

**EVALUATION OF PETROLEUM POTENTIAL OF THE
BALKASSAR BLOCK POTWAR BASIN PAKISTAN, WITH
INTEGRATED INTERPRETATION OF SOURCE,
RESERVOIR AND STRUCTURE**

SYED BILAWAL ALI SHAH

**FACULTY OF SCIENCE
UNIVERSITY OF MALAYA
KUALA LUMPUR**

2019

**EVALUATION OF PETROLEUM POTENTIAL OF
THE BALKASSAR BLOCK POTWAR BASIN
PAKISTAN, WITH INTEGRATED INTERPRETATION
OF SOURCE, RESERVOIR AND STRUCTURE**

SYED BILAWAL ALI SHAH

**THESIS SUBMITTED IN THE FULFILMENT OF THE
REQUIREMENTS FOR THE DEGREE OF DOCTOR OF
PHILOSOPHY**

**DEPARTMENT OF GEOLOGY
FACULTY OF SCIENCE
UNIVERSITY OF MALAYA
KUALA LUMPUR**

2019

UNIVERSITY OF MALAYA
ORIGINAL LITERARY WORK DECLARATION

Name of Candidate: **SYED BILAWAL ALI SHAH**

Matric No: **SHC160079**

Name of Degree: **DOCTOR OF PHILOSOPHY**

Title of Thesis: **EVALUATION OF PETROLEUM POTENTIAL OF THE BALKASSAR BLOCK POTWAR BASIN PAKISTAN, WITH INTEGRATED INTERPRETATION OF SOURCE, RESERVOIR AND STRUCTURE**

Field of Study: **Petroleum Geology**

I do solemnly and sincerely declare that:

- (1) I am the sole author/writer of this Work;
- (2) This Work is original;
- (3) Any use of any work in which copyright exists was done by way of fair dealing and for permitted purposes and any excerpt or extract from, or reference to or reproduction of any copyright work has been disclosed expressly and sufficiently and the title of the Work and its authorship have been acknowledged in this Work;
- (4) I do not have any actual knowledge nor do I ought reasonably to know that the making of this work constitutes an infringement of any copyright work;
- (5) I hereby assign all and every rights in the copyright to this Work to the University of Malaya ("UM"), who henceforth shall be owner of the copyright in this Work and that any reproduction or use in any form or by any means whatsoever is prohibited without the written consent of UM having been first had and obtained.
- (6) I am fully aware that if in the course of making this Work I have infringed any copyright whether intentionally or otherwise, I may be subject to legal action or any other action as may be determined by UM.

Candidate's Signature

Date:

Subscribed and solemnly declared before,

Witness's Signature

Date:

Name:

Designation:

**EVALUATION OF PETROLEUM POTENTIAL OF THE BALKASSAR
BLOCK POTWAR BASIN PAKISTAN, WITH INTEGRATED
INTERPRETATION OF SOURCE, RESERVOIR AND STRUCTURE**

ABSTRACT

Potwar Basin is known to be one of the greatest and oldest oil producing provinces in Pakistan. The subsurface of Potwar Basin consists of large subsurface anticlines, mostly bounded by thrust and reverse faults. The area selected for this study is in Balkassar Oilfield situated in Potwar Basin, which is a compressive region belonging to the active foreland fold and thrust belt of northern Pakistan. In this study, subsurface structure and hydrocarbon potential of the subsurface has been evaluated based on seismic structural interpretation, source and reservoir rock evaluation. An attempt was made to interpret subsurface structure geology and hydrocarbon potential by identifying reflectors, folds, faults, structural trends, styles and trap type using well logs and 2D seismic data. Interpretation reveals the presence of an anticline in the center of the area, bounded by seven major blind faults, four faults are present at south-eastern limb, two faults are present in the north-western limb. The six major faults that bound the structure were previously the normal faults but were reactivated as reverse faults by salt diapirism. In the seismic grid line moving in northeast direction towards center an increase in disturbance can be observed. This structure in the subsurface of the Balkassar block is recognized as a salt-cored anticline structure formed as a result of Indian Plate subduction of an anticlockwise drift and Himalayan orogenic forces. Balkassar structure is at stage 2 known as active diapirism pillow stage. 3D maps show anticline structure is dipping steeply towards northwest side, however, it is dipping gently in southeast side, whereby the limbs have been terminated by the faults present on both sides of the anticline. Chorgali Formation in the subsurface of Balkassar block is covering anticline top flat surface, and the contour map indicates a structural trend that is a four way closure that

could host hydrocarbons accumulation. Furthermore, at the level of Sakesar Limestone in the northwest side, a broad contour closure has been identified which may act as a potential prospect for hydrocarbon accumulation bounded by faults from both sides. Source rock analysis was performed on the Patala Shale Formation from two outcrop sections to evaluate their hydrocarbon generative potential. These samples were analyzed using organic geochemical methods (TOC, Rock-Eval and Py-GC) and organic petrological analysis (vitrinite reflectance). The TOC content of the shales ranges between 0.25 - 1.16 wt. %, while the S₂ values are from 0.11-0.63 mg HC/g rock, consequently low HI values (18-294 mg HC/g TOC) were obtained, thus indicating poor to fair hydrocarbon potential. This is supported by the absence of distinct hydrocarbon peaks in the pyrolysis-GC pyrograms. Observation under the microscope showed the dominant presence of vitrinitic (Type III kerogen) and inertinitic (Type IV kerogen) phytoclasts with minor amount of amorphous organic matter (Type II kerogen). The measured vitrinite reflectance (%R_o) values vary between 0.51-0.84%, indicating immature to peak oil generation window. On the basis of T_{max} values (385 to 429 °C), these samples are immature for hydrocarbon generation, however, these values appear to have been affected by the low S₂. Evaluation of the reservoir rocks was conducted based on well log analysis on the Sakesar and Chorgali formations encountered in three wells. Both formations are shown to possess good reservoir qualities. Sakesar Formation has an average porosity of up to 11.77% and permeability reaches up to 115.81 mD. Having average porosity of 18.13%, the Chorgali Formation has a better potential to act as reservoir rocks compared to the Sakesar Formation in the Balkassar Oilfield.

Keywords: Structure Interpretation, Reservoir, Petrophysics, Potwar, Balkassar.

**PENILAIAN POTENSI PETROLEUM BAGI BLOK BALKASSAR
LEMBANGAN POTWAR PAKISTAN, DENGAN INTEGRASI INTEPRETASI
PUNCA, TAKUNGAN DAN STRUKTUR**

ABSTRAK

Lembangan Potwar dikenali sebagai salah satu wilayah pengeluar minyak yang terbesar dan tertua di Pakistan. Dalam lembangan ini terdapat antiklin antiklin besar yang dibendung oleh sesar-sesar tujuh dan songsang. Kawasan kajian terletak di Balkassar dalam Lembangan Potwar yang merupakan wilayah mampatan dalam Jaluran Lipatan dan Tujahan aktif Pakistan Utara. Dalam kajian ini struktur sub-permukaan dan potensi hidrokarbonnya telah dinilai melalui penafsiran seismos struktur, serta penilaian sumber dan reservoir. Penafsiran sub-permukaan dilakukan dengan menggunakan reflektor-reflektor, lipatan-lipatan, tren dan gaya struktur, perangkap melalui data log-log telaga dan data seismos 2D. Penafsiran berjaya menemui kehadiran satu antiklin ditengah kawasan dibendung oleh tujuh sesar dimana empat terdapat di sayap tenggara dan dua lagi di sayap barat laut. Enam sesar tersebut adalah sesar normal yang telah di aktifkan semula sebagai sesar songsang melalui diapirisme garam. Terdapat peningkatan canggian kearah timur laut yang ditunjukkan pada grid garis seismos. Struktur yang terdapat pada blok Balkassar ini adalah Antiklin Teras-Garam terbentuk akibat dari subduktus Plat Hindi dan putaran lawan jam serta daya orogeni Himalaya. Struktur Balkassar berada pada peringkat kedua Diapirisme Aktif. Peta 3D menunjukkan struktur antklin ini bermiring kearah barat laut tetapi bermiring dengan landai pada sebelah tenggara dimana sayap-sayap telah terputus oleh sesar dikedua-dua belah. Formasi Chorgali melitupi permukaan atas antiklin tersebut dan menunjukkan penutupan empat arah bagi pengumpulan hidrokarbon. Tetapi pada aras Batukapur Sakesar, suatu tutupan lebar telah dikenal pasti yang boleh bertindak sebagai prospek pengumpulan hidrokarbon terbendung oleh sesar. Analisis batuan punca dilakukan keatas sampel Formasi Patala

Shale dari dua keratan singkapan untuk menilai potensi penjanaaan petroleum. Sampel-sampel ini dianalisa menggunakan kaedah geokimia organik (TOC, Rock-Eval dan Py-GC) dan analisa petrologi organik (pantulan vitrinit). Kandungan TOC berjulat diantara 0.25-1.16wt%, sementara nilai S2 Rock-Eval adalah dari 0.11-0.63mgHC/gTOC, yang demikian, nilai HI yang rendah (18-294 mgHCgTOC) diperolehi, dengan itu mencadangkan potensi hidrokarbon adalah lemah ke sederhana. Ini disokong oleh ketiadaan puncak hidrokarbon yang jelas didalam pyrogram Py-GC. Pemerhatian dibawah mikroskop menunjukkan kehadiran phytoklast vitrinit (kerogen Jenis III) dan inertinit (kerogen Jenis IV) yang dominan dengan jumlah bahan organik amorfos (kerogen Jenis II) yang minor. Nilai pantulan vitrinit (%Ro) yang diukur berjulat diantara 0.51-0.84% menunjukkan jendela penjanaaan minyak tidak matang ke puncak matang. Berdasarkan nilai Tmax (385-429°C), sampel-sampel ini adalah tidak matang untuk penjanaaan hidrokarbon, walaubagaimanapun nilai ini nampaknya telah dipengaruhi oleh nilai S2 yang rendah. Penilaian batuan takungan dilakukan keatas Formasi Sakesar dan Chorgali dalam tiga telaga berdasarkan analisis log telaga. Kedua-dua formasi ini mempunyai kualiti takungan yang baik. Formasi Sakesar mempunyai purata keporosan sehingga 11.77% dan ketertelapan mencapai 115.81 mD. Dengan purata keporosan 18.13%, Formasi Chorgali mempunyai potensi yang lebih baik sebagai batuan takungan berbanding Formasi Sakesar di Medan Minyak Balkassar.

Kata kunci: Tafsiran Struktur, Takungan, Petrofizik, Potwar, Balkassar.

ACKNOWLEDGEMENTS

In the name of Allah the Most Gracious the most Merciful. All praises to Allah Subhanaho Wa Taala (SWT) for the strengths and his blessings in completing this thesis. Special appreciation and deepest gratitude go to my supervisors, Prof. Dr. Wan Hasiah Abdullah and AP Prof. Mustaffa Kamal Bin Shuib for their supervision, encouragement and constant support.

Their invaluable help, comments, suggestions and guidance throughout the experimental works and thesis writing have contributed to the success of this research. A deep sense of appreciation to Dr Samina and Adeeb Ahmed for their guidance. I would like to extend my sincere appreciation to the Directorate General of Petroleum Concessions of Pakistan for provision of the data for this study. Special thanks are offered to the Schlumberger for providing Petrel software in the University Malaya Geology computer lab.

I am most grateful to the Department of Geology in the University Malaya for providing facilities to complete this study. I am most grateful to my parents because of who I am here and who were always there for me all the time. I would like to express my appreciation to Dr. Syed Haider Ali Shah and Syed Arshad Ali Shah my brothers for considerable advice and assistance with the study as well as their comments and fruitful discussion all the way from the very start till the end of my thesis. Finally. I am very grateful for all the help provided by the academic staff, visiting professor and supporting staff of the Department of Geology Faculty of Science University of Malaya, and to my colleagues for their continued support and encouragement.

Syed Bilawal Ali Shah. 2019

TABLE OF CONTENTS

ABSTRACT	iii
ABSTRAK	v
ACKNOWLEDGEMENTS	vii
TABLE OF CONTENTS	viii
LIST OF FIGURES	xv
LIST OF TABLES	xx
LIST OF APPENDICES	xxii
CHAPTER 1: INTRODUCTION	1
1.1 Research outline.....	1
1.2 Location and Geological Setting	2
1.3 Problem Statement.....	6
1.4 Objectives	7
1.5 Material and Methods	7
1.5.1 Geochemical data	7
1.5.2 Seismic sections, well logs interpretation and data analysis	8
1.5.3 Microfacies analysis and environment of deposition	8
1.5.4 Lithofacies analysis	8
1.5.5 Seismic facies analysis	9
1.6 Previous studies	9
1.7 Significance of the study	10
CHAPTER 2: GEOLOGICAL SETTINGS AND TECTONICS	12
2.1 General Geology and Tectonics.....	12
2.2 Evolution of Potwar Basin.....	13

2.3	Structural Settings of the Basin	17
2.4	Hydrocarbon Potential	17
2.4.1	Source rocks	18
2.4.1.1	Hangu Formation.....	18
2.4.1.2	Lockhart Formation.....	19
2.4.1.3	Patala Shale Formation.....	19
2.4.2	Reservoir rocks	20
2.4.2.1	Sakesar Limestone Formation	21
2.4.2.2	Chorgali Formation	21
2.4.3	Traps and seals	21
2.4.4	Generation and Migration	22

CHAPTER 3: REVIEW OF SOURCE ROCK CHARACTERISTICS, HYDROCARBON POTENTIALITIES AND GEOPHYSICAL INVESTIGATIONS.....23

3.1	Introduction.....	23
3.2	Source rock characteristics	23
3.2.1	Quantity of organic matter	23
3.2.2	Rock-Eval pyrolysis	24
3.2.3	Type of organic matter	27
3.2.3.1	Kerogen Type I.....	28
3.2.3.2	Kerogen Type II	29
3.2.3.3	Kerogen Type III.....	29
3.2.3.4	Kerogen Type IV.....	29
3.2.4	Thermal maturity	30
3.2.5	Petroleum trap	31
3.2.5.1	Combination traps	32

3.2.5.2	Structural traps	32
3.2.5.3	Salt Dome traps	34
3.2.6	Salt structures movement and development stages	38
3.3	Geophysical well logs analysis.....	41
3.3.1	Gamma ray (GR)	43
3.3.2	Spontaneous potential (SP)	44
3.3.3	Density log	48
3.3.4	Sonic log (DT).....	51
3.3.5	Neutron porosity log (NPHI).....	53
3.4	Reservoir properties.....	54
3.4.1	Mud cake and mud filtrated resistivity correction.....	55
3.4.2	Formation Water resistivity (RW) determination.....	56
3.4.3	Shale Volume (Vsh) determination	56
3.4.4	Formation porosity determination (ϕ)	57
3.4.5	Total porosity	58
3.4.6	Density Log (ϕ_D).....	58
3.4.7	Shaly zones.....	58
3.4.8	Clean zones.....	59
3.4.9	Neutron Porosity Log (ϕ_N)Formation porosity determination (ϕ).....	59
3.4.10	Shaly zones.....	59
3.4.11	Density-Neutron combination	59
3.4.12	Clean zones.....	60
3.4.13	Shaly zones.....	60
3.4.14	Secondary porosity (ϕ_{sec}).....	61
3.4.15	Effective Porosity (ϕ_e)	61
3.4.16	Fluid saturation determination.....	61

3.4.17	Water saturation SW	61
3.4.17.1	Uninvaded zones	62
3.4.18	Hydrocarbon saturation determination Sh.....	62
3.5	Introduction to seismic methods.....	62
3.5.1	Seismic reflection method.....	65
3.5.1.1	Seismic velocities.....	65
3.5.1.2	Interval velocity.....	67
3.5.1.3	Average velocity	67
3.5.1.4	Root mean square velocity	68
3.5.1.5	Dix equation	68
3.5.2	Horizon mapping by 3D contours	69
3.5.3	Seismic interpretation.....	71
3.5.4	Structural analysis	74
3.5.4.1	Time section	75
3.5.4.2	Depth section.....	75
3.5.5	Softwares used for seismic interpretation	75
3.6	Microfacies analysis	75
3.7	Lithofacies analysis	75
3.7.1	Factors effecting interpretation	76
CHAPTER 4: RESEARCH DATA AND METHODOLOGY		79
4.1	Introduction.....	79
4.2	Research data.....	79
4.3	Organic geochemistry methods	85
4.3.1	Sample preparation.....	86
4.3.2	Analytical studies	87

4.3.2.1	Pyrolysis	87
4.3.2.1.1	Rock-Eval pyrolysis and Total organic carbon (TOC)	87
4.3.2.1.1.1	Total organic carbon (TOC)	87
4.3.2.1.1.2	Rock-Eval pyrolysis	87
4.3.2.1.1.3	Pyrolysis-Gas Chromatography	90
4.3.2.1.1.4	Organic petrology : vitrinite reflectance.....	90
4.4	Microfacies analysis	91
4.4.1	Sample preparation.....	91
4.5	Seismic data interpretation	93
4.5.1	Base map	95
4.5.2	Horizon marking and interpretation	96
4.5.3	Parameters required	96
4.5.3.1	Time in seconds.....	96
4.5.3.2	Average velocity	96
4.5.3.3	Depth	97
4.5.3.4	Time interval	97
4.5.3.5	Interval velocity.....	98
4.5.4	3D Horizon mapping	98
4.5.4	Seismic to well tie to mark horizons in petrel	99
4.5.5	Petrel software interpretation	100
4.5	Petrophysical well log analysis.....	102
4.5.1	Corrections and Calculations.....	103
4.5.2	Interpretation	103
4.5.2.1	Shale volume	103
4.5.2.2	Procedure for finding different parameters from logs.....	104
4.5.2.3	Porosity and Water Saturation.....	104

4.5.2.4	Permeability	105
4.5.2.5	Bulk volume of water (BVW).....	105
4.5.2.6	Pay reservoir and net pay	106
4.5.2.7	Saturation of hydrocarbon (Sh).....	106
4.6	Lithofacies analysis	110
4.7	Seismic facies analysis	113
CHAPTER 5: RESULTS AND DISCUSSION		114
5.1	Introduction.....	114
5.2	Source rock evaluation	114
5.2.1	Organic matter richness and source rock quality	114
5.2.1.1	Total organic carbon content and pyrolysis	114
5.2.1.2	Kerogen pyrolysis (Py-GC).....	119
5.2.1.3	Thermal maturity.....	123
5.2.1.2.1	Vitrinite reflectance (%Ro) and (Tmax)	123
5.3	Seismic interpretation	126
5.3.1	Structural Interpretation	126
5.3.2	3D Contour maps.....	134
5.4	Petrophysical analysis.....	143
5.4.1	Results of petrophysical analysis	148
5.5	Micro facies analysis	149
5.5.1	Micro facies and depositional environment identified	149
5.5.1.1	Nummulitic wackestone	150
5.5.1.2	Millioloïdal wackestone	151
5.5.1.3	Bioclastic wackestone	152
5.5.1.4	Diagenetic features	153
5.5.1.4.1	Dissolution	153

5.5.1.4.2	Cementation	153
5.5.1.4.3	Compaction	153
5.5.1.4.4	Neomorphism	154
5.5.1.4.5	Filled fractures and veins	154
5.5.1.5	Thin section visual porosity	155
5.6	Lithofacies identified	159
5.6.1.1	Facies 1	159
5.6.1.2	Facies 2	159
5.6.1.3	Facies 3	160
5.6.1.4	Facies 4	160
5.6.1.5	Facies 5	160
5.6.1.6	Facies 6	160
5.6.2	Identified depositional environments	161
5.6.2.1	Point bar	162
5.6.2.2	Overbank elements	162
5.6.2.3	Channel fill elements	162
5.7	Seismic facies identified	162
CHAPTER 6: CONCLUSIONS.....		165
6.1	Conclusions	165
6.2	Contribution of the study	170
6.3	Recommendations for future work	171
REFERENCES.....		172
LIST OF PUBLICATIONS AND PAPERS PRESENTED		187
APPENDIX		192

LIST OF FIGURES

Figure 1.1	: Geological map displaying various Potwar Basin structural zones, MBT, NDPZ, and showing study area in Balkassar.	3
Figure 1.2	: Major structures of Potwar Basin	4
Figure 2.1	: The landmass movement of Indo-Pak from Australia and collision with Eurasian plate.	13
Figure 2.2	: Stratigraphic column showing the trap stratigraphy of Balkassar-OXY-1 well.	16
Figure 2.3	: Sedimentary maps of Pakistan.	16
Figure 3.1	: Schematic diagram of Rock-Eval program showing output of rock samples (evolution of CO ₂ and hydrocarbons) during heating. Tmax, S1, S2, and S3 are the important measurements	26
Figure 3.2	: Plot of atomic H/C vs atomic O/C showing different types of kerogen and oil/gas generation zone.	27
Figure 3.3	: Kerogen types classification based on HI/OI plot.	28
Figure 3.4	: An example of combination type stratigraphic trap	32
Figure 3.5	: Anticline trap type example.	33
Figure 3.6	: Compressional trap type example.	34
Figure 3.7	: An example of salt dome trap type.	35
Figure 3.8	: Different terminologies and structures in salt systems.	37
Figure 3.9	: Different terminologies and structures in salt systems.	37
Figure 3.10	: Development stages of salt diapir	39
Figure 3.11	: Salt growth rate and sedimentation rate relationship.	40
Figure 3.12	: Showing the GRmax , GRmin and GRlog reading of interested zone in the center.	44
Figure 3.13	: Origin of SP curve.	46
Figure 3.14	: Idealized SP log	47

Figure 3.15	: Idealized Density log.	49
Figure 3.16	: Density log recording equipment source and receiver/detector in well.	50
Figure 3.17	: Idealized Sonic log	52
Figure 3.18	: Neutron log idealized.....	54
Figure 3.19	: Shale distribution in rocks	57
Figure 3.20	: Reflected and refracted seismic waves.	65
Figure 3.21	: Interval velocities of different horizons.....	67
Figure 3.22	: An example of 3D contour output image from horizon mapping.	69
Figure 3.23	: Image showing seismic line number along with shotpoint numbers and coordinates of all shotpoints used for horizon mapping in Petrel, provided by LMKR.	70
Figure 3.24	: A complete seismic interpretation flowchart.	72
Figure 3.25	: An example of an image of velocity analysis (Time-Depth relationship) (velocity model which allows to move data between time domain and depth domain) of seismic dip line SOX-PBJ-04 on excel.	73
Figure 3.26	: Types of lithological facies	78
Figure 4.1	: Mine X-1 and Mine X-2 Mustafabad section near Choa Saidan Shah Village, and on top is Sakesar Formation.	81
Figure 4.2	: Inside mine X-1.	81
Figure 4.3	: Inside mine X-2.	81
Figure 4.4	: Exposed Patala Shale, Mustafabad section near Choa Saidan Shah Village.....	82
Figure 4.5	: Exposed Patala Shale Mustafabad section near Choa Saidan Shah Village.....	82
Figure 4.6	: Exposed Patala Shale near Pail Village (Pail Village Patala Shale and Sakesar section).	83
Figure 4.7	: Sample extraction from Patala Shale near Pail Village.	83

Figure 4.8	: Measuring Patala Shale section near Pail Village.	84
Figure 4.9	: Ten selected samples, acid, geological hammer, notebook and bags.	84
Figure 4.10	: Flow chart of source rock characterization.	86
Figure 4.11	: For TOC analysis Multi EA2000 elemental analyzer.	88
Figure 4.12	: Rock-Eval process and output of Rock-Eval that is recorded	89
Figure 4.13	: Example seismic section SOX-PBJ-04 showing different reflectors and faults in subsurface.	94
Figure 4.14	: Showing the base map that contains all seismic lines and wells location of the study area.	95
Figure 4.15	: Showing the synthetic seismogram along with well tops from Balkassar-OXY-01 well.	101
Figure 4.16	: Data flow chart of well logs interpretation.	102
Figure 4.17	: Determination of formation temperature at various depths	107
Figure 4.18	: Determination of R_w from R_{we}	108
Figure 4.19	: Correction of R_{mf} and R_{we} according to temperature.	109
Figure 4.20	: R_{mf} / R_{we} determination from Self-Potential.	110
Figure 4.21	: Warcha Sandstone generalized stratigraphic characteristics in Potwar Basin.	112
Figure 5.1	: Distribution pyrolysis of S_2 yields versus (TOC) total organic carbon plot.	115
Figure 5.2	: Plot of hydrogen index (HI) vs pyrolysis T_{max} , showing the thermal maturity stages and kerogen type of the analyzed Patala Shale samples.	119
Figure 5.3	: Pyrolysis GC pyrograms of the Patala Shale samples of Mustafabad section.	221
Figure 5.4	: Pyrolysis GC pyrograms of the Patala Shale samples of Mustafabad section.	122
Figure 5.5	: Plot of maturity parameters vitrinite reflectance ($\%R_o$) and T_{max} for the samples.	125

Figure 5.6	: Photomicrographs of amorphous organic matter (brown staining) and inertinite macerals (white phytoclasts) in sediments of the Patala Shale samples.....	125
Figure 5.7	: Seismic line SOX-PBJ-01 without interpretation.....	129
Figure 5.8	: Interpreted seismic line SOX-PBJ-01.....	129
Figure 5.9	: Seismic line SOX-PBJ-04 without interpretation.....	130
Figure 5.10	: Interpreted seismic line SOX-PBJ-04.....	130
Figure 5.11	: Seismic line SOX-PBJ-05 without interpretation.....	131
Figure 5.12	: Interpreted seismic line SOX-PBJ-05.....	131
Figure 5.13	: Seismic line SOX-PBJ-06 without interpretation.....	132
Figure 5.14	: Interpreted seismic line SOX-PBJ-06.....	132
Figure 5.15	: Structural model of Balkassar anticline with well tops of Balkassar-OXY-01.	133
Figure 5.16	: Structural model of Balkassar anticline with tops of interpreted source and reservoir horizons on seismic are displayed.	133
Figure 5.17	: Salt diapir development stages.	134
Figure 5.18	: Chorgali Depth contour map.	137
Figure 5.19	: Sakesar Depth contour map.	138
Figure 5.20	: Patala depth contour map.....	139
Figure 5.21	: Basement depth contour map.....	140
Figure 5.22	: All formations depth contour map.	141
Figure 5.23	: Chorgali time contour map.	142
Figure 5.24	: Sakesar time contour map.....	142
Figure 5.25	: Patala time contour map.	143
Figure 5.26	: Graph showing average percentages of the petrophysical parameters of both reservoirs.....	148
Figure 5.27	: Plate 1, Nummulitic wackestone.	150

Figure 5.28	: Plate 2, Millioidal wackestone.....	151
Figure 5.29	: Plate 2, Millioidal wackestone.....	152
Figure 5.30	: Plate 4: Diagenetic features in Sakesar Limestone, A: dissolution, B: calcite filled vein, C: neomorphism, D: compaction, E: filled fracture and F: cementation, Millioidal wackestone.....	154
Figure 5.31	: Fracture porosity in Pail Village sample 3.	155
Figure 5.32	: Dissolution porosity in Pail Village sample 2.	156
Figure 5.33	: Different gamma ray log responses to the characteristic of Warcha sandstone in the subsurface of Balkassar.	161
Figure 5.34	: Seismic facies identified on seismic section SOX-PBJ-04.....	164

University of Malaya

LIST OF TABLES

Table 2.1	: Balkassar block stratigraphic, developed from Balkassar-OXY-01, Balkassar 7 and Balkassar 8 well	15
Table 2.2	: Oil and gas producing reservoirs formations found in Potwar.....	20
Table 2.3	: Numerous seals and reservoir that are present in many fields of Potwar Basin.....	22
Table 3.1	: The geochemical parameters which describes the source rock petroleum potential.....	24
Table 3.2	: SP log principal uses.....	48
Table 3.3	: Values of common lithologies/fluids densities.....	50
Table 3.4	: For different matrixes sonic velocities and interval transit time	52
Table 3.5	: Facies lithologies, contents variations with gamma ray response	77
Table 4.1	: Seismic and well datasets.....	80
Table 4.2	: Equipment used for sample preparation.....	93
Table 5.1	: Pyrolysis (SRA), TOC data parameters and measured vitrinite reflectance (%Ro) values of the Patala Shale samples of Mustafabad section.....	116
Table 5.2	: Pyrolysis (SRA), TOC data parameters and measured vitrinite reflectance (%Ro) values of the Patala Shale samples of Pail Village.....	117
Table 5.3	: Petrophysical: Different parameters values calculated for Sakesar limestone in Balkassar-OXY-01 well.....	144
Table 5.4	: Petrophysical: Different parameters values calculated for Chorgali Formation in Balkassar-OXY-01 well.....	144
Table 5.5	: Petrophysical: Different parameters values calculated for Chorgali Formation in Balkassar- 7 well.....	145
Table 5.6	: Petrophysical: Different parameters values calculated for limestone Formation in Balkassar- 7 well.....	145
Table 5.7	: Petrophysical: Different parameters values calculated for Formation in Balkassar- 8 well.....	146

Table 5.8	: Petrophysical: Different parameters values calculated for Sakesar limestone Formation in Balkassar- 8 well.	146
Table 5.9	: Criteria for qualitative description of reservoir adopted for this study.....	147
Table 5.10	: Reservoirs petrophysical parameters for the three wells analyzed in this study.....	147
Table 5.11	: Average petrophysical parameters of Chorgali and Sakesar formations.	148
Table 5.12	: Lithology, sample numbers, field description, microfacies, and photomicrographs of Mustafabad Section.	157
Table 5.13	: Lithology, sample numbers, field description, microfacies, and photomicrographs of Pail Village section.....	158
Table 5.14	: Seismic facies identified.	163

LIST OF APPENDICES

Appendix A: VR histograms of Patala shale	192
---	-----

University of Malaya

CHAPTER 1: INTRODUCTION

1.1 Research outline

In Potwar Basin of northern Pakistan hydrocarbon traps are controlled structurally, though it is reported that local stratigraphic traps are also present (Iqbal et al., 2015; Kemal, 1991; Shah & Abdullah, 2016). Tertiary Himalayan orogeny has caused all of the structural traps. Consequently the proposed study of Potwar Basin is to analyse the structural traps. Moreover, Potwar Basin in the past two decades has gained much more petroleum exploration attention (Jaswal, 1990; Kemal, 1991; Kadri, 1995; Moghal et al., 2007). So in this regard a large number of multinational and national petroleum companies have been concerned to understand properly the structural complexities of the region. On the other hand, not much and inadequate data has been published which is emphasizing on the trap configuration and their structural geometries.

The area that has been selected for this study is known as Balkassar, lies in central part of Potwar Basin, Punjab Pakistan, and is 85 km from Islamabad. Its elevation is 499 m above sea level. The coordinates of Balkassar are 32° 55' N and 72° 39' E. Balkassar oilfields were the major producing fields with average production of 386bbl per day in Nov 94 in the Potwar Basin (Iqbal et al., 2015). Attock Oil Company limited (AOCL) and Burmah Oil Company have discovered this field in the 1946 (Iqbal et al., 2014; Shah & Abdullah, 2017).

In terms of petroleum exploration, the Balkassar oilfield is very important as it is host to proven hydrocarbon reserves. The subsurface of Balkassar has Precambrian to recent sediments thick sedimentary cover sequence which is about 4000 m thick, and amongst these rocks units, Eocene age Sakesar and Chorgali formations and Paleocene Hangu Formation are proven reservoirs (Iqbal et al., 2015). In the cover sequence reflection data displays the presence of reverse faults of Precambrian to recent sediments. In the

basement normal fault is present which is also present in reflection seismic data (Lillie et al., 1987; Moghal et al., 2007; Pennock et al., 1989).

The present study makes use of seven fresh outcrop samples and three samples collected from deep mines to evaluate source rock potential. Well logs data from three wells were evaluated for reservoir rock potential and grid of eleven seismic reflection sections (collected by Occidental in project area of Balkassar) for seismic structural interpretation (Fig 1.3). All of these are trustworthy ways for the subsurface interpretation. By using these data, it will help in understanding the complex subsurface geological structure of Balkassar, potentiality of source and reservoir rocks and trap model. All of these techniques when applied together allows an insight into the framework and structural trends of area. The seismic data was acquired from approval from (DGPC) which includes seismic sections and well tops.

1.2 Location and Geological Setting

In the region Potwar Basin is the oldest oil provinces, Attock Oil Company limited made the very first commercial discovery at Khaur in 1914, and since 1914 large number of hydrocarbons fields have been discovered in this area (Zahid et al., 2014). The majority of the discoveries were related with the subsurface faults, associated anticlines and duplexes (Jaswal et al., 1999; Jadoon et al., 2015). Exploratory wells which are in numbers more than 150 so far have been drilled in Potwar. Numerous wells amongst them were prematurely abandoned because of structural complexities and some of them didn't even reach the target depth due to technical drilling difficulties.

Potwar Basin is generally taken to fall between the Jhelum fault in the east and Kalabagh fault in the west. The MBT marks northern periphery, Khairabad-Panjal Thrust, while Salt Range is the southern boundary (Jaswal et al., 1997; Kazmi & Jan, 1997; Rana & Asrarullah 1982). Within these boundaries MBT, Panjal Thrust and Salt Range Thrust,

it can be broadly subdivided into two parts, across the Khairi-Murat Thrust, as 1.NPDZ, 2 SPDZ.

Physical and geographic locations of Potwar Basin are naturally complex. It is bounded from its northern side by Margalla thrust and from its south by Salt Range Thrust. Its eastern limit forms the Jhelum thrust. The Indus River more or less outline the western limit. Over all the in Potwar the structural trend is east-west & northeast-southwest (Gee, 1980; Gee, 1989; Iqbal et al., 2014a; Iqbal et al., 2014b; Kazmi & Abbassi, 2002; Kazmi & Jan 1997; Shah, 2009; Tahirkheli, 1979). Greater part of the area consists of large surface anticlines. In the region most of the subsurface structures consists of reverse and thrust faults. Most of the anticlinal bounded thrust faults are blind and which never emerged on surface. In western, southwestern and eastern Potwar the tectonic styles are different.

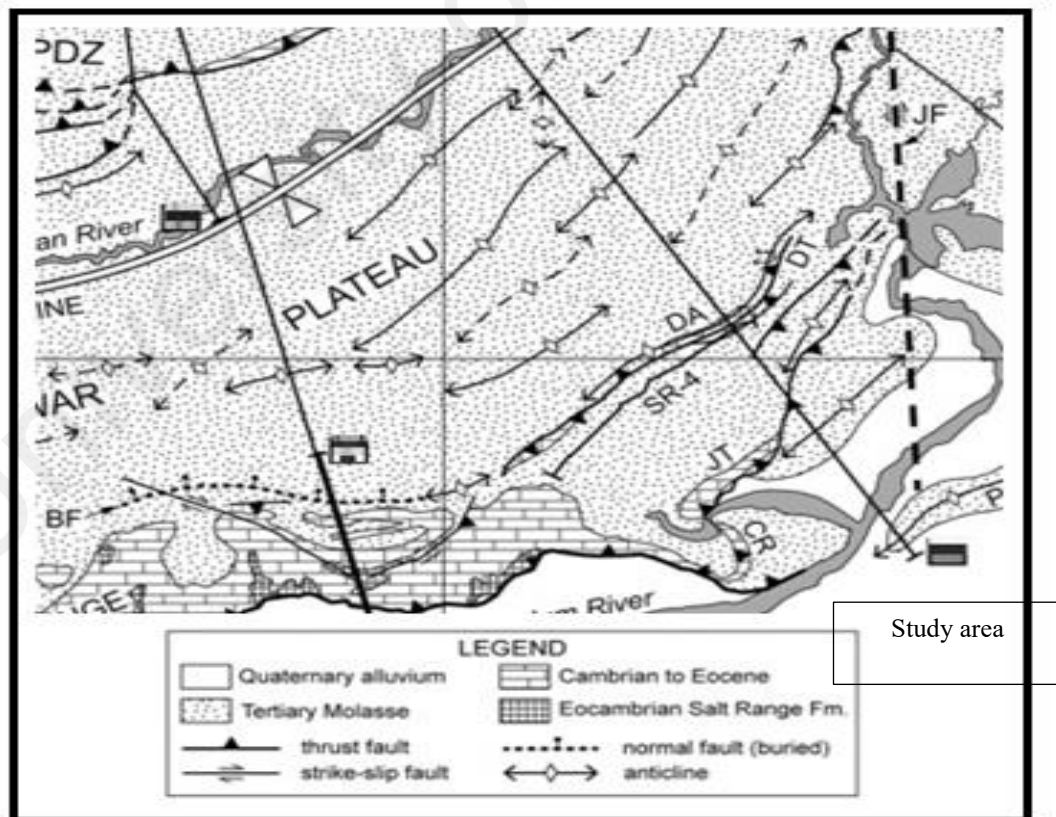


Figure 1.1: Geological map displaying various Potwar Basin structural zones, MBT, NDPZ, and showing study area in Balkassar. Free image.

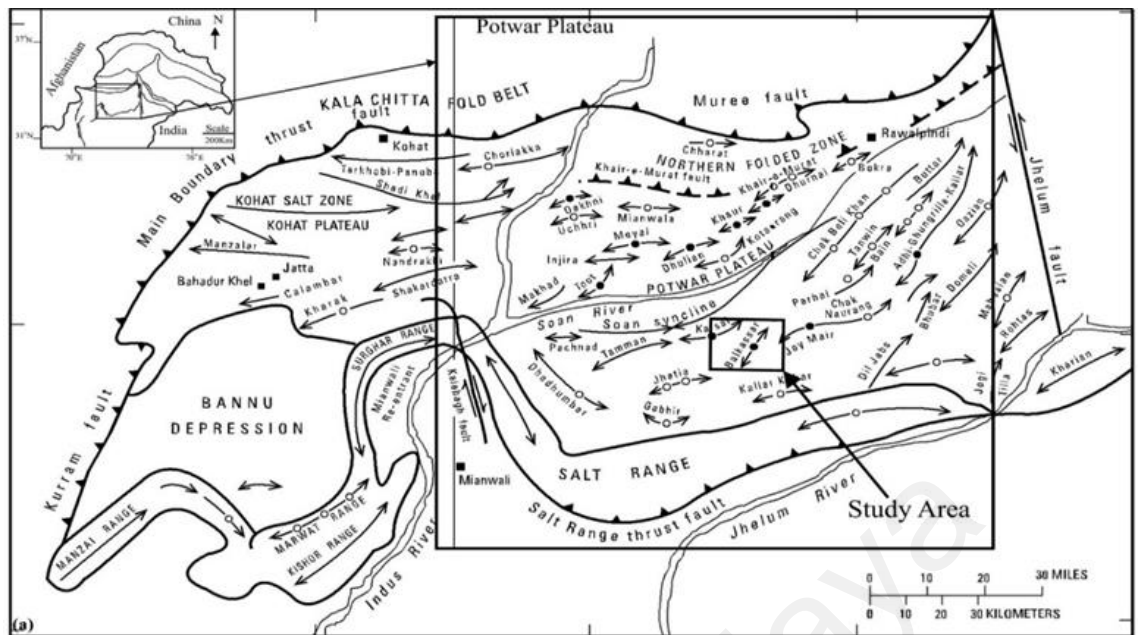


Figure 1.2: Major structures of Potwar Basin. Free image.

Balkassar the study area is a part of active Foreland fold and Thrust Belt of northern Pakistan (Ahsan et al., 2012; Zahid et al., 2014). Tectonically the area lies in compression region. Structurally this area has several tectonic sub divisions such as the Kharsel Fault in its north. While Jhatia and Ghabbir faults lies in its west. In its east it consists of Joya Mair thrust fault. In the south, it consists of Kalar Kahar fault (Fig 1.1 and 1.2) (Ahsan et al., 2012; Ashraf et al., 2016; Shah & Abdullah, 2017). In Balkassar, the major source rocks are Patala Shale and Lockhart limestone and shale of Paleocene ages. These shales are black and marine in nature (Hasany & Saleem, 2012).

In Balkassar area, Miocene age, the seal rock is Murree Formation over Eocene reservoirs (Zahid et al., 2014). This Murree Formation seal is an effective for reservoirs of Eocene age in Potwar Basin. In Balkassar area, the discovery was from Eocene reservoirs. The combined thickness of both formations is 464-600ft (141.43m-182.88m) (Iqbal et al., 2015). In the region the major producing reservoirs are Sakesar and Chorgali formations of Eocene age (Kadri, 1995).

Balkassar Oilfield is an area containing a subterranean store of petroleum. The Potwar Basin consists of numerous anticlines. The hydrocarbon accumulation is associated with anticlinal structure in Balkassar area (Shah & Abdullah, 2017). The combination of seal, reservoir and source rock presents prime hydrocarbon trap in this area.

University of Malaya

1.3 Problem Statement

Source rock evaluation, reservoir rock properties, structural trap model, extensive structure interpretation and 3D horizon mapping are essential and important aspects for understanding the subsurface elements, as Balkassar block has a complex structural type trap, bounded by various faults in the recent cover sequence and in the basement. About 150 exploratory wells have been drilled so far in the region, many of these were prematurely abandoned, as they could not reach their target depths due to structural complexities and associated technical drilling problems (Ahsan et al., 2013; Iqbal et al., 2015).

In past two decades Balkassar has attracted exploration companies attention for petroleum exploration (Ahsan et al., 2013; Iqbal et al., 2015; Kadri, 1995; Kemal, 1990; Moghal et al., 2007). So a large number of multinational and nationwide petroleum companies have been interested to identify the structural complexities of the region. On the other hand, very few and limited data has been published on the source rock potential, reservoir rock potential, trap configuration and their geometries. Although Balkassar has a complex structure and known hydrocarbon potential according to Iqbal et. al. (2015), Jaswal et. al. (1999) and Kadri, (1995), still the reserves are not explored.

Lack of information available regarding complete interpretation of seismic grid sections for structural model of anticline, and horizon mapping for the proven source, reservoir, seals and cap rocks (Ahsan et al., 2013) for understanding the complex structural geometries and evaluation of the reservoir rock potentiality as well as lack of information available regarding petrophysical analysis (Ahsan et al., 2013) which makes this deemed necessary and crucial to carry out the proposed study.

1.4 Objectives

The objectives of this study were focused on the evaluation of petroleum system, all of the processes which control the hydrocarbon potential of Balkassar oilfield by integrating the available subsurface, geophysical and geological data with emphasis on structure interpretation and trap model.

The main aim of proposed study is to evaluate structure and potentiality of the Balkassar Block.

The following are the main research objectives:

- To evaluate source rock potential
- To identify targeted horizons of interest, folds and faults
- To characterize the structural trap geometries of the subsurface based on seismic interpretation;
- To map targeted subsurface horizons (by 3D contour maps)
- To evaluate hydrocarbon potential of reservoir rock.

1.5 Material and Methods

For achieving the objectives, the data and methodologies that have been adopted are described below.

1.5.1 Geochemical data

For source rock characterization, ten outcrop rock samples were utilized which were subjected to TOC, Rock-Eval pyrolysis, Py-GC and vitrinite reflectance measurements. The samples were collected from Pail Village section and Mustafabad section near Choa Saidan Shah Village.

1.5.2 Seismic sections, well logs interpretation and data analysis

Post- stacked time migrated seismic sections were provided by LMKR Resources, after getting permission letter from DGPC, Pakistan. The present study make use of the seismic reflection data acquired through vibrosise acquisition survey and processed by Oil and Gas Development Company Limited (OGDCL) in 1981. For seismic interpretation Schlumberger Petrel Software was used and the for reservoir evaluation Interactive Petrophysics was used based on well logs data. A trustworthy way for the subsurface geological interpretation is the seismic data integration with geological data and wells data (well logs). By using these data, it will help in understanding the subsurface geological structures, structural style, trends, behavior, potentiality of the reservoir rocks and trap model. This form of multi-approach technique is used by the exploration companies to understand the subsurface geological structure in hydrocarbons exploration, and provides an insight into the framework and structural styles of the area.

1.5.3 Microfacies analysis and environment of deposition

In Potwar Basin Sakesar Formation is one of the major producing reservoir (Kadri, 1995; Shah, 2009). In this study Sakesar Formation is investigated for its detailed microfacies analysis at two localities (Mustafabad and Pail Village section) in Eastern Salt Range. Based on detailed sedimentological investigations including outcrop observations and thin section evaluation, microfacies of Sakesar limestone are identified in the study area. Dunham's (1962) classification is used to classify Sakesar Limestone in these microfacies.

1.5.4 Lithofacies analysis

Warcha Formation in Potwar Basin is one of the proven and deeper reservoir rock (Kadri, 1995; Shah, 2009).

Subsurface facies analysis was performed for the Warcha-Sandstone Formation through datasets of Balkassar-OXY-1. Well logs were used in Interactive Petrophysics software. In this software the dataset of gamma ray log was used as a tool to interpret and delineate the subsurface facies, as the gamma ray log is one of the most useful tool due to its best property of its response to different lithologies (Posamentie & Allen, 1999). The aim of the investigation was to investigate subsurface sedimentary facies and depositional cycles and depositional environment based on the variety of characteristics of gamma ray log trends. Both large scaled depositional units and small scale lithofacies organisation were interpreted and the recognition of arrangement of depositional sequences were considered in terms of their paleo-environment significance.

1.5.5 Seismic facies analysis

Seismic facies are three dimensional mappable units of seismic reflections that are different from adjacent units. Seismic facies analysis is interpretation and description of seismic parameters such as continuity, amplitude and configuration. The analysis was performed with an aim to identify seismic facies in Balkassar subsurface, and five major seismic facies have been identified and interpreted in Miocene to Early Cambrian.

1.6 Previous studies

Potwar Basin in terms of petroleum exploration in the past two decades has gained more consideration (Kadri, 1995; Kemal, 1991; Jaswal, 1990; Moghal et al., 2007). Source rock characteristics and petroleum system analysis as well as structural trap model were studied and had attracted the interest of lots of oil companies, geophysicist and geologists to venture into exploration activities. The Potwar Basin is much more famous since 1914 because the very first discovery was made at Kundal western Indian subcontinent in that year (Kadri, 1995; Kazmi & Jan, 1997). First commercial discovery

was on thrust faulted anticline which is near to the Khaur and was made in 1914 by AOC (Iqbal et al., 2015).

The Potwar Basin got more attention of the oil companies and over 340 wells have so far been drilled in Potwar (Iqbal et al., 2015). The oil production from Khaur well was from the Sakesar Formation. In Potwar Basin, according to Kadri (1995), the Balkassar area is very important in terms of petroleum exploration as it is host to proven hydrocarbon reserves, and also Attock Oil Company discovered this field in 1946 and the production was from the same Sakesar Formation (Iqbal & Shah, 1980). In Potwar the first gas field was Adhi which had the discovery in 1979, which was producing from the rocks of ages Eocene and Cambrian rocks (Petroconsultants, 1996). In Potwar region, 3 gas fields over 18 oil discoveries have been made between years 1914 to 1996 (Quadri & Quadri, 1998). In production Potwar Basin, is majorly from faulted anticlinal traps and the rocks are mainly from Eocene age, biggest oil discovery was explored in field of Dhurnal (Jaswal et al., 1997).

1.7 Significance of the study

This study results have mainly highlighted following.

- Source rock potential
- Structural interpretation.
- Subsurface horizons distribution.
- Potential prospect for hydrocarbon accumulation.
- Geometry of the subsurface hydrocarbon trap.
- Reservoir rock potentiality

The results of this study have unrevealed the source and reservoir rock potentiality, geometry of the subsurface hydrocarbon trap, folds and faults present. The main horizons

have been marked, whereby subsurface horizon distribution and potential prospect for hydrocarbon accumulation in the Balkassar oilfield has been identified. This research has a direct applicability to hydrocarbon exploration. All of this work has important information for the body of knowledge and exploration companies regarding subsurface and will help in understanding the complex structure of the Balkassar oilfield for future hydrocarbons exploration.

University of Malaya

CHAPTER 2: GEOLOGICAL SETTINGS AND TECTONICS

This chapter will highlight the structures, subsurface stratigraphy, tectonics and geologic history of Pakistan, with emphasis on the study area Balkassar in Potwar Basin, based on the earlier published literature.

2.1 General Geology and Tectonics

Pakistan is a country in South Asia and it has a coastline along the Arabian Sea and the Gulf of Oman in the south and is bordered by India to the east, Afghanistan to the west, Iran to the Southwest and China in the far northeast respectively. Few of earlier published accounts local geology are by Kadri (1995) and Kazmi & Jan (1997) on Salt mines and Salt range in Punjab province, Carter (1844 and 1861) on hills and soils in between Indus and Hyderabad and geology of provinces Baluchistan and Sindh, whereas Wynne 1870-1891 on the geology of the province Khyber-Pakhtunkhwa (which includes salt range and the Kohat) and Punjab province as well as Kashmir (Kazmi & Jan, 1997). Mainly these and succeeding research were of reconnaissance nature regarding minerals engineering and regional geology. The books which sum up Pakistan's geology are Geology and Tectonics of Pakistan, written by Kazmi & Jan (1997), and Petroleum Geology of Pakistan written by Kadri (1995).

A tectonic plate which travelled about 5000 km carrying Indo-Pakistan landmass, followed by seafloor spreading and opening of Indian Ocean. The landmass moved in northward direction and collided with the Eurasian plate (Fig. 2.1). It is estimated that about 130 million years ago the separation from supercontinent initiated (Johnson et al. 1976), the Proto-ocean fracture zone and the seafloor spreading facilitated the movement was facilitated by transform faulting (Duncan et al., 1988).

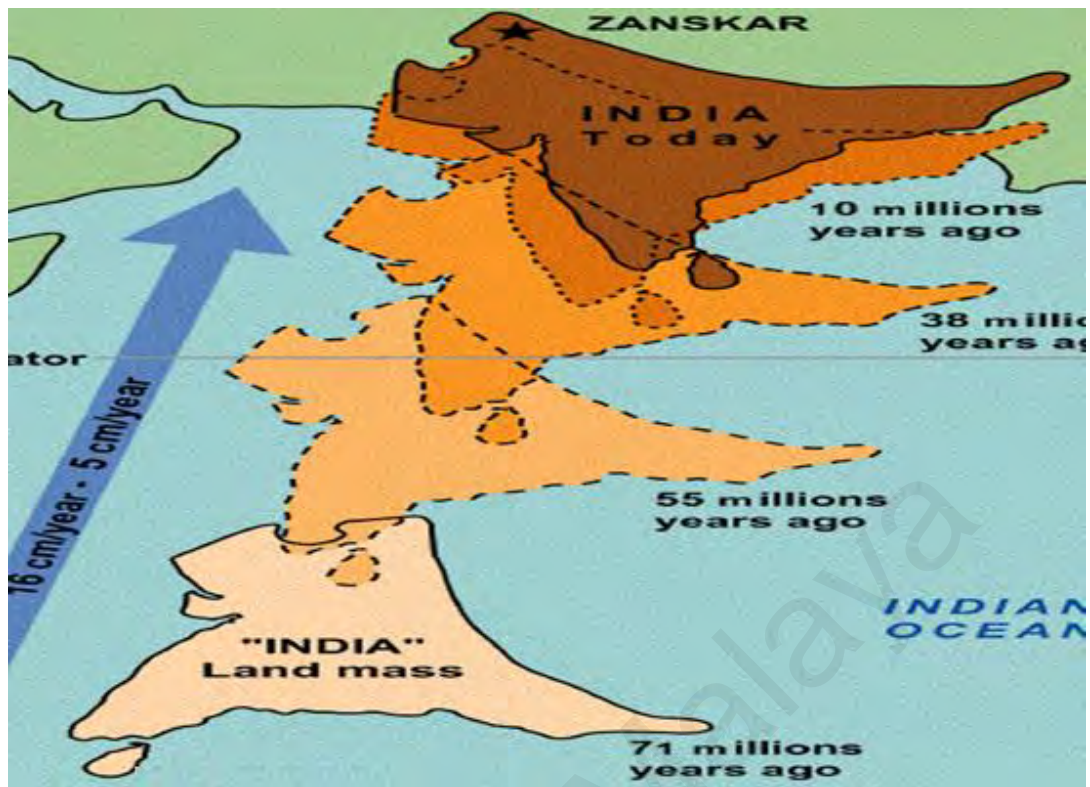


Figure 2.1: The landmass movement of Indo-Pak from Australia and collision with Eurasian plate. Free Image.

2.2 Evolution of Potwar Basin

The area of study lies in Potwar Basin part of upper Indus Basin, located on the Indian Shield northwestern part, Kirthar Fold belt borders its west (Kadri, 1995). This basin covers two thirds of eastern Pakistan. The major characteristics of the Indus Basin are the fore-deep comprising depressions, platform, an inner folded zone and outer folded zone (Memon & Siddiqui, 2005). Almost all of the Pakistan's major oil/condensate and gas fields are located in Indus Basin (Kadri, 1995).

The area that has been selected for this study lies in Potwar Basin (Fig. 2.3), the oilfield area itself is known as Balkassar. The oldest rocks of Indus Basin are characterized by a thick sequence of Infra Cambrian and Cambrian age non-metamorphosed (Bender & Raza, 1995). In the region the Kohat-Potwar Basin has produced and is still producing oil and gas extensively. The Potwar Basin is on subducting margin of Indian Plate, where

collision of the two plates Indian and Eurasian plate resulted in the deformation of the Indian Plate. Along with collision the growing of the Himalayas mountains in north west and northern part further deformed/distorted Indian plate, due to this deformation sediments were juxtapositioned of Precambrian and Tertiary ages (Iqbal et al., 2015; Kadri, 1995; Kazmi & Jan, 1997; Shah & Abdullah, 2017).

Towards the southern periphery of Potwar Basin the sediments of Precambrian age are exposed in Salt Range. Due to this deformation and juxtaposition the sediments of Precambrian and Paleocene age did not faced enough thermal stress to generate hydrocarbons, and are mostly thermally immature (Grelaud et al., 2002, Khan et al., 1986). Whereas on the other hand in case of Pre-Eocene strata lots of factors like compaction disequilibrium with deep burial as well as compression caused sufficient thermal stress to generate hydrocarbons (Fazeelat et al., 2010; Grelaud et al., 2002).

Table 2.1: Balkassar block stratigraphic, developed from Balkassar-OXY-01, Balkassar 7 and Balkassar 8 well.

Age	Formation	Lithology	Environment of Deposition	Top (m)	Thickness
Pliocene	Nagri	Sandstone	Fluvial	0	478.82
Miocene	Chinji	Sandstone and Clay	Fluvial	478.8	929.29
Miocene	Kamlial	Sandstone	Fluvial	1408.1	106.68
Miocene	Murree	Sandstone	Fluvial	1514.8	906.74
Eocene	Chorgali	Limestone and Shale	Marine	2421.5	45.72
Eocene	Sakesar	Limestone	Marine	2467.2	135.63
Paleocene	Patala	Shale	Shallow marine to lagoon	2602.9	21.34
Paleocene	Lockhart	Limestone	Shallow marine	2624.2	35.05
Paleocene	Hangu	Sandstone	Shallow marine	2659.3	27.34
Early Permian	Sardhai	Clays	Lacustrine to shallow marine	2686.7	109.72
Early Permian	Warcha	Sandstone	Fluvial to lagoon	2796.4	143.73
Early Permian	Dandot	Sandstone	Shallow marine	2938.1	60.96
Early Permian	Tobra	Conglomerate	Glacial to Fluvial	2999.1	51.8
Early Cambrian	Khewra	Sandstone	Shallow marine	3050.9	78.33
Pre-Cambrian	Salt Range	Evaporates, marl	Marine hypersaline	3129.2	0.77

TRAP STRATIGRAPHY

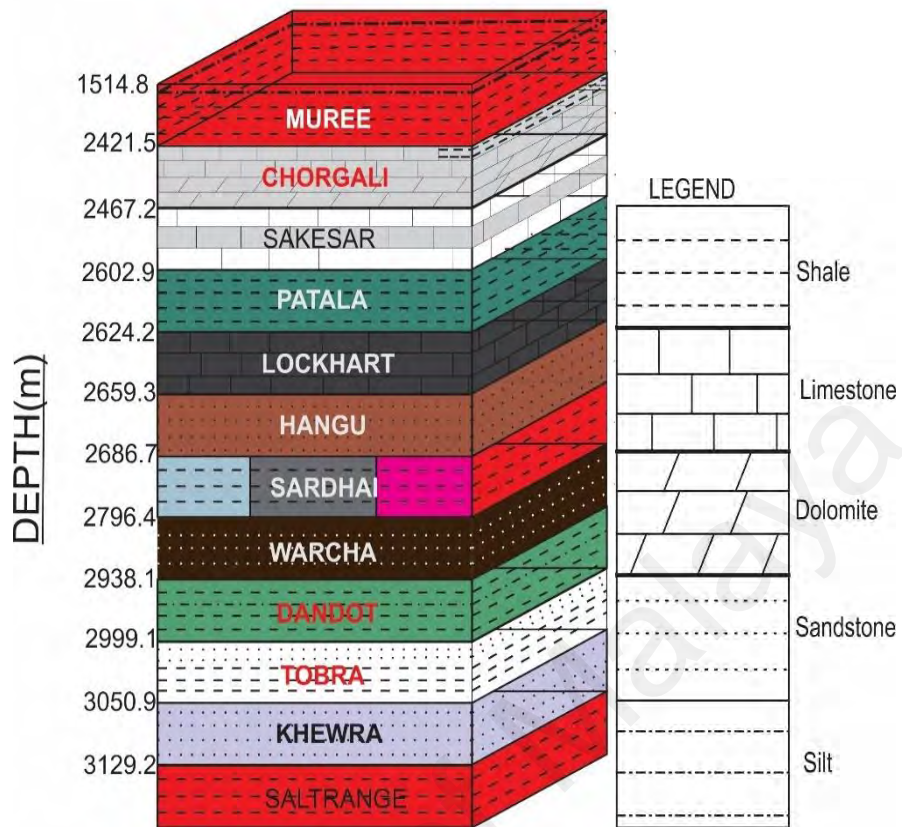


Figure 2.2: Stratigraphic column showing the trap stratigraphy of Balkassar-OXY-1 well.

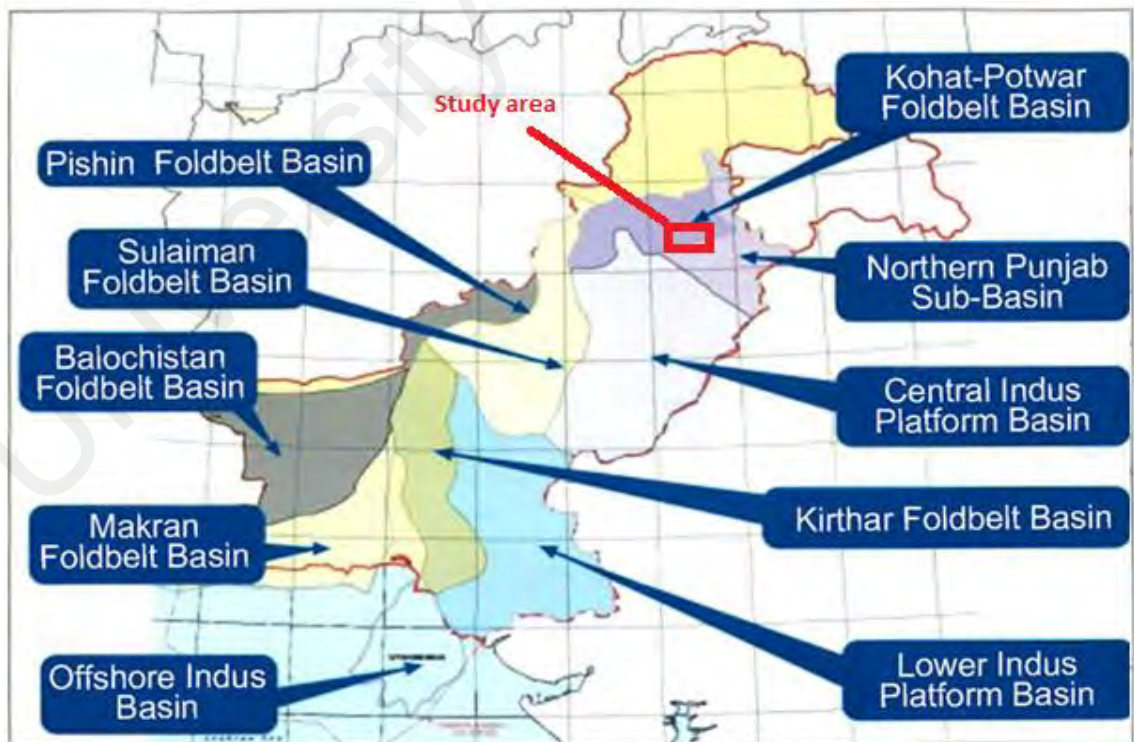


Figure 2.3: Sedimentary maps of Pakistan. Free image.

2.3 Structural Settings of the Basin

The Basin Kohat-Potwar consists of thrust faults and east-west trending folds (Khan et al., 1986). The basin is covered by Neogene Siwalik molasse which forms several large folds a number of which are faulted. These surface structures their size and orientation defines the structural zones within the Basin (Gee, 1989; Iqbal et., 2015; Shah & Abdullah 2016). Oil well data and the seismic reflections suggest that these zones reflect differences in lithostratigraphy and deeper structures.

The Potwar Basin is more or less classified by river Indus to the west and from east by river Jhelum, Salt Range in south and Kalachitta-Margalla hill ranges in north (Ashraf et al., 2016). The basin is predominantly covered by Siwalik sequence. Basin is more extensively deformed in the northern part and is characterized by east-west complex and tight folds that are overturned in the south direction and are sheared by steep angle faults (Ghazi et al., 2015; Iqbal et al., 2015; Kazmi & Jan, 1997). Several east-west gentle and broad folds are present in western part, whereas strike suddenly changes in eastern part towards northeast and the structures consist of broad synclines and anticlines are tightly folded (Pennock et al., 1989). The greater internal deformation at the base and the increased drag formed complicated structures (Lillie et at., 1987).

2.4 Hydrocarbon Potential

First commercial discovery was in the 1914 by Attock Oil Company, after that in 1935 there was a discovery in Dhulian, other discoveries followed with Balkassar in 1946 and 1981, Joya Mair in 1944, Tut in 1967 and in Karsal in 1956. the very first commercial gas discovery was in 1979 in Adhi (Jaswal et al., 1997; Quadri & Quadri, 1998).

In Potwar Basin potential source rocks mostly from the Paleocene age, and the production primarily comes from the faulted anticline traps which are from Cambrian to

Miocene. Source rocks in basin namely, Wargal Formation, Lockhart Formation and Patala Shale Formation (OGDC, 1996; Quadri & Quadri, 1996). The reservoir rocks of Potwar Basin includes Paleogene shelf carbonates, Miocene alluvial sandstones, Jurassic and Permian continental sandstones and alluvial and shoreface Cambrian sandstones (Iqbal & Shah, 1980; Shah, 1977). The oil and gas that has been explored and produced from various formations of Potwar Basin are: Permian Tobra, Wargal, Amb; Cambrian Khewra, Jutana, Kussak, Jurassic Dutta; Patala Shale, Khairabad, Lockhart, Nammal, Sakesar, Margalla Limestone, Chorgali, Bhadrar and Murree (Khan et al., 1986; Petroconsultants, 1996). The oilfields that have been so far discovered in the Potwar are either popup structures, faulted anticline or fault-block traps (Jadoon et al., 1997; Jadoon et al., 2015).

2.4.1 Source rocks

Source rocks in basin includes Lockhart Limestone, Hangu and Patala Shale formations (OGDC, 1996; Quadri & Quadri, 1996). Patala Shale Formation shallow marine shales have thickness in range from 15 to 180 thick and is the most probable predominant oil source in Potwar Basin (OGDCL, 1996; Wandrey et al., 200). In Potwar sub-Basin, the source rock are reported to be organic rich and the kerogen is mature (Fazeelat et al., 2010). In Balkassar area, the major source rock is Patala Shale whose age is Paleocene, whereas Lockhart and Hangu formations are also considered as source rock.

2.4.1.1 Hangu Formation

Hangu Formation has been assigned Early Paleocene age. The Hangu sandstone name was given to Paleocene sequence in the Kohat Basin (Kadri, 1995). The formation consists prominent bands of kaolinite occur in its upper part and laterite and lateritic sandstones. Hangu Formation dominantly contains thick bed, reddish brown and dark grey sandstone with few meters thick grey colored carbonaceous shale intercalations and

rarely conglomerates lenses (Maqsood & Ahmed, 2014). The sandstone in Hangu Formation is fine to medium grain, hard and compact to well sorted. The common depositional features are tabular and trough cross bedding (Shah, 2009). The Hangu Formation is 27 m thick in Balkassar Formation. Lockhart Limestone conformably overlies Hangu Formation.

2.4.1.2 Lockhart Formation

The Lockhart Formation overlies a fossiliferous sandstone at the top of Hangu Formation. The Lockhart limestone of Paleocene age is a cliff forming dark grey crystalline, nodular bubbly limestone. It consists of alternating beds of (marl) limy siltstone and medium beds of silty packstone containing larger foraminifers (Kadri, 1995). The formation has abundant corals, echinoid, foraminifers and algae (Cheema et al., 1977; Latif, 1970c; Raza, 1967; Shah, 2009). Its total organic content ranges between 0.5-2.5% (Fazeelat et al., 2010). The Lockhart Formation overlies the siltstones, carbonaceous shales and a coal bed of Hangu Formation. The limestone of Lockhart in Balkassar is 35 m thick and is well developed throughout Potwar.

2.4.1.3 Patala Shale Formation

Patala Formation age is Paleocene, consist of sandstone interbeds, shale and marl and limestone is medium bedded. Shale is dark greenish grey selenite-bearing (Cheema et al., 1977; Shah, 2009). The Patala shale is considered to be the major source rock, its total organic content ranges between 1-10% (Fazeelat et al., 2010). Patala Formation was deposited in deltaic and shallow marine environments accounting for combination of both marine organic and terrestrial material (Kadri, 1995). Patala Formation lower section sandstone directly overlies the Lockhart limestone (Shah, 2009). In Balkassar it is 21 m thick.

2.4.2 Reservoir rocks

In Balkassar area the oil and gas that was discovered from Sakesar and Chorgali formations (Khan et al., 1986; Petroconsultants, 1996). In Balkassar area, the oil and gas reservoirs were discovered in the fractured limestone of the Chorgali and Sakesar formations of Eocene age. The combined thickness of both Formations is (141.43-182.88m). The main oil horizon is in the top 50-100ft (15.24m-30.48m), which consists of interbedded turquoise shale, limestone and marl. The well logs show that the water resistivity (R_w) of this reservoir is 0.314-0.464 ohm/m (Shah, 1977). The Chorgali and Sakesar formations of Eocene age are the main producing hydrocarbon reservoirs in NPDZ and Central Potwar which include Dhurnal, Chak Naurang, Balkassar, Dakhani oil fields (Table. 2.2). The Jurassic age, Datta sandstone and Samana Suk limestone Formations are the main reservoirs in NPDZ which include Dhulian, Toot and Meyal oil fields (Mehmood et al., 2015). Tobra Conglomerate, Nilawhan sandstone and limestone of Zaluch Group are reservoirs in Adhi and Dhurnal oil fields (Iqbal and Shah, 1980). The Cambrian age, Khewra sandstone is a good reservoir of gas/condensate in Central Potwar that includes Adhi and Missa Keswal Gas fields (Kazmi and Jan, 1997; Shah, 2009).

Table 2.2: Oil and gas producing reservoirs formations found in Potwar.

Formations	Type of reservoir	Age
Murree	Alluvial sandstone	Miocene
Sakesar, Margalla Hill limestone, Chorgali	Carbonates, Shale	Eocene
Patala, Lockhart, Khairabad & Nammal	Carbonates	Paleogene
Warcha	Sandstones	Cretaceous
Datta	Continental sandstones	Jurassic
Amb, Wargal, Tobra	Sandstone	Permian
Khewra, Jutana, Kussak	Alluvial and sandstone	Cambrian

Note: Sandstone porosities observed in Potwar Basin ranges from <5% to 30% having an average of 12 to 16%.

2.4.2.1 Sakesar Limestone Formation

Its age Early Eocene has been assigned by Cheema et. al. (1977) on the basis of foraminifers. The Sakesar contains dominantly limestone and marl. The limestone has a reasonably consistent lithological character all over its distribution (Quadri, 1995). The Sakesar is richly fossiliferous with plentiful mollusks echinoids and foraminifers (Shah, 2009). The Sakesar Limestone Formation in Balkassar acts as a source rock, its thickness is 136 ms, The Sakesar Formation lower section directly overlies the Patala Formation. In Balkassar hydrocarbons have been produced from this Sakesar Formation in Balkassar well 7 (Iqbal et al., 2015; Shah & Abdullah, 2016; Shah & Abdullah, 2017; Zahid et al., 2014).

2.4.2.2 Chorgali Formation

Its age is Eocene and the formation is divisible into two units (Kadri, 1995). Formation's upper part contains shale with one bed of nodular argillaceous limestone near to the top and one thick dark grey limestone bed. However lower part contains medium to thin bedded light grey to white, fine to very finely crystalline dolomites with interbeds of grey to greenish grey calcareous shale (Shah, 2009). The measured Chorgali Formation thickness in Balkassar is 45 m (Ahsan et al., 2012; Khan et al., 1987). Chorgali Formation conformable overlies Sakesar Limestone and is overlain by Murree Formation from top in Balkassar (Shah, 2009).

2.4.3 Traps and seals

In Balkassar Murree Formation of Miocene age, which is 906 m thick, provides a very thick seal rock over Chorgali and Sakesar formation of Eocene age, and is well settled on all of these reservoirs which is not allowing hydrocarbons to escape from it (Table. 2.3) (Ahsan et al., 2013). Murree Formation is composed of dark red to maroon color siltstone

and clay interbeds and grey color Sandstone (Kadri, 1995; Shah, 2009). Where as in entire Potwar the Murree Formation thickness varies and its maximum thickness noted was 3,030 in Kashmir (Shah, 2009). The formation is poorly fossiliferous and is comprised of limited number of plant remains, fish, wood and remains of mammalian bones (Shah, 2009).

Table 2.3: Numerous seals and reservoir that are present in many fields of Potwar Basin.

Seal	Reservoir	Discovered Field
Dandot Formation	Lower Permian Tobra	Adhi
Hangu Formation	Wargal	Dhurnal
Hangu Formation	Datta	Meyal
Shinwari Formation	Datta	Meyal-2
Murree Formation	Sakesar Limestone	Balkassar-4
Murree Formation	Sakesar & Chorgali	Balkassar-1

2.4.4 Generation and Migration

In Potwar Basin generation and migration of hydrocarbon most probably begin in Late Cretaceous time for Cambrian through lower cretaceous source rock and again for younger rocks in Pliocene time (OGDC, 1996; Fazeelat et al., 2010). Whereas suggested by Wandrey et al. (2004) in Potwar Basin the hydrocarbons generation and migration begin at about 30 Ma and therefore indicates only one late and second period of generation which is from 15 Ma to 20 Ma and is still continued.

CHAPTER 3: REVIEW OF SOURCE ROCK CHARACTERISTICS, HYDROCARBON POTENTIALITIES AND GEOPHYSICAL INVESTIGATIONS.

3.1 Introduction

In this chapter, Paleocene to Eocene succession in the Balkassar Potwar Basin area of the upper Indus basin were subjected to source and reservoir rock characterization. The main emphasis of this study is to detect the entrapment style which possibly will add a new way of understanding Balkassar area petroleum system elements. The important features that characterize the source rock, maturity and quality of organic matter, reservoir rock properties as well as the types of traps will be presented.

3.2 Source rock characteristics

In petroleum exploration and production companies' geochemical analysis has become an increasingly important tool for rapid and inexpensive evaluation of large numbers of rock samples. In this study the critical factors which were performed are maturity, organic richness (quantity) and potential type of hydrocarbons. These briefly described in the following sub-sections.

3.2.1 Quantity of organic matter

TOC describes the quantity of organic carbon in a rock sample and contain both bitumen and kerogen (Peters & Cassa, 1994). A Potential source rock ought to contain adequate quantities of organic matter to be able to generate petroleum. According to Peters & Cassa (1994) there are minimum values of TOC % for sediments below which they are unable to produce oil/gas in terms of organic carbon (Table. 3.1). In an earlier study by Lewan (1984), he reported that the minimum TOC (wt. %) value which is required for expelling hydrocarbons ranges between 1.5 and 2 %, whereas 0.5% TOC for

gas to be expelled. >2% TOC content in a source rock is considered to be a good source rock potential.

Table 3.1: The geochemical parameters which describes the source rock petroleum potential.

Petroleum Potential	TOC (Wt. %)		S1 mg/g	S2 mg/g	Hydrocarbons (ppm)
	Shale	Carbonates			
Poor	0-0.5	<0.2	0-0.5	0-2.5	0-300
Fair	0.5-1	0.2-0.5	0.5-1	2.5-5	300-600
Good	1-2	0.5-1	1-2	5-10	600-1200
Very good	2-4	1-2	2-4	10-20	1200-2400
Excellent	>4	>2	>4	>20	>2400
Kerogen type and expelled products					
Kerogen	Hydrogen Index (HI)		S2/S3	Main product	
I	>600		>15	Oil	
II	300-600		10-15	Oil	
II/III	200-300		5-10	Oil/Gas	
III	50-200		1-5	Gas	
IV	<50		<1	Non	
Thermal Maturity					
Maturity		Maturation			
		Ro (%)		Tmax (°C)	
Immature		0.20-0.60		<435	
Mature	Early	0.60-0.65		435-445	
	Peak	0.65-0.90		445-450	
	Late	0.90-1.35		450-470	
	Postmature	>1.35		>470	

3.2.2 Rock-Eval pyrolysis

Pyrolysis is defined as the heating of organic matter in the absence of oxygen to yield organic compounds (Peters, 1986). For source rock evaluation and characterization, the first article was published by Espitalié et. al. (1977) on application and development of standard pyrolysis method. Subsequent Rock-Eval pyrolysis analyzers e.g. Rock-Eval 6, are introduced with new and improved functions since 1977. The Rock-Eval pyrolysis

methods are used to detect petroleum potential in rock samples and are used to identify the organic matter type and maturity (Peters et al., 1983; Peters, 1986). The technique which is widely performed operates at programmed heating temperature in the range of 300-550 °C with small amount of rock (about 100mg) are pyrolyzed, in the absence of oxygen to determine rock samples petroleum potential (Espitalié et al., 1977; Peters, 1986).

Tmax, S1, S2, S3, HI, OI and PI are the parameters which are generated by Rock-Eval pyrolysis (Fig. 3.1) (Tissot & Welte, 1984). All of these are used to evaluate the quality, quantity and maturity of organic matter. Hydrocarbons in free state are represented by S1 which represents milligrams of hydrocarbons that can be thermally distilled from one gram of the rock at 300 °C. During the temperature range of 300-500 °C the hydrocarbons are cracked from kerogen and are represented by S2. The S3 represents CO₂ that has been released by the sample during kerogen cracking and is measured by thermal conductivity detector (TCD) in which it is trapped during cracking and is measured in mg CO₂/g rock (Fig.3.1).

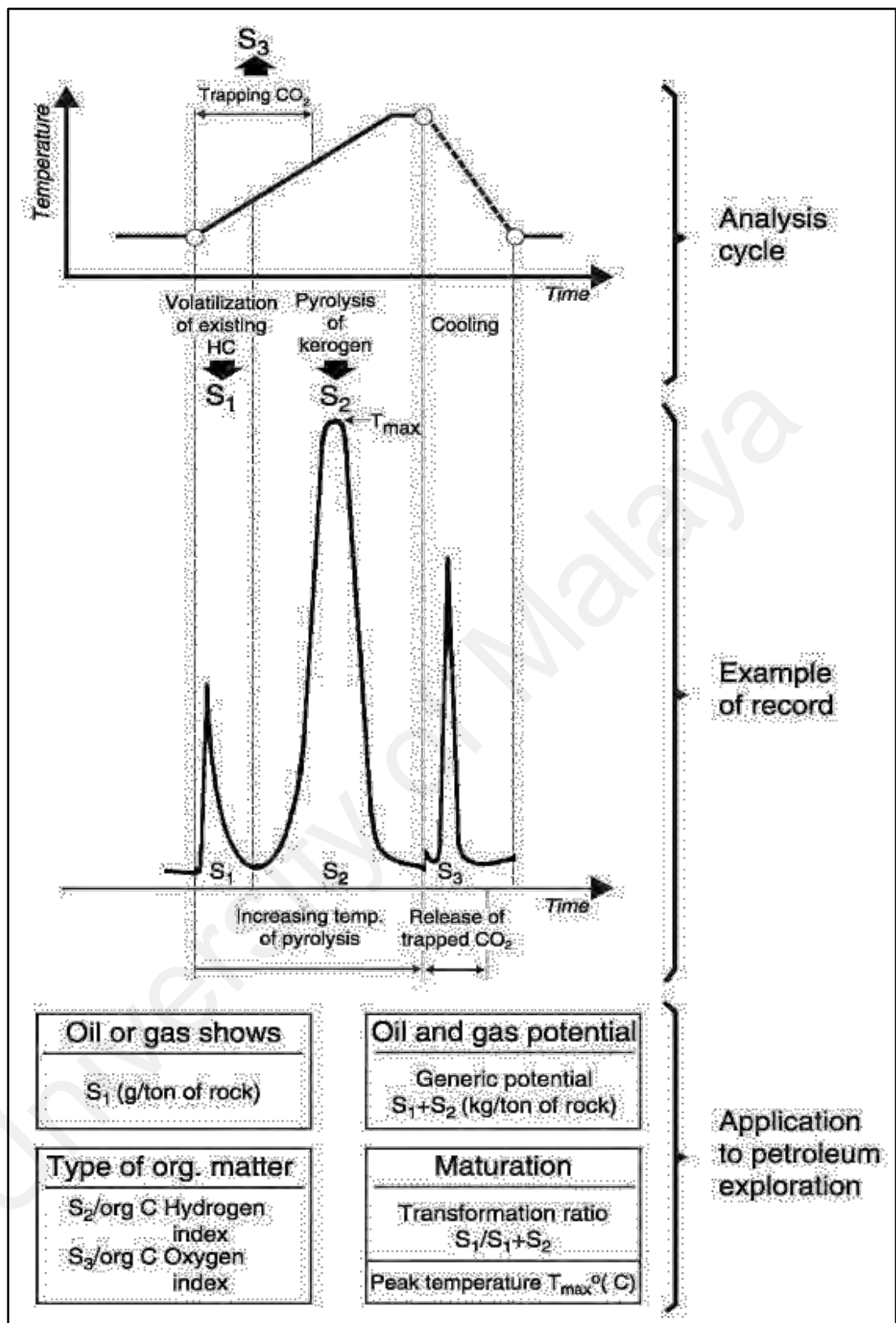


Figure 3.1: Schematic diagram of Rock-Eval program showing output of rock samples (evolution of CO_2 and hydrocarbons) during heating. T_{max} , S_1 , S_2 , and S_3 are the important measurements. Free image.

3.2.3 Type of organic matter

There are various methods that are used to identify the type, or quality of organic matter and to classify the type of kerogen and to evaluate the petroleum potential of rock samples (Peters, 1986). Kerogens are classified mainly into three types. Type-I highly oil prone, Type-II oil prone, Type-III gas prone. There is also Type-IV kerogen which is less studied (Tissot et al., 1974) (Fig. 3.2 and 3.3). By using the Van-Krevelen diagram or atomic H/C vs O/C, kerogen types can be distinguished (Stach et al., 1982; Van-Krevelen, 1961). From HI or the ratio of S₂/S₃ the type of hydrocarbon products that the source rock will generate can also be obtained (Peters, 1986). Rock-Eval pyrolysis technique can be used for both detection of petroleum potential and the identification of organic matter type in the rock samples (Peters, 1986).

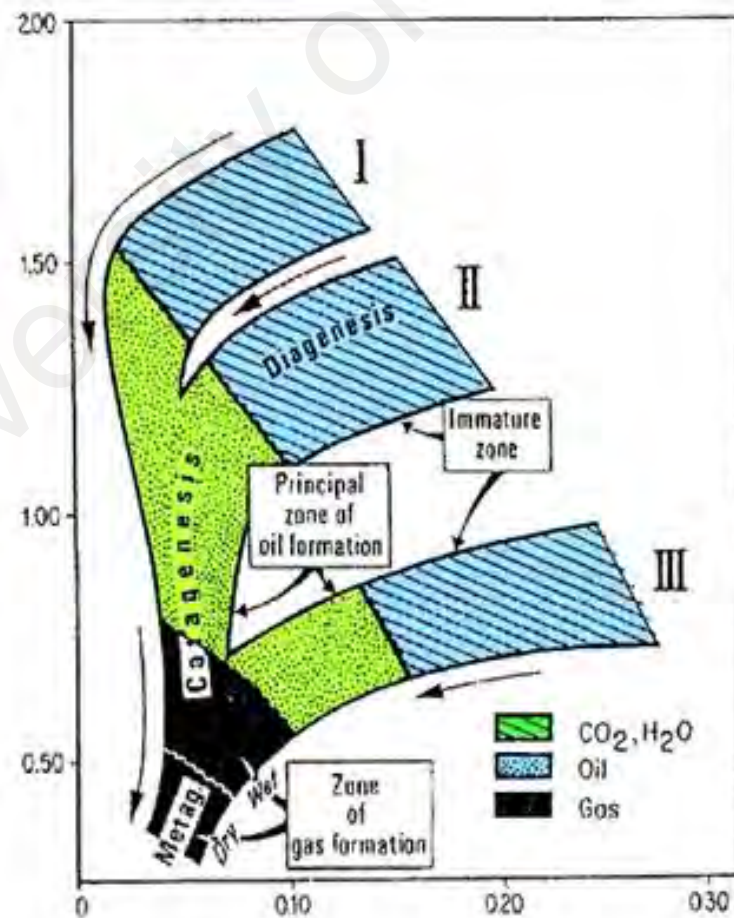


Figure 3.2: Plot of atomic H/C vs atomic O/C showing different types of kerogen and oil/gas generation zone. Free image.

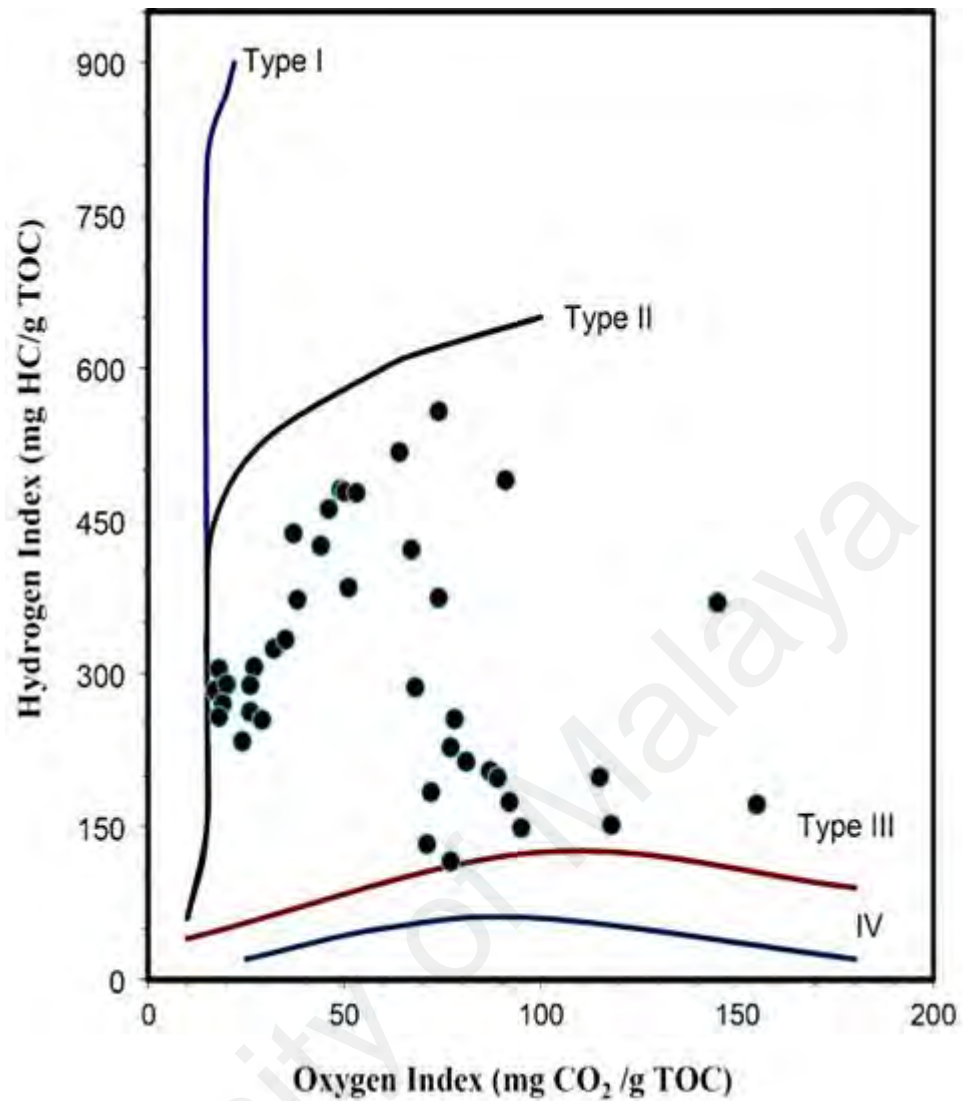


Figure 3.3: Kerogen types classification based on HI/OI plot. Free image.

3.2.3.1 Kerogen Type I

The relatively rare type of kerogen is Type-I (Tissot and Welte, 1984). Immature kerogen Type-I contains highly oil prone organic matter, it shows low O/C < 0.1 and high atomic H/C > 1.5, and it contains low sulfur contents (Stach et al., 1982). Rocks that are rich in organic matter type have been deposited in shallow water column under anoxic environmental condition. The main organic constituents being alga-derived that are mostly deposited in lacustrine settings. Type-I kerogen may also be dominated by amorphous liptinite macerals. Major hydrocarbon components of Type-I kerogen are long

chain n-alkanes, as compare to other kerogen types, NSO and aromatic compounds are less (Peters & Cassa, 1994; Durand, 1980).

3.2.3.2 Kerogen Type II

Type-II kerogen is derived from mixed organic matter (marine and terrigenous) that has been deposited under marine depositional conditions (Dembicki, 2009). It has the potential to produce both oil and gas. The sources of kerogen Type-II are liptinitic macerals such as plant resins, spores, and pollens (Fisher & Miles, 1983). The immature Type-II kerogen is highly oil prone and has high HI values 300-600 mg HC/g TOC (Peters et al., 2005b). Sulphur is high as compare to other types of kerogens (Baskin & Peters, 1992; Lewan, 1984; Orr, 1974 Peters et al., 1990). As shown in Fig. 3.2 at immature stage it shows higher atomic O/C but lower atomic H/C (1.2-1.5) when compared to Type-I kerogen, this type is also dominated by liptinite macerals.

3.2.3.3 Kerogen Type III

Kerogen is mainly gas prone although small amount of oil can be expected during maturation (Hunt, 1996). It shows high atomic O/I < 0.3 and low atomic H/C < 1.0 It has ketone, carboxylic acid and polyaromatic nuclei groups, with small quantity of aliphatic compounds (Peters & Cassa, 1994; Stach et al., 1982).

3.2.3.4 Kerogen Type IV

Type-IV kerogen is dead carbon which shows low to high atomic O/C < 0.3 and very low 0.5-0.6 atomic H/C. This type of kerogen is dominated by inertinite macerals that generate no or very little hydrocarbons during maturation stage (Peters and Cassa, 1994; Stach et al., 1982).

3.2.4 Thermal maturity

In addition to the type and quantity of the organic matter, the level of thermal maturity of organic matter is also an essential part for evaluation of the source rock potential. The extent of temperature driven reactions are described by thermal maturity, in which sedimentary organic matter is converted into petroleum (Peters & Moldowan, 1993). The biological material (plant debris and bacterial) in sediments are converted by early diagenetic processes into kerogen and bitumen. Afterwards thermal processes convert fragment of this kerogen and bitumen into hydrocarbons and finally into gas (Tissot & Welte, 1984).

Various parameters are used for the evaluation of thermal maturity degree of organic matter. The widely used indicator of thermal maturity is vitrinite reflectance (%Ro), and this indicator is extensively used in petroleum studies (Copard et al., 2002; Suggate, 1998).

The values of vitrinite reflectance between 0.5% Ro and 1.3% Ro shows that the samples are within oil generation window, the values that are less than 0.5% are considered as thermally immature, and the values that are more than 1.3% Ro are considered to be in gas window maturity (Tissot & Welte, 1984). There are various limitations of this method that are related to recycled vitrinite practices, mud additives and cavings (Hunt, 1995). The vitrinite reflectance values were reported to be lower at about 0.4 %Ro for top oil window in coaly sediments dominated by Type II higher plant kerogen, such as resinite, suberinite and bituminite (Abdullah, 1997). The vitrinite reflectance and Tmax values are known to be suppressed in sequences that are rich in liptinite.

The Tmax parameters for the Rock-Eval pyrolysis can also be used for thermal maturity (Behar et al., 1997). During Rock-Eval pyrolysis the Tmax is the temperature at which the maximum amount of S2 hydrocarbons are produced. The Tmax values that ranges from 430 °C to 465 °C shows top oil window to gas window. According to Espitalié (1986), the beginning of oil window can start from 430 °C to 435 °C Tmax and the values of vitrinite reflectance will be in range of 0.5%Ro to 0.6% for Type I and II kerogen.

3.2.5 Petroleum trap

A rock unit in the subsurface that blocks the movement of hydrocarbons and cause it to be preserved in the reservoir is a petroleum trap (Gluyas & Swarbrick, 2013; Van der Pluijm, 2004). The oil in the petroleum trap is always accompanied by water and natural gas, all these are confined in the porous and permeable reservoir rock unit, usually composed of sedimentary rocks such as sandstone, fissured limestone, dolomites and arkoses. Being the lightest from all the natural gas occupy the top of trap underlain by oil and then by water. A layer present at the top of reservoir rock unit that is impermeable and prevents the upward movement or escape of hydrocarbons is cap rock, that part of the trap which occupies the oil and gas in it is known as petroleum reservoir (Hunt, 1979, Russel, 1955).

There are many petroleum traps classifications but one simple system divides them into four types:

- Structural traps
- Stratigraphic traps
- Combination traps and
- Hydrodynamic traps

In this study only structural and combination traps are discussed.

It is the structural or stratigraphic feature that ensures the juxtaposition of reservoir and seals, such that hydrocarbons reserves remain trapped in the subsurface instead of escaping (Davis et al., 1996). The common types are Structural, Stratigraphic, hydrodynamic and Combination Traps. (Levorsen & Berry, 1967).

3.2.5.1 Combination traps

Numerous oil and gas fields around the globe are not due to the result of stratigraphic, structural, or hydrodynamic flow but are due to the combination of two or more forces. Such kind of traps maybe named as combination traps, maximum of them are the result of stratigraphic and structure processes (Fig. 3.4).

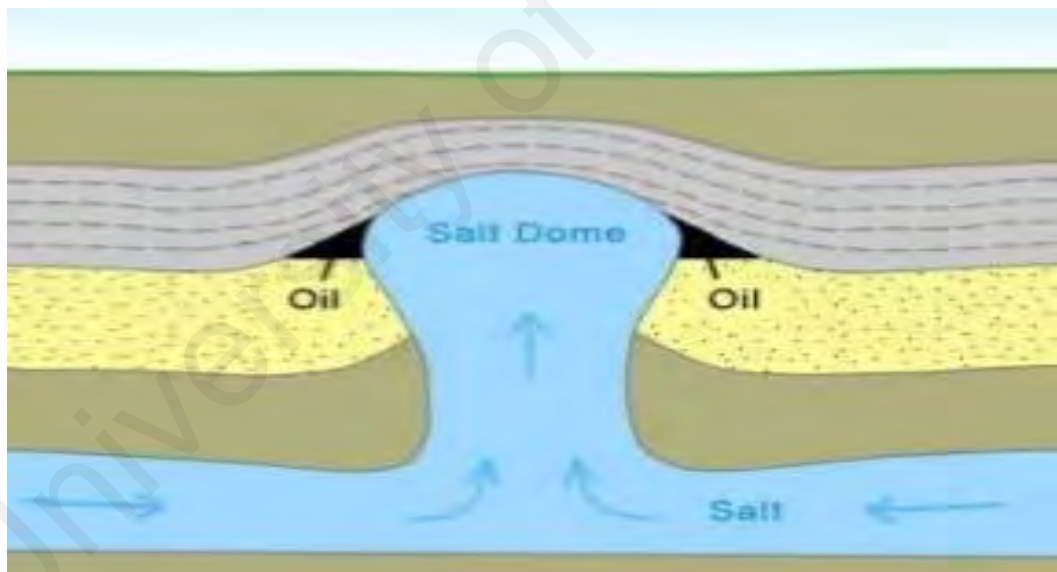


Figure 3.4: Shows an example of combination type stratigraphic trap. Free image.

3.2.5.2 Structural traps

A structural trap is a geological trap that is formed as a result of changes in the subsurface structure, due to diapiric, gravitational and compressional processes and tectonic activity (Gluyas & Swarbrick, 2013). These kind of changes in the subsurface

results in the blockage of hydrocarbons which can lead to the generation of hydrocarbons and can form petroleum reservoir. Structural traps are the most important type of traps around the globe because majority of the oil discovered in the world are from structural type traps (Allen & Alleen, 2013). There are three basic types of structural traps (Gluvas & Swarbrick, 2004; Hunt, 1979).

- Anticline trap
- Fault trap
- Salt Dome trap

Anticline trap

An area in the subsurface where the strata has been bent into a dome/arch and was previously flat is anticline. If there is an impermeable rock present in the dome and oil that can move and accumulate at the crest of an arch/dome and gets trapped there is known as anticline traps (Fig. 3.5) (Sheriff & Geldart, 1995). These kind of traps are most significant type of traps for exploration companies. Anticline traps are commonly very long and have oval domes of land which can be seen by only looking at a seismic sections/ geological maps (Allen & Allen, 1990).

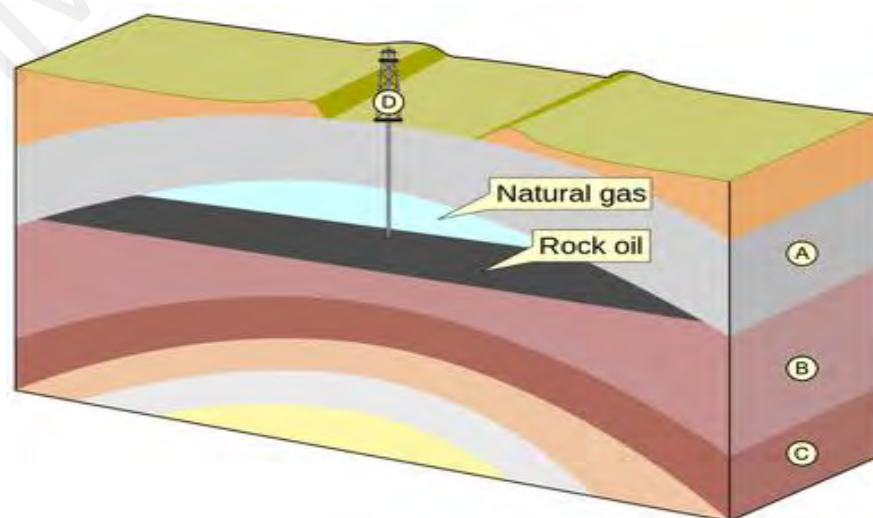


Figure 3.5: Anticline trap type example. Free image.

Compressional traps

Anticlinal, or fold, traps may be subdivided into two classes:

a) Compressional anticline

The anticlines that are formed at convergent plate boundaries due to the compressive stresses are known as compressional anticlines (Fig. 3.6) (Davis et al., 1996; Tarbuck et al., 2005). Such fields are found adjacent to mountain chains in many parts of the world. One of the best example of such trap with production from compressional anticlines is in Iran.

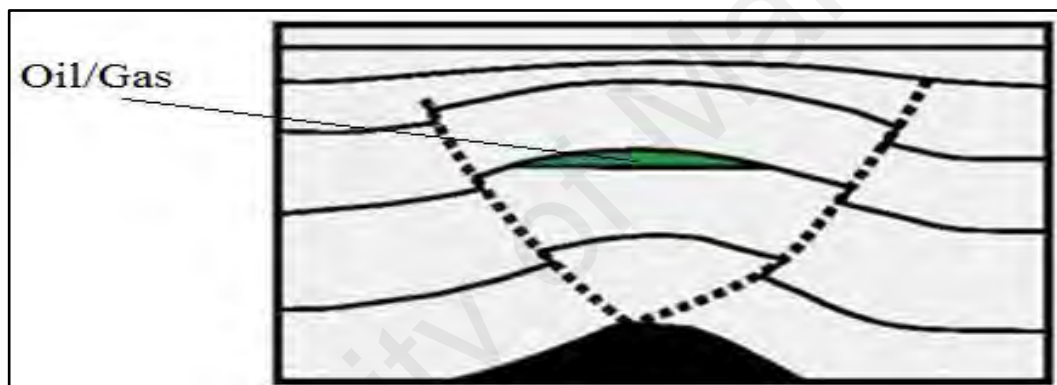


Figure 3.6: Compressional trap type example. Free image.

3.2.5.3 Salt Dome traps

When masses of salt are forced and pushed upwards through clastic rocks due to their greater buoyancy, and ultimately breaking through and rising towards the surface, a dome like structure is formed, known as salt dome trap (Fig. 3.7). These salts are impermeable and when they cross a layer of impermeable rock unit in which hydrocarbons are migrating, salts block the path ways as same as fault trap (Gluyas and Swarbrick, 2004).

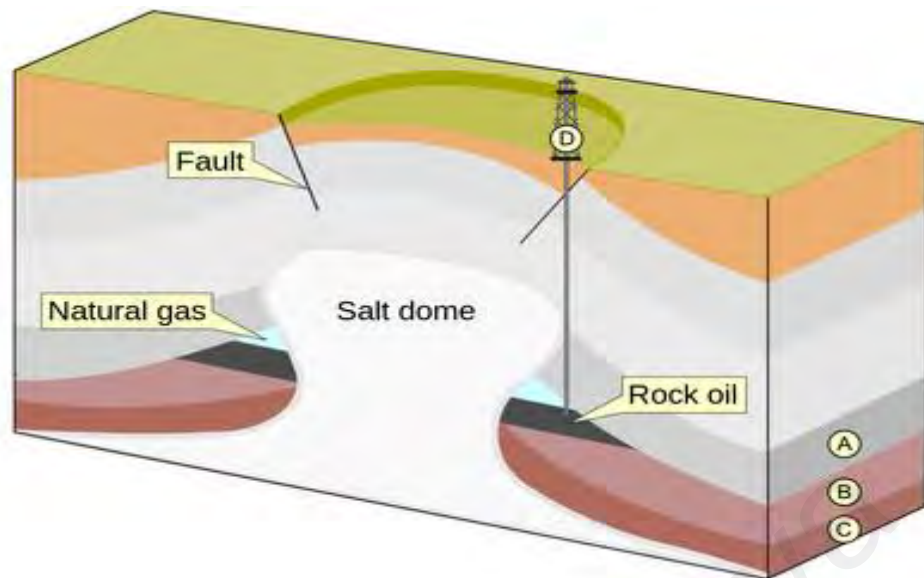


Figure 3.7: An example of salt dome trap type. Free image.

The Balkassar anticline structure is a salt-cored, where diapirism process has taken place. Diapirism are processes involved when a formation is under sufficient stress to flow, break and pierce through overlying strata which is of lower viscosity and higher density, whereby it can be or may not be associated with regional deformation (Dixon, 1975; Brun, 1983; Koyi, 1998). Salt diapirs are also called salt domes. Salt domes exists in many places like Germany and Persian Gulf. Salt bodies contains varying amount of evaporites with anhydrite and hydrated form gypsum. Salts and evaporites are sedimentary rocks that play very important role in deformation (Koyi, 1998).

Salts have properties different from other rocks i.e. they have low equivalent viscosity, low and depth independent density of 2.15 to 2.2 g/cm and also depends on its composition, they easily become mobile and ductile, their movement is aided if temperature increases or small amount of water is present, and they are relatively incompressible (Al-Fahmi et al, 2014; Krzywiec, 2010).

For the process of diapirism to be triggered, three conditions are very necessary to exist (Alsop, 2012; Archer, 2012; Hudec & Jackson, 2007), first is density inversion that occurs below critical depth, the depth below which evaporites become less dense than

overburden, below this level the system becomes unstable gravitationally, and the evaporites become buoyant and rise if the overburden is overcome. Secondly when salt thickness is more than 300 m it begins to react as viscous fluid when the overburden reaches to a thickness of more than 1000 to 1500 m, this is the depth at which other sediments become denser than salt. At a depth of 1 to 3 km due to low strength of salt, they start to flow under low differential stresses (Al-Fahmi, 2014; Archer, 2012; Schultz-Ela, 1993;).

Third and the very important condition to initiate diapirism process is the disturbance required to initiate the process, the initial impulse is oftenly caused by tectonic event i.e. faulting and folding or plate movement. For example, in the study area of Balkassar, folding, faulting and plate movement all can be observed (Archer, 2012; Schultz-Ela, 1993). If the above strata on salt layer are perfectly horizontal uniform and regular and also no unstable gravitational force can be observed. However, any lateral variation in the thickness present in overlying strata can lead to differences in the pressure over salt layer which will trigger the salt and it will flow towards those areas which pressure is low in the above strata. This differential in pressure ultimately leads the salts to flow through the strata towards the surface (Vendeville, 2002).

Various analogue and numerical experiments have suggested that salt diapirs vary in position and shape as a function of depth and its flux rate and time (Alsop, 2012; Archer, 2012; Vendeville, 2002; Hudec & Jackson; 2007) (Fig. 3.8, 3.9, 3.10 and 3.11). The shape and position of salt structures depends on overburden i.e. how it deforms.



Figure 3.8: Different terminologies and structures in salt systems. Free Image

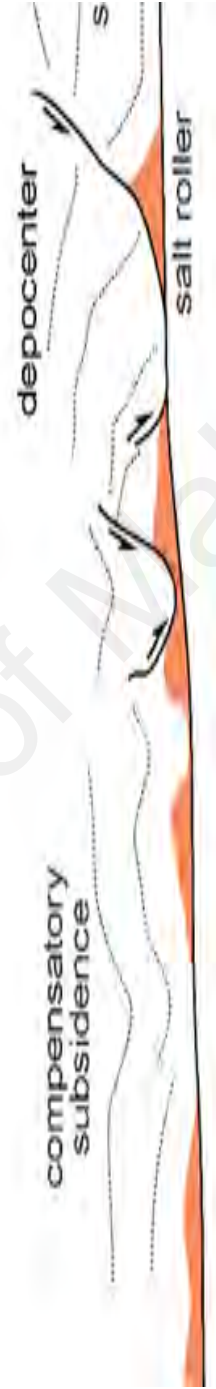


Figure 3.8: Different terminologies and structures in salt systems. Free image.

There are variety of salt structure shapes which depends on upward movement of salt (stages of development of salt-cored structure), the rising salt part may detach from the low density source (Edgell, 1991; Edgell, 1996) (Fig. 3.16 and 3.17). The diameter of salt domes can be of few kilometers and the sides of the salt dome are very steeply dipping which can extend downward for numerous kilometers that forms a relatively narrow neck that displays a tight folding. In extensional systems the diapirs rise up fracture zones, and takes up advantage of the spaced that has been created by the separation and thinning (Krzywiec, 2010).

3.2.6 Salt structures movement and development stages

There are various stages of salt movement, the model that has been adopted in this study is the Trushelm's Original Model, who has developed the salt movement model after studying 200 salt structures of northern Germany. Trushelm summarized the main characteristics of the structures and used a synthetic cross section of diapirs and associated depocenters (Al-Fahmi, 2014; Krzywiec, 2010; Vendeville, 2002). The model consists of four stages (Fig. 3.10):

1. Initial stage
2. Pillow stage
3. Diapir stage
4. Postdiapir stage (present day stage)

These stages have been divided into three groups according to the movement of salts:

1. Pre-kinematic
2. Active diapirism
3. Passive Diapirism

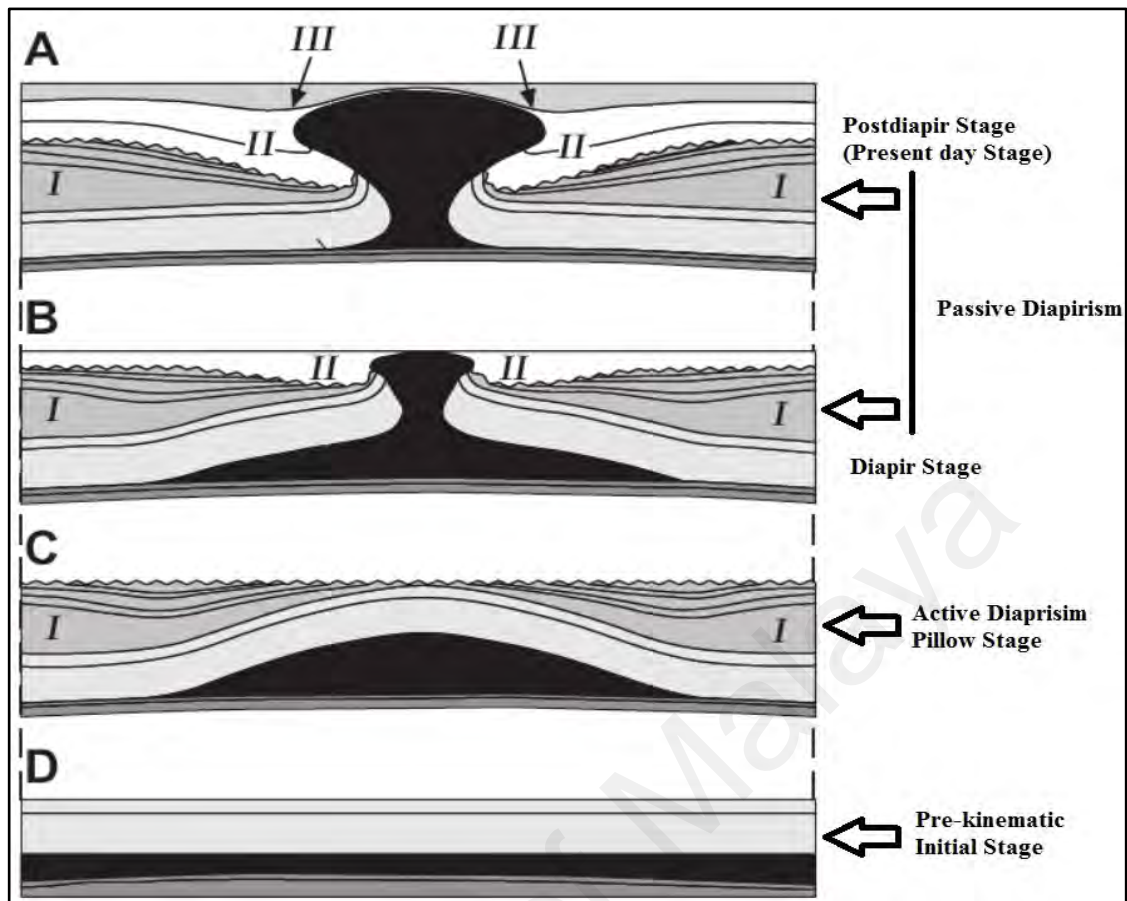


Figure 3.9: Development stages of salt diapir systems. Free image.

In Figure 3.18 D: is the initial stage of salt before movement, C: is the pillow stage displaying the strata I in the primary peripheral sink which is thinning towards the diapir, B: is the diapir stage displaying strata II to be thickening towards the diapir, A: is the Postdiapir stage displaying strata III to be thinning above diapir.

At the initial stage there is no movement of salts, when the movement is triggered by any tectonic event i.e. (folding, faulting, plate movement or pressure differential) the salts create pillow structures, the overburden is moved upward, and the movement of salt upward creates depo-centers (mini-basins) on sides of salt structures, and these are called primary rim synclines (Figure 3.10 C). The thickness of the sediments deposited in the depo-centers decreases towards salt pillow. Due to the differential loading of overburden the salt continues moving upward from the salt source layer towards the diapir and now this movement of diapir stage forms second rim synclines which are filled by growth

strata. If the source salt layer stops salt supply or the diapir is no more connected with source layer then the salt movement will stop and due to lack of supply of salt from source layer the diapir will be buried and covered by sediments. If the source salt layer continues to supply salt than third generation of rim synclines will be developed.

Shape and salt structure types depends on various factors such as thickness of source salt layer, sedimentation rate, erosion rate, tectonic regime and overburden properties. The general ideas on which the salt structure shape depends on, are sedimentation rate and salt supply rate (Fig. 3.11) (Giles et al., 2002; McGuinness et al., 1993).

1. When sedimentation rate is less than salt supply rate, than the diapir has a widening shape and the overturned beds have a dip greater than 90° .
2. When sedimentation rate is similar as salt supply rate than salt structure develop with vertical flank with a dip of 90° .
3. When the sedimentation rate is higher than salt supply rate than the dip of salt sediment is less than 90° .

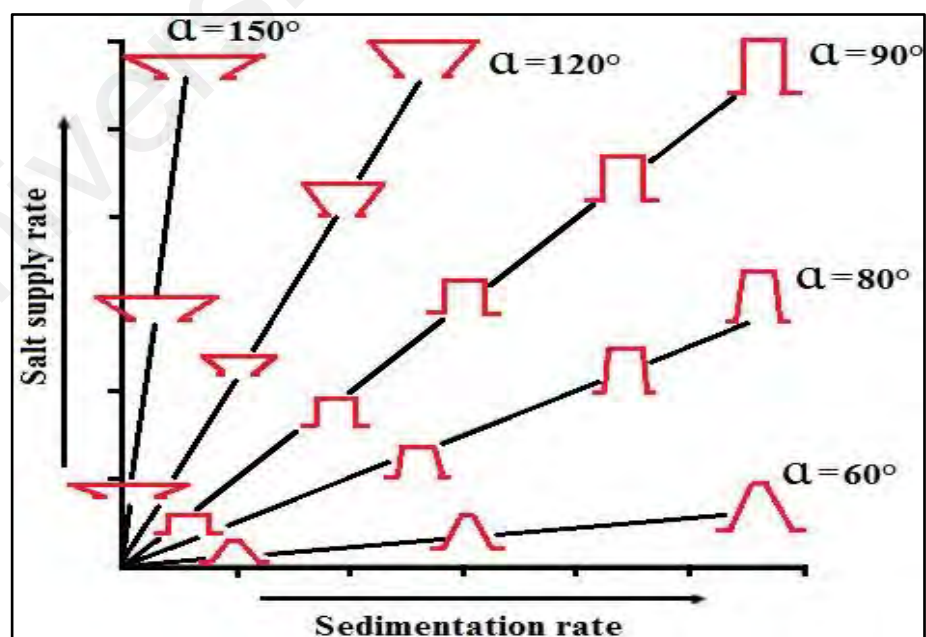


Figure 3.10: Salt growth rate and sedimentation rate relationship. Free image.

3.3 Geophysical well logs analysis.

The procedure of making a detail record of geological formation is called well logging (Asquith & Krygowski, 2004). It is done when the drilling equipment's are more in borehole, it is a very powerful tool for physical measurements of rock properties and are measured by lowering the instruments into the borehole that are drilled for oil/gas exploration (Telford et al., 1990). The wireline logging is done by tool attached at the end of wireline and lowered into the borehole and different sensors attached to it records formation properties. Now a day well log is very important and is performed in almost every exploration and development of wells because well logs have proved so successful to provide a more accurate information of reserves evaluation.

Well logs are implemented when the drilling activity has been stopped. Well logging methods includes numerous active methods and mechanical methods and also includes several nuclear, acoustic logging, thermal and measurement of magnetic properties (Telford et al., 1990). For petroleum exploration the main emphasis will be on logging because this is the main and major application of well logging (Pickett, 1970; Telford et al., 1990). The very first time well logging was run by Schlumberger brothers in 1927 in France Pechelbronoil field and they measured resistivity (Segesman, 1980; Snyder & Fleming, 1985; Telford et al., 1990). With the passage of time, well logging received much more attention and updates and in 1932 two types of well logging resistivity and spontaneous potential were in use. Archie introduced empirical equations in 1942 relating resistivity measurements to water saturation and porosity. The main aim of well logging is to measure the properties of rocks, identifying the potential reservoir, determining their porosity, permeability and the fluids that they contain (Telford et al., 1990). The very first step in petrophysical analysis is determination of lithological content before further proceeding to reservoir properties (Lashin et al., 2016).

There are three general types of well logs:

1. Electrical e.g.
 - Spontaneous Potential
 - Resistivity
2. Nuclear e.g.
 - Gamma Ray
 - Density
 - Neutron
3. Acoustic/Sonic e.g.
 - Transit time

There are two general types of log measurements

1. Active Measurements
2. Passive Measurements

Gamma Ray logs and Spontaneous Potential logs measures the natural potential in rocks, no artificial currents are applied, whereas in resistivity logs artificial current is applied to measure the resistivity.

To identify thickness and depth of productive zone and to differentiate between water, oil and gas in reservoir and the estimation of hydrocarbon reserves well logs are used (Asquith and Krygowski, 2004). There are various types of well logs, in this study, the used logs are Spontaneous Potential (SP), Sonic log (DT), Gamma ray log (GR), Density log (RHOB), Neutron porosity (NPHI) and Deep Laterolog (LLD).

3.3.1 Gamma ray (GR)

Gamma ray log is used to identify lithologies, it is measured in API units (Asquith et al., 2004). This log is very useful in differentiating between shales and sands. In shaley rocks normally radioactive elements are concentrated, because of which shale and clay bearing rocks have high readings of gamma ray log whereas the carbonates and sandstones that are clay free are very weakly radioactive and shows low readings of GR (Fig. 3.12). Radioactivity of sandy shale is low compare to the shales which have high radioactivity therefore it is trusting to differentiate between these stratigraphic units from other rocks (Selley, 1996). Volume of shale can be calculated using gamma ray log (Larionov, 1969; Lashin et al., 2016) In this study, Gamma Ray log is used for calculating shale volume by using the following equation (Schlumberger, 1972).

$$GR = \frac{GR_{log} - GR_{min}}{GR_{max} - GR_{min}}$$

Whereas:

GR_{log} = Gamma ray log reading of target zone

GR_{max} = Gamma ray log reading maximum against shale zone

GR_{min} = Gamma ray log reading minimum against clean zone

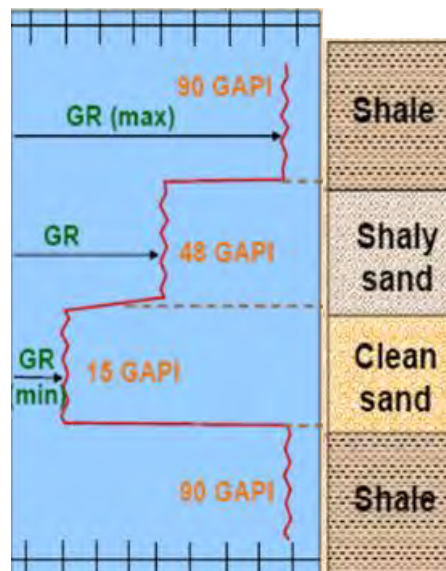


Figure 3.11: Showing the GR_{max} , GR_{min} and GR_{log} reading of interested zone in the center. Free image.

After calculating from log and equation the value obtained are used in another formula to get shale volume (Charts, 1983).

For younger rocks i.e. rocks of Tertiary age:

$$V_{sh} = 0.083[2^{(3.7 \cdot IGR)} - 1.0]$$

For older rocks i.e. rocks of Paleozoic and Mesozoic age:

$$V_{sh} = 0.033[2^{(2 \cdot IGR)} - 1.0]$$

In this study the first formula for rocks of tertiary age was used.

3.3.2 Spontaneous potential (SP)

In the petroleum industry the very first earlier measurements that were recorded was spontaneous potential log (SP), which has played very important role in log interpretation.

The SP log was first discovered in 1928 by Schlumberger (Serra, 1983). Now a day's

most of the wells have this log. Spontaneous potential logs are primarily used for gross lithology to differentiate between permeable and non-permeable zones (Asquith and Krygowski, 2003).

Spontaneous potential log measure natural potential difference between an electrode placed at the surface and electrode placed in the well (Fig. 3.13), in spontaneous potential no artificial currents are used. It is measured in millivolts of electric voltages arising from electrochemical factors within adjacent rocks and borehole creates the spontaneous potential log (Asquith & Krygowski, 2003; Serra, 1983) (Fig. 3.14). The electrochemical factors are brought by differences in the salinities' between formation water and mud filtrate within permeable beds. The potential varies from formation to formation, usually within range of few millivolts to hundred millivolts, measured relative to the level of shales (Serra, 1983).

Conductive fluids are necessary for SP log in borehole to generate these voltages. SP log cannot be used in the nonconductive fluids that is oil-base drilling muds or in air-filled holes. When mud filtrate from the drilling mud is forced into the formation under the differential pressure between formation and the mud column electrokinetic potential appears, when the filtrate flow takes place, electrokinetic potential is generated: 1) In front of permeable formation across mud-cake, 2) across permeable formation, 3) across shale bed (Serra, 1983).

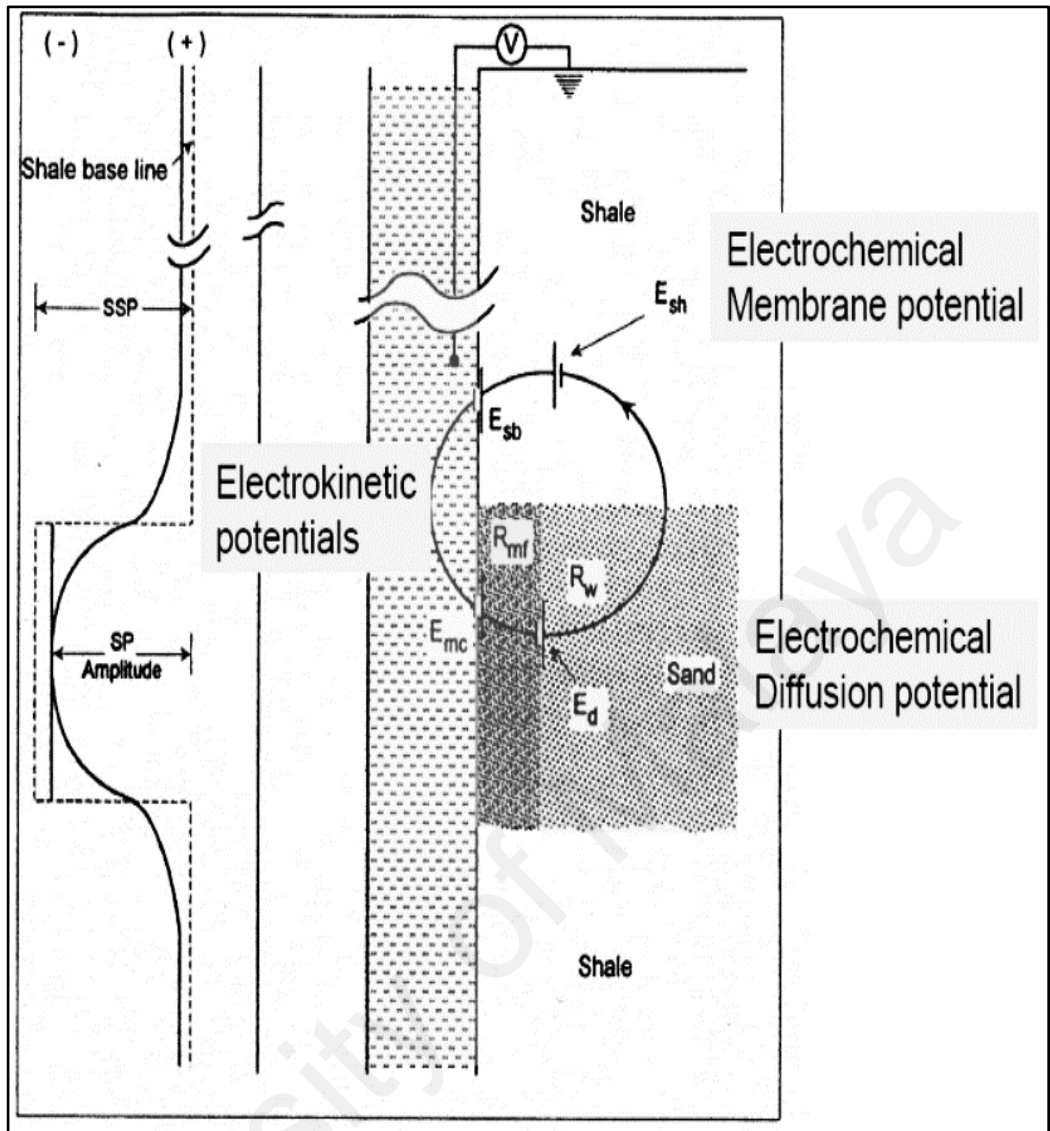


Figure 3.12: Origin of SP curve. Free image.

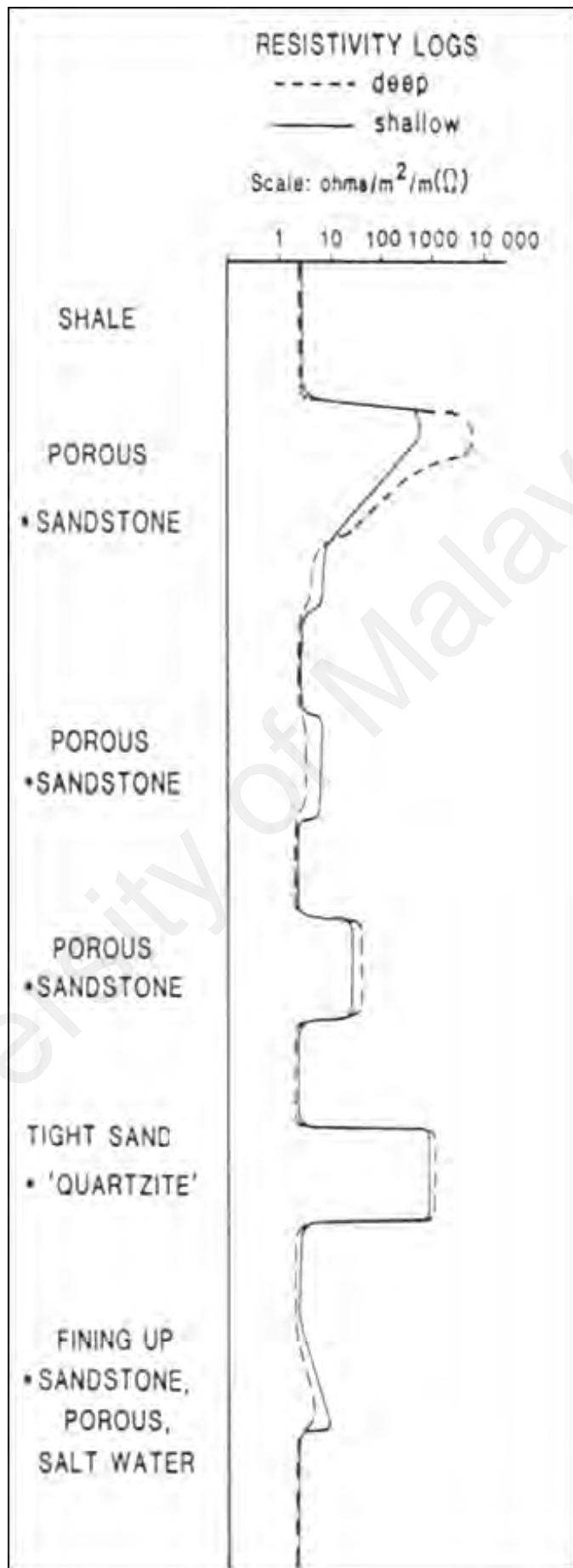


Figure 3.13: Idealized SP log. Free image.

Table 3.2: SP log principal uses

	Knowing	Used for
Quantitative	Static SP and shale line	Shale volume
	Formation temperature and Mud filtrate resistivity	Formation water resistivity
Qualitative	Grain/Clay sizes relations	Shaliness
	Shale line	Permeability indicator
		Correlation

3.3.3 Density log

Variations in the density of lithologic column that is cut by the borehole and the continuous record of these variations in the density is density log (Fig 3.15 and 3.16). The main and significant use of this log is to measure the porosity of the formation. It is also very useful in identifying the gas-bearing formations. The term density is used for gross density of formation. In porous rocks it also includes the fluids density present in the pore spaces of the formation and the grain density of rock itself. There is evidence of a relation between the fluids present in rock pores and porosity of the rock which contributes to the bulk density.

To measure porosity from density log this relation is the base of density log (Asquith and Krygowski, 2003; Serra, 1983; Rider, 1986). For measuring formation bulk density a beam of gamma ray is bombarded on the rock. At a very fixed distance, a counting system detects the changes in the intensity of bombarded gamma rays beams from the source, resulting from the changes in the formation density.

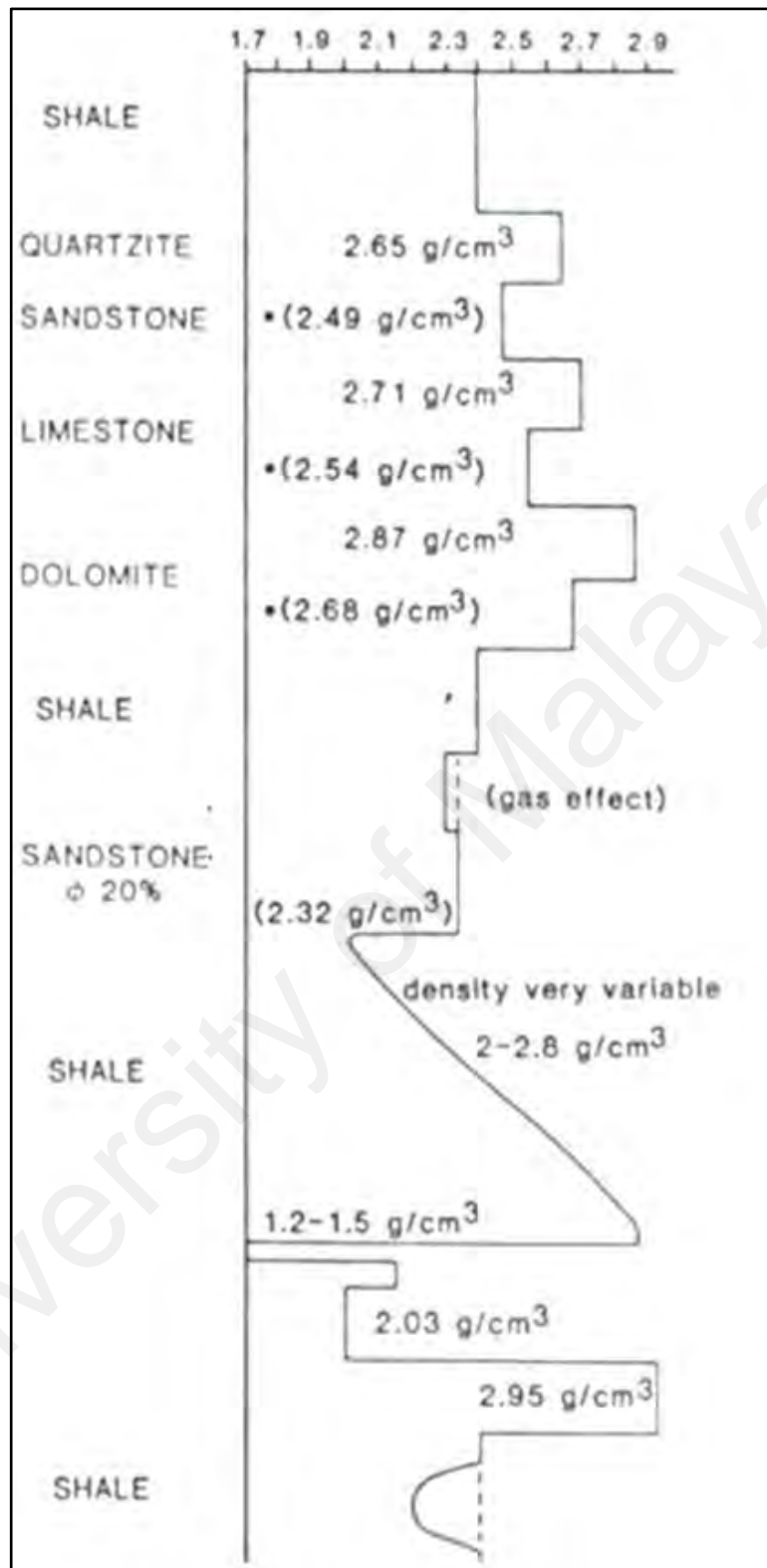


Figure 3.14: Idealized Density log. Free image.

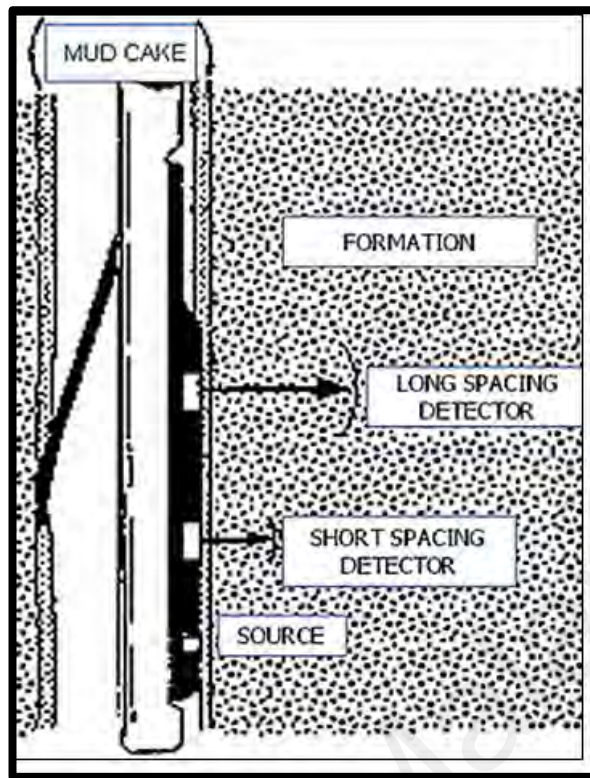


Figure 3.15: Density log recording equipment source and receiver/detector in well. Free image.

Table 3.3: Values of common lithologies/fluids densities.

Lithologies	ρ_{ma} or ρ_{fl} g/cm^3 [kg/m^3]	ρ_e (b/e)
Limestone	2.710 (2710)	5.08
Sandstone	2.644 (2644)	1.81
Dolomite	2.877 (2877)	3.14
Salt	2.040 (2040)	4.65
Anhydrite	2.960 (2960)	5.05
Fluids		
Salt water	1.15 (1150)	-
Fresh water	1.0 (1000)	-
Barite (mud additive)	-	267

3.3.4 Sonic log (DT)

Sonic log also known as acoustic log. Sonic log measures the travel time of elastic wave through formation. This log was originally designed as an aid in the interpretation of seismic data, but it was found very effective in porosity determination, and this made it a standard wireline tool for the porosity estimation. The information recorded can also be used to derive the velocities of elastic waves through the formation. The main and significant use of this log is to calculate the porosity of a formation (Serra, 1983). Sonic log is also very effective for correlation when used with Gamma Ray log.

In Sonic log the device measures the transit time of as sonic impulse through required length of rock, mostly 3 ft to 5 ft (Fig 3.17). The propagation rate of compressional waves through rock depends on rock matrix elastic properties and fluids it contain (Asquith and Krygowski, 2003).

Sonic log important uses are:

- Porosity determination
- Creating synthetic seismograms
- Stratigraphic correlation
- Lithologies identification
- Shaliness recognition
- Fracture identification
- Source rock identification

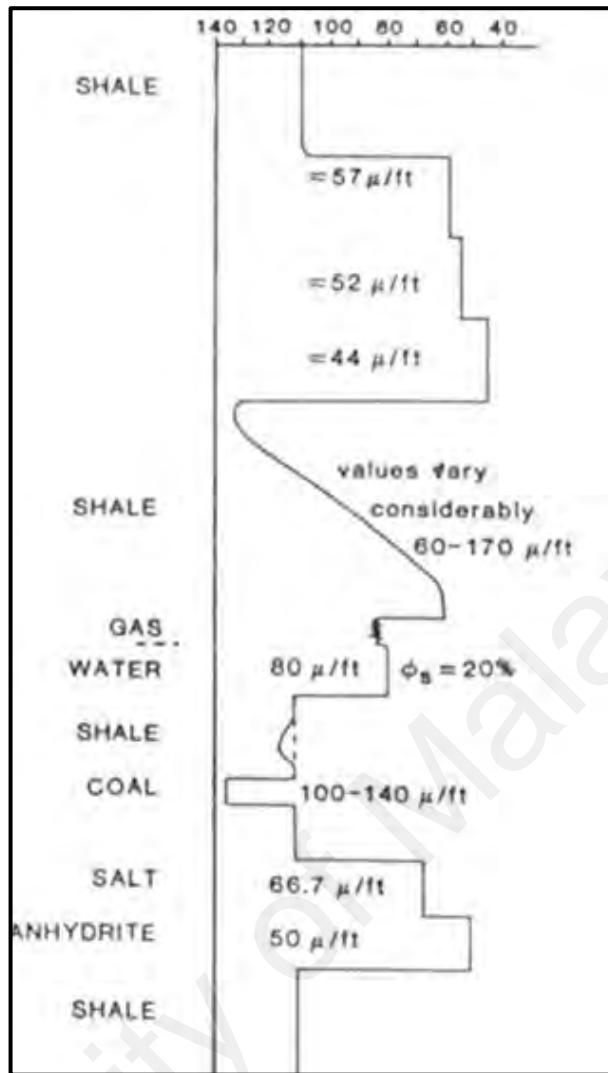


Figure 3.16: Idealized Sonic log. Free image.

Table 3.4 For different matrixes sonic velocities and interval transit time.

Lithologies/Fluids	Matrix velocities ft/sec	Δt_{matrix} or Δt_{fluid} $\mu\text{sec}/\text{ft}$ ($\mu\text{sec}/\text{m}$)	Δt_{matrix} (RGH) $\mu\text{sec}/\text{ft}$ ($\mu\text{sec}/\text{m}$)
Limestone	21000 to 23000	47.5 [156]	49 [161]
Sandstones	18000 to 19500	55.5 to 51.0 [182 to 186]	56 [184]
Dolomite	23000 to 26000	43.5 [143]	44 [144]
Salt	15000	66.7 [219]	-
Anhydrite	20000	50.0 [164]	-
Casing (Iron)	17500	57.0 [187]	-
Saltwater mud filtrate	5980	185 [607]	-
Fresh water mud filtrate	5280	189 [620]	-

3.3.5 Neutron porosity log (NPHI)

Neutron logs are porosity logs that measures the hydrogen concentration in a formation that are shale free where the pores are filled with oil or water, whereby these logs measure liquid filled porosity.

These neutrons are produced with chemical source usually a mixture of beryllium and americium which emits neutrons continuously (Fig 3.18). When these neutrons collides with the nuclei of formation they lose some energy, with adequate collisions neutron is absorbed by nucleus and a gamma ray is emitted. Therefore the energy loss is dominated by formation hydrogen concentration, because hydrogen in a porous formation is more concentrated in fluid filled pores, and energy loss can be related to the formation's porosity (Asquith & Krygowski, 2003).

The neutron log response varies with:

- Detector types i.e. neutron or gamma rays of different energies
- Source and detector spacing
- Lithology (limestone, sandstone, dolomite)

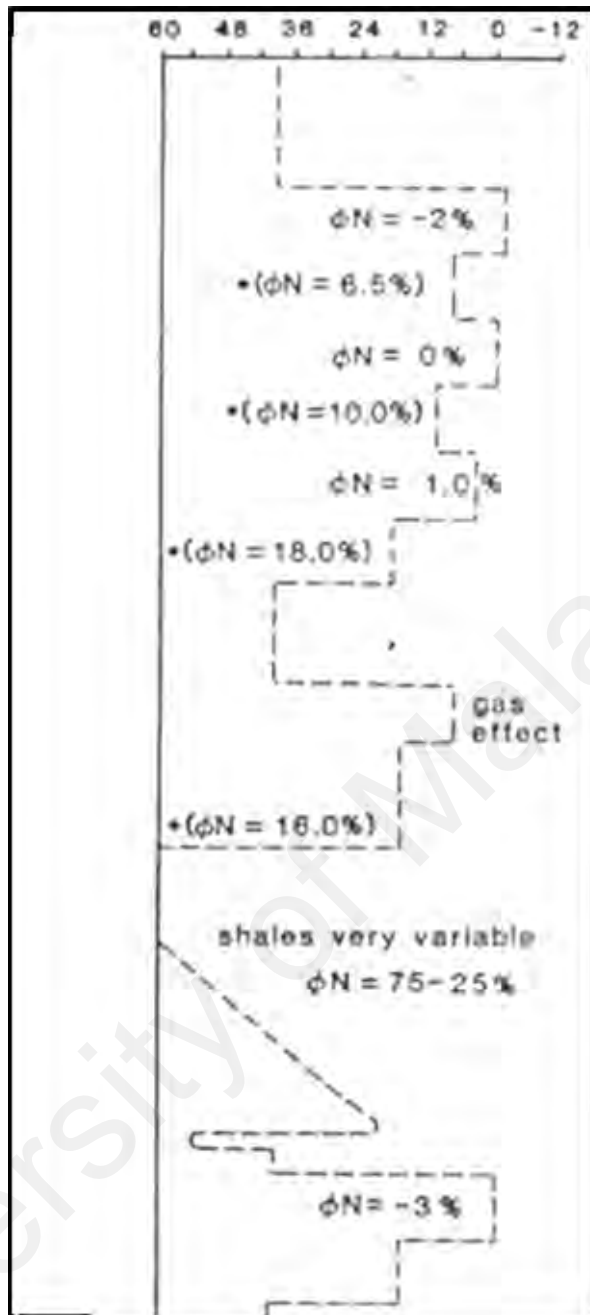


Figure 3.17: Neutron log idealized. Free image.

3.4 Reservoir properties

Formation temperature is very important in logs analysis. With temperature, resistivity of all mud cake (R_{mc}), drilling mud (R_m), mud filtrate (R_{mf}) and formation water (R_w) vary. So, it is important to calculate it at depth of interest and for that the equation used is as follows (Asquith et al., 2004).

$$FT = ST + \left(\frac{BHT - ST}{TD} \right) * FD$$

Whereas:

FT = Formation temperature °F

BHT = Bottom hole temperature °F

FD = Total depth (ft)

ST = Surface temperature °F

FD = Formation depth (ft)

3.4.1 Mud cake and mud filtrated resistivity correction

The mud cake (R_{mc}) and mud filtrate (R_{mf}) resistivity can be determined if the mud weight and mud resistivity are known (Schlumberger, 1977).

$$R_{mf} = K_m (R_m)^{1.07}$$

$$R_{mc} = 0.69 (R_{mf}) \left(\frac{R_m}{R_{mf}} \right)^{2.65}$$

Whereas:

R_{mc} = Resistivity of mud cake

R_{mf} = Resistivity of mud filtrate

K_m = Constant that is linked to mud weight

R_m = Resistivity of mud

So, after calculating on surface temperature the R_{mc} and R_{mf} must be corrected for formation temperature using Dresser Atlas, (1979) equation.

$$R_{ft} = R_{st} * [(ST + 6.77) / (FT + 6.77)]$$

Whereas:

ST = Surface temperature °F

FT = Formation temperature °F

R_{ST} = Resistivity of mud cake/filtrate at surface temp °F

R_{FT} = Resistivity of mud cake/filtrate at formation temp °F

3.4.2 Formation Water resistivity (R_w) determination

For fluid saturation formation water resistivity (R_w) correction is essential. Methods that are used for calculating the formation water resistivity are, porosity resistivity cross plot, Spontaneous Potential and apparent water resistivity log. Formation water resistivity calculated by:

$$R_w = \frac{(R_t * R_{mf})}{R_{xo}}$$

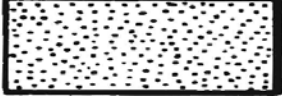
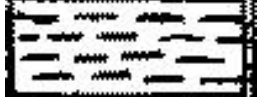

3.4.3 Shale Volume (V_{sh}) determination

For the calculation of porosities of targeted formations shale volume is very important to be measured (Charts, 1983; Poupon & Gavmard, 1970; Schlumberger, 1972). Probable shale volume can be calculated by several equations by interpreting well logs either single or double curve indicators. Every well log that is used, is supposed to give actual or upper limit of actual value. Shale volume can be calculated from several shale indicator logs. From single log the shale volume can be calculated from Gamma Ray, Resistivity (LLD/LLS), Spontaneous Potential and Neutron logs. In this study, Gamma Ray log (GR) was used for calculating the Shale volume. On the basis of shale volume, shale can be differentiated according to their physical properties (Table. 3 and Fig. 3.19).

- Laminated Shale: Shales that exists in sand as thin beds.

- Dispersed Shale: Shales that are dispersed throughout rock unit.
- Structural Shale: Shales present by means of nodules or grains in the rock unit.

Table 3. Shale distribution in rocks.

Types of Rocks	Pattern	Shale volume
Clean (Sandstone, sand)		$V_{sh} < 10\%$
Shale (shale)		$V_{sh} > 40\%$
Shaly sand		$< 10\% V_{sh} < 40\%$

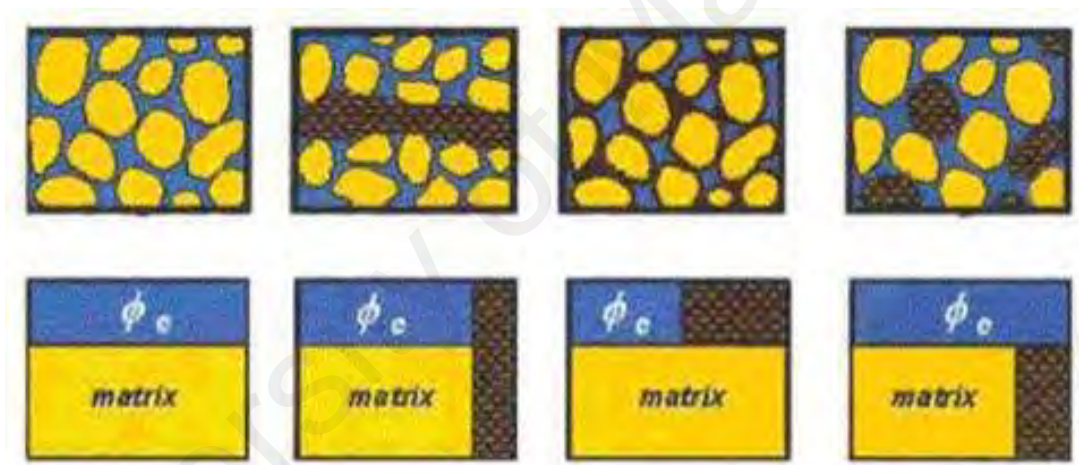


Figure 3.18: Shale distribution in rocks. Free image.

3.4.4 Formation porosity determination (ϕ)

Percent of void space in a total rock volume is porosity (Horgan, 1999). Porosity that has been developed by original sedimentation process is known as primary porosity (Horgan, 1999). In deep and older rock due to cementation and overburden the porosity is generally low. For measuring fluid saturation porosity is very important to calculate and correct it by using several different porosity tools. Porosity is mainly calculated from well logs. The most common logs used for calculating the porosity are Density (RHOB),

Sonic (DT), Neutron (NPHI) or combination of Neutron-Density logs (Fazeelat et al., 2010). These logs help in calculating the total, effective as well as secondary porosity.

3.4.5 Total porosity

Sonic neutron or density log can be used for measuring the total porosity, or combining the reading of neutron and density log.

3.4.6 Density Log (ϕ_D)

It is another application of gamma rays for collecting important information about the subsurface formations, and offers continuous record of bulk density of formation. The very main use of this log is to derive a value for total porosity of formation. The total porosity can be calculated through following equations for clean and shaly zones.

3.4.7 Shaly zones

Formations in which shales are present the density log displays low to moderate values of porosity, whereas the values for same zones in sonic and neutrons the values are moderate to relatively high as compare to density log reading. For the density log reading should be corrected to remove unwanted effects and for that following equation is used (Charts, 1983).

$$\phi_D = \left(\frac{\rho_{ma} - \rho_b}{\rho_{ma} - \rho_f} \right) - V_{sh} * \phi_{D_{sh}}$$

$$\phi_{D_{sh}} = \left(\frac{\rho_{ma} - \rho_{sh}}{\rho_{ma} - \rho_f} \right)$$

Whereas:

ρ_{sh} = opposite thick shale bed, the typical density log reading.

ρ_b = Bulk Density

ρ_{ma} = Matrix density

ρ_f = Fluid density

3.4.8 Clean zones

In formations, where there are no shales the following formula is used for calculating total porosity (Wyllie, 1963).

$$\phi_D = \left(\frac{\rho_{ma} - \rho_b}{\rho_{ma} - \rho_f} \right)$$

3.4.9 Neutron Porosity Log (ϕ_N) Formation porosity determination (ϕ)

The Neutron porosity log were firstly introduced and used in 1940, which had single detector and an isotopic source and later on the tool gets updated (Asquith et al., 2004). This log is mainly used for measuring the porosity of formation. This log mainly counts the number of hydrogen atoms in the formation (Fazeelat et al., 2010). This log is very much effected by gas saturation.

3.4.10 Shaly zones

Whenever shale exists in a formation, neutron log readings will be too high, for that an equation is used to correct the readings (Allen et al., 1965):

$$\phi_{NC} = \phi_{Nlog} - (V_{sh} * \phi_{Nsh})$$

3.4.11 Density-Neutron combination

Porosity can be determined from combination of density-neutron log by using equations for clean and shaly zones.

3.4.12 Clean zones

Porosity can be determined from combination of density-neutron log by using equations for clean and shaly zones.

For calculating total porosity in clean zone following formula can be used (Schlumberger, 1972):

$$\phi_{ND} = \sqrt{\frac{\phi_{ND}^2 - \phi_D^2}{2}}$$

$$\phi_{N=} \phi_N - \phi_{sh} * \phi_{Nsh}$$

$$\phi_D = \phi_D - \phi_{sh} * \phi_{Dsh}$$

3.4.13 Shaly zones

For shale zone, there is another equation used (Schlumberger, 1972):

$$\phi_{ND} = \phi_D - \left(\frac{\phi_{Dsh}}{0.45}\right) * 0.13 * V_{sh}$$

$$\phi_{NC} = \phi_D - \left(\frac{\phi_{Nsh}}{0.45}\right) * 0.13 * V_{sh}$$

$$\phi_{ND} = \sqrt{\frac{\phi_N^2 - \phi_D^2}{2}}$$

Whereas:

ϕ_{Dsh} and ϕ_{Nsh} are neutron and density porosity of a shale zone, and ϕ_{NC} and ϕ_{DC} are corrected for shale effect.

3.4.14 Secondary porosity (Φ_{sec})

Secondary porosity is the difference between Density-Neutron combine porosity and primary porosity from sonic log. Secondary porosity can be calculated by subtracting primary porosity from total porosity by the following equation (Schlumberger, 1972):

$$\Phi_{sec} = \Phi_{ND} - \Phi_S$$

3.4.15 Effective Porosity (Φ_e)

Effective porosity depends on the number of pores connected in rock. It can be calculated by using the following equation (Schlumberger, 1972):

$$\Phi_e = \Phi_t * (1 - V_{sh})$$

Whereas:

Φ_e = Effective porosity

Φ_t = Total porosity

V_{sh} = Shale volume

3.4.16 Fluid saturation determination

For completing the petrophysical parameters of reservoir, determination of fluid saturation is essential (Zahid et al., 2014). Fluid determination is mainly done for calculating hydrocarbon and water presence in the zone of interest.

3.4.17 Water saturation S_w

Water saturation tells about the presence of water in pore space. For flushed zone it is denoted by S_{x0} and in uninvaded zone it is denoted by S_w . Water saturation is expressed

by volume percent or fraction. Proper interpretation and calculation of water saturation is very important because hydrocarbon saturation calculation totally depends on water saturation calculation (Poupon & Leveaux, 1971; Schlumberger, 1972). Water Saturation calculation for clean zones are as follows:

3.4.17.1 Uninvaded zones

By Archie's equation water saturation in clean zone is calculated by following formula:

$$S_w = \left(F * \frac{R_w}{R_t} \right)^{1/n}$$

Where F is formation factor and can be expressed as:

$$F = \left(\frac{a}{\phi^m} \right)$$

ϕ = Formation porosity

R_w = Water resistivity

R_t = Uninvaded zone resistivity

3.4.18 Hydrocarbon saturation determination S_h

Hydrocarbon saturation is directly calculated from water saturation by following equation:

$$S_h = 1 - S_w$$

3.5 Introduction to seismic methods

All seismic methods basic principle is the controlled generation of elastic waves that penetrates the earth subsurface generated by seismic source and reflects back from

different points due to change in lithology. The change in elastic waves are recorded in order to obtain an image of the subsurface. These waves are pulse of strain energy that travels through solids and liquids. There are two major types of waves produced by seismic energy sources. These are:

- Body waves
- Surface waves

In body waves the energy is transported in all directions, whereas in surface waves the energy travels near or along the surface. The criteria that distinguish these waves from each other is the direction of ground movement relative to the propagation direction and the propagation zones.

In seismic methods the prime interest is in body waves which are of two types namely:

- Primary waves (P-waves)
- Secondary waves (S-Waves)

P-waves are longitudinal or compressional waves have particle motion parallel to the direction of propagation, whereas in S-waves are shear or transverse waves have particle motion perpendicular to the direction of propagation. Surface waves are oftenly considered as source of noise, which may contain valuable information regarding material properties present in shallow ground.

In seismic methods the most important fundamental parameter is velocity of seismic waves, which depends on different properties like porosity, lithology, mineral content, pore fluid saturation and compaction. P-waves have higher velocity than S-waves. P-Waves can travel through both solids and fluids, but S-waves can only travel through solids.

Seismic waves during their propagation within earth's subsurface are refracted, reflected or diffracted when elastic contrast occurs at boundaries between rock masses or layers of different properties (Fig. 3.28). The seismic waves that are recorded after reflecting back from the subsurface allows drawing conclusion on lithological composition and structures of the subsurface. By carefully measuring the travel-times of seismic waves and by defining their material specific velocities, a subsurface geological model can be constructed. In seismic survey there are different energy sources to produce elastic waves (e.g. dynamite, vibrator, sledgehammer and weight drop).

The most classical methods of seismic are reflection and refraction seismics. In refraction seismic method head waves are used which arise at boundary of two layers when reflection at critical angle occurs, the main aim of seismic refraction survey is to determine refractor topography, depth of different layers and layers velocities (Van Overmeeren, 2001). Seismic reflection method is most important and powerful geophysical technique to prospect for oil and gas at greater depths. The very basic technique of seismic method used by exploration companies is generation of seismic waves and measuring the waves travel time from source to subsurface and reflecting back at receivers (geophones).

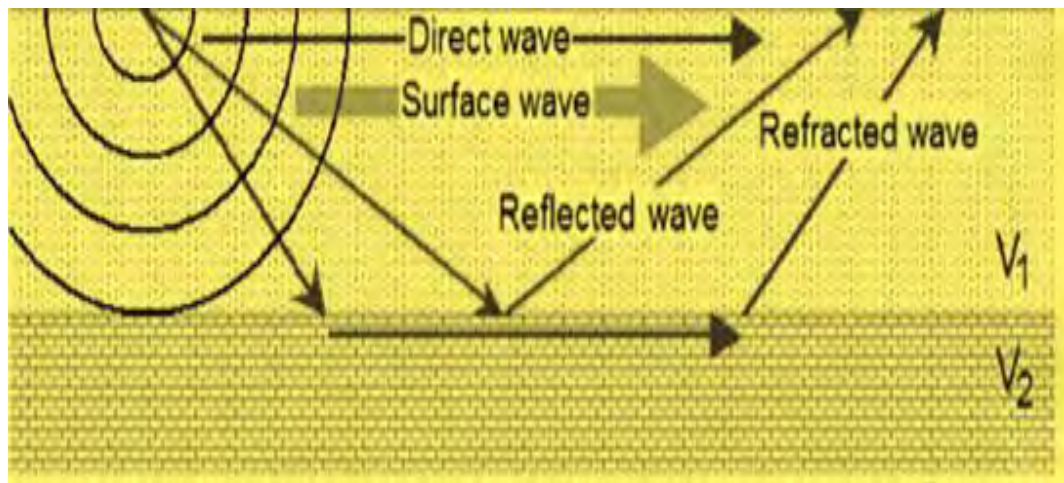


Figure 3.19: Reflected and refracted seismic waves. Free image.

3.5.1 Seismic reflection method

To map subsurface geological structures seismic reflection method is used. In this method measurements are made by measuring the arrival time of reflected seismic waves from interfaces where the acoustic impedance (density) changes. Keeping in mind the main two objectives, variations in depth and attitude of boundaries (Sheriff, 1980).

The seismic reflection methods works by penetrating the sound waves that travels between different boundaries/rock layers and fluids, the reflected back sound waves are recorded on digital instruments and on large sheet (seismic section) papers having dark lines on it, which is later interpreted to delineate subsurface structures. In the subsurface the seismic waves travels at a speed of 6000 m/s, this time is two way travel time which is divided by two to get one way travel time which is the actual depth of horizon of interest.

3.5.1.1 Seismic velocities

In seismic interpretation the most important step is to estimate seismic velocities for good and proper interpretation, for delineating the following:

- True depth
- Migration of seismic section
- Stacking of seismic data
- Probable lithological determination
- Porosity estimation

Velocities are so important because this allows to convert time seismic section into depth section, because seismic sections are always recorded in time. These velocities can also be used in more complex interpretation of seismic section for probable determination of porosities, geological ages, fluid content, fracturing etc.

Relationship of seismic velocity with density and elasticity is given by:

$$V^2 = \frac{E}{\rho}$$

By this relation the velocity is directly proportional to elasticity and inversely to density. However the reverse of this is true because the denser the rock, the more will be the velocity because of compaction its elasticity increases in such a way that it reduces the effect introduced by the density.

Types of Seismic velocities

In seismic interpretation the term velocity refers to seven different velocity concepts;

- Instantaneous Velocity
- Interval Velocity
- Apparent Velocity
- Average Velocity
- Root Mean Square Velocity
- Stacking Velocity and

➤ Migration Velocity

3.5.1.2 Interval velocity

The average speed of a wavefront between two points is interval velocity, measured perpendicular to the velocity layers (Fig 3.21).

$$V_{\text{int}} = \frac{z_2 - z_1}{t_2 - t_1} = \frac{2\Delta z}{\Delta t}$$

Δt = Two way travel time

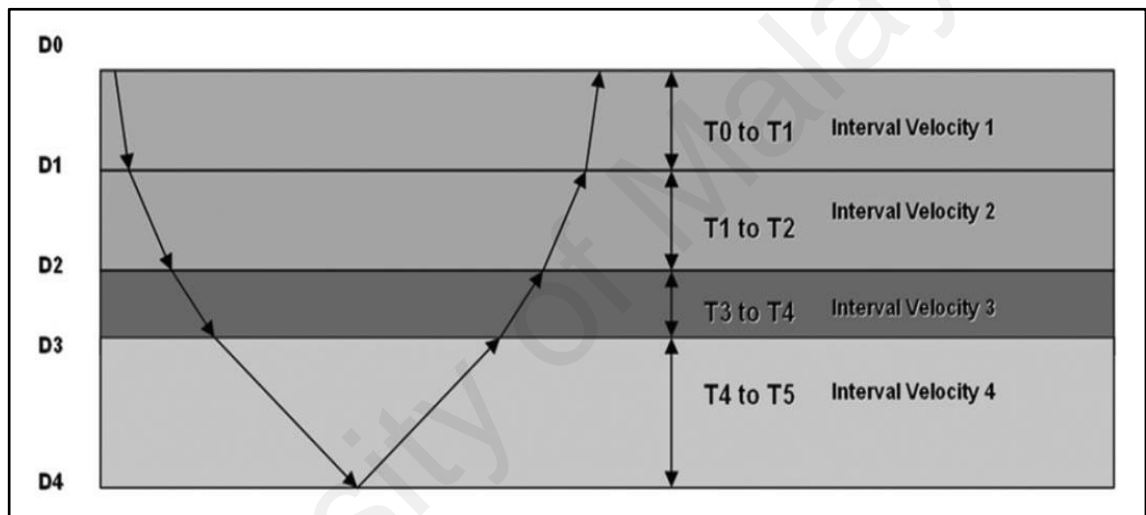


Figure 3.20: Interval velocities of different horizons. Free image.

3.5.1.3 Average velocity

In seismic methods the average velocity is the depth divided by travel-time of a wave to that depth. Formula to calculate average velocity is:

$$V_{\text{avg}} = \frac{2\sum_{k=1}^n z_k}{\sum_{k=1}^n t_k}$$

3.5.1.4 Root mean square velocity

When the subsurface layers are horizontal having interval velocities as V_1, V_2, \dots, V_n and the two way travel times are t_1, t_2, \dots, t_n then root mean square velocity of n-layers will be:

$$V_{\text{rsm},n} = \frac{\sum V_i^2 t_i}{\sum t_i}$$

The root mean square velocity is always determined from surface to a specific interface.

3.5.1.5 Dix equation

This is the velocity which is obtained from the application of NMO normal move out correction to the common depth point CDP gather.

The equation which always used for determining the interval velocities between two reflectors from RMS root mean square velocities is dix equation.

$$V_{\text{int}} = \frac{(t_2 V_{\text{RMS}2}^2 - t_1 V_{\text{RMS}1}^2)}{(t_2 - t_1)^2}$$

V_{int} = Interval Velocity

t_1 = Traveltime of first reflector

t_2 = Traveltime of second reflector

$V_{\text{RMS}1}$ = Root mean square velocity of first reflector

$V_{\text{RMS}2}$ = Root mean square velocity of second reflector

3.5.2 Horizon mapping by 3D contours

The line drawn by joining points of equal value is known as contour. Velocity analysis of all seismic dip and strike lines are conducted in which interval, average and mean average velocities are used to map the horizons, for mapping horizons of interest, time is picked from all seismic section below all short point and then combining the time picked with the shotpoint coordinates (Fig. 3.23) of all shotpoints and using it to model horizons by generate time and depth contour 3D contour maps (Fig. 3.22).

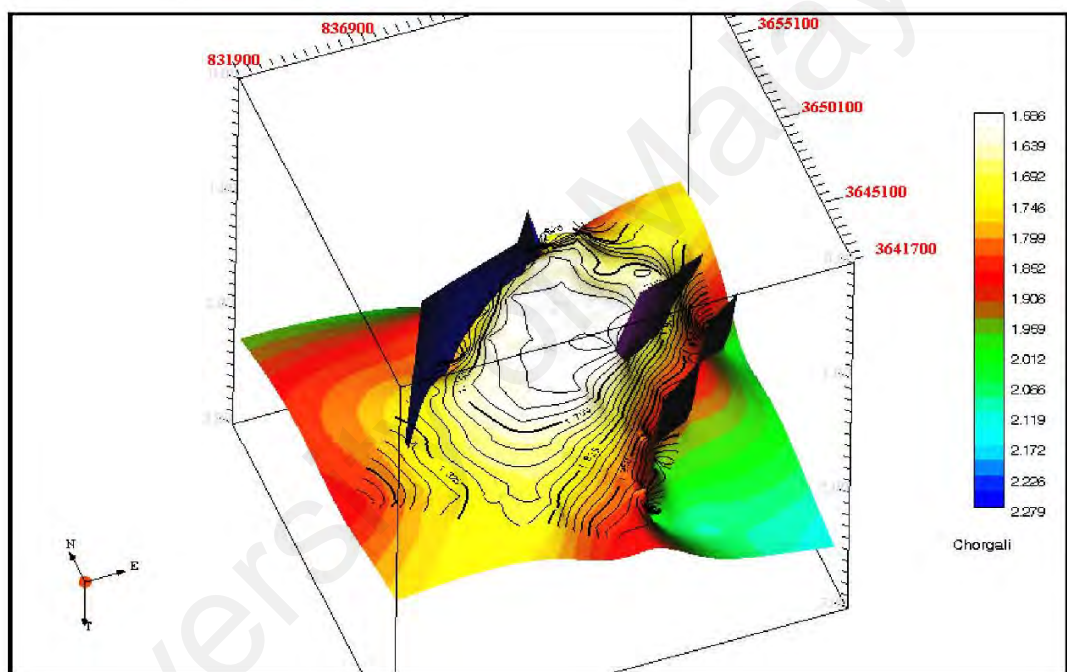


Figure 3.21: An example of 3D contour output image from horizon mapping.

A	B	C	D	E	F	G	H	I	J	K	L	M	N	O	P	Q	R	S	T	U	V	W	X	Y	Z	AA	AB	
1	Line number	Shotpoints	lat	long																								
2	SOX-PB1-1	85	32524.89	72327.06																								
3	SOX-PB1-1	86	32523.7	72300.37																								
4	SOX-PB1-1	87	32522.45	72303.12																								
5	SOX-PB1-1	88	32521.07	72305.95																								
6	SOX-PB1-1	89	32519.51	72308.92																								
7	SOX-PB1-1	90	32517.69	72312.06																								
8	SOX-PB1-1	91	32515.59	72315.4																								
9	SOX-PB1-1	92	32513.33	72318.91																								
10	SOX-PB1-1	93	32511.03	72322.56																								
11	SOX-PB1-1	94	32508.84	72326.29																								
12	SOX-PB1-1	95	32506.9	72330.06																								
13	SOX-PB1-1	96	32505.3	72333.83																								
14	SOX-PB1-1	97	32503.94	72337.56																								
15	SOX-PB1-1	98	32502.66	72341.21																								
16	SOX-PB1-1	99	32501.3	72344.72																								
17	SOX-PB1-1	100	32499.7	72348.06																								
18	SOX-PB1-1	101	32497.76	72351.2																								
19	SOX-PB1-1	102	32495.57	72354.16																								
20	SOX-PB1-1	103	32493.26	72356.99																								
21	SOX-PB1-1	104	32491.7	72359.74																								
22	SOX-PB1-1	105	32489.9	72362.45																								
23	SOX-PB1-1	106	32487.09	72365.16																								
24	SOX-PB1-1	107	32484.52	72367.91																								
25	SOX-PB1-1	108	32482.15	72370.75																								
26	SOX-PB1-1	109	32479.9	72373.72																								
27	SOX-PB1-1	110	32477.7	72376.85																								
28	SOX-PB1-1	111	32475.5	72379.98																								
29	SOX-PB1-1	112	32473.23	72383.11																								
30	SOX-PB1-1	113	32470.96	72386.24																								
31	SOX-PB1-1	114	32468.69	72389.37																								
32	SOX-PB1-1	115	32466.42	72392.5																								
33	SOX-PB1-1	116	32464.15	72395.63																								
34	SOX-PB1-1	117	32461.88	72398.76																								
35	SOX-PB1-1	118	32459.61	72401.89																								
36	SOX-PB1-1	119	32457.34	72405.02																								
37	SOX-PB1-1	120	32455.07	72408.15																								
38	SOX-PB1-1	121	32452.8	72411.28																								

Figure 3.22: Image showing seismic line number along with shotpoint numbers and coordinates of all shotpoints used for horizon mapping in Petrel, provided by LMKR.

3.5.3 Seismic interpretation

The process which is used for determining about the subsurface information of the earth from seismic section is seismic interpretation. In the seismic interpretation an interpreter concentrates on specific lineups of wiggles on the seismic section. It is very important to decide what formations they are representing, how their behavior is, i.e. how they are going higher and lower in the section, where the wiggles have suddenly broken up and discontinue, where the fault is appearing.

Two basic records are contained by seismic section one is the record of arrival time of reflection from geological surface, the real depth of this surface is calculated by solving variety of parameters e.g. thickness and velocity of overlying rock layers, the second record is reflection shape, which contains information about frequencies, how much signal is strong and how the frequencies are distributed (Kearey et al., 2013). This is the information which can be used for the lithology and fluid content identification.

The very first activity of an interpreter is picking and marking of a horizon that are appearing on the section, the reflection may be representing a reliable reflection of a horizon that is appearing as strong wiggles. These reflections are picked and marked on the section by noting the shotpoints along the vertical sections. The picked horizons are timed by reading the reflection times on the seismic section. These picked time can then be plotted to map the horizons and convert time seismic section into depth section by applying different algorithms (Coffeen, 1978).

There are various problems that appear in seismic interpretation like the very first thing is identification of the reflections and after identifying staying on the same reflection throughout the seismic sections which covers the area, identifying the faults, folds and discontinuity and at last presenting your results of interpretation (Coffeen, 1978). When there is a seismic section which has been recorded in good quality and there a various

reflections on the resulting section, then the very first step is identifying the reflection, in identification of a reflection the most common method is comparing all the seismic section with each other, that will help in understanding the behavior of the horizons, but this becomes difficult when the sections are recorded far away from each other.

After marking the horizons and fault times with CDP numbers and navigation coordinates X, Y (Fig. 3.24) of all interpreted seismic sections are then put as an output for contouring and mapping (Fig. 3.24 and .25) to model the subsurface horizons structure by 3D maps and on the 3D maps if there is a prospective zone a well point is marked on the section.

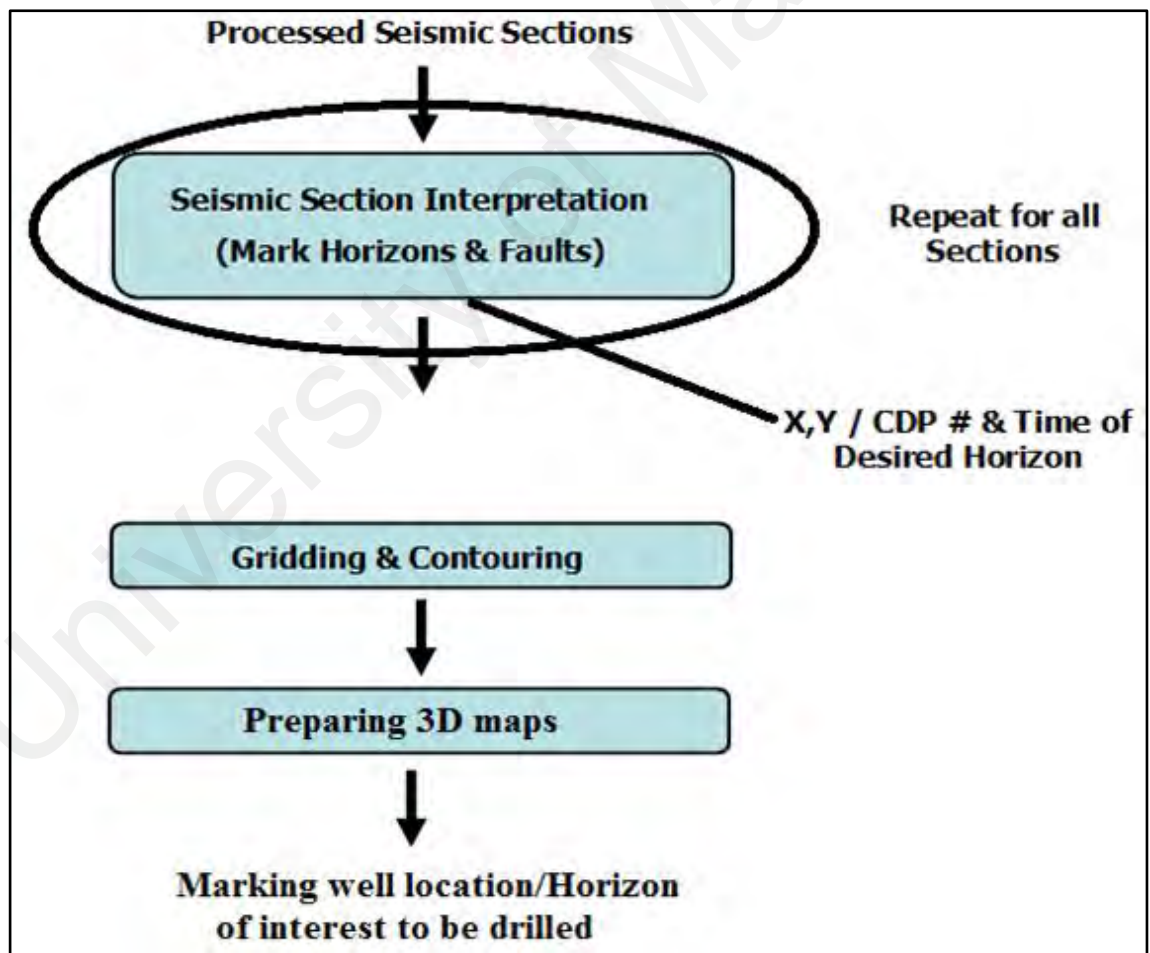


Figure 3.23: A complete seismic interpretation flowchart.

VP 108				VP 123				VP 138																	
A	B	C	D	E	F	G	H	I	J	K	L	M	N	O	P	Q	R	S	T	U	V	W			
Time (msec)	Time in Sec	Vrms (m/msec)	Vint	Depth(m)	Time (msec)	Time in Sec	Vrms (m/msec)	Vint	Depth(m)	Time (msec)	Time in Sec	Vrms (m/msec)	Vint	Depth(m)	Time (msec)	Time in Sec	Vrms (m/msec)	Vint	Depth(m)	Time (msec)	Time in Sec	Vrms (m/msec)	Vint	Depth(m)	
1	0	0.001	2300	0	0	0.001	2400	0	0	0	0.001	2400	0	0	0	0.001	2400	0	0	0	0.001	2400	0	0	
2	1	0.001	2300.581395	1.150290688	1	0.001	2400.970149	2.400.970149	1.20045075	1	0.001	2400.970149	2.400.970149	1.20045075	1	0.001	2400.970149	2.400.970149	1.20045075	1	0.001	2400.970149	2.400.970149	1.20045075	
3	2	0.002	2301.162791	2.300.872093	2	0.002	2401.940299	2.401.940299	2.401.453224	2	0.002	2401.940299	2.401.940299	2.401.453224	2	0.002	2401.940299	2.401.940299	2.401.453224	2	0.002	2401.940299	2.401.940299	2.401.453224	
4	3	0.003	2301.744186	3.01.162791	3.451744186	3	0.003	2402.910448	2.402.910448	2.402.910448	3	0.003	2402.910448	2.402.910448	2.402.910448	3	0.003	2402.910448	2.402.910448	2.402.910448	3	0.003	2402.910448	2.402.910448	2.402.910448
5	4	0.004	2302.325581	3.202.325581	4.602906977	4	0.004	2403.880597	2.403.880597	2.403.880597	4	0.004	2403.880597	2.403.880597	2.403.880597	4	0.004	2403.880597	2.403.880597	2.403.880597	4	0.004	2403.880597	2.403.880597	2.403.880597
6	5	0.005	2302.906977	3.202.325581	5.754360465	5	0.005	2404.850746	2.404.850746	2.404.850746	5	0.005	2404.850746	2.404.850746	2.404.850746	5	0.005	2404.850746	2.404.850746	2.404.850746	5	0.005	2404.850746	2.404.850746	2.404.850746
7	6	0.006	2303.488372	3.203.488372	6.906104651	6	0.006	2405.820896	2.405.820896	2.405.820896	6	0.006	2405.820896	2.405.820896	2.405.820896	6	0.006	2405.820896	2.405.820896	2.405.820896	6	0.006	2405.820896	2.405.820896	2.405.820896
8	7	0.007	2304.069767	3.204.069767	8.058139535	7	0.007	2406.791045	2.406.791045	2.406.791045	7	0.007	2406.791045	2.406.791045	2.406.791045	7	0.007	2406.791045	2.406.791045	2.406.791045	7	0.007	2406.791045	2.406.791045	2.406.791045
9	8	0.008	2304.651163	3.204.651163	9.210465116	8	0.008	2407.761194	2.407.761194	2.407.761194	8	0.008	2407.761194	2.407.761194	2.407.761194	8	0.008	2407.761194	2.407.761194	2.407.761194	8	0.008	2407.761194	2.407.761194	2.407.761194
10	9	0.009	2305.232558	3.205.232558	10.3630814	9	0.009	2408.731343	2.408.731343	2.408.731343	9	0.009	2408.731343	2.408.731343	2.408.731343	9	0.009	2408.731343	2.408.731343	2.408.731343	9	0.009	2408.731343	2.408.731343	2.408.731343
11	10	0.01	2305.813953	3.205.813953	11.51598837	10	0.01	2409.701493	2.409.701493	2.409.701493	10	0.01	2409.701493	2.409.701493	2.409.701493	10	0.01	2409.701493	2.409.701493	2.409.701493	10	0.01	2409.701493	2.409.701493	2.409.701493
12	11	0.011	2306.395349	3.206.395349	12.66918605	11	0.011	2410.671642	2.410.671642	2.410.671642	11	0.011	2410.671642	2.410.671642	2.410.671642	11	0.011	2410.671642	2.410.671642	2.410.671642	11	0.011	2410.671642	2.410.671642	2.410.671642
13	12	0.012	2306.976744	3.206.976744	13.82267442	12	0.012	2411.641791	2.411.641791	2.411.641791	12	0.012	2411.641791	2.411.641791	2.411.641791	12	0.012	2411.641791	2.411.641791	2.411.641791	12	0.012	2411.641791	2.411.641791	2.411.641791
14	13	0.013	2307.55814	3.207.55814	14.97645349	13	0.013	2412.61194	2.412.61194	2.412.61194	13	0.013	2412.61194	2.412.61194	2.412.61194	13	0.013	2412.61194	2.412.61194	2.412.61194	13	0.013	2412.61194	2.412.61194	2.412.61194
15	14	0.014	2308.139535	3.208.139535	16.13052326	14	0.014	2413.58209	2.413.58209	2.413.58209	14	0.014	2413.58209	2.413.58209	2.413.58209	14	0.014	2413.58209	2.413.58209	2.413.58209	14	0.014	2413.58209	2.413.58209	2.413.58209
16	15	0.015	2308.72093	3.208.72093	17.28488372	15	0.015	2414.552339	2.414.552339	2.414.552339	15	0.015	2414.552339	2.414.552339	2.414.552339	15	0.015	2414.552339	2.414.552339	2.414.552339	15	0.015	2414.552339	2.414.552339	2.414.552339
17	16	0.016	2309.303236	3.209.303236	18.43953488	16	0.016	2415.522388	2.415.522388	2.415.522388	16	0.016	2415.522388	2.415.522388	2.415.522388	16	0.016	2415.522388	2.415.522388	2.415.522388	16	0.016	2415.522388	2.415.522388	2.415.522388
18	17	0.017	2309.883721	3.209.883721	19.59447674	17	0.017	2416.492537	2.416.492537	2.416.492537	17	0.017	2416.492537	2.416.492537	2.416.492537	17	0.017	2416.492537	2.416.492537	2.416.492537	17	0.017	2416.492537	2.416.492537	2.416.492537
19	18	0.018	2310.465116	3.210.465116	20.74979793	18	0.018	2417.462687	2.417.462687	2.417.462687	18	0.018	2417.462687	2.417.462687	2.417.462687	18	0.018	2417.462687	2.417.462687	2.417.462687	18	0.018	2417.462687	2.417.462687	2.417.462687
20	19	0.019	2311.046512	3.211.046512	21.90532556	19	0.019	2418.432836	2.418.432836	2.418.432836	19	0.019	2418.432836	2.418.432836	2.418.432836	19	0.019	2418.432836	2.418.432836	2.418.432836	19	0.019	2418.432836	2.418.432836	2.418.432836
21	20	0.02	2311.627907	3.211.627907	23.06104651	20	0.02	2419.402985	2.419.402985	2.419.402985	20	0.02	2419.402985	2.419.402985	2.419.402985	20	0.02	2419.402985	2.419.402985	2.419.402985	20	0.02	2419.402985	2.419.402985	2.419.402985
22	21	0.021	2312.209302	3.212.209302	24.21715116	21	0.021	2420.373134	2.420.373134	2.420.373134	21	0.021	2420.373134	2.420.373134	2.420.373134	21	0.021	2420.373134	2.420.373134	2.420.373134	21	0.021	2420.373134	2.420.373134	2.420.373134
23	22	0.022	2312.790698	3.212.790698	25.37354651	22	0.022	2421.343284	2.421.343284	2.421.343284	22	0.022	2421.343284	2.421.343284	2.421.343284	22	0.022	2421.343284	2.421.343284	2.421.343284	22	0.022	2421.343284	2.421.343284	2.421.343284
24	23	0.023	2313.372093	3.213.372093	26.53032556	23	0.023	2422.313433	2.422.313433	2.422.313433	23	0.023	2422.313433	2.422.313433	2.422.313433	23	0.023	2422.313433	2.422.313433	2.422.313433	23	0.023	2422.313433	2.422.313433	2.422.313433
25	24	0.024	2313.953488	3.213.953488	27.6872093	24	0.024	2423.283582	2.423.283582	2.423.283582	24	0.024	2423.283582	2.423.283582	2.423.283582	24	0.024	2423.283582	2.423.283582	2.423.283582	24	0.024	2423.283582	2.423.283582	2.423.283582
26	25	0.025	2314.534884	3.214.534884	28.84447674	25	0.025	2424.253731	2.424.253731	2.424.253731	25	0.025	2424.253731	2.424.253731	2.424.253731	25	0.025	2424.253731	2.424.253731	2.424.253731	25	0.025	2424.253731	2.424.253731	2.424.253731
27	26	0.026	2315.116279	3.215.116279	30.00203488	26	0.026	2425.223881	2.425.223881	2.425.223881	26	0.026	2425.223881	2.425.223881	2.425.223881	26	0.026	2425.223881	2.425.223881	2.425.223881	26	0.026	2425.223881	2.425.223881	2.425.223881
28	27	0.027	2315.697674	3.215.697674	31.15988372	27	0.027	2426.19403	2.426.19403	2.426.19403	27	0.027	2426.19403	2.426.19403	2.426.19403	27	0.027	2426.19403	2.426.19403	2.426.19403	27	0.027	2426.19403	2.426.19403	2.426.19403
29	28	0.028	2316.27907	3.216.27907	32.31802526	28	0.028	2427.164179	2.427.164179	2.427.164179	28	0.028	2427.164179	2.427.164179	2.427.164179	28	0.028	2427.164179	2.427.164179	2.427.164179	28	0.028	2427.164179	2.427.164179	2.427.164179
30	29	0.029	2316.860465	3.216.860465	33.47645349	29	0.029	2428.134328	2.428.134328	2.428.134328	29	0.029	2428.134328	2.428.134328	2.428.134328	29	0.029	2428.134328	2.428.134328	2.428.134328	29	0.029	2428.134328	2.428.134328	2.428.134328
31	30	0.03	2317.44186	3.217.44186	34.63517442	30	0.03	2429.104478	2.429.104478	2.429.104478	30	0.03	2429.104478	2.429.104478	2.429.104478	30	0.03	2429.104478	2.429.104478	2.429.104478	30	0.03	2429.104478	2.429.104478	2.429.104478
32	31	0.031	2318.023256	3.218.023256	35.79418605	31	0.031	2430.074627	2.430.074627	2.430.074627	31	0.031	2430.074627	2.430.074627	2.430.074627	31	0.031	2430.074627	2.430.074627	2.430.074627	31	0.031	2430.074627	2.430.074627	2.430.074627
33	32	0.032	2318.604651	3.218.604651	36.95348837	32	0.032	2431.044776	2.431.044776	2.431.044776	32	0.032	2431.044776	2.431.044776	2.431.044776	32	0.032	2431.044776	2.431.044776	2.431.044776	32	0.032	2431.044776	2.431.044776	2.431.044776
34	33	0.033	2319.186047	3.219.186047	38.1130814	33	0.033	2432.014925	2.432.014925	2.432.014925	33	0.033	2432.014925	2.432.014925	2.432.014925	33	0.033	2432.014925	2.432.014925	2.432.014925	33	0.033	2432.014925	2.432.014925	2.432.014925
35	34	0.034	2319.767442	3.219.767442	39.27296512	34	0.034	2432.985075	2.432.985075	2.432.985075	34	0.034	2432.985075	2.432.985075	2.432.985075	34	0.034	2432.985075	2.432.985075	2.432.985075	34	0.034	2432.985075	2.432.985075	2.432.985075
36	35	0.035	2320.348837	3.220.348837	40.43313953	35	0.035	2433.955224	2.433.955224	2.433.955224	35	0.035													

Seismic interpretation process can be divided into three sub categories which are interrelated, lithologic, structure and sequence stratigraphy (Telford et al., 1990). The seismic sequence stratigraphy reveals the cyclic episodes of deposition, the lithologic interpretation gives information regarding changes in porosity, fluid, fracture intensity and lithology from seismic data, the direct hydrocarbon indicators DHI, bright spots and dim-outs are those elements employed in this process. The structure interpretation is used to create structural maps of the subsurface from the observed waves arrival times records. In this study 2D seismic interpretation has been done.

3.5.4 Structural analysis

The most important objective of structural analysis on the seismic section is to mark structural traps that may contain hydrocarbons trapped in it. That are variety of section sections which shows structure images that are easy to interpret, but also there are sections that are very difficult to interpret and requires expert to interpret properly, the discontinuity of a reflection indicates presence of faults, and undulating reflections indicates folded beds presence. Almost all of the structural interpretation is carried out in units of two way reflection time rather than depth, and mostly time structure/contour maps are generated to display geometry of horizons of interest by means of contours of equal reflection time. The constructed time contour maps can be converted into depth maps and sections by applying correct algorithms and using correct velocity information.

Structural analysis is done by two approaches:

- Time Section
- Depth Section

3.5.4.1 Time section

It is the reproduction of seismic section, time section consist of vertical scale and horizontal scale.

3.5.4.2 Depth section

Accurate measurements of seismic velocities is very critical and most important step in seismic data processing and interpretation, seismic velocity determination is the base of all seismic interpretation.

3.5.5 Softwares used for seismic interpretation

Variety of softwares packages have been designed for seismic interpretation either 2-D, 3-D or 4-D. Petrel E&P Interpretation software from Schlumberger was used in this study.

3.6 Microfacies analysis

Deposition of sediment is controlled primarily by physical and biological features of prevailing environment of deposition. These features are helpful in identifying and interpreting the place of deposition in the basin. Flugel (2004) referred the term microfacies as the total of all paleontological and sedimentological criteria, which can be classified using thin sections.

3.7 Lithofacies analysis

Gamma ray is one of the main and most useful tool for subsurface facies analysis due to its response to different lithological horizons (Posamentier and Allen, 1999; Ghazi & Mountney, 2010). Gamma ray log have different response to radiations emitted by rocks. Generally the decay of thorium, uranium and potassium compounds and their values can

be used as proxy for lithology identification (Rider, 1990; Hampson et al., 2005; Ghazi & Mountney, 2010). Gamma ray logs are very useful in identifying clays and clay-rich horizons as they contain greater amount of radioactive minerals. Nevertheless sand rich facies have different characteristic gamma ray log trends (Rider, 1990). The amount of clay makes the gamma ray log increase systematically and the values goes progressively upward (Ghazi et al., 2010).

3.7.1 Factors effecting interpretation

There are various factors need to be taken care of during interpretation. The first thing is response of gamma ray log that is the shape/trend of gamma ray log to various lithologic units present, the presence of potassium feldspar content in sandstone can record high values of gamma ray then in clean zones (Ghazi & Mountney, 2010; Rider, 1990). The presence of mica contents can also increase the values of gamma ray log (Rider, 1990). Hence the sand size detrital components cannot all be expected to have low values, and also not all of the clay minerals can be assumed to have higher response because clay minerals have variety of compositions. The example for this can be the values of gamma ray which were higher for illite as compare to the chlorite and kaolinite (Ghazi & Mountney, 2010; Hurst, 1990; Rider, 1990). Minerals such as gypsum, quartz and calcite have low gamma ray log values, however the units which are rich in clays records much higher gamma ray values on logs (Ghazi & Mountney, 2010).

At the start gamma ray log trends indicates variations in grain size, however in fluvial successions the relationship between sandstone facies and grain size change is effected by the presence of clay matrix within sand dominated beds (Ghaz & Mountney, 2010). In channels the presence of mud pebbles deposition will generate higher gamma ray values even though the parent material is a clean sandstone, similarly an increase in gamma ray values can be observed when there is presence of carbonaceous material (Chow et al.,

2005). Facies lithologies content variations, lithologies types and gamma ray variations are given in Table 3.5 and Figure 3.26.

Table 3.5: Facies lithologies, contents variations with gamma ray response.

Facies No.	Lithology of the facies	Characteristics	Gamma ray variations	Average thickness of facies in this type of bed
1	Coarse-grained to pebbly sandstone.	Cylindrical trend in the gamma-ray logs.	20 to 50%	3 m In thin beds and 9 m in thick beds.
2	Coarse- to medium-grained sandstone with rare shale and claystone.	Log character shows a change in grain size from base to top reflecting a fining-upward character.	30 to 60%	1 m In thin beds and 5 m in thick beds
3	Medium- to fine-grained sandstone with siltstone and claystone.	Bell-shaped trend in the gamma ray logs, Facies lower boundaries show an abrupt deflection towards sand base line whereas upper boundaries show a deflection towards shale base line.	40 to 70%	4-5 m average thickness.
4	Sandstone with interbedded siltstone and claystone with Carbonaceous material in places.	Funnel shape and cleaning-upwards trends. Facies lower boundaries show a sharp base and a gradual upward-shifting trend towards sand base line, whereas upper boundaries show a sharp deflection towards the shale base line.	20 to 90%	4 m average thickness.
5	Claystone and siltstone with interbeds of very fine to fine grained micaceous sandstone.	Irregular to symmetrical shape and trend of log. Facies lower boundaries have rounded base, and the trends gradually shifts towards sand base line.	30 to 80%	3 m average thickness.
6	Shale, mudstone, claystone with fine beds of sandstone and thin beds of siltstone.	These have irregular shape of log, upper and lower both boundaries are towards shale base line.	50 to 90%	0.2 to 0.4 m-thick, thinner beds

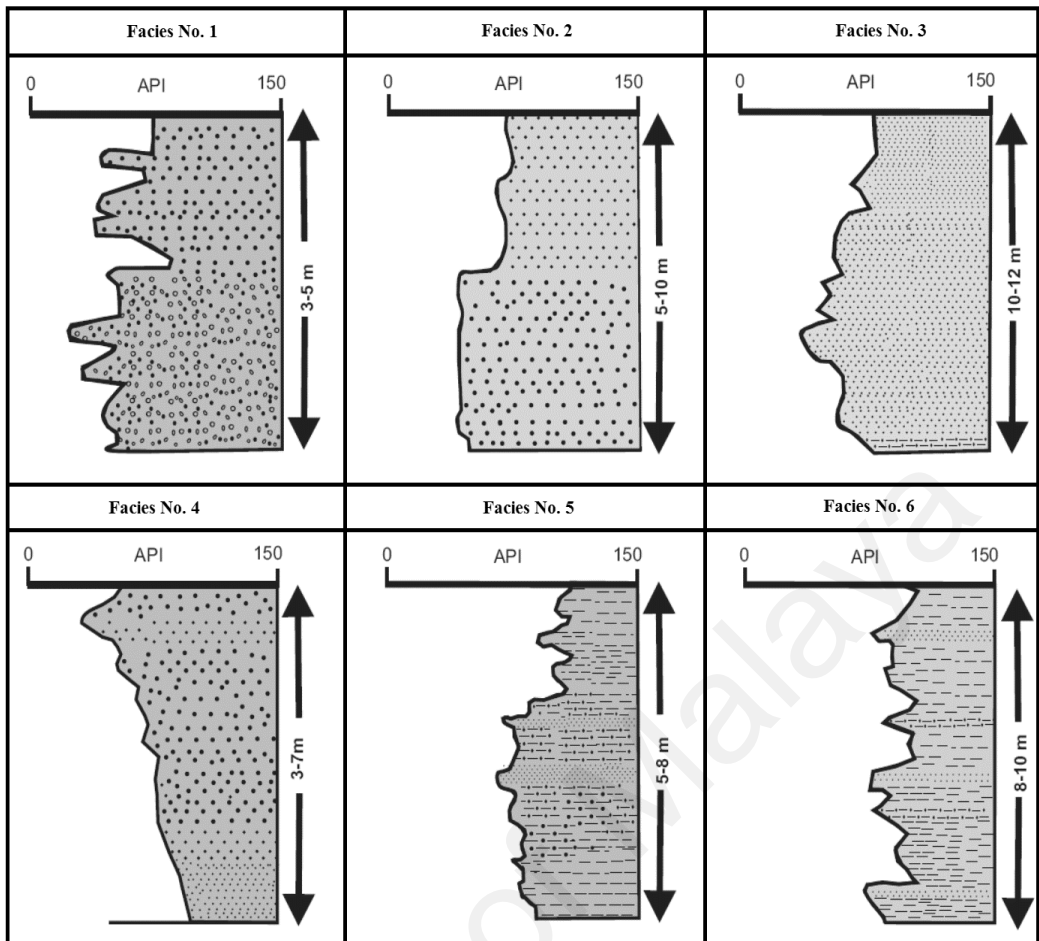


Figure 3.25: Types of lithological facies. Free image.

CHAPTER 4: RESEARCH DATA AND METHODOLOGY

4.1 Introduction

To achieve the targeted objectives of this study, multidisciplinary methods were used. These include evaluation of the source and reservoir rocks potentiality, structural interpretation and to propose a trap model of the Balkassar anticline. This chapter is summarizes the research methods applied on samples, data and the software that were used.

4.2 Research data

Seven outcrops and 3 deep mines rock samples were obtained from two different outcrop sections, namely Pail Village section and Mustafabad section near Choa Saidan Shah Village, At Mustafabad section, three rock samples were obtained from two different mines, namely Mine-X1 which was 248 feet deep and Mine-X2 which was 252 feet deep $32^{\circ} 43' 0.99296''$ N, $72^{\circ} 56' 28.12434''$ E, and two samples were obtained from 17 feet outcrop section exposed from bottom to top with an interval of 5.6 feet $32^{\circ}43'04.9''$ N $72^{\circ}56'23.4''$ E (Fig. 4.1 to 4.5). The remaining five samples were obtained from outcrop of Patala Shale section at Pail Village, which is also the type section of Patala Shale $32^{\circ} 35' 57''$ N, $72^{\circ} 27' 22''$ E. (Shah, 2009) (Fig. 4.6 to 4.9). For seismic structure interpretation, the seismic sections includes (Printed seismic sections and in soft form).

In soft form, grid of eleven seismic dip and strike lines in SEG-Y (see section 1.5.2) (Fig. 1.3) format were used along with complete logging datasets that has penetrated the Paleocene source and Eocene reservoir rocks until Salt Range Formation which is the oldest formation. For microfacies analysis 19 outcrop samples were obtained from Mustafabad and Pail Village section and were subjected to petrographic analysis using

petrographic polarizing microscope in laboratory. For lithofacies analysis data from well log datasets have been used in Interactive Petrophysics software, this includes gamma ray log with resolution of 1 meter vertical, having counts measured on horizontal scale from 0 to 150 and were calibrated in API units. The research data also includes subsurface geological information and structural maps. Seismic and well data details are given below:

Table 4.1: Seismic and well datasets.

Dip lines	Strike lines	Wells
SOX-PBJ-01	SOX-PBJ-08	Balkassar-OXY-01
SOX-PBJ-02	SOX-PBJ-09	Balkassar 7
SOX-PBJ-03	SOX-PBJ-10	Balkassar 8
SOX-PBJ-04	SOX-PBJ-11	
SOX-PBJ-05		
SOX-PBJ-06		



Figure 4.1: Mine X-1 and Mine X-2 Mustafabad section near Choa Saidan Shah Village, and on top is Sakesar Formation.



Figure 4.2: Inside mine X-1.



Figure 4.3: Inside mine X-2.



Figure 4.4: Exposed Patala Shale, Mustafabad section.



Figure 4.5: Exposed Patala Shale Mustafabad section.

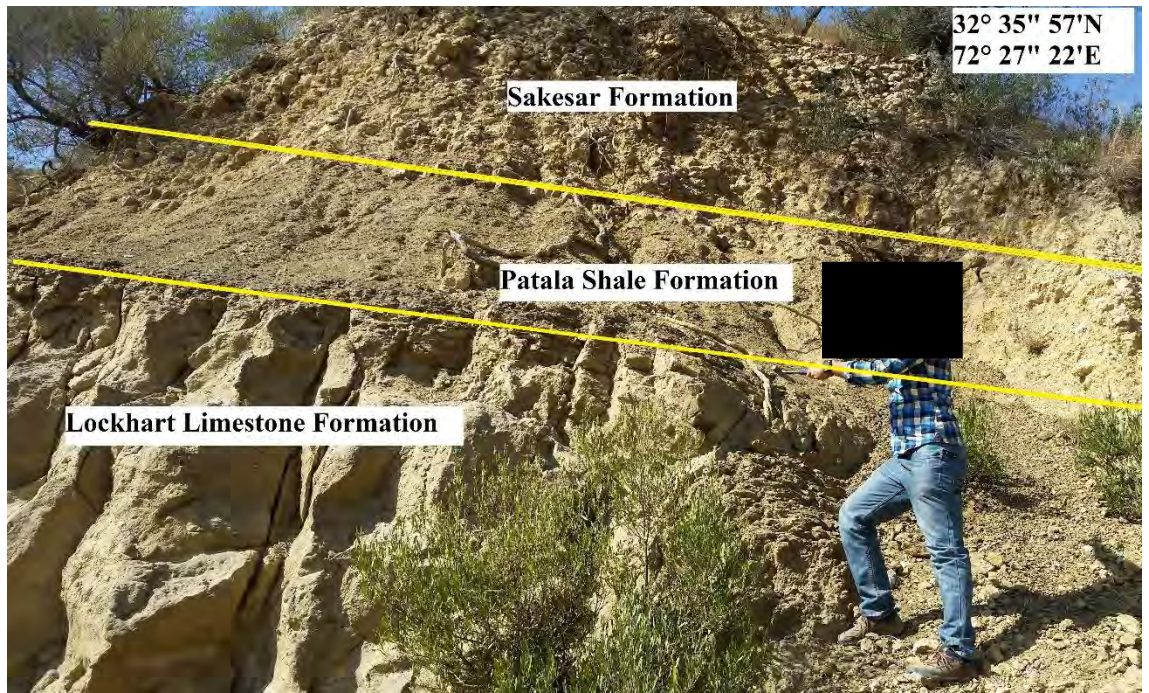


Figure 4.6: Exposed Patala Shale near Pail Village (Pail Village Patala Shale and Sakesar section).



Figure 4.7: Sample extraction from Patala Shale near Pail Village.



Figure 4.8: Measuring Patala Shale section near Pail Village.



Figure 4.9: Ten selected samples, acid, geological hammer, notebook and bags.

4.3 Organic geochemistry methods

For rapid and inexpensive evaluation of large amount of rock samples from the outcrop, source rock geochemical analysis are the practical exploration tools. In this study organic geochemical analysis were performed on ten fresh outcrop cutting samples from two outcrop units of Patala Shale Formation at Pail Village and Mustafabad section near Choa Saidan Shah Village (Figs. 4.1 to 4.9).

The main purpose of these analysis was to evaluate the shales organic matter type, organic content and thermal maturity. The assessment of source rock was based on geochemical analysis which includes TOC (Total Organic Carbon), Rock-Eval and vitrinite reflectance measurements (Tables 5.1 and 5.2).

University of Malaya

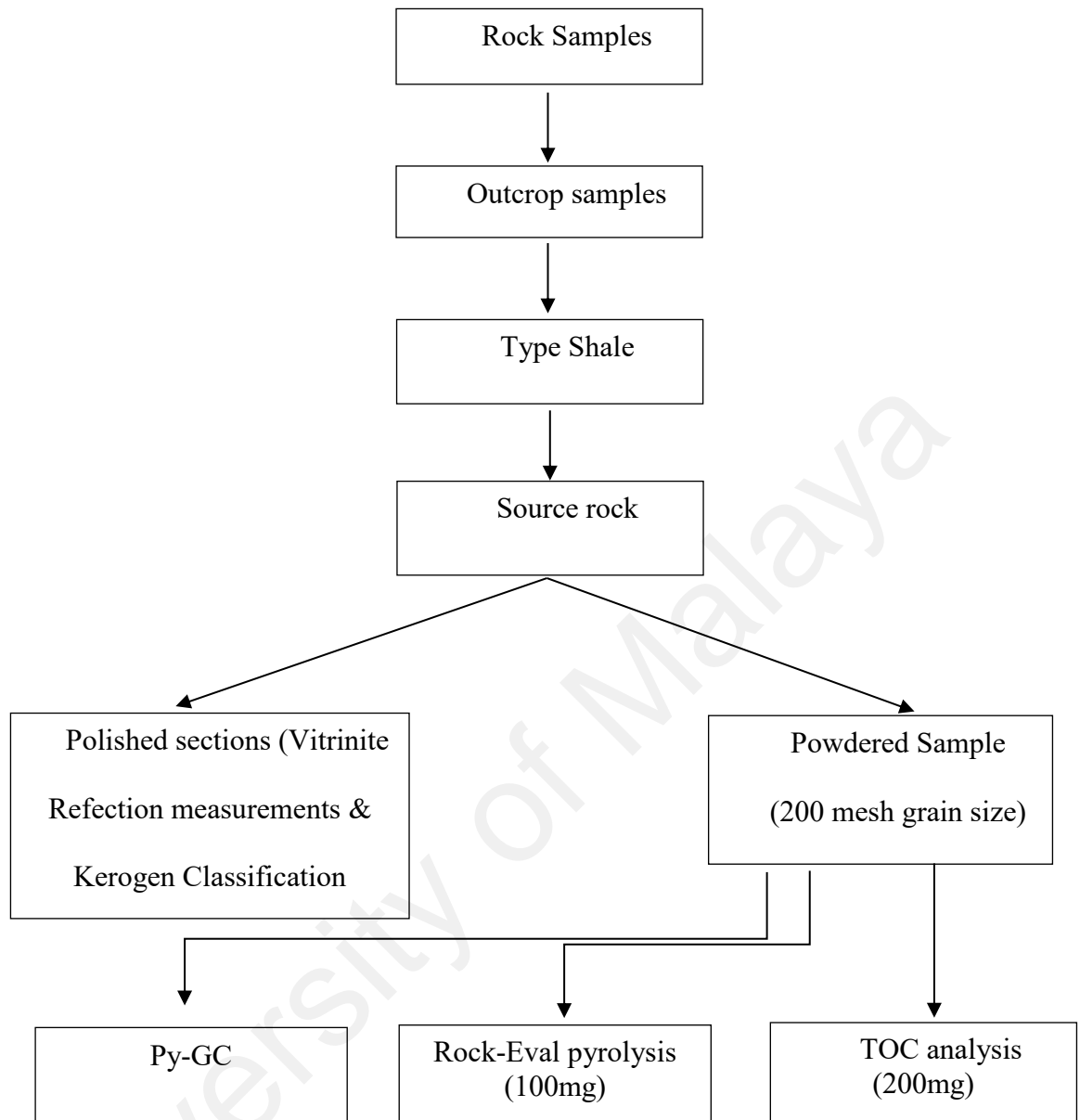


Figure 4.10: Flow chart of source rock characterization.

4.3.1 Sample preparation

The preparation of rock samples for organic geochemical study was done by following the procedure and instructions of Peters & Cassa (1994). The samples were washed by fresh water followed by purified organic free water to remove mud. In this process the cuttings were wet-sieved with 2 μm top sieve and 180 μm bottom sieve, and then the samples were left to dry at room temperature. The samples which were greater than 180

μm and less than 2 mm in size were used for geochemical analysis (Peters and Cassa, 1994).

4.3.2 Analytical studies

4.3.2.1 Pyrolysis

The heating of organic matter to decompose it chemically in the absence of oxygen or any other reagent is known as pyrolysis. In the chemical analysis, it is used for breaking down the organic matter into simpler molecules for identification of type, quantity and thermal maturity of organic matter e.g. using Rock-Eval (RE).

4.3.2.1.1 Rock-Eval pyrolysis and Total organic carbon (TOC)

Rock-Eval pyrolysis (RE) as well as TOC determination was carried out for samples to determine kerogen type, source richness, and level of thermal maturity.

4.3.2.1.1.1 Total organic carbon (TOC)

The quantity of organic carbon in a rock sample is describe by total organic carbon (TOC, wt. %). In this study the samples were crushed and weighted with a very sensitive balance to measure 100 mg of rock sample from each sample. The TOC content of the samples were determined by utilizing a MultiEA2000 elemental analyzer instrument (Fig. 4.11).

4.3.2.1.1.2 Rock-Eval pyrolysis

To describe the petroleum generative potential of the potential source rock, Rock-Eval pyrolysis is used, by providing information about their organic matter (type, quantity and thermal maturity) (Fig. 4.12). Using Rock-Eval VI unit with total organic carbon module pyrolysis analysis was completed, and was carried out at Hydrocarbon Development

Institute of Pakistan (HDIP) Islamabad. The samples were analyzed by this procedure and the parameters that were measured which include S1, S2, S3 and Tmax (temperature of maximum pyrolysis yield). Then hydrogen index (HI) and oxygen index (OI) were calculated as per described by Espitalié et. al. (1977) and Peters & Cassa (1994). For kerogen type (quality) identification from Rock-Eval pyrolysis plots of Tmax (°C) against (HI) Hydrogen Index and (HI) Hydrogen Index against (OI) oxygen Index were used, whereas for quantity of organic matter identification, graph of TOC against S2 (mg HC/g rock) were plotted and the level of maturity was estimated by utilizing Tmax and (PI) production Index.



Figure 4.11: For TOC analysis Multi EA2000 elemental analyzer.

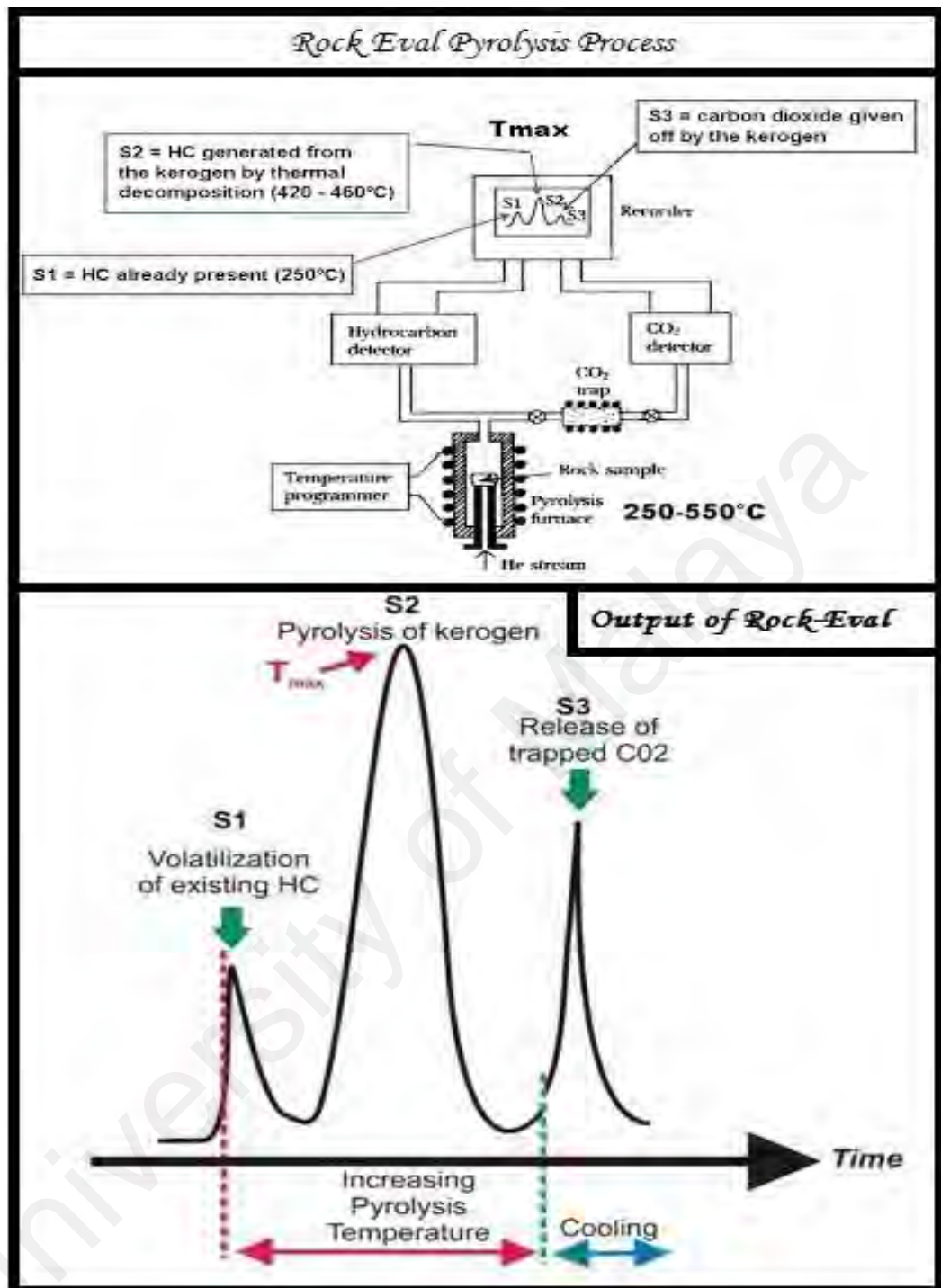


Figure 4.12: Rock-Eval process and output of Rock-Eval that is recorded. Free image.

4.3.2.1.1.3 Pyrolysis-Gas Chromatography

Pyrolysis-Gas Chromatography (Py-GC) analysis were performed using a single shot (for S2 analysis) Pyrolyzer Py-2020iD. The pyrolysis gas chromatography analysis of the S2 peak material gives information regarding the quantitative and qualitative chemistry of the thermal decomposition products of the kerogen (Dembicki, 2009). This provides direct indicator of kerogen type and types of hydrocarbons that can be generated by the kerogen during maturation process (Giraud, 1970; Larter & Douglas, 1980).

Py-GC was applied to provide compositional and structural characteristics of the kerogen and hydrocarbon potential possessed by the kerogen. This pyrolysis analysis is carried out using Pyrolyzer System which can perform thermal distortion (from 40-300°C) and pyrolysis at 600°C. The system is coupled to an inert (quartz and Ultra Alloy-5), 30 mm, 0.25 mm internal diameter column (0.52 μ m film thickness) fitted to an Agilent GC chromatograph equipped with flame ionization detector. The pyrolysis products passed through a GC column and released over a temperature range of 300-600 °C at 25°C/min. Identification of peaks based on reference chromatograms was done manually with Agilent ChemStation software.

4.3.2.1.1.4 Organic petrology : vitrinite reflectance

The degree of organic maturity was also investigated by vitrinite reflectance analysis. In this petrological analysis, the vitrinite reflectance (%Ro) was measured on dispersed organic matter in the studied Patala Shale. The analysed samples were first dried and crushed (about 1-2mm fragments). The sediments were mounted in setting polyester (Serifix) resin with hardener and the sediments were allowed to set. The samples were then subjected to ground flat on diamond lap and afterwards polished on isopropyl alcohol-lubricated silicon carbide paper of various grades. Lastly, the samples were

polished to a highly reflecting surface using progressively finer alumina powder (5/20, 3/50 and gamma).

Vitrinite reflectance measurement was performed using a Leica CTR6000M microscope equipped with Diskus Fossil software. A leuko-saphir standard (0.589%Ro) was used for calibration. Considering the availability and mode of occurrence of the vitrinite particles, between 15 to 50 measurements were obtained. The measurements were carried out under white light using an oil immersion X50 objective. The measured vitrinite reflectance values are shown in table 5.1 and table 5.2.

4.4 Microfacies analysis

For identification and interpretation of microfacies and their depositional environment, field study was carried out at two outcrop sections of Sakesar Formation, namely Mustafabad and Pail Village section, in Eastern Salt Range area. The study was carried out to decipher the microfacies, diagenetic properties, environment of deposition and reservoir potential of carbonate rocks only and not for the sandstone and shales samples due to their friable nature. Thin section laboratory investigations were performed using petrographic polarizing microscope for detailed petrographic analysis. For the interpretation of reservoir potential, stained thin sections were prepared from outcrop samples. A total of 19 samples were collected from both sections.

4.4.1 Sample preparation

Limestone is a sedimentary rock which is composed of largely minerals aragonite and calcite and these are the different forms of calcium carbonate CaCO_3 . Various limestones consist of skeletal fragments of marine organism such as foraminifera or coral. Following procedure was used to prepare sample for analysis.

1. The sample was first cut to 8-10mm piece from main sample by Geofoms's left side cutting station, then the glass slides were grind to make its surface rough so that the sample can fix on the slide. And then the sample flat surface were rubbed with silicone carbide and water so that its surface become rough.
2. The samples were then fix to glass slide using KEPT epoxy resins and were placed in the Geofix for bonding samples to the slide under pressure.
3. The glass slide were then put in vacuum chuck and were cut to ~2.0 mm thickness using special slide cut on the Geoform. The sample were touch with micrometer to adjust the digital position of sample to zero, and then the samples were grinded with grinding cup from 2.0 mm to 80 microns. The Kemtech vacuum jig was set to 30 mic to get the final thickness of sample and were mount to vacuum jig face.
4. The samples were lap on the Kemtech III machine using silicone carbide and water until the jigs diamond faced stopped ring fully contacts the cast iron lapping plate, there is an obvious change in sound which can be heard when this point is reached which confirms that the sample slide have lapped to the set thickness.
5. Then the slide was removed from jig and cleaned and inspected, and were further subjected for polishing on Kemtech III. After cleaning the vacuum jig using ultra sonic cleaner for removing the lapping slurry contamination the diamond stop ring was adjusted above the vacuum face late. Then cast iron lapping plate was replaced with aluminium lift off disc and PSUM polishing pad was mounted.
6. With diamond suspension the Aku-Disp slurry pump was charged and programmed the pump to dispense a 2 second supply of slurry every 8-10 second. Now the lapped samples were mount to the clean vacuum jig and polished on PSU and MBL cloths working down to the diamond suspension micron size to the required thickness and surface finish i.e. 30 micron. In this way the samples were prepared for analysis.

After preparing the sample the analysis was done using Michel-Levy interference color chart. Usually quartz is used as a gauge for determining the thickness as it is one of the most abundant mineral. Then the sample slide were placed between two polarizing filters set at right angles to each other, the optical properties of minerals in thin section alter the color and light intensity. Different minerals have different properties and most rock forming mineral can be identified easily.

Table 4.2: Equipment used for sample preparation.

For Cutting & Grinding		For Polishing	
Equipment Used:	GEOFORM Precision Thin Section Cutting and Grinding Machine	Equipment Used:	Kemtech III Thin Section Lapping Machine
Cutting Disc	Ø200 Diamond Cut-off wheels (Metal Bonded, high conc.)	Sample Holder	Vacuum jig (Specimen Fixture)
Grinding Wheel	Ø 175 Diamond cup grinding wheel, 35 mic	Plate/Pad	Cast Iron Lapping Plate, PSU-M & MBL-M Polishing Pad
	Standard Slides 27 x 46 x 1.27, 144 pcs.		

4.5 Seismic data interpretation

The study area of Balkassar was surveyed by seven dip lines and four strike lines. The orientation of these seismic lines are northwest-southeast and north-south. The Seismic lines were recorded by Oil and Gas Development Company Limited (OGDCL) in 1981. 4ms processing sample was used. Vibrosise were used as energy source and symmetric and A-symmetric Geophone spread geometry were used to acquire data. The main and most important objective of seismic data interpretation is the extraction of all possible information of the subsurface from processed seismic data (Onajite, E., 2013). This contains stratigraphy, structure, subsurface rock properties, stress, velocity and also fluid changes in reservoir in time and space. Good knowledge of the area and local geologic

history is very important to interpret the seismic section and make quality decisions of the seismic data (Gadallah & Fisher, 2008; Onajite, E., 2013).

Seismic sections are kind of display of seismic data along a line, that can be 2D seismic profile or a single profile that has been extracted form 3D seismic data (Gadallah & Fisher, 2008; Telford, 1990). In this study 2D seismic sections were used for interpretation (e.g. Fig. 4.13). First the printed seismic sections were interpreted manually and later using Petrel software for the interpretation of seismic sections in soft form (SEG-Y format). A seismic section has various traces with location which is along x-axis and a two-way travel time or sometimes depth along the y-axis (Telford, 1990).

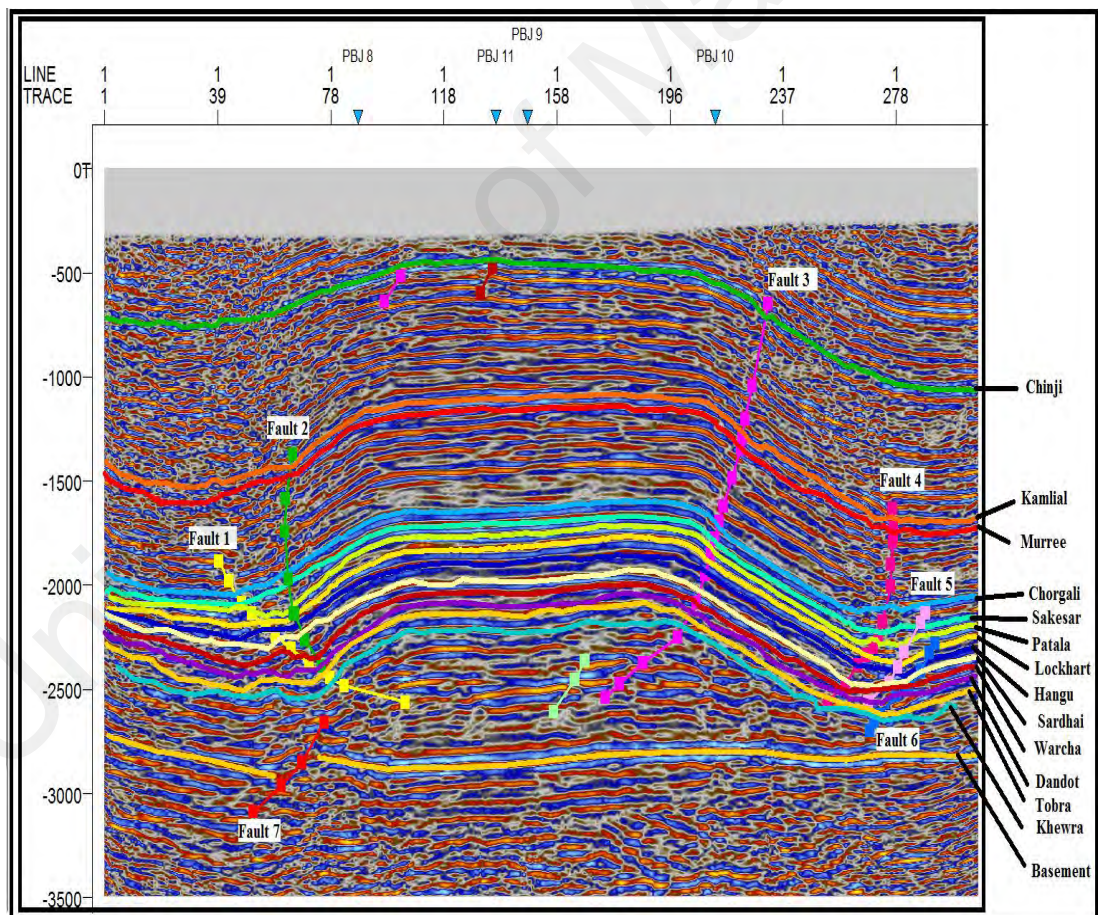


Figure 4.13: Example seismic section SOX-PBJ-04 showing different reflectors and faults in subsurface.

4.5.1 Base map

The Petrel software was used to generate the base map through loading the navigation SEG-Y file to import all shot points of the studied seismic sections. Three wells Balkassar OXY-1, Balkassar 7 and Balkassar 8 were also imported on the base map by importing their las file to show their location on base map (Fig. 4.14).

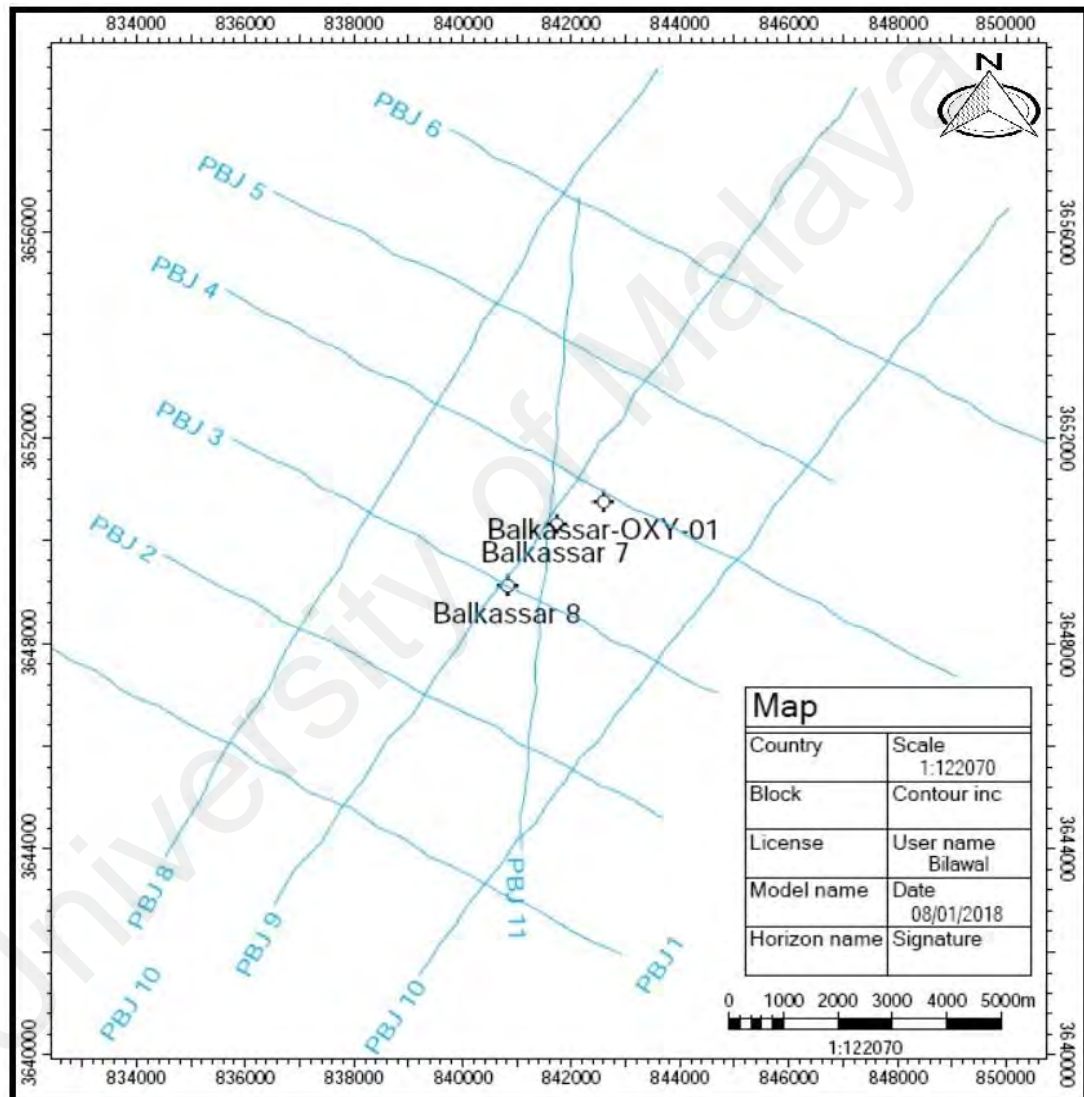


Figure 4.14: Showing the base map that contains all seismic lines and wells location of the study area.

4.5.2 Horizon marking and interpretation

On seismic section horizon is an event, something that can be picked and tracked. Horizon interpretation implies tracking and picking of consistent seismic reflectors on seismic section with the aim to spot hydrocarbon accumulation, calculating their volumes and delineating their extent (Onajite, E., 2013).

Horizon marking is mapping laterally consistent geologic structures by marking the reflectors on seismic section (Kearey, 2013). For marking the horizons of interest manually of printed seismic sections, in this study, velocity functions on top of all shotpoints on all seismic lines were used, which contains interval, root mean square velocity, shotpoint number, time in millisecond, latitude and longitude.

All of this information were used in excel to find all other parameters required for marking the horizons of interest manually on seismic section. The required parameters were: time in seconds, average velocity, interval time, depth (ft) and depth in meters.

4.5.3 Parameters required

4.5.3.1 Time in seconds

As time on seismic section is in milliseconds that was converted by using formula

$$T_{\text{sec}} = \frac{T_{\text{ms}}}{1000}$$

4.5.3.2 Average velocity

Average velocity of seismic P-waves were calculated by using following parameters in a formula.

$$V_{\text{avg}} = \frac{V_{\text{int}} \times (T_1 - T_2) \times (V_0 - T_2)}{T_1}$$

Where as

V_{avg} = average velocity

V_{int} = Velocity interval

T_1 = time in second of same velocity

T_2 = time of upper velocity

V_o = assumed upper velocity

4.5.3.3 Depth

Depth is calculated by using a formula:

$$S = \frac{VT}{2}$$

S= depth

V= calculated average velocity of specific horizon

T=time of specific horizon two-way time

The depth is calculated by applying the above formula on parameters given in velocity functions, as in the velocity functions the time is two-way travel time so the depth calculated from velocity functions were then divided by 2 to get one-way travel time and get accurate depth.

4.5.3.4 Time interval

Time interval is noted by eliminating the picked trough time of the horizon from the picked crest time of horizon.

$$T_{int} = T_2 - T_1$$

T_1 = trough time

T2 = crest time

By using the solved velocity function from the excel work sheet T1 and T2 are used to pick their corresponding depth that is D1 and D2 at every shotpoint.

4.5.3.5 Interval velocity

Interval velocity of every horizon is calculated by using the formula,

$$V_{avg} = \frac{D2 - D1}{T2 - T1}$$

Whereas

D1 = Depth at T1 in solved velocity function

D2 = Depth at T2 in solved velocity function

T1 = Trough time

T2 = Crest time

After getting all of these required parameters solved, the horizons of interest were marked on seismic sections and were matched with the depths given in well tops wells las file.

4.5.4 3D Horizon mapping

The velocity analysis that has been conducted for horizon marking in which interval, average and mean average velocities were calculated for all horizons, were later used for horizon mapping. For mapping horizons by Petrel software, the time picking was conducted for all horizons of interest below all shotpoints and noting down all shotpoint number and combining these with coordinates of all short point and using them to

generate 3D maps of horizons. For depth horizon mapping, first the time seismic sections were converted into depth section (domain conversion which allows to take data from time domain and convert it to depth domain) and then contour maps are integrated (Fig. 3.27).

4.5.4 Seismic to well tie to mark horizons in petrel

The depths of wells are measured either in meters or in feet. In seismic recording TWT two way travel time is used as a vertical scale. The procedure used for comparing well data with seismic section is known as seismic to well tie to pin point mark horizons on seismic section. In this procedure synthetic seismogram is generated. A synthetic seismogram is created by convolving reflectivity derived from density logs and digitized acoustic logs with the wavelet derived from seismic data. The quality of match between synthetic seismogram depends of the seismic data quality and recorded well logs quality.

By analyzing the well location on base map, Balkassar OXY-1 is near to three seismic lines: SOX-PBJ-4, SOX-PBJ-9 and SOX-PBJ-11. SOX-PBJ-11 and SOX-PBJ-9 are strike lines and SOX-PBJ-4 is dip line, as all shotpoints were plotted on base map on the seismic lines (Fig. 4.11). By noticing nearest shotpoints to Balkassar OXY-1 well on these three seismic lines, the dip line SOX-PBJ-4 was used for generating synthetic seismogram. The nearest shotpoints of this major seismic line to the Balkassar OXY-1 well is shotpoint number 170 and 172.

Density and sonic logs from Balkassar-OXY-01 well digitized in Las file format, well ID, well name, well location (lat long), KB, datum, depth of formations and names of formations were used for generating synthetic seismogram in Schlumberger Petrel Interpretation software.

The formations marked on seismic section by using synthetic seismogram from the top are Chinji Formation, Kamliyal Formation, Murree Formation, Chorgali Formation, Sakesar Formation, Patala Formation, Lockhart Formation, Hangu Formation, Sardhai Formation, Warcha Formation, Dandot Formation, Tobra Formation, Khewra Formation and Salt Range Formation respectively.

After marking the horizons on seismic line SOX-PBJ-4, then all the other seismic lines, SOX-PBJ-1, SOX-PBJ-2, SOX-PBJ-3, SOX-PBJ-5, SOX-PBJ-6, SOX-PBJ-7, SOX-PBJ-8, SOX-PBJ-9, SOX-PBJ-10 and SOX-PBJ-11 in Petrel Software were tied with the SOX-PBJ-4 seismic line, called seismic to seismic tie to mark horizons on all seismic lines. Seismic to seismic tie is an essential step in seismic interpretation work flow (Gadallah, 2008; Kearey, 2013; Onajite, E., 2013; Telford, 1990). The procedure for seismic to seismic tie was performed to mark horizons on other seismic lines that cuts the major seismic line which is near to the Balkassar-OXY-01 well and hence for checking miss ties effect by comparing the seismic lines.

4.5.5 Petrel software interpretation

Petrel Software was used for the interpretation of seismic sections and well data. A total of seven major faults were marked on seismic section using fault polygon option and all of the horizons were picked and marked using synthetic generation option on petrel. Synthetic seismogram was generated by using SOX-PBJ-04 seismic line along with well logs of Balkassar-OXY-01 well (RHOB and DT) for acoustic impedance, well tops of Balkassar-OXY-01 well and check-shot survey file. The validity of this study interpretation was confirmed using the existing literature and geological maps (Kadri 1995; Lillie et al., 1987; McDougall & Khan 1990; Moghal et al., 2007; Pennock et al., 1989). The interpreted seismic sections were correlated with the well tops of Balkassar-

OXY-01 well by generating synthetic seismogram for enhancing and validation of the interpretation process (Fig. 4.15).

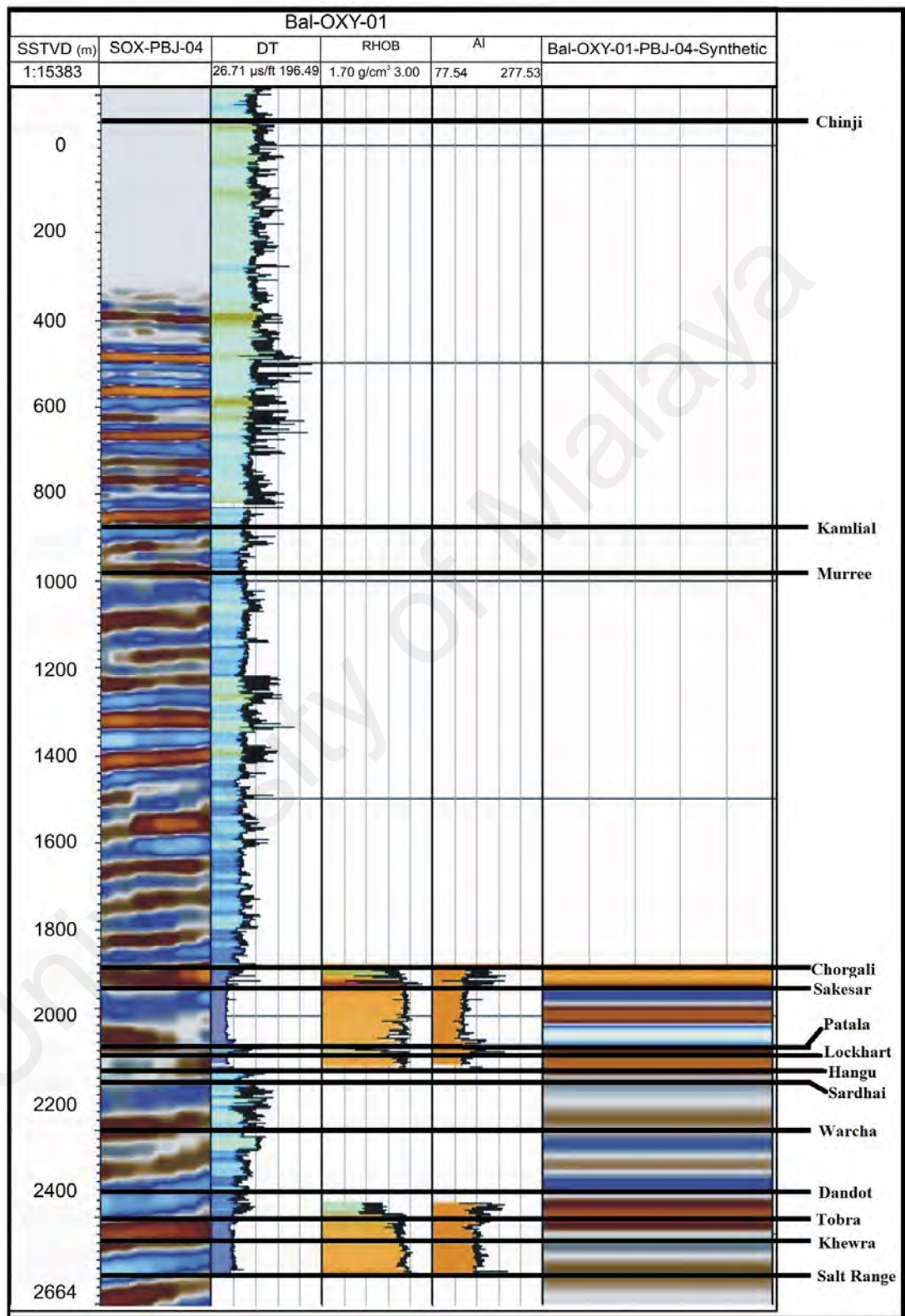


Figure 4.15: Showing the synthetic seismogram along with well tops from Balkassar-OXY-01 well.

4.5 Petrophysical well log analysis

Now a days well logs analysis is one of the most significant and powerful tool for investigating and acquiring information about reservoir properties like volume of shale, permeability, porosity, fluid saturation etc. (Asquith & Krygowski, 2004; Serra, 1983; Serra, 1986). All of the reservoir qualitative and quantitative petrophysical properties have been achieved by interpretation of well logs using a number of procedures (Lashin et al., 2003, 2006, Lashin, 2007; Lashin & Mogren, 2012; Lashin et al., 2016; Nabawy et al., 2009). Identification of lithology is essential for all other properties to be measured from logs especially fluid saturation.

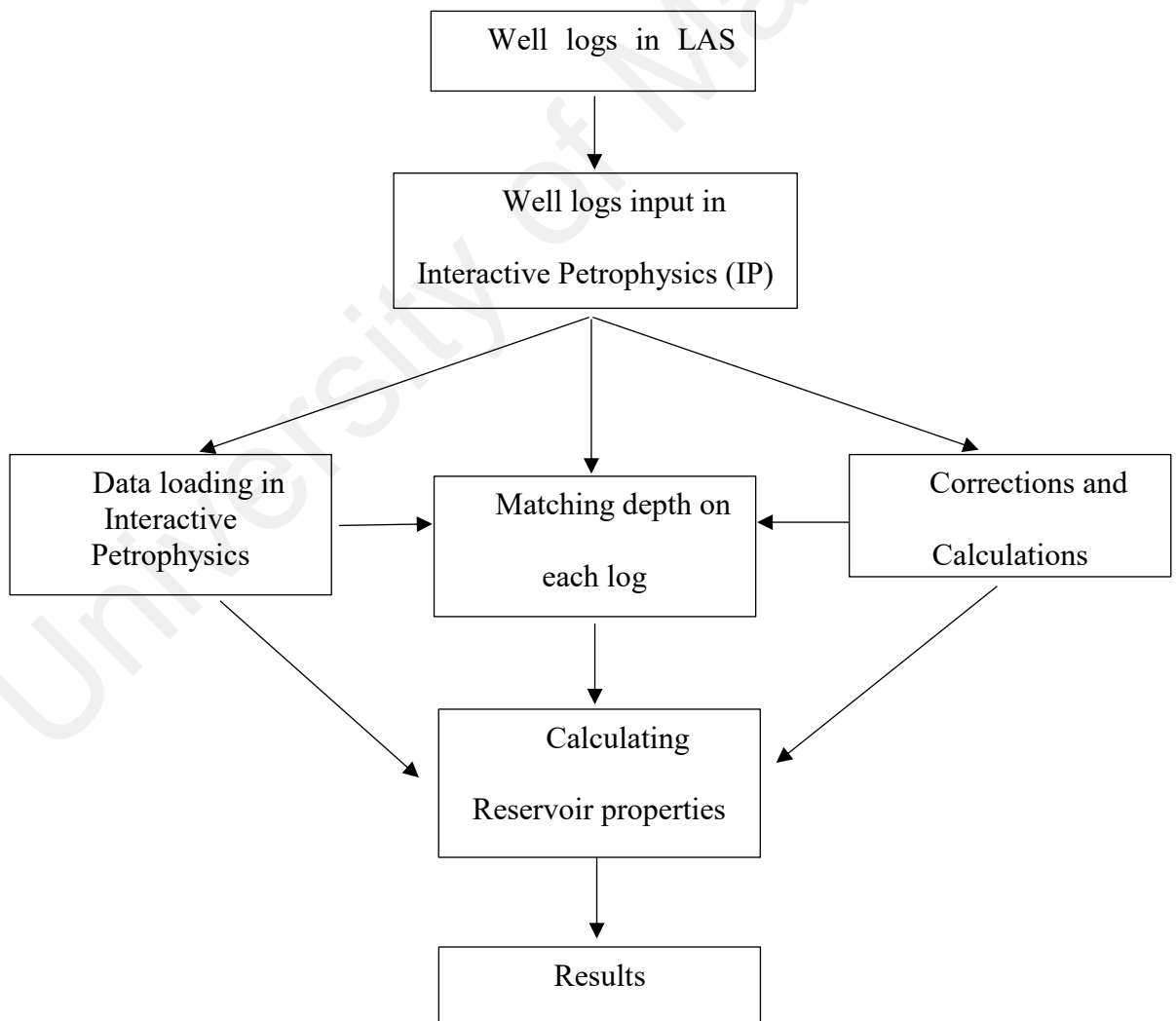


Figure 4.16: Data flow chart of well logs interpretation.

In this study, process of well logs analysis (Fig. 4.16) has been achieved by using Interactive Petrophysics (IP) software. This software has been used for delineating reservoir properties and evaluation presented by Schlumberger. The necessary corrections were applied to correct data for different environment and then the data was used for interpretation. Several processes were performed in this study for interpretation and are described below.

4.5.1 Corrections and Calculations

The depths of all well logs sets were matched with each other, and then were divided vertically into zones of interest of fixed intervals and thickness. Reservoir parameters and corrected well logs were plotted against depth. All different environmental calculations like mud weight, mud cake thickness, borehole size, mud salinity, temperature, pressure and formation water salinity in this study were corrected using Schlumberger corrections.

4.5.2 Interpretation

The main aim of well log interpretation is to define amounts and types of fluids in the formations. For determining all those properties formation porosity and shale volume estimation are required.

4.5.2.1 Shale volume

The most important parameter to be measured from well log is calculation of shale content. Shale volume is essential for correcting water saturation and porosity. Shale volume is considered a good indicator of reservoir quality, whereas lower shale content shows good reservoir quality. Shale volume can be measured from Gamma Ray log (Lashin et al., 2016), Resistivity logs and Spontaneous Potential log. In this study the Gamma Ray log was used for calculating the shale volume. For calculating shale volume, the following equations were used (Schlumberger, 1972).

$$IGR = (GR_{log} - GR_{min}) / (GR_{max} - GR_{min})$$

$$V_{sh} = 0.083 [2^{(3.7 * IGR)} - 1.0]$$

4.5.2.2 Procedure for finding different parameters from logs

Following few parameters were directly read from log track using Interactive Petrophysics (IP).

- i. Bulk resistivity of the formation (LLD) scale 0-2000 ohm.m
- ii. Formation depth in feet
- iii. Neutron porosity (NPHI) scale -0.15 to 0.45
- iv. Spontaneous potential (SP) scale 0-100mv
- v. Bulk density of formation (RHOB) scale 1.95 to 2.95

4.5.2.3 Porosity and Water Saturation

For calculating fluid saturation porosity measuring is an essential parameter. Porosity is mostly measured from well logs and several porosity tools are used for its correction (density, sonic and neutron tools are most commonly used). These tools for calculation are also effected by geological factors like lithology, fluid type, porosity type and formation matrix. For porosity to be measured accurately nearly actual value require knowledge of formation matrix, shale volume and fluid.

Readings from two logs, density and neutron were used from measuring total porosity. Total porosity can be measured by utilizing (Schlumberger, 1972) equation 1. for clean zone and Equation 2 for shaly formation.

Equation 1:

$$\phi_{ND} = \sqrt{\frac{\phi_N^2 - \phi_D^2}{2}}$$

Equation 2:

$$\phi_{ND} = \sqrt{\frac{\phi_{NC}^2 - \phi_{DC}^2}{2}}$$

4.5.2.4 Permeability

In this study, The Timur's (1968) equation of permeability was used to determine permeability.

$$K = (93 * \phi_a^{2.2} / S_{w\ iir})^2$$

Whereby:

ϕ_a = average porosity

$S_{w\ iir}$ = irreducible water saturation

K = Permeability.

4.5.2.5 Bulk volume of water (BVW)

BVW of hydrocarbons bearing zone was calculated based on the equation by Islam et al., (2013):

$$BVW = S_w * \phi_a$$

Whereby:

BVW = bulk volume of water

S_w = water saturation

ϕ_a = average porosity.

4.5.2.6 Pay reservoir and net pay

The criteria that has been adopted for reservoirs pay and net pay were adopted from Mehmood et al. (2015) who defined reservoir by shale volume less than 40% and porosity greater than 7%, this cut-off of 7% and shale volume cut-off of 40% was used for defining the reservoir quality in this study, or defining the pay reservoir water saturation cut-off of 50% was used. Whereas for net pay if the reservoir water saturation is less than 50% than the reservoir is considered to contain hydrocarbons in it (Mehmood et al., 2015).

4.5.2.7 Saturation of hydrocarbon (Sh)

Schlumberger log interpretation charts along with several equations were used in the process to find out certain unknown values to determine saturation of hydrocarbons.

- i. Formation temperature was determined by following formula, whereas bottom-hole temperature of 180 °F and 72 °F surface temperature was given on wireline logs and were used: (Fig. 4.17). $T_f = T_s + D_f (BHT - T_s / TD)$
- ii. Corrected R_{mf} Mud filtrate and R_m resistivity of mud at formation temperature. (Figure. 4.19).
- iii. Self-Potential determination directly by reading it from SP curve on log chart.
- iv. For R_{mf} / R_{we} ratio. Figure. (4.20) was used to measure the value.
- v. R_{we} was determined by dividing the corrected value for R_{mf} by the ratio of R_{mf} / R_{we} value.
- vi. Equation for R_{we} is: $R_{we} = R_{mf} / (R_{mf} / R_{we})$
- vii. R_{we} correction to R_w by using Figure. (4.18) and the value of R_{we} in step 5 to determine the correct R_{we} value.

viii. Saturation of water was determined by using the following equation:

$$S_w = \sqrt{\frac{R_w}{\phi^m * R_t}}$$

ix. Saturation of hydrocarbon can be determined at a given temperature by using

equation: $S_H = 1 - S_w$

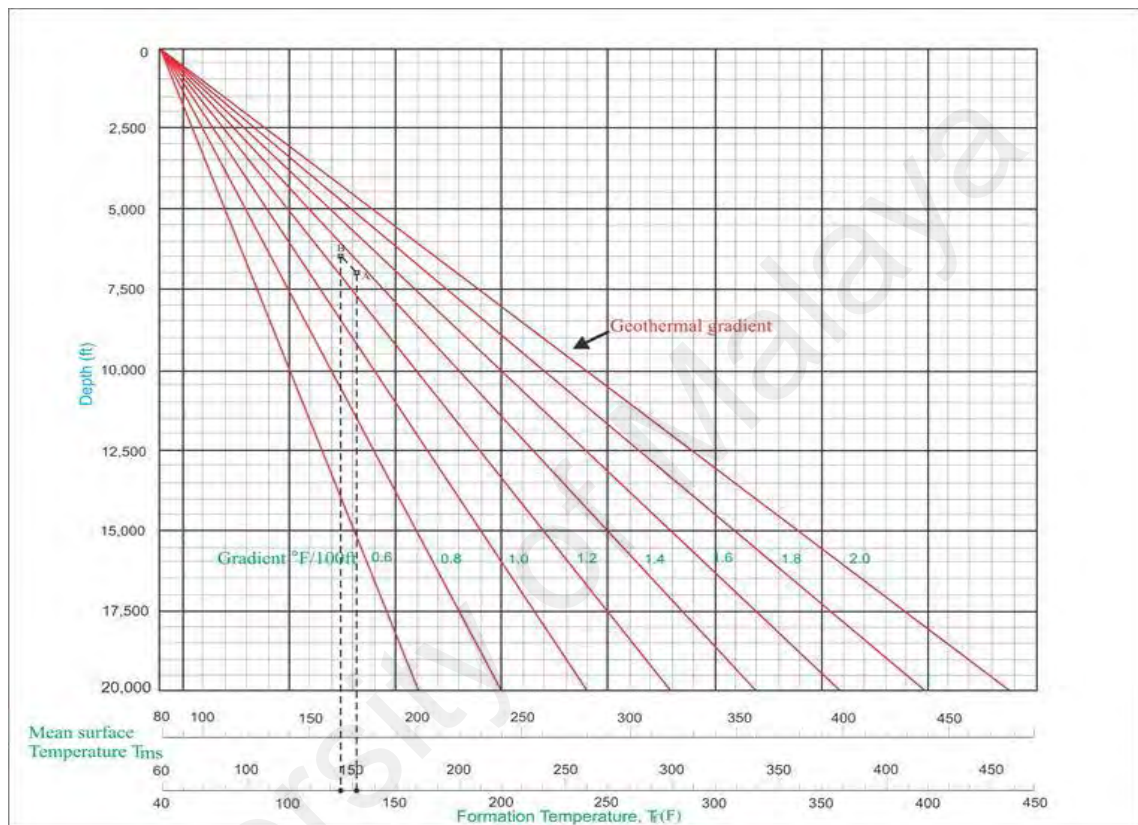


Figure 4.17: Determination of formation temperature at various depths. Free image.

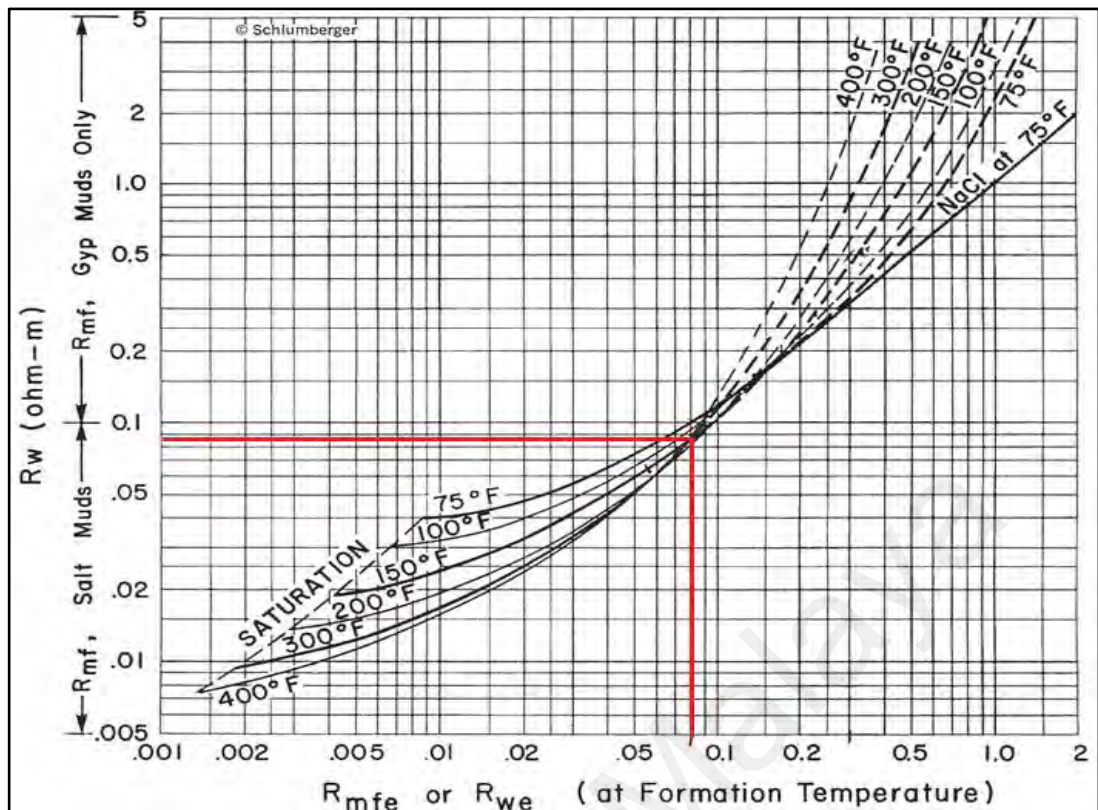


Figure 4.18: Determination of R_w from R_{we} .

As the mud filtrate resistivity values were obtained now these values were utilized in Figure (4.18) to convert them to equivalent mud filtrate resistivity then this equivalent mud filtrate resistivity values were used in a formula shown in step 6 to get equivalent water resistivity. This equivalent water resistivity were converted to water resistivity and ultimately this water resistivity were used to obtain water saturation.

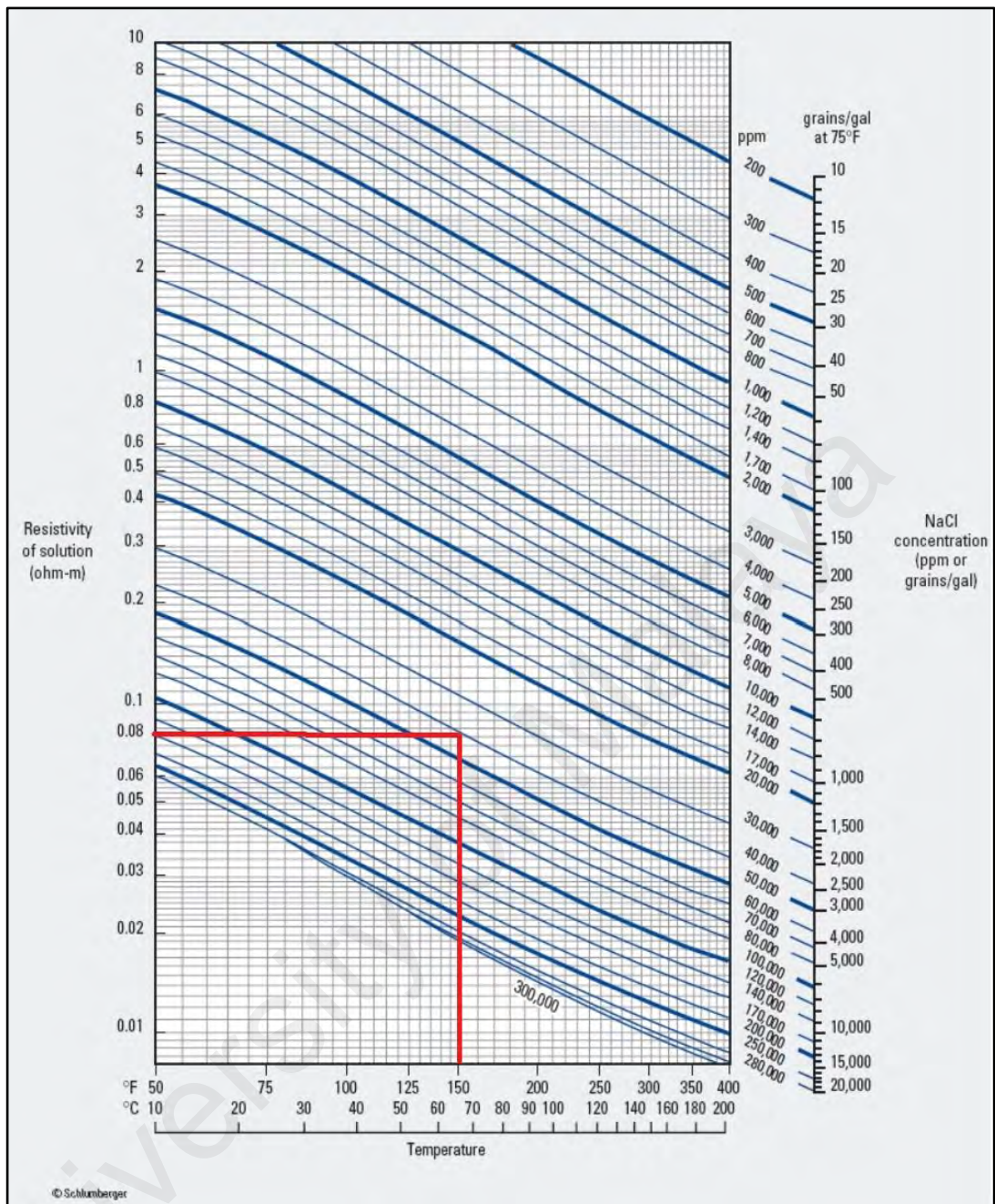


Figure 4.19: Correction of R_{mf} and R_{we} according to temperature.

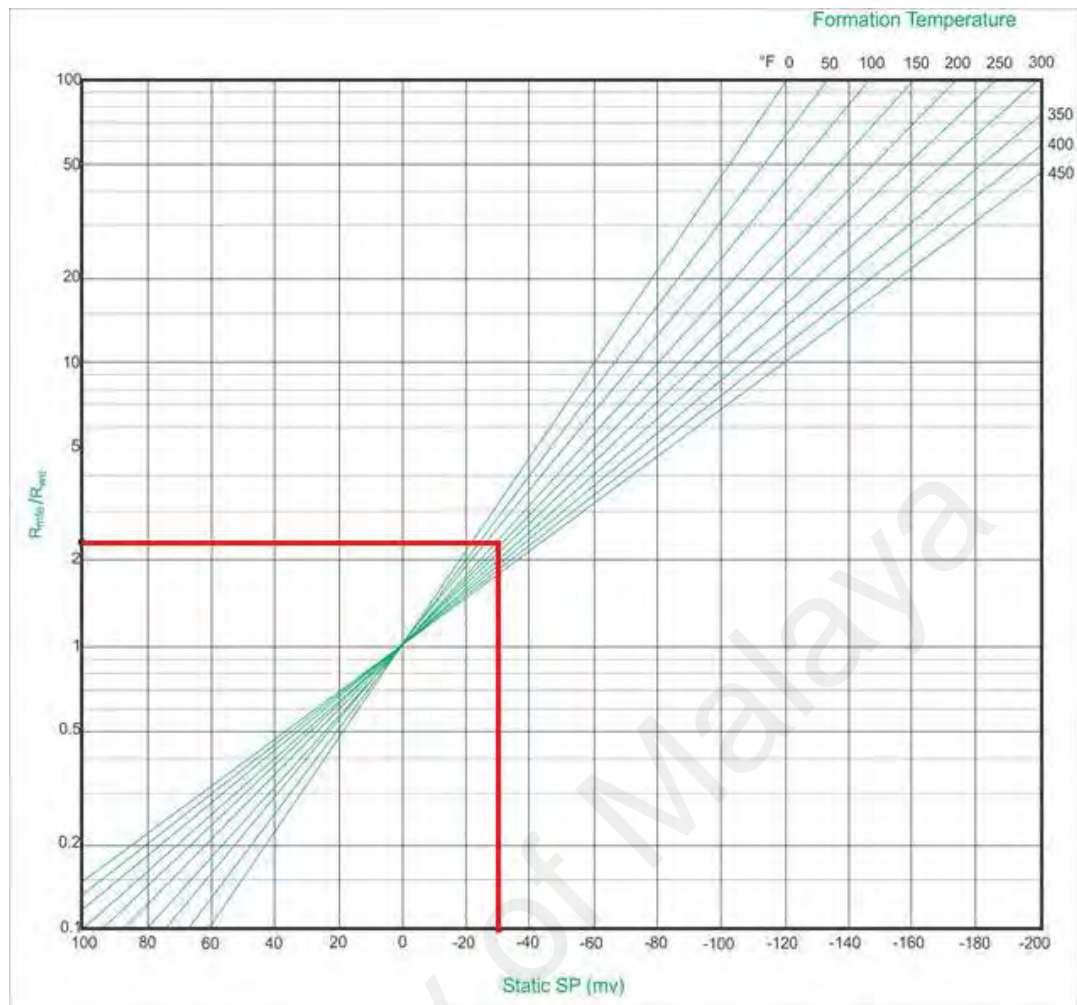


Figure 4.20: R_{mf} / R_{we} determination from Self-Potential.

As the mud filtrate resistivity in log header was measured at surface temperature which needs to be corrected at formation temperature for each value at certain depth to get mud filtrate resistivity at formation temperature. For this correction Figure (4.19) was utilized.

4.6 Lithofacies analysis

Gamma ray tool is one of the most important tool (Rider, 1990; Ghazi & Mountney, 2010), and this tool has been used in this study for subsurface facies analysis due to the characteristic response to different lithologies. Many difficulties were encountered in the interpretation of gamma ray logs shape because of the naturally existing radioactive

minerals, carbonates within some sandstone facies and detrital mica which gave rise to the values of gamma ray uncharacteristically.

To minimize this problem, the gamma ray logs generalized log trends were recognized and were compared to, gamma ray logs trends encountered in the Balkassar-OXY-01 well, the trends were also compared with existing nearest stratigraphic section of the rock as well as with the previous literature and work done in other parts of the Potwar Basin to enhance and validate the interpretation. The sequences of rocks were examined and identified by the trend of gamma ray curves at 1 m interval. Facies associations of sedimentary succession which were principally repeating and fining in the upward cycles were identified.

University of Malaysia

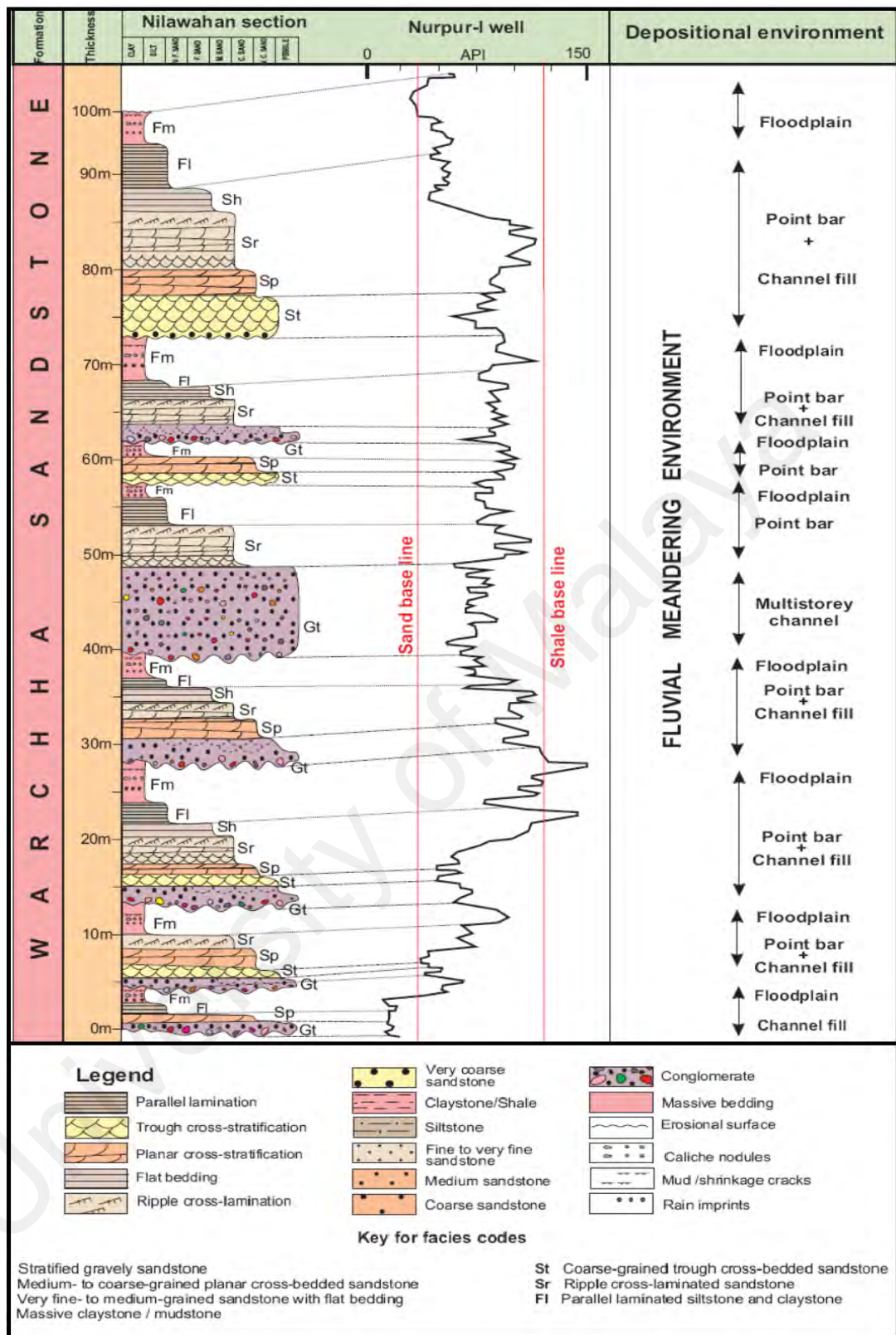


Figure 4.21: Warcha Sandstone generalized stratigraphic characteristics in Potwar Basin.

Free image.

4.7 Seismic facies analysis

Seismic facies analysis is interpretation and description of seismic parameters such as continuity, amplitude and configuration. The analysis was performed with an aim to identify different seismic facies in Balkassar subsurface using SOX-PBJ-04 seismic dip line. The procedure used in this study has been adopted from Futalan et al (2012). In this study four reflection attributes have been used to differentiate between seismic facies.

1. Internal configuration
2. Reflector continuity
3. Amplitude
4. External geometry

Internal configuration is the internal bedding patterns (wavy, convergent, oblique, parallel to subparallel and parallel to wavy), external geometry is the external behavior of reflectors with other strata (sheet to wedge, lens to wedge, sheet to mound), reflector continuity is the lateral continuity of strata and amplitude is the bedding thickness, spacing, density contrast and velocity,

CHAPTER 5: RESULTS AND DISCUSSION

5.1 Introduction

This chapter presents all of the results from organic geochemistry, seismic interpretation and petrophysical analyses performed in this study and their relevance are discussed in the following sub-sections.

5.2 Source rock evaluation

Source rock evaluation techniques that have been adopted in this study are explained below sub sections.

5.2.1 Organic matter richness and source rock quality

The organic richness and quality of the organic matter of the analysed potential source rock are evaluated based on the ratios and parameters that have been obtained from total organic carbon (TOC) and pyrolysis (Rock-Eval) and Py-GC.

5.2.1.1 Total organic carbon content and pyrolysis

Data of the total organic carbon and whole rock pyrolysis are as shown in Tables 5.1 and 5.2. Based on these data, kerogen type and source rock richness for the preserved organic matter in Patala Shales, as well as their thermal maturity were revealed. Within a sedimentary basin, among the prerequisite for source rock to generate oil or gas is the presence of sedimentary organic material in sufficient amount (see section 3.2.1) (Nixon, 1973; Peters & Cassa, 1994). The minimum amount of TOC acceptable for a source rock is 0.5% for shales and 0.2% for carbonates (see section 3.2.1 and Table 3.1) (Peters and Casa. 1994). The TOC vs S₂ plot (Fig. 5.1) indicates that all samples of the Patala Shale Formation possess a poor to fairly good source rock potential, having the values of TOC ranging from 0.25 to 1.16 wt% with average of 0.55 wt%. However based on the pyrolysis

hydrocarbon yield (S2) that ranges between 0.11 to 0.63, with average of 0.34 mg/g (Table 5.1 and Table 5.2), all the analysed rocks can be categorized as having poor source potential for petroleum generation. This is further indicated by the plot of S2 vs TOC as shown in Fig. 5.1. This plot has been applied by many previous workers such as Hakimi et. al. (2012), Shah & Ahmed (2018), and Fazeelat et. al. (2010).

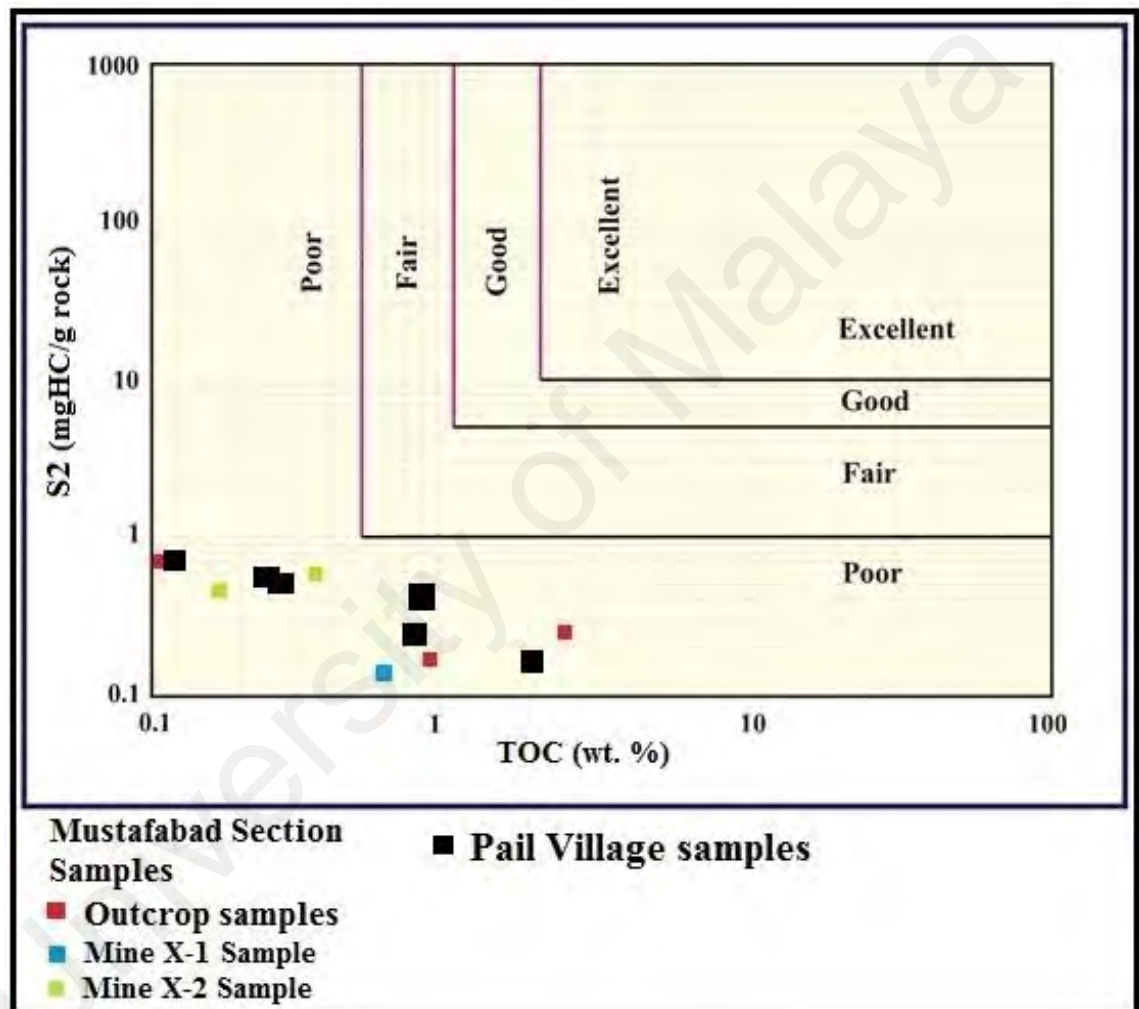


Figure 5.1: Distribution pyrolysis of S2 yields versus (TOC) total organic carbon plot.

Table 5.1 Pyrolysis (SRA), TOC data parameters and measured vitrinite reflectance (%Ro) values of the Patala Shale samples of Mustafabad section.

Sr. No.	Sample No.	%TOC	S1 (mg/g)	S2 (mg/g)	S3 (mg/g)	T-max (°C)	S2/S3 (mg/g)	HI	OI	PI	G.P (S1+S2) (mg/g)	S1*100/TOC	%Ro
1	Mine X-2, Sample 2	0.33	0.01	0.56	0.11	429	5.09	170	33	0.02	0.57	3.03	0.75
2	Outcrop # 3	1.16	0.01	0.24	0.18	419	1.33	21	16	0.04	0.25	0.86	0.73
3	Mine X-2 #1	0.16	0.01	0.47	0.23	427	2.04	294	144	0.06	0.48	6.25	0.84
4	Outcrop # 2	0.93	0.01	0.17	0.08	415	2.12	18	9	0.06	0.18	1.07	0.70
5	Mine X-1	0.57	0.01	0.11	0.08	417	1.37	19	14	0.08	0.12	1.75	0.74

HI: Hydrogen Index = S2 x 100/ TOC, mg HC/g TOC

S1: Volatile hydrocarbon (HC) content, mg HC/g rock

S3: Carbon dioxide yield, mg CO₂/ g rock

GP: Genetic potential = S1+S2

Ro: Vitrinite reflectance (%)

OI: Oxygen Index = S3 x 100 / TOC, mg CO₂/g TOC

S2: remaining HC generative potential, mg HC/g rock

Tmax: Temperature at maximum S2 peak

PI: Production index = S1 (S1+S2)

TOC: Total organic carbon, wt.%

Table 5.2 Pyrolysis (SRA), TOC data parameters and measured vitrinite reflectance (%Ro) values of the Patala Shale samples of Pail Village.

Sr. No.	Sample No.	%TOC	S1 (mg/g)	S2 (mg/g)	S3 (mg/g)	T-max (°C)	S2/S3 (mg/g)	HI	OI	PI	GP(S1+S2) (mg/g)	S1*100/TOC	%Ro
1	Sample 2	0.25	0.03	0.63	0.17	429	3.70	252	68	0.01	0.66	12	0.60
2	Sample 3	0.98	0.08	0.34	0.26	422	1.30	34	26.5	0.03	0.42	8.16	0.51
3	Sample 4	0.28	0.09	0.52	0.19	429	2.73	185	67.8	0.05	0.61	32.14	0.66
4	Sample 5	1.06	0.05	0.17	0.12	424	0.91	16	10.7	0.008	0.16	4.46	0.64
5	Sample 6	0.75	0.06	0.24	0.09	427	2.66	32	12	0.018	0.3	8	0.66

HI: Hydrogen Index = S2 x 100/ TOC, mg HC/g TOC

S1: Volatile hydrocarbon (HC) content, mg HC/g rock

S3: Carbon dioxide yield, mg CO₂/ g rock

GP: Genetic potential = S1+S2

Ro: Mean vitrinite reflectance in oil immersion (%)

OI: Oxygen Index = S3 x 100 / TOC, mg CO₂/g TOC

S2: remaining HC generative potential, mg HC/g rock

Tmax: Temperature at maximum S2 peak

PI: Production index = S1 (S1+S2)

TOC: Total organic carbon, wt.%

The type of organic matter (OM) was characterized by pyrolysis analysis based on HI values (see section 3.2.3 and Table 3.1 for standard acceptable values). In general, the HI values are less than 300mg HC/g TOC. Samples with moderate HI values can be of either marine or lacustrine origin (Harris et al., 2004; Hakimi et al., 2012; Hakimi & Abdullah, 2013). Previous studies by Shami (2002), Fazeelat et al. (2010) and Zahid et al. (2014) had recognized the probable shallow marine origin of the Patala Shale Formation. The kerogen classification based on the HI vs Tmax plot was also carried out by previous workers (Fazeelat et al., 2010), which was also used to determine the maturity and kerogen types.

The Patala Shales are generally of poor quality and possess low to moderate HI values ranging between 18 mg HC/g TOC to 294 mg HC/g TOC (Table 5.1 and Table 5.2). The generally low HI values suggest that the Patala Shales are dominated by Type IV kerogen with Type III and mixed Type II-III kerogens as shown in Fig. (5.2) (see Table 3.1).

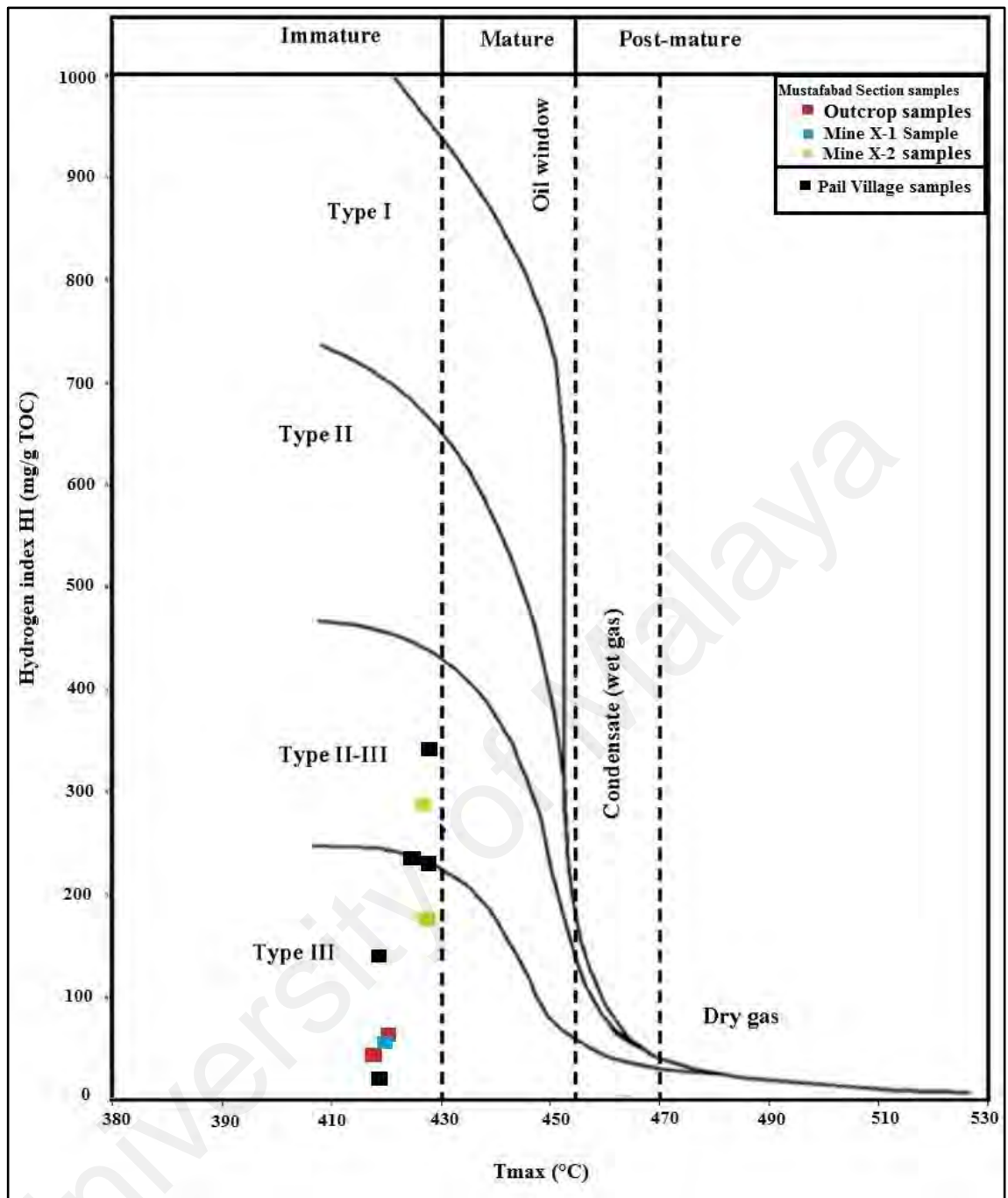


Figure 5.2: Plot of hydrogen index (HI) vs pyrolysis T_{max} , showing the thermal maturity stages and kerogen type of the analyzed Patala Shale samples.

5.2.1.2 Kerogen pyrolysis (Py-GC)

The pyrolysis-gas chromatography (Py-GC) technique was developed in the sixties as a tool to elucidate structural features of kerogens (Giraud, 1970; Larter & Douglas, 1980).

This method has been used in the petroleum exploration to provide a direct indicator of

the kerogen composition and type of hydrocarbons that can be generated by the kerogen during the maturation process (see section 4.3.2.1.1.3) (Dembicki et al., 1983; Larter & Douglas, 1980). Many examples showing the differentiation of algal, marine or terrestrial kerogens by Py-GC fingerprints are published in literature. (e.g. Horsfield, 1989; Larter, 1984). Behar and Pelet, 1985 also show clearly how the three main types of kerogens can be distinguished by the carbon number distribution of n-alkanes. These authors stated that type I pyrograms contains large amount of n-alkanes/ n-alkenes in C₂₀- C₃₀ range, whereas in type II pyrograms most of these compounds have less than 20 atoms of carbon. Dembicki, (2009) also suggested that a high concentration of >C₁₅ compounds is characteristics of type I kerogens, whereas Type III pyrograms shows most products in the <C₁₀ fraction. Thus besides pyrolysis (Rock-Eval) data the composition of pyrolysis products fragments (Py-GC) can be used to interpret kerogen characteristics of source rocks (e.g. Giraud, 1970; Larter & Douglas, 1980).

Examples of pyrograms of the analysed Patala Shale samples are as shown in figures (5.3 and 5.4). The program showed that no hydrocarbon has been generated, and thus no peaks can be identified. This is expected as the S₂ values are very low in all of these samples. In support, petrographic observations revealed that the dominant organic matter type (maceral) is inertinite, with common presence of reworked vitrinite (Fig. 5.6). These types of organic matter are categorized as Type-IV kerogen which does not generate hydrocarbons (see section 3.2 and Table 3.1), except possibly small amounts of methane (Hunt, 1996).

S2 Pyrolysis GC Traces

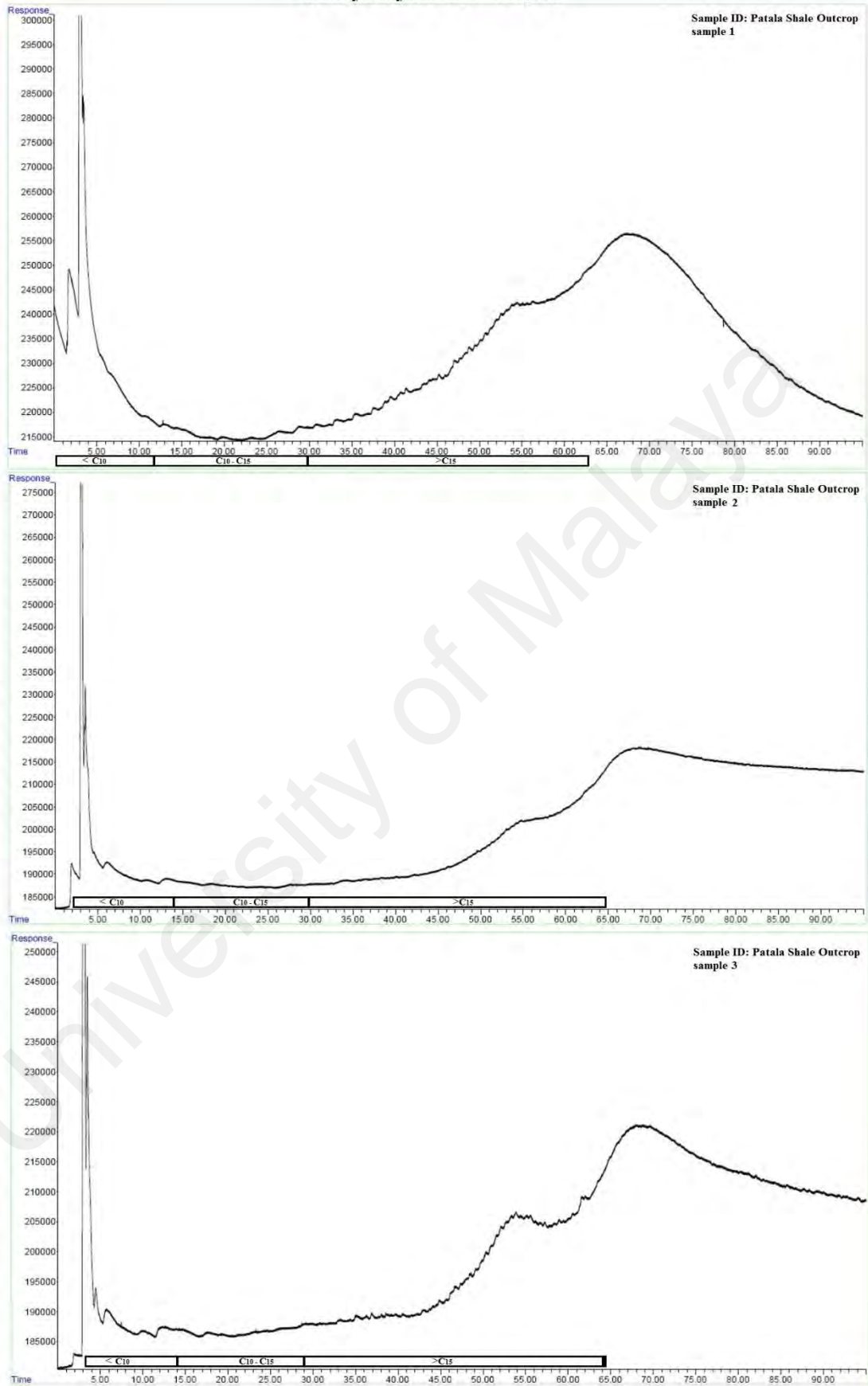


Figure 5.3: Pyrolysis GC pyrograms of the Patala Shale samples of Mustafabad section.

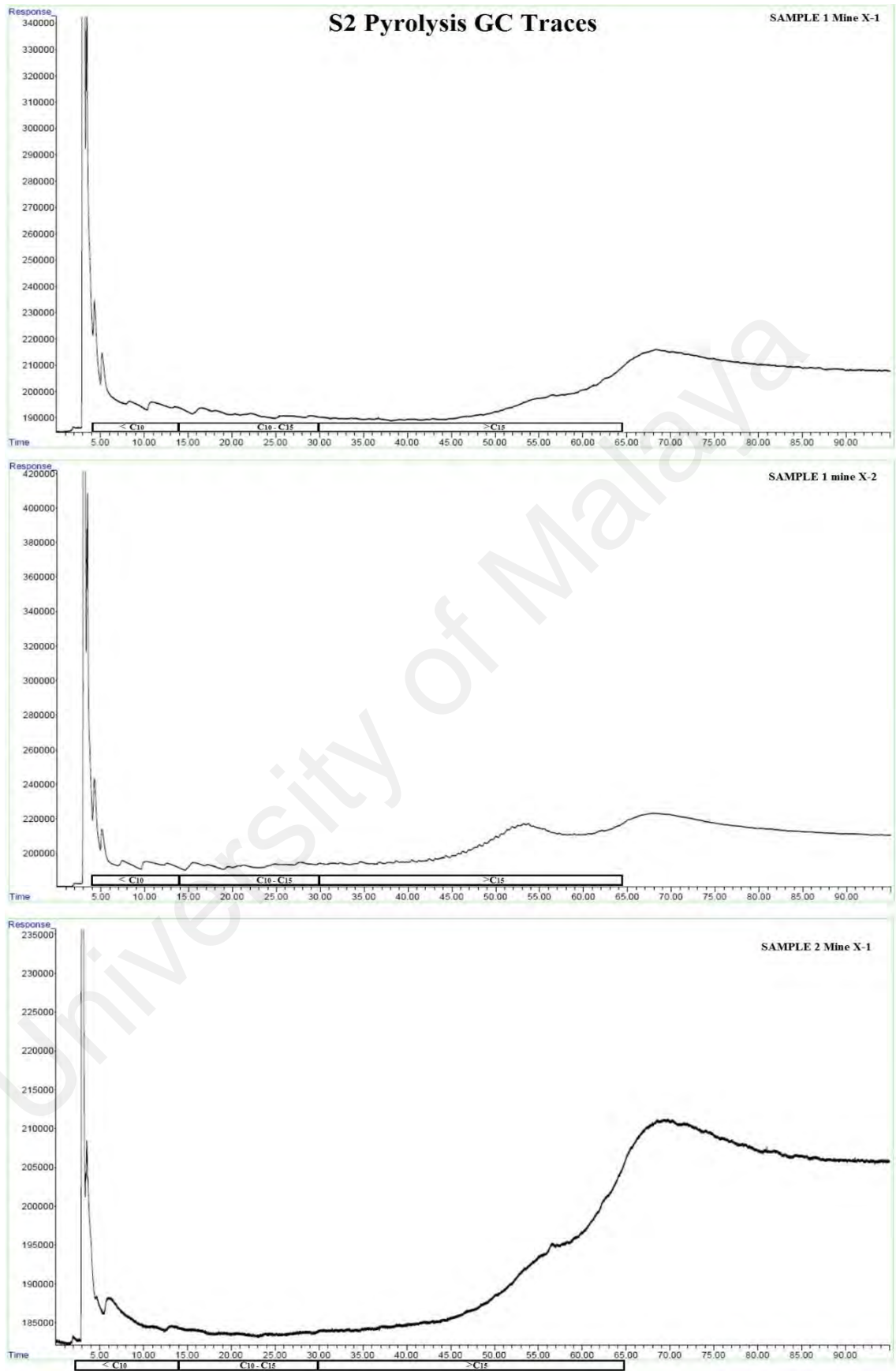


Figure 5.4: Pyrolysis GC pyrograms of the Patala Shale samples of Mustafabad section.

5.2.1.3 Thermal maturity

The extent of heat driven reaction is described by thermal maturity, which convert sedimentary organic material into petroleum (see section 3.2.4) (Peters and Moldowan, 1993). This thermal exposure converts kerogen into petroleum. In this study two of maturity indicators have been used to evaluate the thermal maturity level of the Patala Shale sediments; these include pyrolysis Tmax and mean vitrinite reflectance (%Ro).

5.2.1.2.1 Vitrinite reflectance (%Ro) and (Tmax) temperature maximum

The term vitrinite is applied to a group of kerogen/macerals with certain definite, chemical and variable optical properties (Carr, 2000). The maceral of the vitrinite group is telocollinite, subgroup telovitrinite, with a homogenous, more or less structure-less appearance. To determine the rank/level of thermal maturation of coal and organic matter in the sediments, vitrinite (in particular telocollinite) reflectance value (%Ro) is widely used (see section 3.2.4) (ICCP, 1998). The measured reflectance values can be compared to the Tmax values obtained from Rock-Eval pyrolysis (see table 3.1).

Now a days in petroleum exploration studies, both vitrinite reflectance (VR) and Tmax are widely used as indicators for level of thermal maturation of organic matter (Copard et al., 2002; Dow, 1977; Espitalié & Bordenave, 1993; Tissot & Welte, 1984; Suggate, 1998). In this study the values of the vitrinite reflectance measurement that were obtained ten samples are as shown in Table 5.1 and Table 5.2.

It is commonly accepted that the vitrinite reflectance values between 0.5 to 1.3% suggest oil generation window, whereas values less than 0.5% are commonly considered as thermally immature, whilst values that are greater than 1.3% indicate gas window maturity (see Section 3.2.4). According to Peters (1986), Tissot et. al. (1987) and Espitalié & Bordenave (1993) the Tmax values ranges between 400° to 430°C

characterize immature organic matter, the Tmax values that lies between 435° to 450°C characterize oil zone or mature organic matter, whereas the Tmax values that are greater than 450°C characterize over-mature zone.

The analysed samples have mean %Ro values ranging between 0.69-0.84 % for Mustafabad section and 0.51-0.66 % for Pail Village section. The studied samples appear to have higher level of thermal maturation based on VR values when compared to Tmax values (Fig. 5.3). It ought to be noted that Tmax is a crude measurement of maturity and that conclusion regarding maturity should be supported by other geochemical analysis, such as vitrinite reflectance (Peters, 1986). Considering the values of S2 are very low (0.11-0.63 mg/g) in all of the analysed samples, whereby low values are known to give anomalous Tmax values, thermal maturity assessment based on vitrinite reflectance is considered to be more reliable in this study. Consequently, the analysed samples from Pail Village section are evaluated to be thermally immature to early mature whilst samples from Mustafabad section are peak mature for oil generation based on Peters & Cassa (1994) classification.

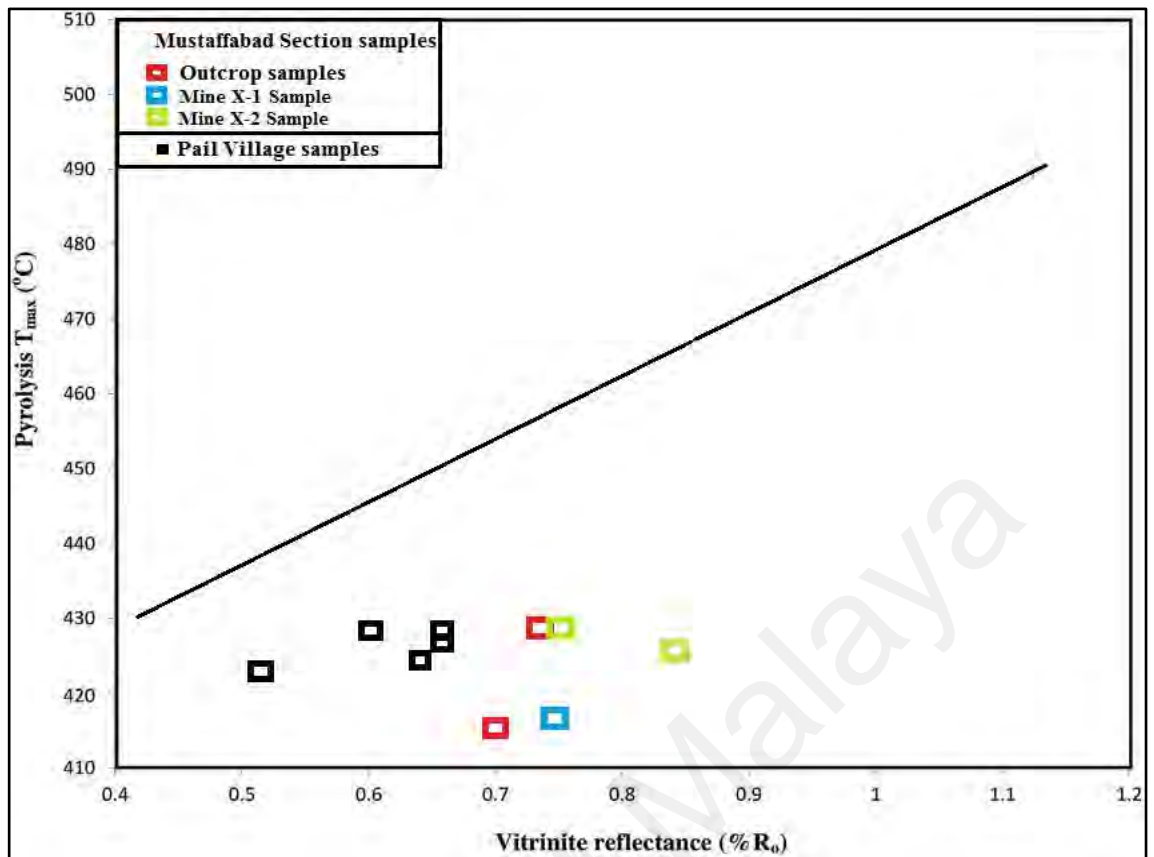


Figure 5.5: Plot of maturity parameters vitrinite reflectance (%R₀) and T_{max} for the samples.

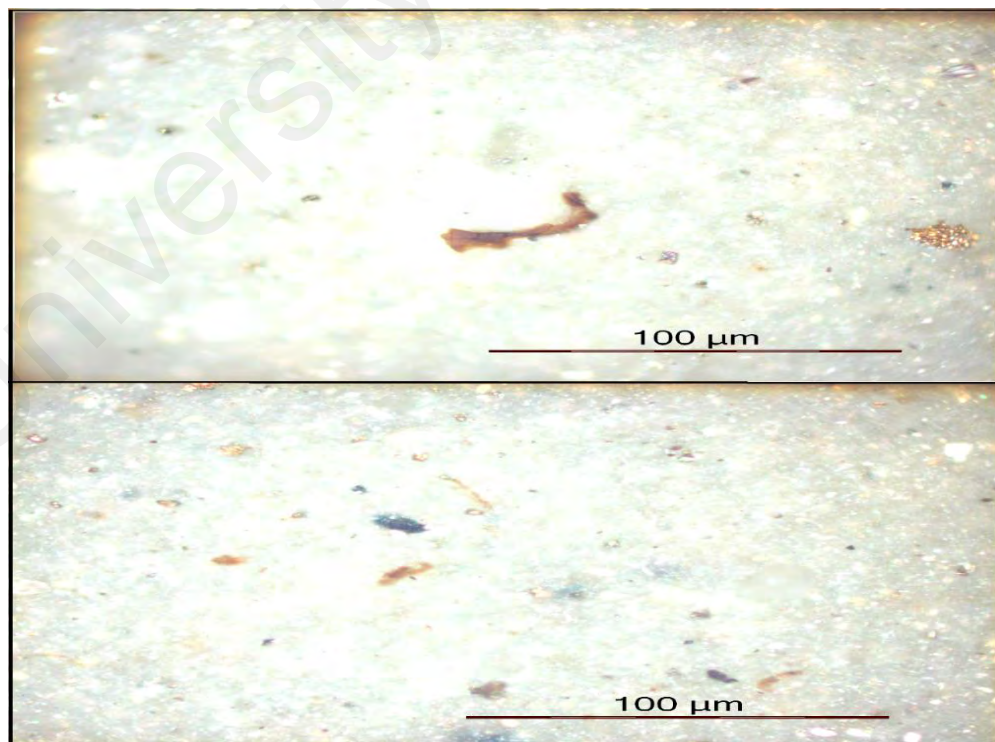


Figure 5.6: Photomicrographs of amorphous organic matter (brown staining) and inertinite macerals (white phytoclasts) in sediments of the Patala Shale samples.

5.3 Seismic interpretation

Seismic interpretation is the representation of seismic reflections data into structural picture by applying complex algorithms; corrections, calculations, migration and time depth conversion (TDR time-depth relationship) (Dobrin & Savit, 1988). The objective of seismic interpretation is to mark and identify the major structure (folds and faults) and top of reflectors of interest (Seal-/Cap rock, source and reservoir formations and basement), as well as identifying the geometry (type and style) of the prevailing faults in the subsurface of Balkassar (see section 3.6.1). The interpretation mainly relies on reflectors identification and calculating their positions (depth) and placing them at their true positions in the subsurface on the basis of geology of the area and correlating it with the already drilled well data, details of these were presented in section (4.4.2).

5.3.1 Structural Interpretation

Based on the seismic strike lines SOX-PBJ-08, SOX-PBJ-09, SOX-PBJ-10 and dip lines SOX-PBJ-01, SOX-PBJ-02, SOX-PBJ-03, SOX-PBJ-04, SOX-PBJ-05 and SOX-PBJ-06, the structure of the study area has been interpreted (Figs. 4.14 and 5.7-5.16). The images shown here are the compressed images and are exaggerated to meet and fit the output screen for printing purposes.

On seismic dip lines SOX-PBJ-01, SOX-PBJ-04, SOX-PBJ-05 and SOX-PBJ-06, fourteen reflectors have been marked and interpreted from Chinji to Salt Range Formation and basement (Figs. 5.10-5.15). These are:

1. Chinji Formation
2. Kamlial Formation
3. Murree Formation (Seal)
4. Chorgali Formation (Reservoir)

5. Sakesar Limestone (Reservoir)
6. Patala Shale Formation (Source)
7. Lockhart Limestone Formation
8. Hangu Formation
9. Sardhai Formation
10. Warcha Formation
11. Dandot Formation
12. Tobra Formation
13. Khewra Formation
14. Salt Range Formation and
15. Basement

In the center of the seismic dip line SOX-PBJ-01 a noticeable bulge can be observed that has been developed in the basement strata (Fig. 5.7 and 5.8). Lots of studies exist that verify that this bulge/anticline structure has been produced from post tertiary Himalayan compression (Iqbal et al., 2015; Kadri, 1995; Kazmi & Abbassi, 2008; Shah & Abdullah, 2017; Shah, 2009; Zahid et al., 2014). On the dip line SOX-PBJ-04 an anticline structure can be identified which is bounded by various faults from both sides. Seven major faults have been identified in the interpretation. Six major faults are reverse faults and the seventh is normal fault present in basement. Four reverse faults (Fault 3, 4, 5 and 6) can be observed at the southeastern limb of the anticline (Fig. 5.9 and 5.10), and two reverse faults (Fault 1) and (Fault 2) can be observed in the northwestern limb of the anticline (Fig. 5.9 and 5.10). Faults 1, 2, 3, 4, 5 and 6 were the normal faults in the structure but were reactivated as a reverse fault by a salt diapir, the faults have dip angles of 60° to 75° .

The reactivation of normal fault to reverse fault is the same as in the Northern Chilean Fore Arc where due to subduction zone the normal faults were reactivated as reverse faults. The same has happened in Arabian Gulf and Salt Diapirs in Santos and Campos

Basins, Brazil (Al-Fahmi et al., 2014; Loveless et al., 2010; Harding & Huuse, 2015; Quirk et al., 2012). Increase in disturbance in the structure can be observed while moving in the northeast direction from seismic line SOX-PBJ-01 towards the center of the anticline that is seismic line SOX-PBJ-04. While moving further towards northeast, the southeastern limb of the anticline has received much more disturbance due to the Himalayan Orogenic Forces and Indian Plate anticlockwise movement and subduction of the Indian Plate. This anticline structure is known as Balkassar anticline (Figs 5.9 and 5.10). In the basement rocks, normal fault can be observed (Fig. 5.9 and 5.10). This normal fault is a result of tectonic loading of the Indo-Pak Plate in north (Pennock et al., 1988).

Fault 3 and 4 are the major faults in the sedimentary sequence which is extending toward the basement. A reverse fault (Fault 1) is present on the north-western flank of the anticline which is extending downward towards the Salt Range Formation in Late Precambrian rocks (Fig. 5.9, 5.10, 5.15 and 5.16). Fault 3 (reverse fault) in the structure disappears after cutting Chinji Formation of Miocene age (Fig. 5.9 and 5.10). All identified normal and reverse faults are blind faults. The disturbance in the structure has increased towards east. The structure in the subsurface of Balkassar block is a Salt-Cored anticline structure formed as a result of Indian Plate subduction and drift (anticlockwise rotation), salt diapirism and Himalayan orogenic compressional forces (Fig. 15 and 16). In the diapir development stages, the structure of Balkassar is at stage 2 known as Active Diapirism Pillow Stage, in which the strata is thinning towards the center and thickening towards the limbs (see section 3.3.2.1.9.1 and Fig. 3.18 and 5.17).

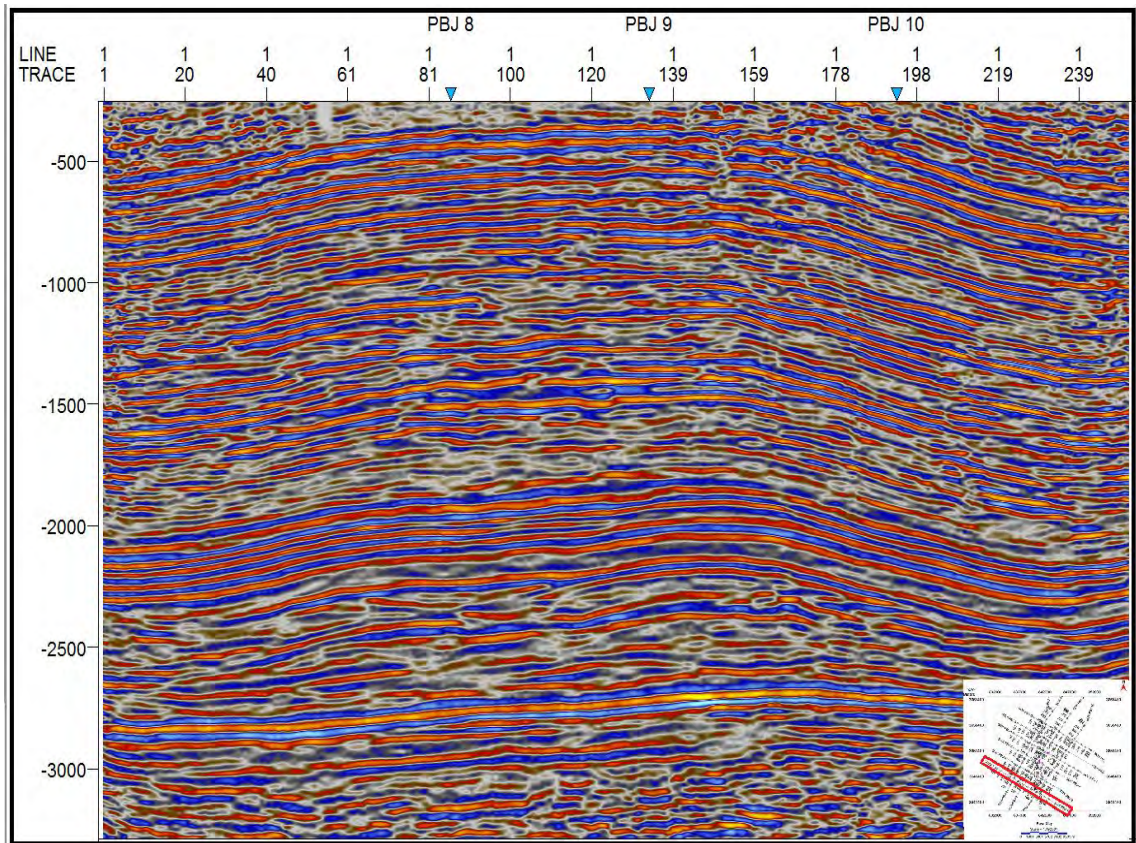


Figure 5.7: Seismic line SOX-PBJ-01 without interpretation.

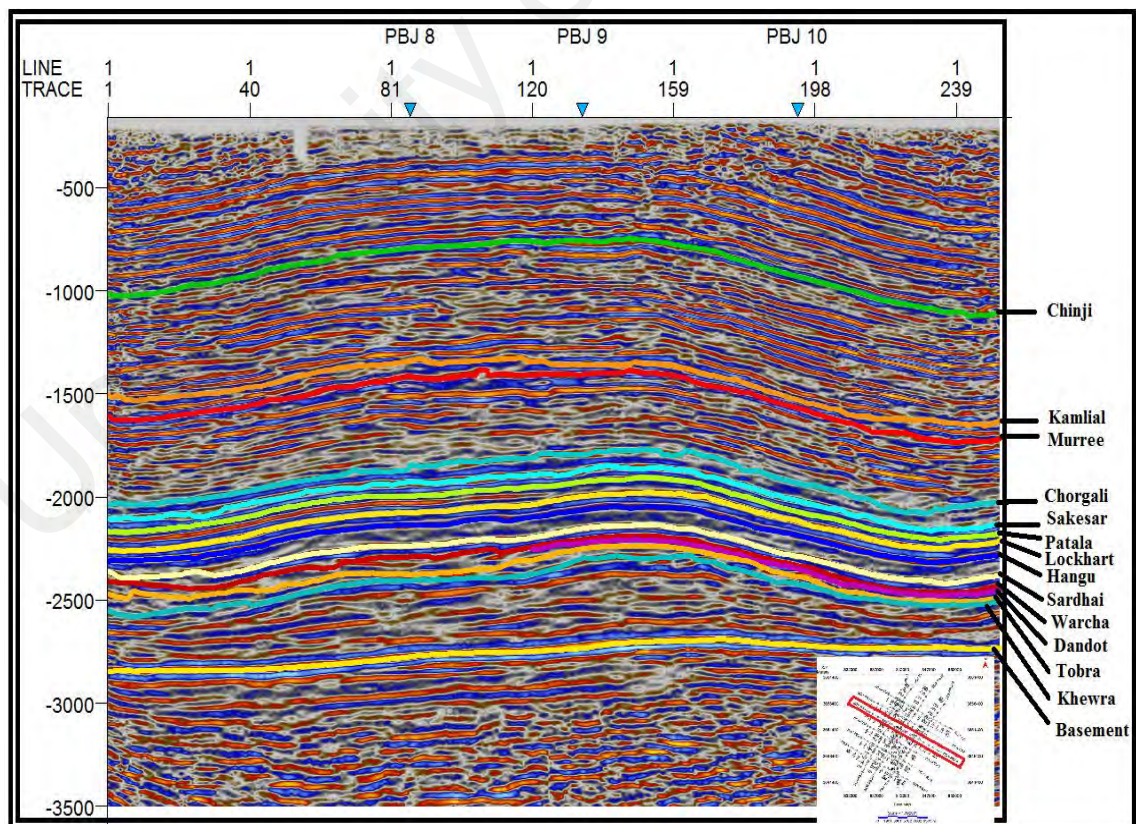


Figure 5.8: Interpreted seismic line SOX-PBJ-01.

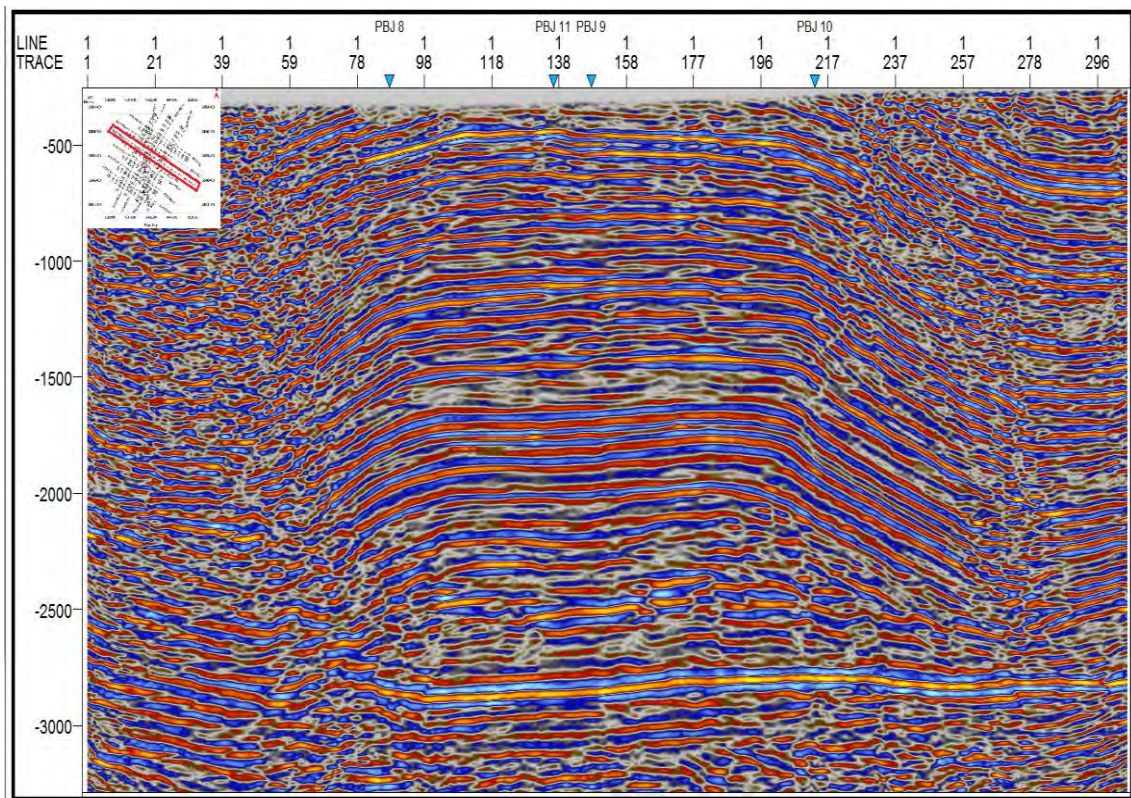


Figure 5.9: Seismic line SOX-PBJ-04 without interpretation.

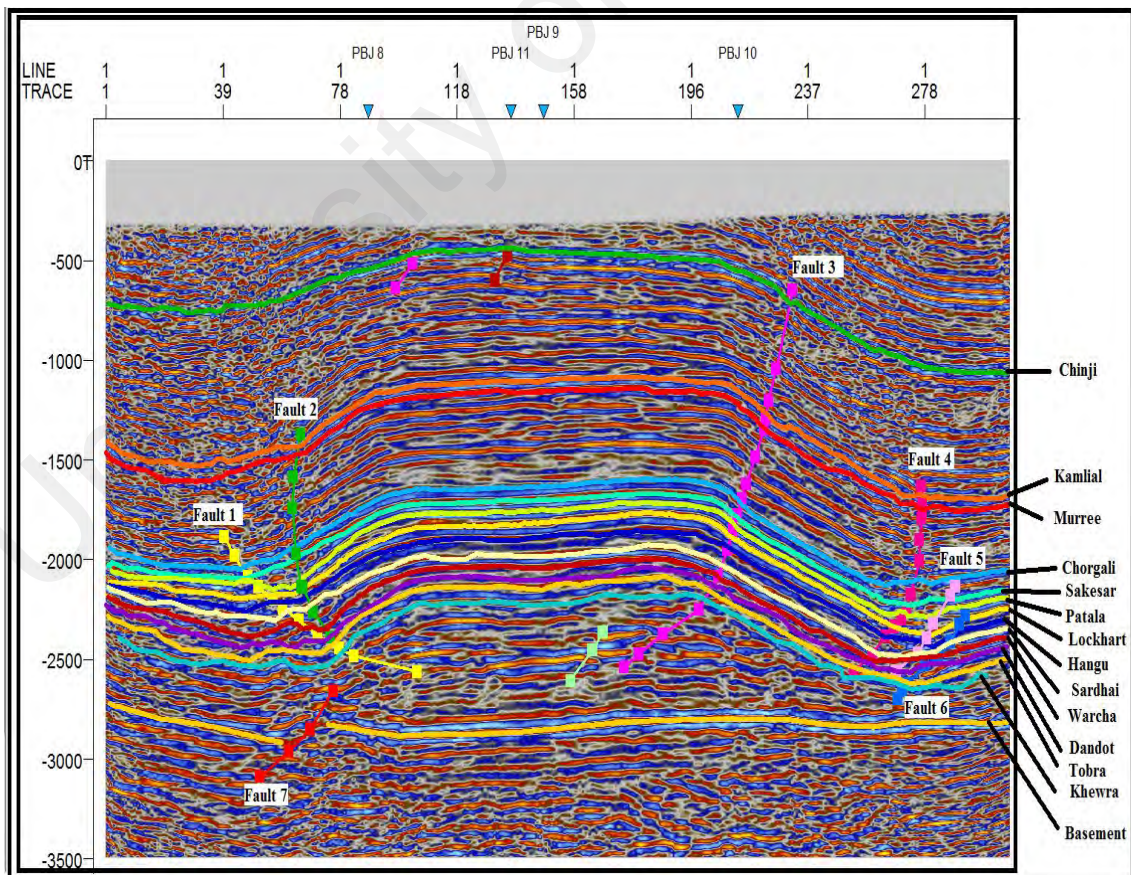


Figure 5.10: Interpreted seismic line SOX-PBJ-04.

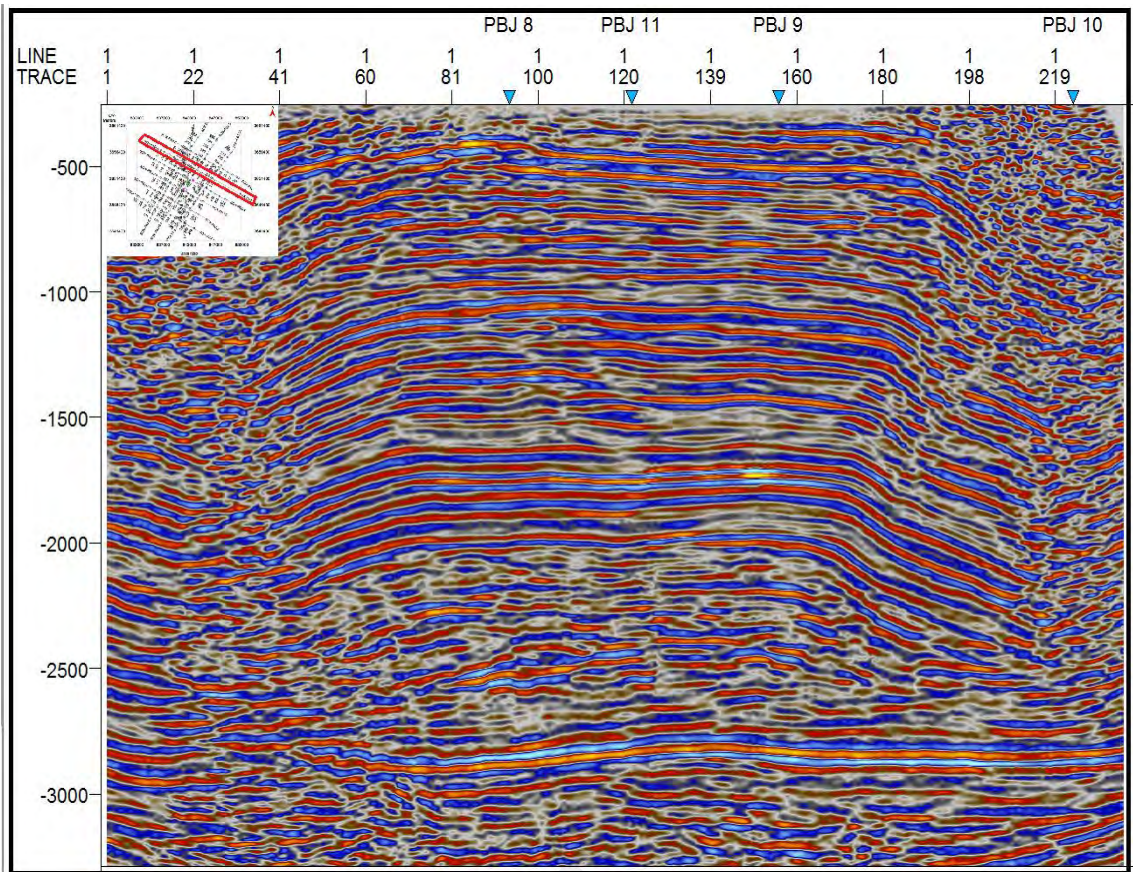


Figure 5.11: Seismic line SOX-PBJ-05 without interpretation.

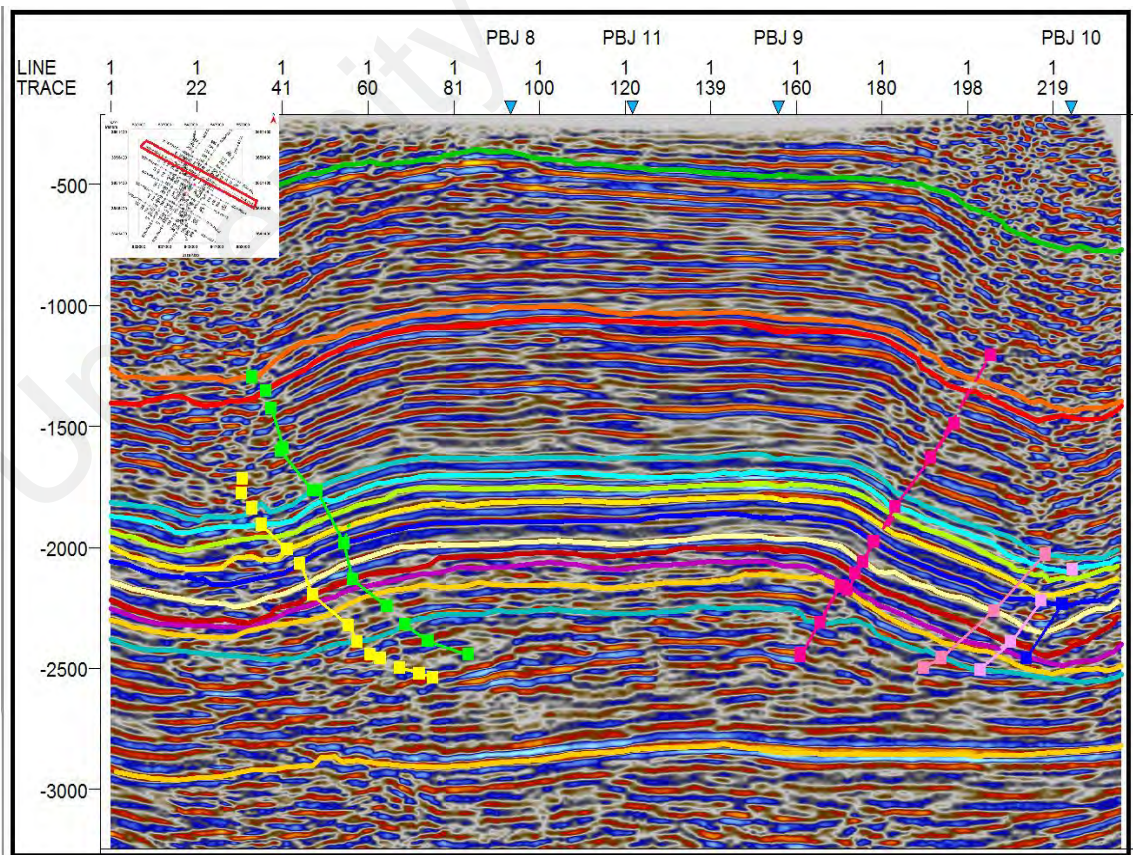


Figure 5.12: Interpreted seismic line SOX-PBJ-05.

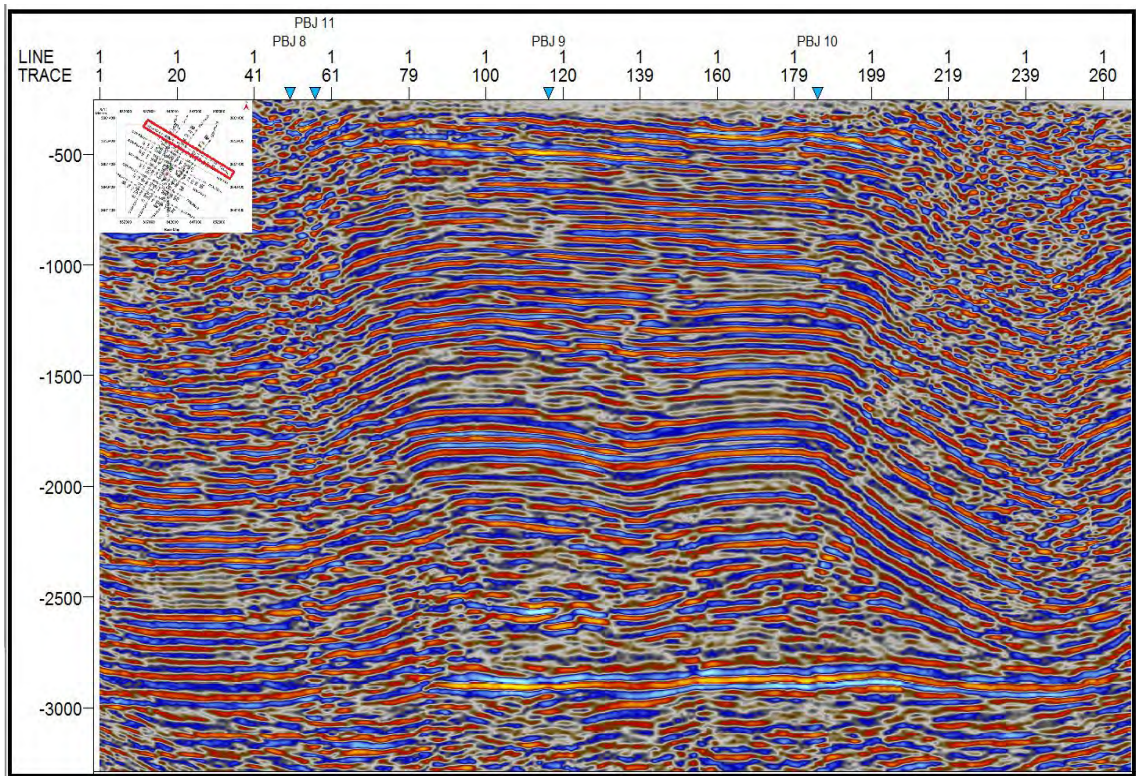


Figure 5.13: Seismic line SOX-PBJ-06 without interpretation.

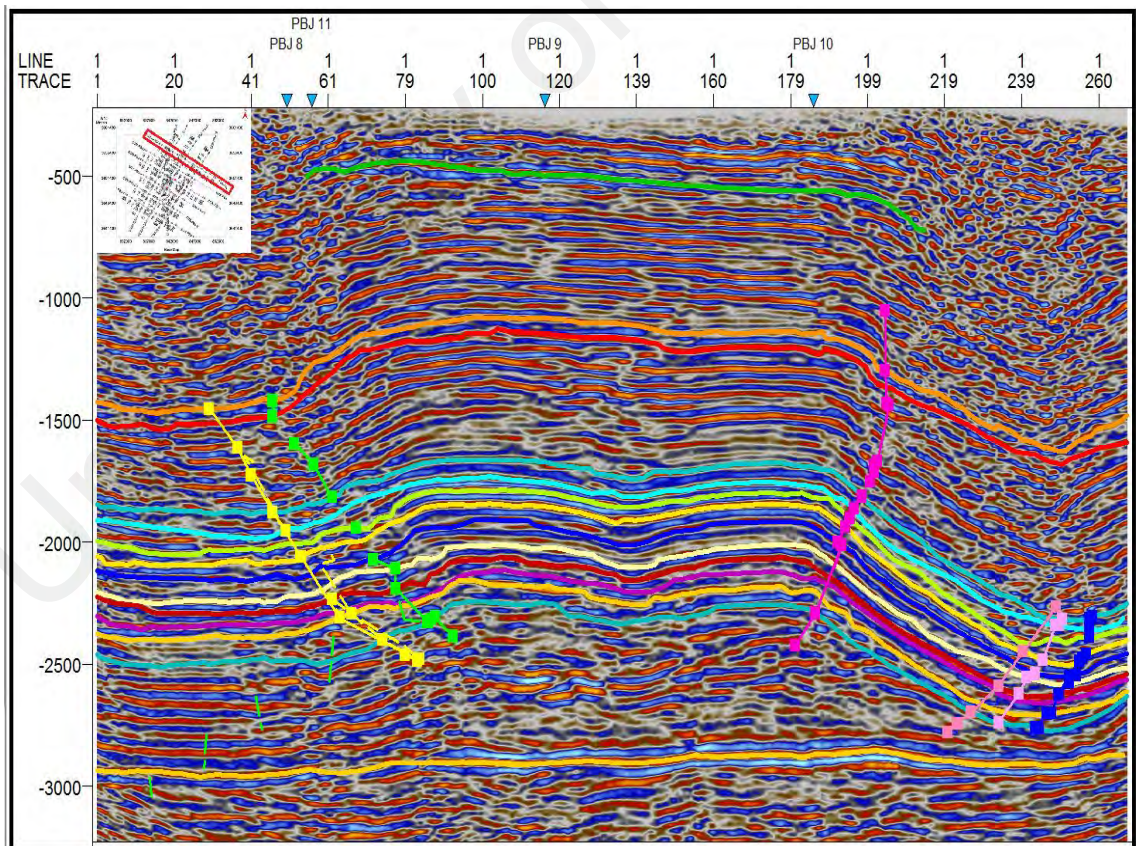


Figure 5.14: Interpreted seismic line SOX-PBJ-06.

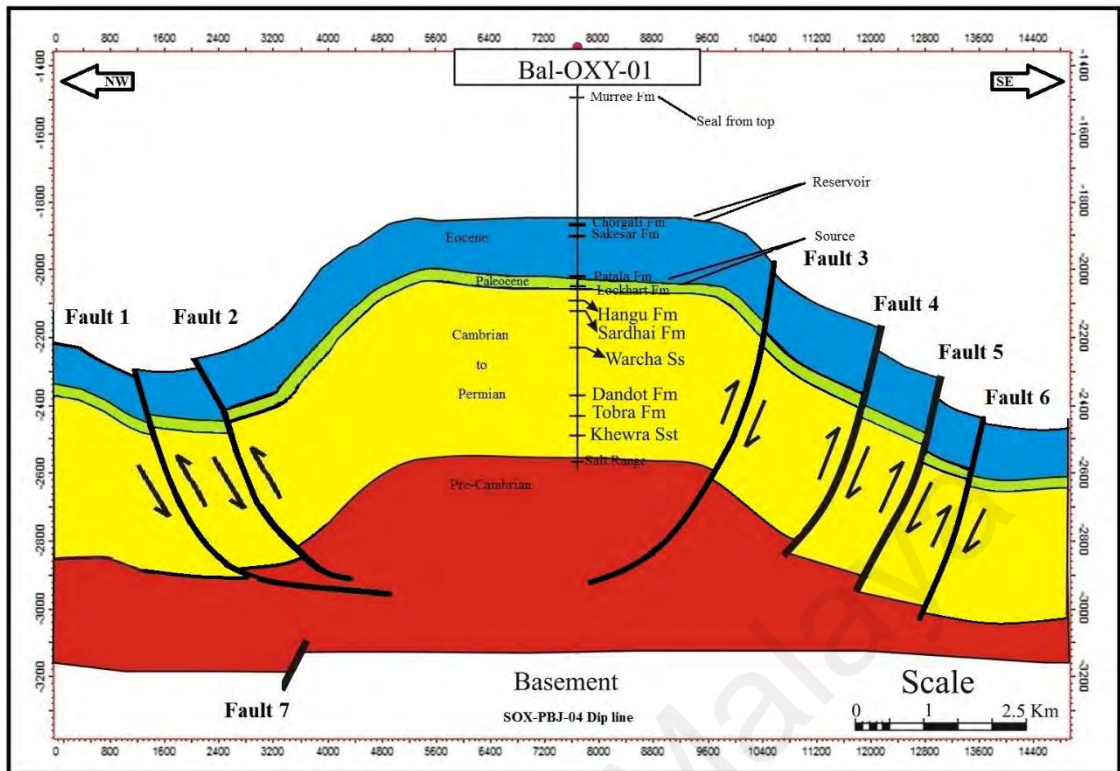


Figure 5.15: Structural model of Balkassar anticline with well tops of Balkassar-OXY-01.

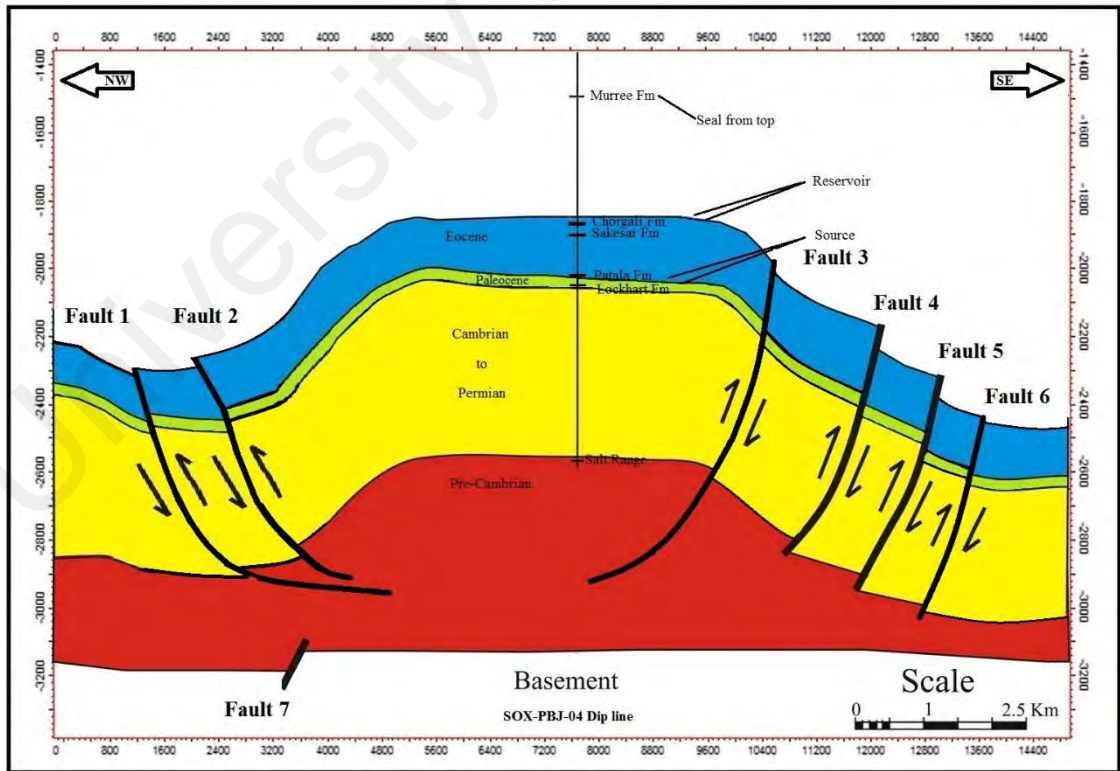


Figure 5.16: Structural model of Balkassar anticline with tops of interpreted source and reservoir horizons on seismic are displayed.

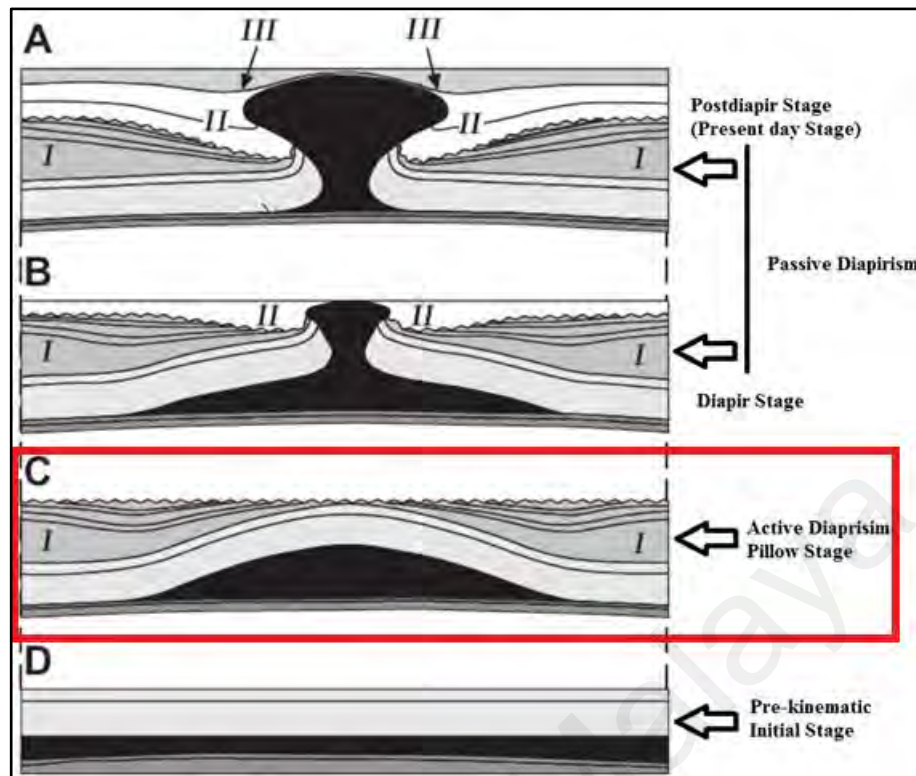


Figure 5.17: Salt diapir development stages. Free image.

5.3.2 3D Contour maps

The velocity analysis that has been conducted for horizon marking was further used for horizon mapping by 3D contours (time and depth surfaces maps) to interpret the subsurface structural trend, behavior of the horizon, distribution of the horizon and uplift and downward movement of the horizon throughout the block. Horizons were mapped both by time and depth contour maps.

Murree Formation in the Balkassar block is providing a thick seal and is about 890 to 907 meters thick, it is uniformly distributed over Chorgali Formation in the block, disturbance can be observed in northwestern corner where the horizon is dipping steeply due to the fault. The contours are very close depicts that the throw of the fault is quite high, the structure is extended in northeast and southwest direction.

The 3D depth model of Chorgali horizon depicts that the formation has been raised from original position if we focus on northwest corner of the map, it also depicts that Fault 3, 4, 5 and 6 are dipping towards northwest and Fault 1 and 2 are dipping in the opposite direction (Fig. 5.18). The Balkassar anticline structure is dipping steeply towards northwest side whereas it is dipping gentle on southwest side the faults interpreted have dip angles between 60° – 75° . The Chorgali Formation is covering the Balkassar anticline top flat surface, and shows a structure that is a four way closure bounded by faults from both sides.

The behavior of Balkassar anticline at the level of Sakesar Limestone, and Patala Shale formations are same as the Chorgali Formation (Fig. 5.19 and 5.20), but rocks of Cambrian age have been effected by Salt tectonics whereas the Basement horizon is relatively smooth (Fig. 5.21). Overall the structure trend of Balkassar anticline indicates a four way closure for the hydrocarbons accumulation, and the dip observed from the 3D models is in northwest direction, which is as same as the dip observed in the rest of the Basin present in Indian plate. This type of four way closure increases the strata thickness in the northwest direction and therefore facilitating updip migration of hydrocarbons to accumulate at the center of the anticline.

The time contour map of Chorgali Formation (Fig. 5.23) shows a shallow and flat area at the center and in the northeast direction, the formation is making top flat part of the anticline. The structure present in the northwest and southeast is ambiguous and forms saddles and peaks and the limbs are steeply dipping 65° – 75° . at the sides. The saddles and peaks may have been generated by the compressional forces. The contour map also depicts that both limbs of the anticline are steeply dipping 65° – 75° . and the limbs have been terminated by the faults present on both sides of the anticline, in the northwest side a small contour closure can be observed which may act as a potential prospect for hydrocarbon accumulation at level of Chorgali Formation (Fig. 5.23).

The time contour maps at the level of Sakesar and Patala formations depicts a flat crestal part (Fig. 5.24 and 5.25), the contours observed in these formations depicts that the limbs are steeply dipping 65° – 75° in the northwest direction as compare to the limbs in southeast direction, the anticline limbs are steeply dipping 60° – 65° between Fault 3 and Fault 4, whereas moving away from Fault 6 the limbs again become gentler as the compressional forces are fading as much as moving away from the anticline center. At the level of Sakesar Limestone in the northwest side a broad contour closure can be observed and has been identified which may act as a potential prospect for hydrocarbon accumulation (Fig. 5.24).

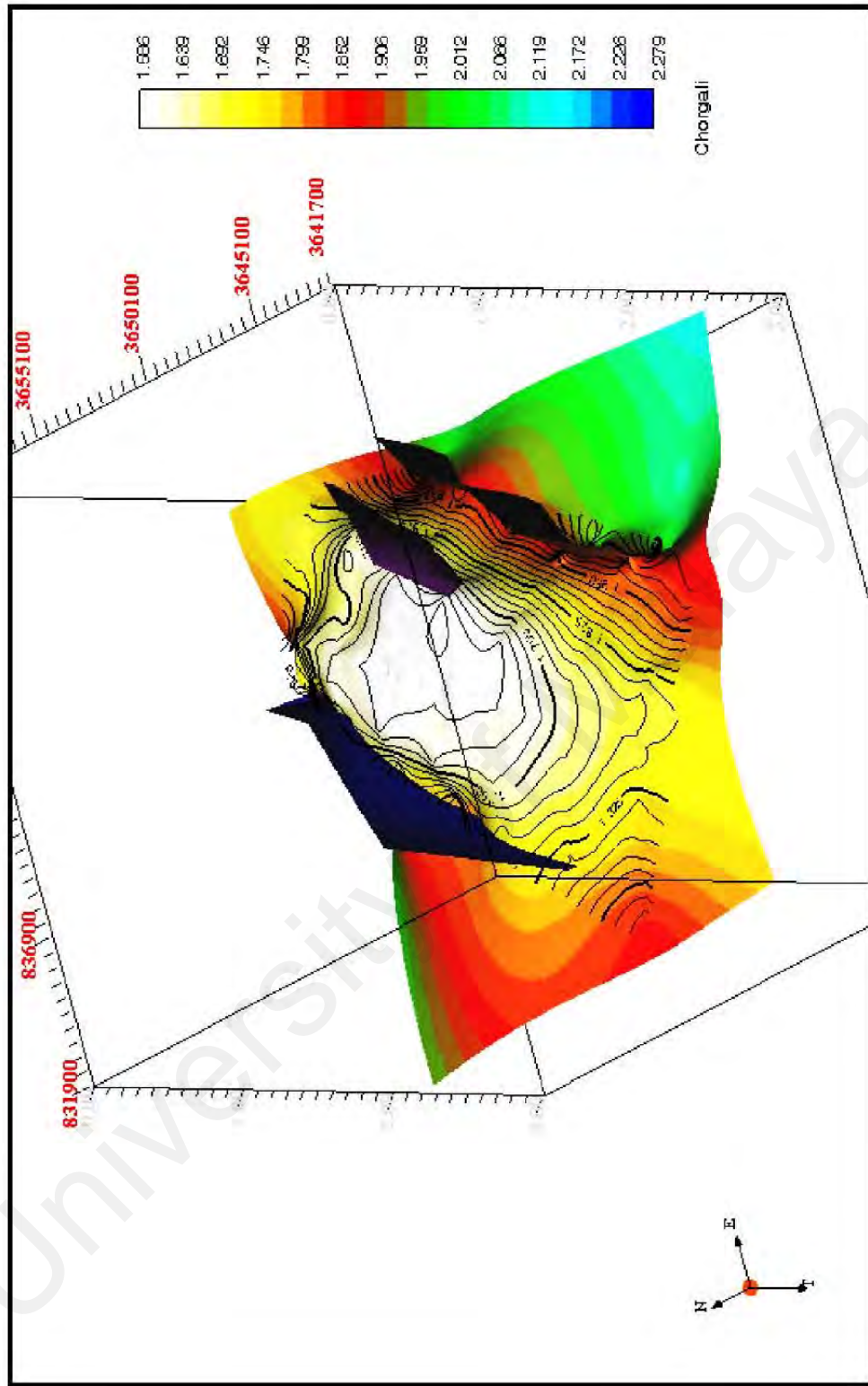


Figure 5.18 Chorgali Depth contour map.

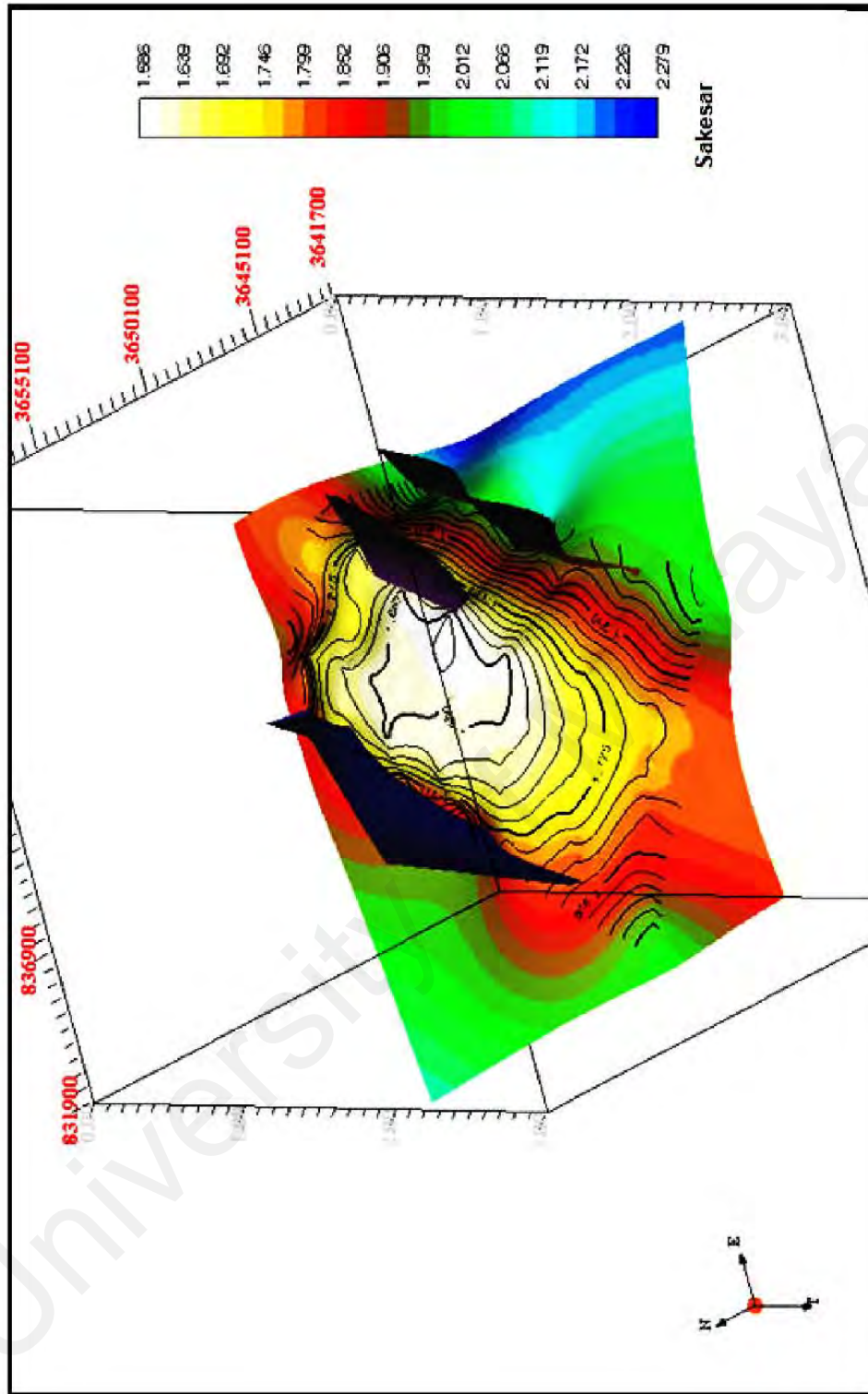


Figure 5.19 Sakesar Depth contour map.

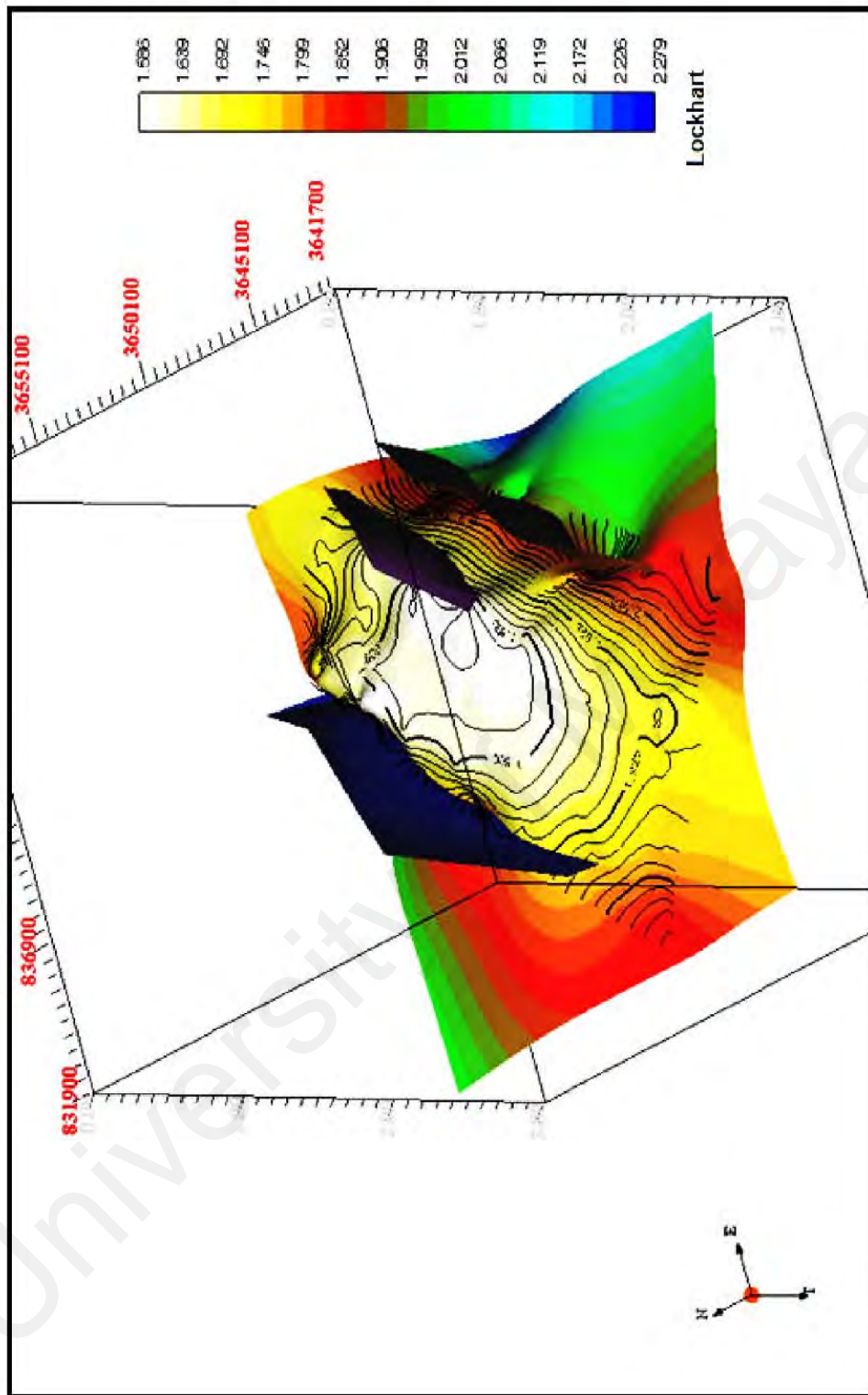


Figure 5.20 Patala depth contour map.

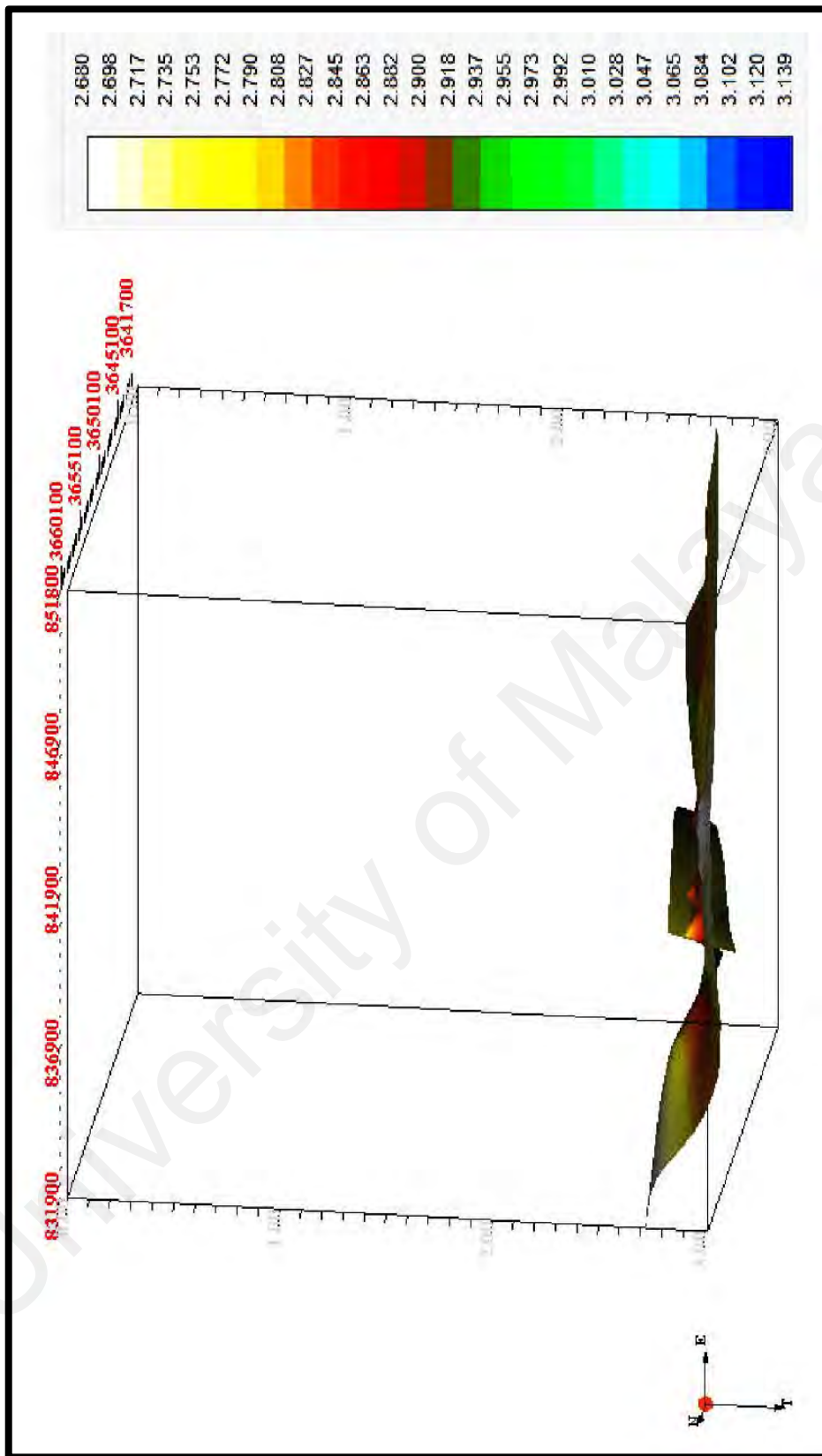


Figure 5.21 Basement depth contour map.

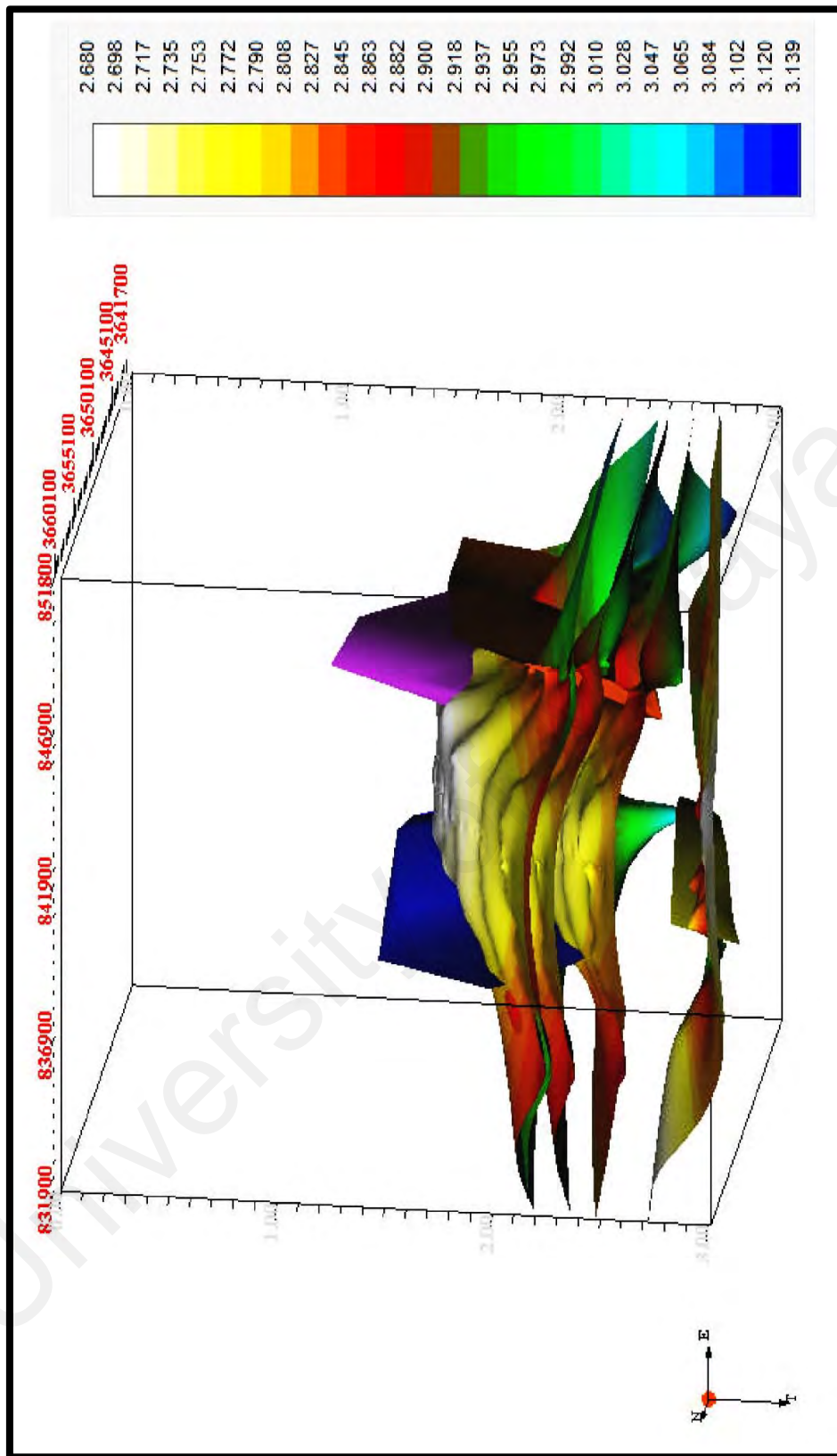


Figure 5.22 All formations depth contour map.

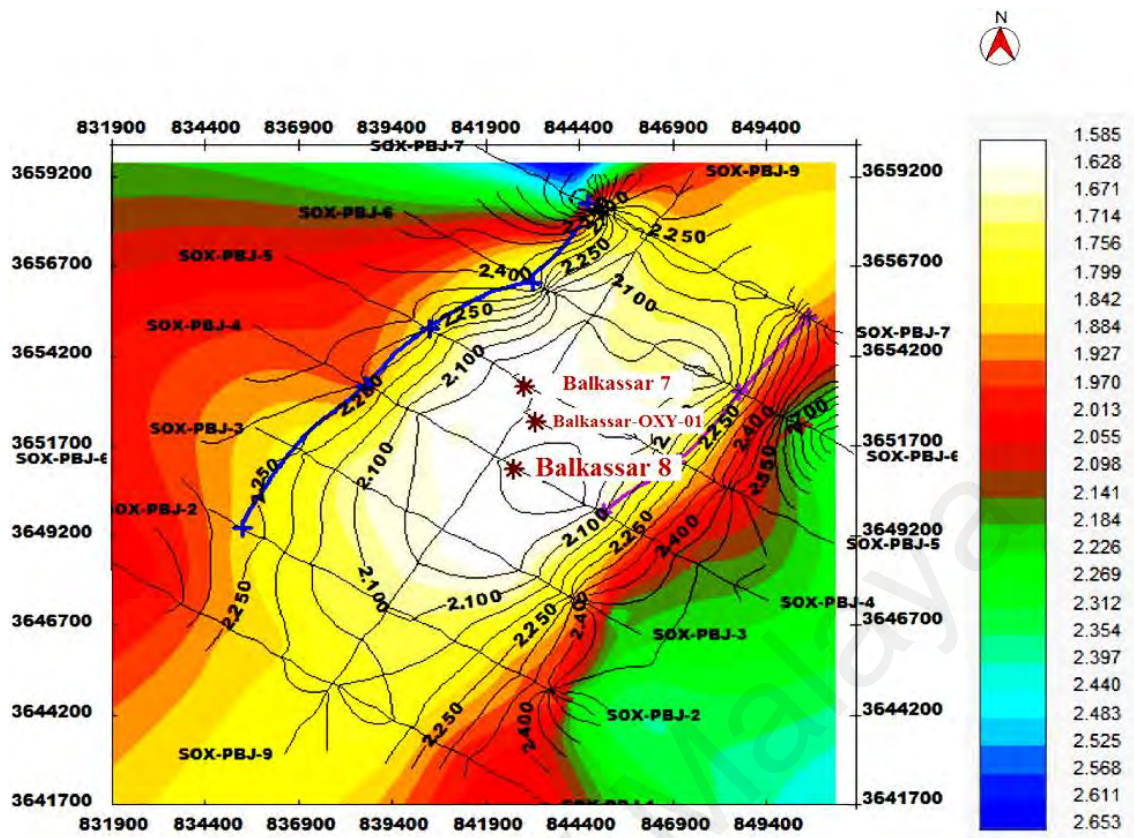


Figure 5.23: Chorgali time contour map.

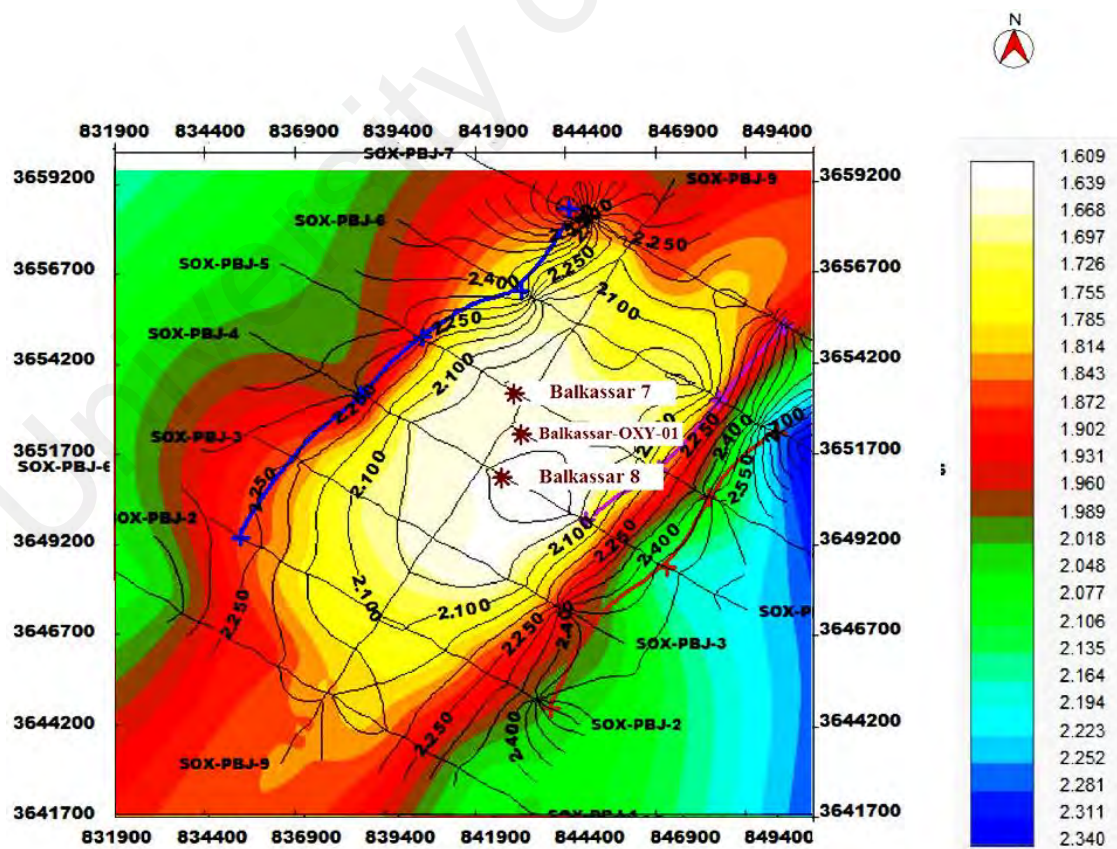


Figure 5.24: Sakesar time contour map.

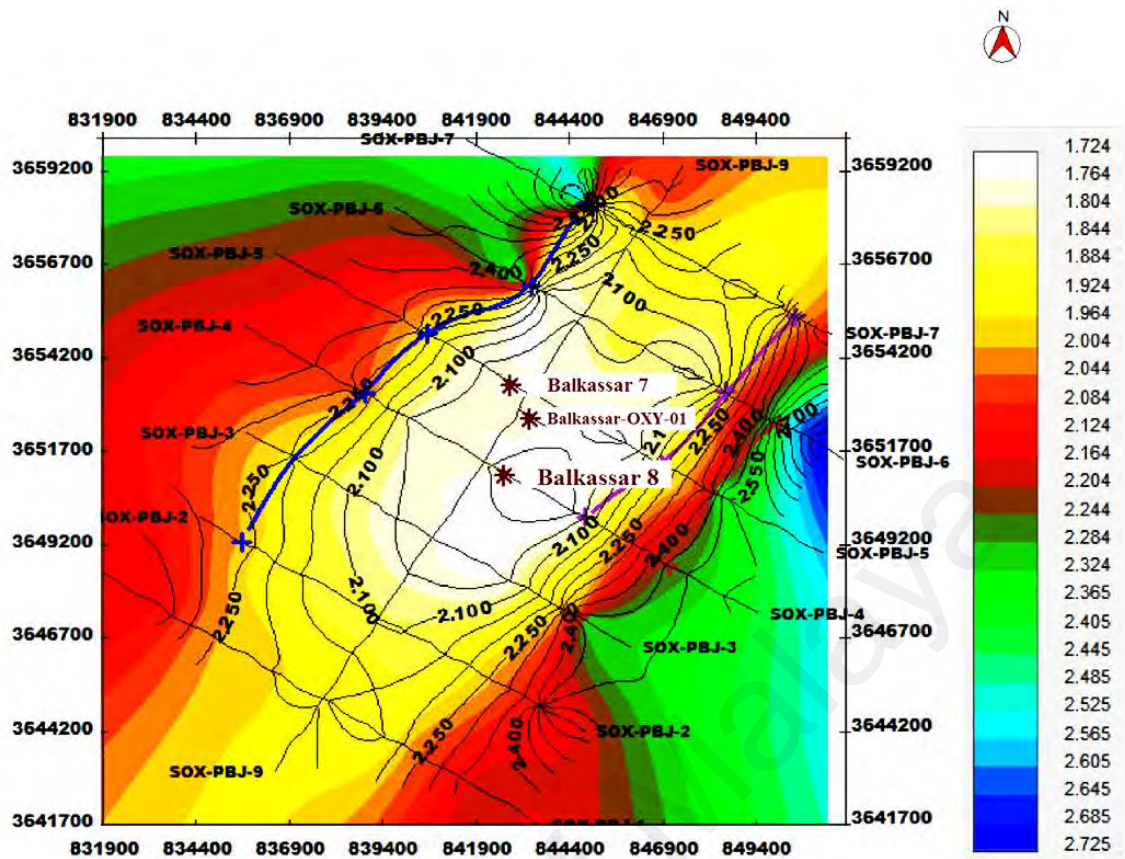


Figure 5.25: Patala time contour map.

5.4 Petrophysical analysis

The petrophysical analysis through wireline logs- (Neutron, Density, Resistivity, Gamma Ray and Spontaneous-potential) for Eocene age Sakesar Formation and Chorgali Formation in Balkassar-OXY-1 well, Balkassar-7 and Balkassar 8 well are conducted. The analysis was made to calculate volume of shale, porosity, water saturation, formation water resistivity, and saturation of hydrocarbon. All of these parameters are very useful in investigating the reservoir hydrocarbon potential.

Table 5.3: Petrophysical: Different parameters values calculated for Sakesar limestone in Balkassar-OXY-01 well.

Depth (ft)	Temp	RHOB	Φ_D	SP	Φ (N.D)	Rt (LLD)	Rwe	Rw	Sw	SH	Lithology
8149	153.4	2.8	0.39	-28	0.36	300	0.40	0.70	14%	86%	Limestone
8205	154	2.72	0.35	-11	0.19	1118	0.6	0.81	19%	81%	Limestone
8260	154.6	2.65	0.04	-31	0.21	1511	0.39	0.62	13%	87%	Limestone
8315	155.1	2.69	0.19	-34	0.32	1860	0.35	0.31	14%	86%	Limestone
8371	155.7	2.58	0.07	-45	0.26	1677	0.37	0.6	37%	63%	Limestone
8426	156.2	2.68	0.29	-35	0.23	1754	0.36	0.46	15%	85%	Limestone
8481	156.8	2.45	0.21	-30	0.27	804	0.38	0.43	6%	94%	Limestone

Note: Average saturation of hydrocarbon (SH) calculated is 83.1% in Sakesar limestone Formation encountered in Balkassar-OXY-01 well. The abbreviated parameters are described in the text.

Table 5.4 Petrophysical: Different parameters values calculated for Chorgali Formation in Balkassar-OXY-01 well.

Depth (ft)	Temp	RHOB	Φ_D	SP	Φ (N.D)	Rt (LLD)	Rwe	Rw	Sw	SH	Lithology
7944	151.8	2.63	0.15	-27	0.11	320	0.41	0.69	34%	66%	Limestone
7969	152.1	2.66	0.11	-11	0.13	300	0.49	0.82	37%	63%	Limestone
7994	152.9	2.61	0.09	-29	0.10	160	0.61	0.63	36%	64%	Limestone
8019	153.3	2.67	0.12	-30	0.08	900	0.58	0.42	32%	68%	Limestone
8044	153.7	2.62	0.14	-27	0.14	1430	0.27	0.34	39%	61%	Limestone
8069	154.1	2.68	0.07	-31	0.11	1680	0.66	0.47	23%	77%	Limestone
8094	154.4	2.69	0.10	-35	0.12	450	0.35	0.37	27%	73%	Limestone

Note: The average saturation of hydrocarbon (SH) calculated is 67.42 % in Chorgali Formation encountered in Balkassar-OXY-01 well.

Table 5.5: Petrophysical: Different parameters values calculated for Chorgali Formation in Balkassar- 7 well.

Depth (ft)	Temp	RHOB	Φ_D	SP	Φ (N.D)	Rt (LLD)	Rwe	Rw	Sw	SH	Lithology
7864	156.1	2.69	0.32	-29	0.27	390	0.59	0.69	33%	67%	Limestone
7891	156.4	2.67	0.30	-11	0.16	1230	0.31	0.67	38%	62%	Limestone
7919	156.7	2.71	0.14	-31	0.25	1630	0.32	0.71	24%	76%	Limestone
7946	157	2.66	0.19	-33	0.23	1810	0.31	0.42	36%	64%	Limestone
7974	157.3	2.62	0.12	-46	0.24	1690	0.36	0.68	28%	72%	Limestone
8001	157.6	2.69	0.29	-31	0.22	1770	0.34	0.45	37%	63%	Limestone
8029	157.9	2.63	0.27	-33	0.18	980	0.32	0.49	39%	61%	Limestone

Note: The average saturation of hydrocarbon (SH) calculated is 66.5%. Chorgali Formation encountered in Balkassar well 7.

Table 5.6: Petrophysical: Different parameters values calculated for Sakesar limestone Formation in Balkassar- 7 well.

Depth (ft)	Temp	RHOB	Φ_D	SP	Φ (N.D)	Rt (LLD)	Rwe	Rw	Sw	SH	Lithology
8031	153.1	2.73	0.38	-26	0.34	430	0.41	0.72	21%	79%	Limestone
8086	153.7	2.71	0.32	-13	0.17	1130	0.59	0.79	22%	82%	Limestone
8141	154.2	2.67	0.07	-29	0.20	1550	0.37	0.66	33%	67%	Limestone
8196	154.8	2.63	0.15	-36	0.29	1790	0.38	0.33	8%	92%	Limestone
8251	155.3	2.56	0.09	-46	0.24	1720	0.35	0.62	16%	87%	Limestone
8306	155.8	2.62	0.24	-33	0.26	1730	0.37	0.41	12%	88%	Limestone
8361	156.3	2.49	0.25	-31	0.23	930	0.36	0.43	19%	81%	Limestone

Note: The average Saturation of hydrocarbon (SH) calculated is 82.2% in Sakesar limestone Formation encountered in Balkassar well 7.

Table 5.7: Petrophysical: Different parameters values calculated for Chorgali Formation in Balkassar- 8 well.

Depth (ft)	Temp	RHOB	Φ_D	SP	Φ (N.D)	Rt (LLD)	Rwe	Rw	Sw	SH	Lithology
7864	153.2	2.71	0.37	-26	0.20	540	0.39	0.70	41%	59%	Limestone
7890	153.6	2.73	0.33	-14	0.17	1150	0.57	0.77	39%	61%	Limestone
7917	154.3	2.66	0.06	-30	0.16	1590	0.33	0.65	33%	67%	Limestone
7944	154.9	2.61	0.14	-34	0.18	1720	0.36	0.32	39%	61%	Limestone
7970	155.5	2.54	0.08	-45	0.12	1740	0.32	0.60	46%	54%	Limestone
7997	156.1	2.60	0.25	-32	0.13	1710	0.34	0.41	37%	63%	Limestone
8024	156.8	2.48	0.25	-30	0.11	980	0.32	0.42	43%	57%	Limestone

Note: The average Saturation of hydrocarbon (SH) calculated is 60.21% in Chorgali Formation encountered in Balkassar well 8.

Table 5.8: Petrophysical: Different parameters values calculated for Sakesar limestone Formation in Balkassar- 8 well.

Depth (ft)	Temp	RHOB	Φ_D	SP	Φ (N.D)	Rt (LLD)	Rwe	Rw	Sw	SH	Lithology
8031	153.2	2.69	0.35	-25	0.22	610	0.37	0.69	24%	76%	Limestone
8096	153.6	2.72	0.31	-16	0.19	1230	0.54	0.75	37%	63%	Limestone
8161	154.3	2.65	0.09	-29	0.17	1520	0.35	0.67	26%	74%	Limestone
8226	154.9	2.62	0.18	-36	0.19	1840	0.34	0.34	16%	84%	Limestone
8291	155.5	2.53	0.11	-44	0.13	1610	0.31	0.62	23%	77%	Limestone
8356	156.1	2.59	0.27	-35	0.14	166	0.33	0.43	14%	86%	Limestone
8421	156.8	2.46	0.22	-32	0.11	890	0.30	0.39	17%	83%	Limestone

Note: The average Saturation of hydrocarbon (SH) calculated is 77.68% in Sakesar limestone Formation encountered in Balkassar well 8.

For qualitative description of reservoirs and Van Golf-Racht (1982), Rider (1986) and Amigun & Odole (2013) have reported on criteria used for porosity. Table 5.9 shows the criteria that has been adopted for this study.

Table 5.9: Criteria for qualitative description of reservoir adopted for this study.

Qualitatively Evaluation of Permeability		Qualitatively Evaluation of Porosity	
Average K value (md)	Qualitative description	Average Porosity	Qualitative description
<10	Poor to fair	0-5	Negligible
10-50	Moderate	5-10	Poor
50-250	Good	10-20	Good
250-1000	Very Good	20-30	Very Good
1000>	Excellent	>30	Excellent

The analyzed petrophysical parameters computed for Sakesar and Chorgali formations are as shown in (Table 5.10 and 5.11).

Table 5.10: Reservoirs petrophysical parameters for the three wells analyzed in this study.

Parameters	Wells					
	Balkassar 7		Balkassar 8		Balkassar-OXY-01	
Reservoirs	Chorgali	Sakesar	Chorgali	Sakesar	Chorgali	Sakesar
Depth	2398-2447	2448-2567	2397-2446	2447-2535	2421-2466	2467-2602
Gross (m)	14.80	22.01	14.20	12.31	12.38	11.37
Net (m)	06.60	20.80	12.32	09.38	07.62	08.96
Net/Gross (%)	44.50	89.74	88.70	87.64	61.32	88.67
Net Pay (%)	05.60	16.63	8.79	09.67	06.49	03.76
Vsh (m)	40.80	15.62	23.11	31.21	36.74	10.49
ϕ_a (%)	15.29	16.32	27.93	9.12	11.19	09.87
K (mD)	90.30	143.87	255.79	1.87	01.36	07.68
BVW (%)	02.20	02.72	8.14	2.37	02.48	04.63
S_w (%)	39.79	22.32	46.54	37.66	32.65	21.87
S_H (%)	60.21	77.68	53.46	62.34	67.35	78.13

Table 5.11: Average petrophysical parameters of both Chorgali and Sakesar formations.

Reservoir	Well Name	S _H (%)	S _w (%)	K (mD)	Ø _a (%)	Net/Gross (%)
Chorgali	Balkassar 7	60.21	39.79	90.30	15.29	44.50
	Balkassar 8	53.46	46.54	255.79	27.93	88.70
	Balkassar-OXY-01	67.35	32.65	01.36	11.19	61.32
	Average	60.34	39.66	115.81	18.13	64.84
Sakesar	Balkassar 7	77.68	22.32	143.87	16.32	89.74
	Balkassar 8	62.34	37.66	1.87	9.12	87.64
	Balkassar-OXY-01	78.13	21.87	07.68	09.87	88.67
	Average	72.71	27.28	51.14	11.77	88.68

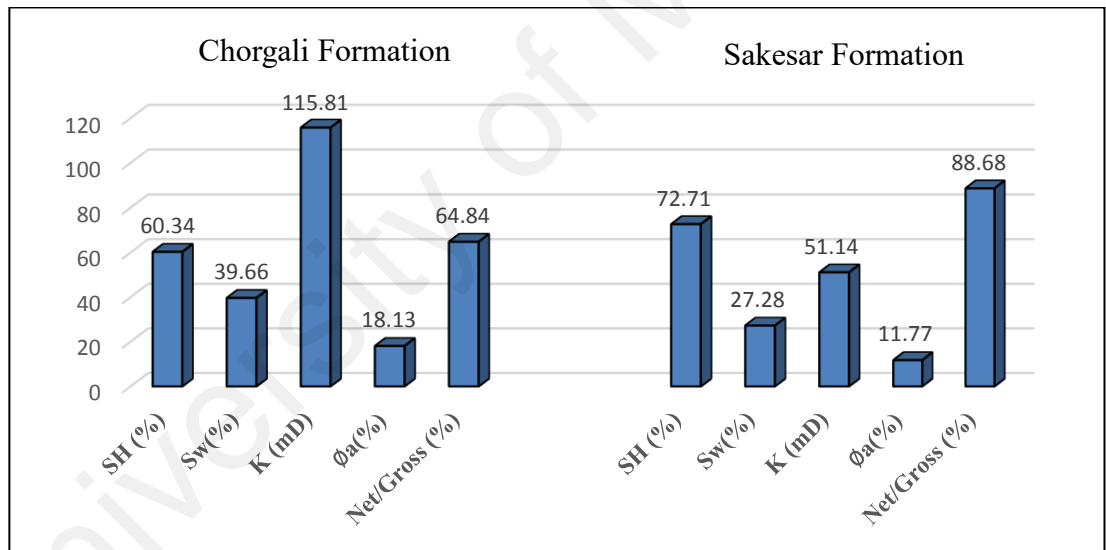


Figure 5.26: Graph showing average percentages of the petrophysical parameters of both reservoirs.

5.4.1 Results of petrophysical analysis

Net/Gross 44.50 to 89.74 indicates that Chorgali and Sakesar formations can act as good reservoir. Net pay thickness in the three wells varies from 3.76 m to 16.63 m. Average permeability and porosity ranges from 01.36 mD to 255.79 and 9.12% to 27.93% (Table 5.10). Maximum values of average porosity and permeability were recorded in

Balkassar-8 well, where values are qualitatively in range from good to very good, according to Amigun & Odoles (2013), Rider (1986) and Van Golf-Racht (1982). Bulk volume of water ranges from 2.20% to 8.14%, whereas hydrocarbon saturation ranges from 53.46% to 78.13%. As from the petrophysical analysis, Chorgali Formation is a good reservoir as compare to Sakesar Formation, considering that Chorgali Formation has higher permeability, average porosity, hydrocarbon saturation and net/gross ratio (Figure 5.26 and Tables 5.10 and 5.11).

5.5 Micro facies analysis

Micro facies analysis was performed on Sakesar Formation outcrop samples. Based on detailed sedimentological investigations, including outcrop observations and thin section evaluation, three microfacies of Sakesar Limestone are identified namely Numulitic wackestone, Milliolooidal wackestone and Bioclastic wackestone. Numulitic wackestone and Milliolooidal wackestone are the microfacies identified in samples taken from Badshah Pur section while Bioclastic wackestone is the microfacies identified in samples taken from Tatrul section. Dunham's (1962) classification is used to classify Sakesar Limestone in these microfacies. According to Dunham's classification a carbonate rock is termed as Wackestone having 10-25 % grains.

5.5.1 Micro facies and depositional environment identified

Microfacies analysis of thin sections indicates that Sakesar Limestone is mainly comprising of wackestone microfacies i.e. Nummulitic wackestone, Milliolooidal wackestone and Bioclastic wackestone. Faunal association includes species of Nummulites, Lockhartia, Assilina, Alveolina and Milliolooids. These microfacies are explained as below.

5.5.1.1 Nummulitic wackestone

Nummulitic wackestone microfacies in (Plate 1) is identified in four thin sections Mustafabad (MD) (MD 1, MD 4, MD 5 and MD 6) of samples taken at interval of 0.2 m, 3.25 m, 3.7 m and 6.5 m from base (Table 5.12). Nummulitic wackestone is mainly dominated by larger benthic foraminifera. Nummulities species are abundant in larger benthic foraminifera. Other benthic foraminifera include *Alveolina* species, *Lockhartia hamei* and *Assilina*. Abundance of these benthic foraminifera is about 15-25 % with average of 20 % while abundance of matrix is about 75-85 % with average 80 % representing the wackestone depositional texture.

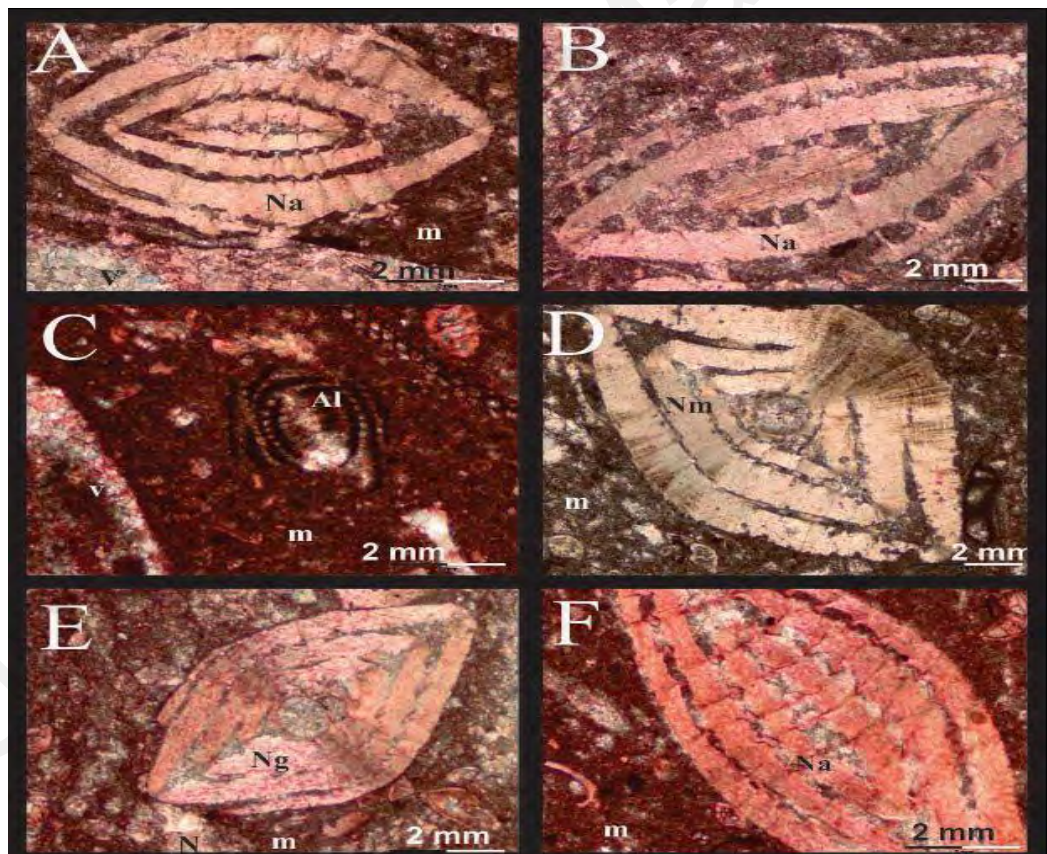


Figure 5.27: Plate 1, Nummulitic wackestone.

Description of plate 1: Nummulitic wackestone: A and B: *Nummulites ataticus* (Na), Micrite matrix (m) and spar filled vein (V). C: *Alveoline* (Al), Micrite matrix (m) and spar filled vein (v). D: *Nummulites mamillatus* (Nm) and micrite matrix (m). E:

Nummulites globules (Ng), micrite matrix (m) and neomorphism (N). F: Nummulites atacicus (Na) and Micrite matrix (m).

5.5.1.2 Milliolooidal wackestone

The Milliolooidal wackestone microfacies (Plate 2) is identified in 7 thin sections (MD 2, MD 3, MD 7, MD 8, MD 9, MD 10 and MD 11) of samples taken at the interval of 1.5 m, 1.6 m, 9.5 m, 10.3 m, 15.3 m, 15.8 m and 18.5 m from base (Table 5.12). Selected thin sections show the abundance of Milliolooids along with algal growth, Nummulites species and some Alveolina species. Percentage of benthic foraminifera is about 15-25 % with the average of 20 % while matrix % is 75 to 85 % with the average of 80 %.

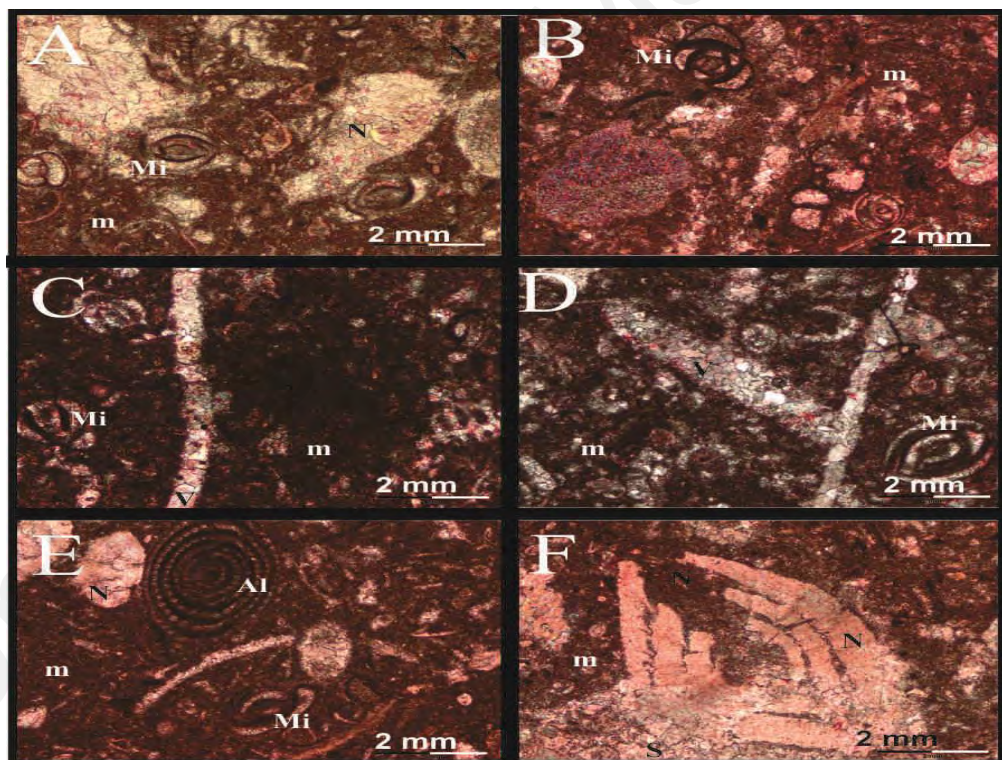


Figure 5.28: Plate 2, Milliolooidal wackestone.

Description of plate 2: The Milliolooidal wackestone microfacies is identified in 7 thin sections (MD 2, MD 3, MD 7, MD 8, MD 9, MD 10 and MD 11) of samples taken at the interval of 1.5 m, 1.6 m, 9.5 m, 10.3 m, 15.3 m, 15.8 m and 18.5 m from base (Table 5.12). Selected thin sections show the abundance of Milliolooids along with algal growth,

Nummulites species and some Alveolina species. Percentage of benthic foraminifera is about 15-25 % with the average of 20 % while matrix % is 75 to 85 % with the average of 80 %.

5.5.1.3 Bioclastic wackestone

Bioclastic wackestone is identified in 4 thin sections (PV 1, PV 2, PV 3 and PV 4 samples description are given in table below) taken at the interval of 0.25 m, 3.7 m, 4.8 m and 5.5 m from top (Table 5.13). Bioclastic wackestone is comprised mainly of larger benthic foraminifera including Nummulites, Lockhartia, Assilina species and Algal growth (Plate 3). Smaller benthic foraminifera are represented by miliolids. The abundance of benthic foraminifera is in the range of 20 to 30 % while matrix percentage is about 70 % to 80 %.

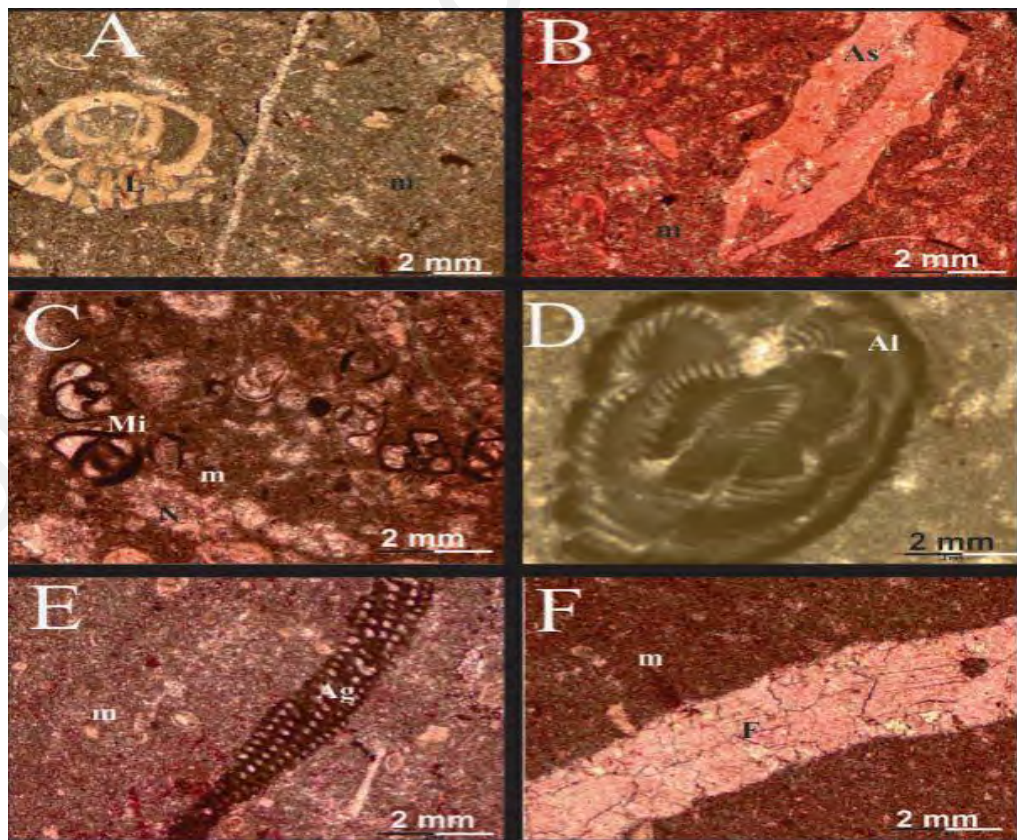


Figure 5.29: Plate 2, Milioloidal wackestone.

Description of plate 3 Bioclastic wackestone: A: *Lockhartia tipperi* (L), micrite matrix (m) and calcite filled vein. B: *Assilina subspinoso* (As) and micrite matrix (m). C: *Milliolids* (Mi), micrite matrix (m) and neomorphism (N). D: *Alveolina* species (Al). E: Algal growth (Ag) and micrite matrix (m). F: Spar filled fracture (F) and micrite matrix (m).

5.5.1.4 Diagenetic features

Detailed petrographic studies and field observations suggest the following diagenetic features in Sakesar Limestone (Plate 4):

5.5.1.4.1 Dissolution

Water supersaturated in calcite, results in the filling of the void spaces and micro fractures (Flugel, 2004). Dissolution causes the formation of voids, veins and refilling of the cement in these voids.

5.5.1.4.2 Cementation

Cementation provides strength and stability to carbonate sediments (Flugel, 2004). Cementation results in the precipitation of the very fine material in the carbonate sediments. Spar cementation is observed in various samples.

5.5.1.4.3 Compaction

Compaction is the post and syn-depositional feature. Compaction results in porosity and permeability reduction, reduction in stratigraphic thickness and breakage of grains (Flugel, 2004). Presence of broken fragments in thin sections points towards compaction.

5.5.1.4.4 Neomorphism

Neomorphism is the process which leads to the replacement of pre-existing carbonate particles with calcite (Flügel, 2004). Neomorphism has choked the void spaces and as a result porosity is reduced. This phenomenon has taken place in most of the microfacies.

5.5.1.4.5 Filled fractures and veins

In carbonate rocks mechanical compaction or regional tectonic stresses causes the fractures. Calcite precipitation results in filling of these fractures and subsequently formed calcite veins (Flügel, 2004). Calcite filled fractures are observed both at outcrop level as well as in thin sections.

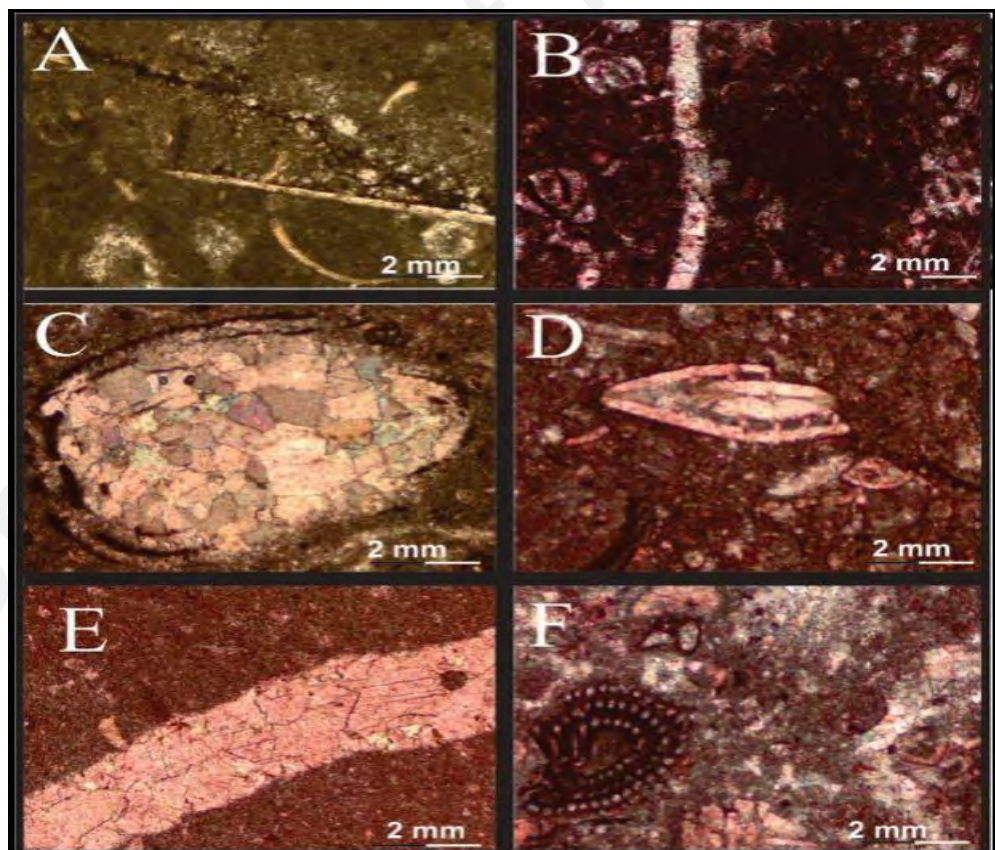


Figure 5.30: Plate 4: Diagenetic features in Sakesar Limestone, A: dissolution, B: calcite filled vein, C: neomorphism, D: compaction, E: filled fracture and F: cementation, Millioloidal wackestone.

5.5.1.5 Thin section visual porosity

The two samples that showed a distinct presence of porosity are (PV-2 and PV-3). The porosity in PV-2 is due to the dissolution whereas PV-3 shows fracture porosity which was later choked due to precipitation of secondary materials. The porosity estimated from these samples is about 14.46%. Detailed microscopic study shows fractures in the Sakesar Limestone are filled by secondary materials due to the process of neomorphism and calcite filling. Other diagenetic features that reduced porosity are micritization, cementation, compaction and pressure. In other samples, porosity range is negligible at outcrop level. Pores that are present in PV-2 are not connected due to which no channelization was developed and resulting in poor permeability.

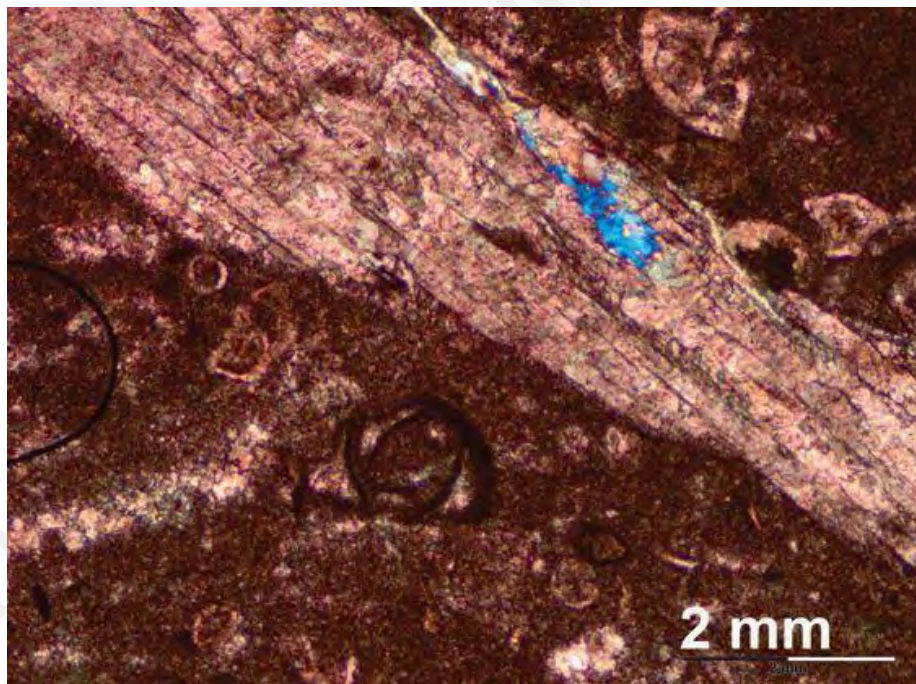


Figure 5.31: Fracture porosity in Pail Village sample 3.

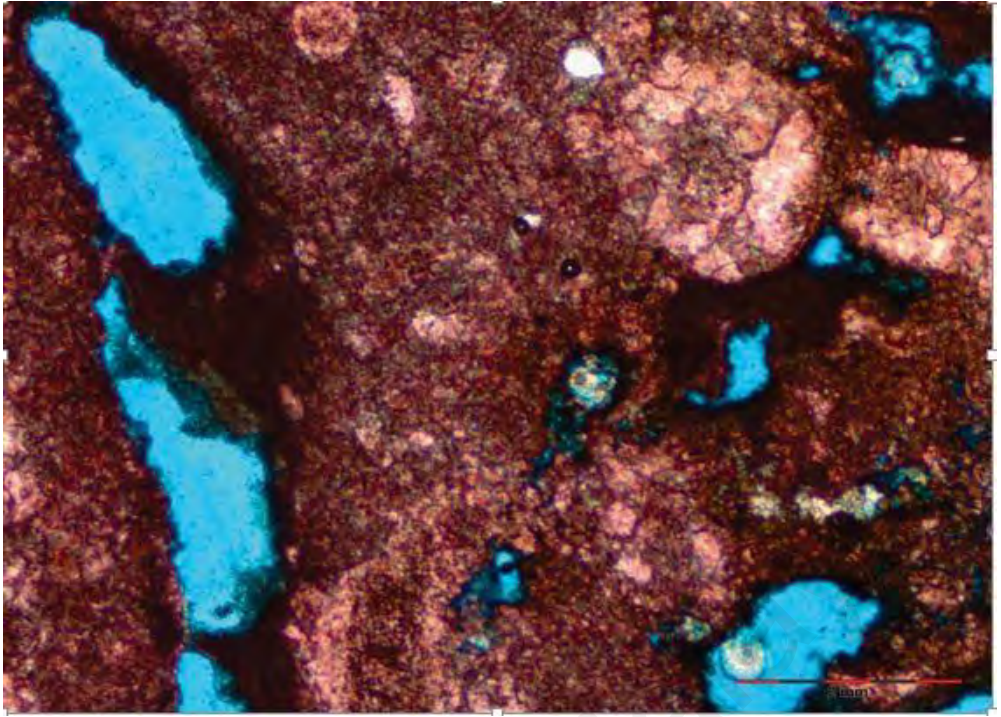


Figure 5.32: Dissolution porosity in Pail Village sample 2.




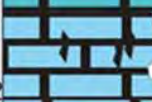









University of Manitoba

Table 5.12: Lithology, sample numbers, field description, microfacies, and photomicrographs of Mustafabad Section.


Age	Formation	Thickness (meters)	Sample number	Lithology	Description	Field photograph	Photomicrographs	Microfacies
Eocene	Sakesar Limestone	18.7	MD 11		Limestone, grey to yellowish brown, Nodular and fractured, massive, chert development.			Millioloidal Wakestone
		17						Millioloidal Wakestone
		16	MD 10		Limestone, brownish grey to yellowish grey, massive, fractured, development of chert.			Millioloidal Wakestone
		15						MD 9
		14	MD 8		Limestone, grey to yellowish grey, massive, well developed nodules.			Numulitic Wakestone
		13						MD 7
		12	MD 6		Limestone, light to yellowish grey, Marl, calcite veins, chert development, less developed nodules.			Numulitic Wakestone
		11						MD 5
		10	MD 4		Limestone, light to brownish grey, Maralcalcite veins, fossil rich, chert development and nodular.			Millioloidal Wakestone
		9						MD 3
		8	MD 2		Limestone, light to brownish grey, Maralcalcite veins, fossil rich, chert development and nodular.			Numulitic Wakestone
7	MD 1	Numulitic Wakestone						
6								
5								
4								
3								
2								
1								
0 m								

LEGEND		
Marl	Limestone	Limestone with chert


Table 5.13: Lithology, sample numbers, field description, microfacies, and photomicrographs of Pail Village section.

Age	Formation	Thickness (meters)	Sample number	Lithology	Description	Field photograph	Photo-micrographs	Micro-facies
Eocene	Sakesar Limestone	6.8	PV-1		Limestone, light grey to cream grey colored, well developed nodularity and chert.			Bioclastic wackestone
		6	PV-2		Limestone, brownish grey colored, calcite veins and nodular			Bioclastic wackestone
		5	PV-3		Limestone, brownish grey to cream grey, chert development, nodular, calcite veins.			Bioclastic wackestone
		4	PV-4					Bioclastic wackestone
		3				Limestone, light grey to cream grey, calcite veins fractured.		
		0	PV-5					


LEGEND



Nodular Limestone



Calcite veins in Limestone



Fractured Limestone

5.6 Lithofacies identified

Facies analysis was conducted on the basis of shape and trend of gamma ray and stacking of vertical profile lithology identification to make various environmental interpretations (Cant, 1992; Chow et al. 2005; Martinius et al. 2002; Posamentier & Allen, 1999; Selley, 1985; Serra, 1985). Detailed analysis has made a six fold facies scheme to be developed in Warcha sandstone Formation present in the subsurface of Balkassar block (Fig. 3.26 and 5.26).

5.6.1.1 Facies 1

The trends which lacks in any particular vertical shape is one of the characteristic of a succession which is clean and is channel deposit indicative (Cant, 1992; Chow et al. 2005). In this facies the high value spikes represents the indication of shale-clast conglomerate. Facies 1 corresponds to a very coarse to coarse grained sandstone and consists of trough cross-stratified facies that is stratified gravely sandstone and coarse-grained trough cross bedded sandstone produced from migrating sinuous crested bars or sand dunes (Ghazi & Mountney, 2010).

5.6.1.2 Facies 2

A fluvial environment is indicated by the significance absence of deposits of mudstone and finning upward elements along with thick gamma ray response (Ghazi and Mountney, 2010; Posamentier and Allen, 1999). Channel fill deposit is indicated by downward cleaning successions (Ghazi & Mountney, 2010; Martinius et al. 2002). The facies 2 have channel fill elements which are coarse-medium grained and also consists of planar and trough cross-stratified facies.

5.6.1.3 Facies 3

A point bar is indicated by characteristics of abrupt change at the base and finning upward vertical scale and have thick shape of gamma ray with bell shape trend. These facies have fine to medium grained sandstone. The serrated character may be caused by blocks of clay derived from the undercut bank by collapse during flood stages (Ghazi, 2009).

5.6.1.4 Facies 4

Sandstone is indicated by the trend which is coarsening upward and cleaning-upward having sharp top boundaries and basin and the trend is toward the shale base line (Cant, 1992; Chow et al. 2005; Posamentier & Allen, 1999). This kind of sandstone facies are recognized mostly in floodplain deposit and are medium to fine grained. The gamma ray curve is irregular whenever there is presence of carbonaceous material (Chow et al., 2005).

5.6.1.5 Facies 5

This kind of facies have coarse grained sandstone with irregular gamma ray curve. These facies tallies laminated siltstone, fine grained sandstone and claystone. The curve may be irregular if there is presence of pebbles and mica interbeds (Chow et al., 2005).

5.6.1.6 Facies 6

Floodplain deposits are indicated by the thick and irregular response shape of gamma ray log, having siltstone, intervening fine grained sandstone and erosional top (Cant, 1992). This kind of facies have laminated siltstone, mudstone, fine sandstone and claystone facies. The irregular log curve is the response of interbedded sandstone and siltstone (Cant, 1992).

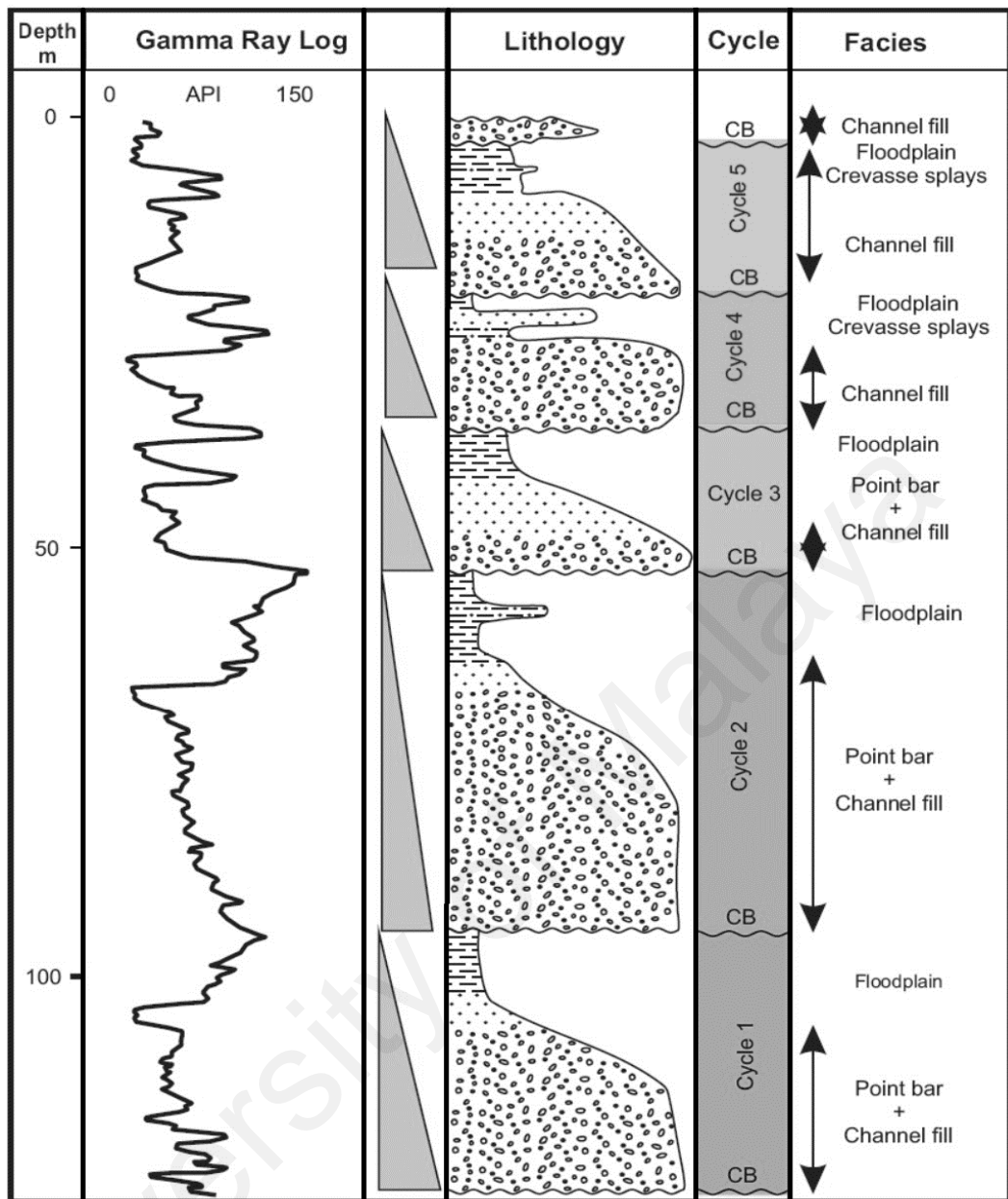


Figure 5.33: Different gamma ray log responses to the characteristic of Warcha sandstone in the subsurface of Balkassar.

5.6.2 Identified depositional environments

The main depositional elements that have been identified are channel, overbank and point bar.

5.6.2.1 Point bar

Point bar elements have been identified which are ranging from 2-5 m thickness (Fig 5.27). They have bell shaped log characteristics (Cant, 1992). The point bar shows a thinning and fining upward succession trend. They change abruptly to thin shale and sandstone beds and generally overlies the channel lag and channel fill elements can be observed in 3 cycles in Fig (5.27).

5.6.2.2 Overbank elements

These are fine grained flood plain deposited elements ranging in thickness from 2 to 10 m and can be observed and present on all 5 cycles (Fig. 5.27). High variability in shape and in trend of logs can be observed due to these elements and are symmetrical and extremely serrated.

5.6.2.3 Channel fill elements

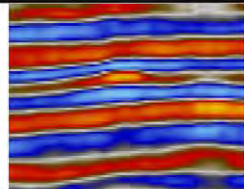
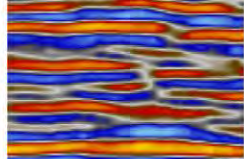

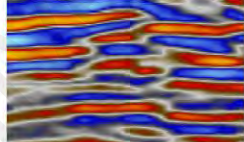
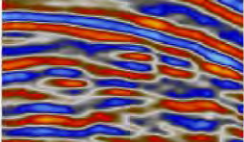
On the gamma ray the appearance and characteristics of channel fill elements are bell shaped, cylindrical and slightly serrated (Cant, 1992, Posamentier & Allen, 1999) (Fig 5.27).

5.7 Seismic facies identified

The seismic facies were identified by adopting the procedure used by (Futalan et al., 2012). After marking all of the seismic horizons and inputting the well tops and making synthetic seismogram to pin point mark the horizons, the seismic facies in the horizons have been identified. Five seismic facies (A, B, C, D, E) have been identified in the study area (Table 5.14). The distribution of facies are usually parallel, the facies have amplitude mostly moderate to high in Early Permian to Eocene horizons. The internal configurations are mostly parallel to wavy in almost all horizons succession except for Early Miocene

Murree horizon in the bottom, continuity is high in Paleocene, Eocene and in Miocene successions however it is disrupted in Cambrian and Early Permian successions this is caused by salt diapir development which initiated above basement horizon. The external geometry of all successions is sheet to wedge. There is an apparent transition in the facies type from Type A (Eocene horizons) to Type B (Miocene horizons) which is the effect of continuous development of salt diapir as it is in early stage of development.

Table 5.14: Seismic facies identified.

Seismic Facies	Reflection Attributes a) External geometry b) Internal configuration c) Continuity d) Amplitude strength	Age
A 	a) sheet to wedge b) parallel to wavy c) high continuity d) moderate to high	Paleocene- Eocene
B 	a) sheet to wedge b) parallel to wavy c) semi-continuous to high continuity d) low to moderate	Miocene
C 	a) sheet to mound b) wavy to hummocky c) disrupted to discontinuous d) moderate to high	Early Miocene
D 	a) sheet to wedge b) parallel to subparallel c) semi-continuous to disrupted d) low to moderate	Pre-Cambrian- Early Permian
E 	a) lens to wedge b) subparallel to convergent to oblique c) semi-continuous to high continuity d) low to moderate	Early-Permian

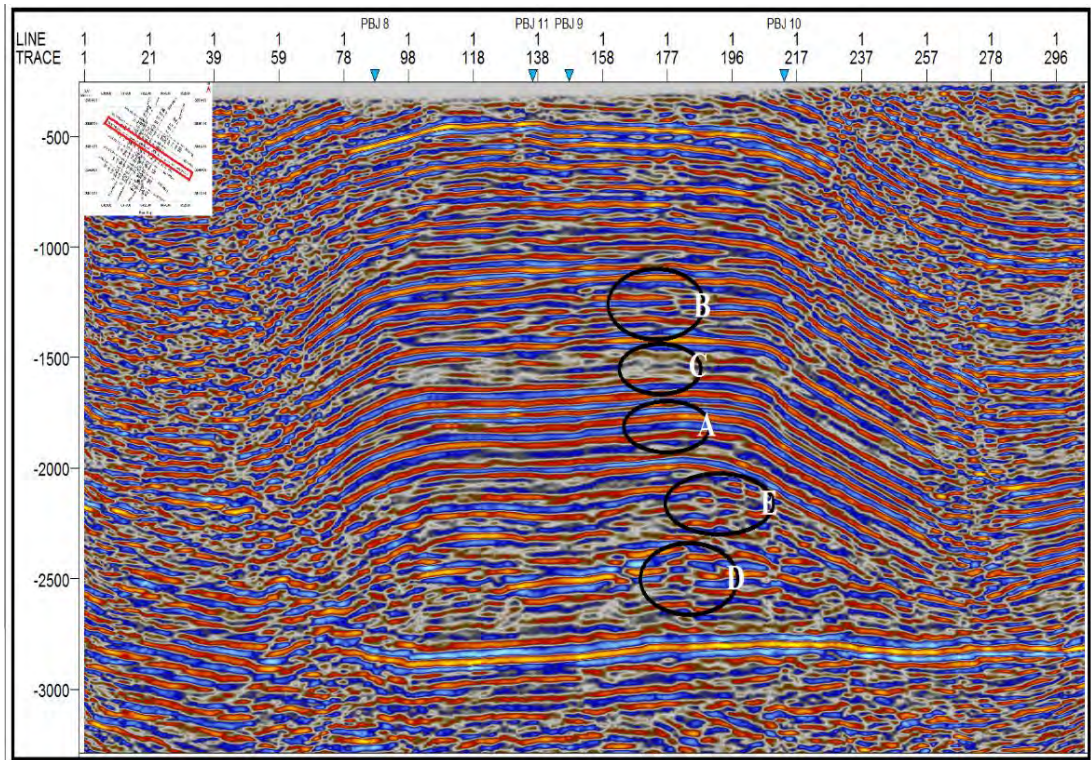


Figure 5.34 Seismic facies identified on seismic section SOX-PBJ-04.

University of M

CHAPTER 6: CONCLUSIONS

6.1 Conclusions

In this study, a combination of approaches including organic geochemistry, thin section analysis, structure interpretation and petrophysical analysis were performed to characterize source and reservoir rocks. The aim is to evaluate the hydrocarbon potential of the Balkassar block, and to interpret probable structural trap for the petroleum accumulation within the study area of the Balkassar region. The study area lies in the Upper Indus Basin, particularly in the Eastern Potwar Basin, Pakistan; its coordinates are 32°55' N and 72°39' E.

The data and samples that were used in this study includes outcrop source rock samples, complete well logs from three selected wells that have penetrated the reservoir and source rocks of the Balkassar oilfield block. Grid of eleven seismic dip and strike lines in SEG-Y format has been used in this study, whereby the well logs and seismic data was provided by Directorate General of Petroleum Concessions (DGPC) and LMKR Pakistan.

In this study, the organic geochemical analyses were performed on ten rock samples of Patala Shale Formation from two different exposed sections namely Pail Village section and Mustafabad section. From Mustafabad section three rock samples from two different mines were obtained and the other five samples were obtained from Pail Village section. The main objective was to evaluate the source rock organic matter richness, thermal maturity and the kerogen type. The assessment of source rock was based on organic geochemical analyses, which includes TOC, Rock-Eval pyrolysis and vitrinite reflectance measurements.

For determination of the source rock richness a total of ten samples were subjected to TOC analyses. Data related to thermal maturity assessment based on Rock-Eval pyrolysis and vitrinite reflectance analyses were compared using table 3.1. The kerogen type was interpreted based on the HI vs Tmax plot (see section 3.2.3 and 5.2.) (Fig. 5.2).

Generally, the petroleum source rock potential of the Balkassar is poor to fair for the studied samples with total organic carbon (TOC) ranging from 0.25 wt. % to 1.16 wt. % (see Table 3.1, 5.1 and 5.2). The Rock-Eval S2 values show poor potential with values ranging from 0.11 mg HC/g rock to 0.63 mg HC/g rock, thus the results indicate that the Patala Shale Formation has poor potential to generate hydrocarbons (see Table 3.1 for standard values) (Fig. 5.1). S2 vs TOC and hydrogen index (HI) vs Tmax were plotted to verify the type of organic matter. The HI vs Tmax plot indicates predominantly Type III and mix Type II-III kerogens. The Py-GC analysis of the analyzed samples in contrast, suggests all the analysed samples contain predominantly Type IV kerogen that may produce minor gas. This is in agreement with Rock-Eval pyrolysis data (low HI values), suggest that the shales have poor oil generating potential. With regard to maturity the VR data suggest the samples are immature to peak mature for oil generation (see section 3.2.4 and Table 3.1, 5.1 and 5.2). On the other hand Tmax of the studied samples that range from 385 to 429 °C suggesting these samples are immature for hydrocarbons generation. However, the Tmax data are regarded as anomalous considering the very low S2 values in all of the analysed samples.

Petrophysical analysis was performed to evaluate the reservoir rocks potential. A suite of wireline logs that contains spontaneous potential (SP) log, sonic log, density log, gamma ray log, neutron log, and resistivity logs of three wells were interpreted carefully to estimate reservoir rock potential of Sakesar Limestone and Chorgali formations encountered in these three wells. The analysis were performed to evaluate and estimate permeability, volume of shale, porosity, bulk volume of water, water saturation,

hydrocarbon saturation, net/gross thickness, net/gross ratio and net pay thickness of reservoir. The criteria adopted in this study for qualitative description of reservoir was adopted from Amigun & Odole (2013), Rider (1986) and Van Golf-Racht (1982) (see section 5.4 and Table 5.9).

The results of petrophysical analysis shows that both Chorgali and Sakesar Formation can act as a good reservoir, whereby both formations possess good to very good porosity and permeability quality. As per qualitative description adopted after Rider, (1986), the maximum values of average porosity and permeability were recorded in the Balkassar well 8 (see section 5.2 and Table 5.10 and 5.11). The petrophysical analysis shows that the Chorgali Formation encountered in all of the three wells possess good petrophysical reservoir rock properties. The Chorgali Formation has higher permeability, average porosity and have higher hydrocarbon saturation when compare to Sakesar Formation.

The analysis of both formations shows that the average porosity indicates a suitable reservoir ranges from 9.12% to 27.93%, permeability ranges from 01.36 mD to 255.79 and hydrocarbon saturation ranges from 53.46% to 78.13% indicating a high hydrocarbon production. Based on the statistical analysis performed, it can be concluded that the Chorgali Formation in the Balkassar oilfield possess good petrophysical properties thus it is a better reservoir to be firstly targeted for hydrocarbons exploration as compared to Sakesar Formation.

Based on the structural analysis performed in this study, the following observation and inference made can be summarized as follows.

The Balkassar anticline structure has been generated and developed by Himalayan Orogenic related compressional forces and salt diapirs. The Balkassar subsurface structure is a salt cored anticline. According to the “Development stages of salt diapir” the Balkassar structure at present is at stage 2 which is known as Active Diapirism Pillow

Stage (see section 3.3.2.1.9.1 and Fig 3.17). The initial kick start for salt movement was provided by tectonic plate's movement and Himalayan orogeny. The structure of Balkassar is recognized as a salt cored anticline structure bounded by various major faults on both sides, and the faults are found to be sealing on both sides of the anticline. The anticline has a complex structure with six major faults present in the sedimentary sequence, and with one normal fault present in the basement.

The faults are the result of Himalayan orogenic, Indian plate movement and Salt Range uplift forces. In Balkassar, the reservoir rocks are Chorgali and Sakesar formation of Eocene age that occurs at depths of ~2421 and ~2467 m respectively as interpreted from seismic and well data. Source rock is the Patala Shale Formation, which contributed to the major oil and gas producing reservoir in the region. In the contour model, a broad four way closure structure has been identified at the level of the Sakesar Formation (see section 5.3.2 and Fig. 5.27). Disturbance in the structure increase, while moving in the north-east direction from the very beginning of the structure. The contour models indicate steep limbs of anticline at NW side and gentle limbs at SE side. Note that in all of the wells that have been drilled on the Balkassar anticline, this closure has not been targeted (see section 5.3.2 and Fig 5.20 and 5.27), yet hydrocarbons may have accumulated in this closure area. For that reason this study have identified hydrocarbon traps that may have accumulation in the Sakesar Formation at the depth of ~2467 m that could potentially be explored in the near future.

Detailed petrographic studies has been conducted for Eocene Sakesar Limestone, to interpret the carbonate microfacies, diagenetic properties, environment of deposition and reservoir potential. Lithologically, Sakesar Limestone is mainly comprising of massive limestone which is light to medium grey in color, hard, fractured, fossiliferous and having cherty nodules at upper part. The lower part shows some intercalations of marl and shale in places. Three microfacies are identified based on microscopic analysis of stained thin

sections, namely Numulitic wackestone, Millioloïdal wackestone (identified in samples from Mustafabad section) and Bioclastic wackestone (identified in samples from Pail Village section).

The faunal association includes *Nummulities atacicus*, *Nummulities mamillatus*, *Nummulities globulus*, *Alveolina*, *Lockhartia tipperi*, Millioloïds, *Assilina subspinosa* and some algal growth. This faunal association and wackestone depositional texture suggests a deposition at a shallow portion of middle shelf. Diagenetic events observed in these microfacies include, cementation, compaction, dissolution, neomorphism, and calcite filling of veins and fractures. Stained thin sections data was used to evaluate reservoir potential at surface level. Process of neomorphism and calcite filling have reduced porosity and permeability at outcrop level. However two samples of Bioclastic wackestone microfacies have shown dissolution porosity in stained thin sections which is about 14%. The wackestone texture and observed faunal association suggests that the environment of deposition of Sakesar Limestone in this area is a shallower portion of the middle shelf.

The gamma ray log data interpretation indicates the presence of both sand and clay dominated lithology in Warcha Formation. The formation is bounded by marine deposits both below and above by Dandot and Sardhai formations and represents a clastic wedge of non-marine fluvial strata. The Warcha Sandstone has accumulated in a meandering fluvial environment which has been interpreted by the indication of repeating the fining upward cycles and the range of facies. The presence of high portion of overbank and flood plain deposits as compare to channel deposits indicates a broad floodplain across which channel meandered. In each succession cycle the deposition of fine grained sediments indicates that Warcha sandstone had extensive network of channel belt which drained across low relief fluvial plain. The lithofacies arrangement within Warcha Sandstone

indicates a fluvial depositional succession. As fining upward cycles are common in meandering fluvial successions these are uniform in Warcha Sandstone (Fig 5.27).

Five different seismic facies have been identified in the Balkassar block from Early Cambrian to Miocene successions (Table 5.14 and Fig 5.34). Cambrian to Early Permian successions have an apparent transition and has been disrupted as also indicated by salt diapir development stages, as the structure is at initial stage in this regard more disruption can be observed in the Cambrian-Permian successions (Figs 5.10, 5.17 and 5.34), however the Paleocene, Eocene and Miocene successions are parallel to wavy and are to disrupted, the wavy effect has been caused by the diapir movement.

6.2 Contribution of the study

Three methodologies together have been used for the first time to evaluate the structure and petroleum potential of the Balkassar Oilfield block. Advanced structural interpretation has been carried out in which three major faults were identified that were not previously identified. All of the sedimentary horizons from recent to older and basement have been marked for the first time on all seismic sections and subsequently all horizons have been mapped by 3D contour maps. The study reveals that the Balkassar anticline has been developed by salt diapirs and is on stage 2 known as “Active Diapirism Pillow Stage” in salt diapir development stages. Petrophysical analyses were conducted on the reservoir rocks of the Sakesar and Chorgali formations encountered in the three investigated wells for the first time (this gap was previously been identified by Ahsan et al., 2013). A four way closure has been identified at the level of the Sakesar Formation which may act as a potential prospect for hydrocarbon accumulation and this closure to date has not been targeted by any well in the Balkassar block. Paleocene and Eocene successions (formations) have been evaluated (this gap was also identified by Ahsan et

al., 2013). All of this research output will add significant information to the body of knowledge within the studied region and its surroundings.

6.3 Recommendations for future work

- High resolution seismic 3D data should be acquired for interpretation so that the neglected structure can also be identified.
- Fault seal analysis should be done for the length of potential prospect.
- Hangu, Lockhart, Sardhai and Warcha Sandstone formation should be evaluated for hydrocarbons.

Extensive seismic facies analysis and if available should be supported with core description study should be carried out.

REFERENCES

- Aadil, N., Sohail, G. M. (2014). 3D geological modelling of Punjab Platform, Middle Indus Basin Pakistan through Integration of wireline Logs and seismic data. *Journal of the Geological Society of India*, 83(2), 211-217.
- Abdullah, W. H. (1997). Evidence of early generation of liquid hydrocarbon from suberinite as visible under the microscope. *Organic Geochemistry*, 27(7-8), 591-596.
- Ahsan, N., Faisal, M. A., Mehmood, T., Ahmed, N., Iqbal, Z., Sameeni, S. J. (2012). 3D Modeling of subsurface stratigraphy and structural evolution of Balkassar area, Eastern Potwar, Pakistan. *Pakistan Journal of Hydrocarbon Research*, 22(2), 25-40.
- Afife, M., Littke, R., Lashin, A., All, M. A. (2018). Petrophysical reservoir-rock properties and source-rock characterization of Abu Roash Formation in Wadi El-Rayan oil field, Western Desert, Egypt. *Arabian Journal of Geosciences*, 11(14), 378.
- Afzal, J., Khan, F. R., Khan, S. N., Alam, S., Jalal, M. (2005). Foraminiferal biostratigraphy and paleoenvironments of the Paleocene Lockhart limestone from Kotal Pass, Kohat, northern Pakistan. *Pakistan Journal of Hydrocarbon Research*, 15(1), 9-24.
- Ahmed, K. A., Man, H. Q., Zeb, Y. (2012). Seismic facies modelling of Potwar Basin using seismic and well log data. *Geosciences*, 2(6), 192-211.
- Al-Fahmi, M., Plesch, A., Shaw, J., Cole, J. (2014). Evolution of Structures above a Salt Diapir. *Case Study from the Arabian Gulf Region*. 1(1), 1-27.
- Allen, L. S., Mills, W. R., Caldwell, R. L. (1965). The effects of fluid invasion in pulsed neutron logging. *Geophysics*, 30(3), 389-395.
- Allen, P. A., Allen, J. R. (2013). Basin analysis: Principles and application to petroleum play assessment. *John Wiley and Sons*. 1(3), 360-373.
- Alsop, G. I. (Ed.). (2012). Salt tectonics, sediments and prospectivity. *Geological Society of London*, 2(4), 21-28.
- Al-Fahmi, M., Cooke, M. L., Cole, J. C. (2014). Modeling of the Dammam outcrop fractures: Case study for fracture development in salt-cored structures. *GeoArabia*, 19(4), 49-80.
- Amigun, J.O. Odole, O.A., 2013. Petrophysical Properties Evaluation for Reservoir Characterisation of SEYI Oil Field (Niger-Delta). *International Journal of Innovation and Applied Studies*, 3(3), 756-773.
- Archer, S. G., Alsop, G. I., Hartley, A. J., Grant, N. T., Hodgkinson, R. (2012). Salt tectonics, sediments and prospectivity: an introduction. *Geological Society, London, Special Publications*, 363(1), 1-6.

- Asquith, G. B., Krygowski, D., Gibson, C. R. (2004). Basic Well Log Analysis. Tulsa. *American Association of Petroleum Geologists*, 16(2), 36-43.
- Ashraf, U., Zhu, P., Anees, A., Abbas, A., Talib, M. A. (2016). Analysis of Balkassar Area Using Velocity Modeling and Interpolation to Affirm Seismic Interpretation, Upper Indus Basin. *Geosciences*, 6(3), 78-91.
- Baker, D. M. (1987). Balanced structural cross-sections of the central Salt Range and Potwar Plateau of Pakistan: shortening and overthrust deformation. *Geology*, 3(4), 36-40.
- Baker, D. M., Lillie, R. J., Yeats, R. S., Johnson, G. D., Yousuf, M., Zamin, A. S. H. (1988). Development of the Himalayan frontal thrust zone: Salt Range, Pakistan. *Geology*, 16(1), 3-7.
- Balme, B. E. (1970). *Palynology of Permian and Triassic strata in the Salt range and Surghar range, West Pakistan* (1st ed., Vol. 1, pp. 1-80). Lawrence Publisher, University Press of Kansas.
- Bassiouni, Z. (1994). *Theory, measurement, and interpretation of well logs* (2nd ed., Vol. 4, pp. 1-320). Henry L. Doherty Memorial Fund, New York, Society of Petroleum Engineers Press.
- Baskin, D. K., & Peters, K. E. (1992). Early Generation Characteristics of a Sulfur-Rich Monterey Kerogen. *American Association of Petroleum Geologist Bulletin*, 76(1), 1-13.
- Beardsmore, G. R., & Cull, J. P. (2001). *Crustal Heat Flow: a Guide to Measurement and Modelling* (4th ed., Vol. 4, pp. 1-280). UK, Cambridge University Press.
- Behar, F., & Pelet, R. (1985). Pyrolysis-gas chromatography applied to organic geochemistry: structural similarities between kerogens and asphaltenes from related rock extracts and oils. *Journal of Analytical and Applied pyrolysis*, 8(1), 173-187.
- Behar, F., Tang, Y., Liu, J. (1997). Comparison of rate constants for some molecular tracers generated during artificial maturation of kerogens: influence of kerogen type. *Organic Geochemistry*, 26(3-4), 281-287.
- Bannert, D., Bender, F. K., Bender, H., Grüneberg, F., Kazmi, A. H., Raza, H. A., Shams, F. A. (1995). Geology of Pakistan. *Gebrüder Borntraeger, Berlin*, 2(1), 12-17.
- Bjorlykke, K. (1989). *Sedimentology and Petroleum Geology* (3rd ed., Vol. 4, pp. 30-390). New York, United States: Springer press.
- Brun, J. P. (1983). L'origine des domes gneissiques; modeles et tests. *Bulletin de la Société Géologique de France*, 7(2), 219-228.
- Burbank, D. W., Reynolds, R. G. (1988). Stratigraphic keys to the timing of thrusting in terrestrial foreland basins: Applications to the north-western Himalaya (1st ed., Vol. 1, pp. 20-45). *New Perspectives in Basin Analysis*. New York, Springer.

- Burnham, A. K., Sweeney, J. J. (1989). A chemical kinetic model of vitrinite maturation and reflectance. *Geochimica et Cosmochimica Acta*, 53(10), 2649-2657.
- Busch, D. A. (1959). Prospecting for stratigraphic traps. *American Association of Petroleum Geologist Bulletin*, 43(12), 2829-2843.
- Carr, A. D. (2000). Suppression and retardation of vitrinite reflectance, Part 1. Formation and significance for hydrocarbon generation. *Journal of Petroleum Geology*, 23(3), 313-343.
- Cheema, M. R., Raza, S. M., Ahmad, H. (1977). Cainozoic. *Stratigraphy of Pakistan*, 12(1), 56-98.
- Chenoweth, P. A. (1971). Unconformity traps. *American Association of Petroleum Geologist Bulletin*, 55(2), 333-333.
- Coffeen, J. A. (1978). *Seismic exploration fundamentals* (1st ed., Vol. 1, pp. 40-277). Houston, Texas U.S.A. PennWell Publishing Company.
- Copard, Y., Disnar, J. R., Becq-Giraudon, J. F. (2002). Erroneous maturity assessment given by Tmax and HI Rock-Eval parameters on highly mature weathered coals. *International Journal of Coal Geology*, 49(1), 57-65.
- Davis, G. H., Reynolds, S. J., Cruden, A. R. (1996). Structural Geology of Rocks and Regions. *Economic Geology and the Bulletin of the Society of Economic Geologists*, 91(6), 1163.
- Davis, L. M. (1926). Notes on the correlation of Pinfold's Chharat Series with the Eocene stages of Sind and Europe. *Transition Mining Geology Institute India*, 20(2), 195-215.
- Davies, L. M. (1930). The fossil fauna of the Samana range and some neighboring areas: part VI. *Memoirs Geological Survey India*, 15(1), 66-81.
- Davis, L. M., Pinfold, E. S. (1937). The Eocene Beds of the Punjab Salt Range; Appendix: Correlation of the Salt Range beds with—Eocene beds of Tibet. *Memoirs Geological Survey India*, 24(1), 68-71.
- Dembicki Jr, H., Horsfield, B., Ho, T. T. (1983). Source rock evaluation by pyrolysis-gas chromatography. *American Association of Petroleum Geologist Bulletin*, 67(7), 1094-1103.
- Dembicki Jr, H. (2009). Three common source rock evaluation errors made by geologists during prospect or play appraisals. *American Association of Petroleum Geologist Bulletin*, 93(3), 341-356.
- Dixon, J. M. (1975). Finite strain and progressive deformation in models of diapiric structures. *Tectonophysics*, 28(1-2), 89-124.

- Dobrin, M.B. and Savit, C.H. (1988). *Introduction to Geophysical Prospecting* (4th ed., Vol. 1, pp. 20-867). McGraw-Hill, New York. Scientific Research an Academic Publisher.
- Dobrin, M. B. (1977). Seismic exploration for stratigraphic traps. *American Association of Petroleum Geologist Memoirs*, 26(2), 329-351.
- Duncan, R. A., Varne, R. (1988). The age and distribution of the igneous rocks of Macquarie Island. *Royal Society of Tasmania*, 122(1), 45-50.
- Duppenbecker S. J., Eliffe J. E. (1998). Basin Modelling: Practice and Progress, *Geological Society Special Publication*, 2(9), 98-103.
- Duroy, Y., Farah, A., Lillie, R. J. (1989). Subsurface densities and lithospheric flexure of the Himalayan foreland in Pakistan. *Geological Society of America Special Papers*, 232(3), 217-236.
- Durand, B. (Ed.). (1980). *Kerogen: Insoluble organic matter from sedimentary rocks* (1st ed., Vol. 5, pp. 35-53). Paris, France. Editions technip, Paris Publisher.
- Eames, F. E. (1951). A contribution to the study of the Eocene in western Pakistan and western India: A. The geology of standard sections in the western Punjab and in the Kohat district. *Quarterly Journal of the Geological Society*, 107(1-4), 159-171.
- Edgell, H. S. (1991). Proterozoic salt basins of the Persian Gulf area and their role in hydrocarbon generation. *Precambrian Research*, 54(1), 1-14.
- Edgell, H. S. (1996). Salt tectonism in the Persian Gulf basin. *Geological Society, London, Special Publications*, 100(1), 129-151.
- Espitalié, J., Laporte, J. L., Madec, M., Marquis, F., Leplat, P., Paulet, J., Boutefeu, A. (1977). Méthode rapide de caractérisation des roches mères, de leur potentiel pétrolier et de leur degré d'évolution. *Revue de l'Institut Français du Pétrole*, 32(1), 23-42.
- Espitalié, J., Bordenave, M. L. (1993). *Rock-eval* pyrolysis. *Applied Petroleum Geochemistry*, 2(2), 2-11.
- Farah, A., Abbas, G., De Jong, K. A., Lawrence, R. D. (1984). Evolution of the lithosphere in Pakistan. *Tectonophysics*, 105(1), 207-227.
- Farah, Abul, Mirza, M.A., Ahmad, M.A., Butt, M.H., 1977, Gravity field of the buried shield in the Punjab Plain, Pakistan: *Geological Society of America Bulletin*, 88(1), 1147–1155.
- Fatmi, A. N. (1974). Lithostratigraphic units of the Kohat-Potwar province, Indus basin, Pakistan. *Geological Survey of Pakistan*, 10(1), 1-80.
- Fazeelat, T., Jalees, M. I., Bianchi, T. S. (2010). Source rock potential of Eocene, Paleocene and Jurassic deposits in the subsurface of the Potwar Basin, northern Pakistan. *Journal of Petroleum Geology*, 33(1), 87-96.

- Fossen, H. (2016). *Structural geology* (1st ed., Vol. 1, pp. 35-480). UK, Cambridge University Press.
- Gadallah, M. R., Fisher, R. (2008). *Exploration Geophysics* (1st ed., Vol. 1, pp. 1-228).. Berlin, Springer Science and Business Media Publisher.
- Gadallah, M. R., Fisher, R. (2009). *Seismic Interpretation*. In *Exploration Geophysics* (2nd ed., Vol. 1, pp. 1-266). Springer Berlin Heidelberg Publisher.
- Gansser, A. (1979). The Himalayas a fascinating geological challenge. *Tectonophysics*, 4(1), 17-21.
- Gansser, A. (1980). The significance of the Himalayan suture zone. *Tectonophysics*, 62(1-2), 3743-4052.
- Gee, E. R. (1980). Pakistan geological Salt Range series. *Geological Society of America Special Papers*, 2(1), 12-17.
- Gee, E. R., Gee, D. G. (1989). Overview of the geology and structure of the Salt Range, with observations on related areas of northern Pakistan. *Geological Society of America Special Papers*, 232(3), 95-112.
- Gill, W. D. (1951). The stratigraphy of the Siwalik Series in the northern Potwar, Punjab, Pakistan. *Quarterly Journal of the Geological Society*, 107(1-4), 375-394.
- Giraud, A. (1970). Application of pyrolysis and gas chromatography to geochemical characterization of kerogen in sedimentary rock. *American Association of Petroleum Geologist Bulletin*, 54(3), 439-455.
- Ghazi, S., Mountney, N. P. (2010). Subsurface Lithofacies Analysis of the Fluvial Early Permian Warchha Sandstone, Potwar Basin, Pakistan. *Journal of the Geological Society of India*, 76(5), 505-517.
- Ghazi, S., Ali, S. H., Sahraeyan, M., Hanif, T. (2015). An overview of tectonosedimentary framework of the Salt Range, northwestern Himalayan fold and thrust belt, Pakistan. *Arabian Journal of Geosciences*, 8(3), 1635-1651.
- Gill, W. D. (1953). Facies and fauna in the Bhadrar beds of the Punjab Salt Range, Pakistan. *Journal of Paleontology*, 3(2), 824-844.
- Giles, K. A., Lawton, T. F. (2002). Halokinetic sequence stratigraphy adjacent to the El Papalote diapir, northeastern Mexico. *American Association of Petroleum Geologist Bulletin*, 86(5), 823-840.
- Gluyas, J., and Swarbrick, R. (2013). *Petroleum Geoscience* (1st ed., Vol. 1, pp. 20-376).. John Wiley and Sons Publishers.
- Gondouin, M., Hill, H.J., Waxman, M.H. 1962. A Tri-Chemical Component of the SP Curve. *Journal Petroleum Technology*, 14 (3), 301-305.

- Grelaud, S., Sassi, W., de Lamotte, D. F., Jaswal, T., Roure, F. (2002). Kinematics of eastern Salt Range and South Potwar basin (Pakistan): a new scenario. *Marine and Petroleum Geology*, 19(9), 1127-1139.
- Hakimi, M. H., Abdullah, W. H. (2013). Organic geochemical characteristics and oil generating potential of the Upper Jurassic Safer shale sediments in the Marib-Shabowah Basin, western Yemen. *Organic Geochemistry*, 54(1), 115-124.
- Hakimi, M. H., Abdullah, W. H., Shalaby, M. R. (2012). Geochemical and petrographic characterization of organic matter in the Upper Jurassic Madbi shale succession (Masila Basin, Yemen): origin, type and preservation. *Organic Geochemistry*, 49(2), 18-29.
- Halbouty, M. T. (1972). Rationale for deliberate pursuit of stratigraphic, unconformity, and paleogeomorphic traps. *American Association of Petroleum Geologist Bulletin*, 56(3), 537-541.
- Handhal, A. M., Mahdi, M. M. (2016). Basin modeling analysis and organic maturation for selected wells from different oil fields, Southern Iraq. *Modeling Earth Systems and Environment*, 2(4), 189-194.
- Hantschel, T., & Kauerauf, A. I. (2009). *Fundamentals of basin and petroleum systems modeling* (1st ed., Vol. 1, pp. 2-404). Berlin, Springer Science and Business Media Publishers.
- Harding, R., & Huuse, M. (2015). Salt on the move: multi stage evolution of salt diapirs in the Netherlands North Sea. *Marine and Petroleum Geology*, 61(3), 39-55.
- Harding, T., & Lowell, J. D. (1979). Structural styles, their plate-tectonic habitats, and hydrocarbon traps in petroleum provinces. *American Association of Petroleum Geologist Bulletin*, 63(7), 1016-1058.
- Harris, N. B., Freeman, K. H., Pancost, R. D., White, T. S., Mitchell, G. D. (2004). The character and origin of lacustrine source rocks in the Lower Cretaceous synrift section, Congo Basin, west Africa. *American Association of Petroleum Geologist Bulletin*, 88(8), 1163-1184.
- Hasany, S. T., Saleem, U. (2012). An integrated subsurface geological and engineering study of Meyal field, Potwar plateau, Pakistan. *Search and Discovery Article*, 2015(1), 1-41.
- Horgan, G. W. (February 1999). "An investigation of the geometric influences on pore space diffusion". *Geoderma*, 88 (1-2), 55-71.
- Horsfield, B. (1989). Practical criteria for classifying kerogens: some observations from pyrolysis-gas chromatography. *Geochimica et Cosmochimica Acta*, 53(4), 891-901.
- Hudec, M. R., Jackson, M. P. (2007). Terra infirma: Understanding salt tectonics. *Earth-Science Reviews*, 82(1-2), 1-28.

- Hunt, J. M. (1996). *Petroleum Geochemistry and Geology* (2nd ed., Vol. 133, pp. 200-743). New York, WH Freeman Company Publishers.
- Hussain, B. R. (1967). Saiduwali Member, a new name for the lower part for the Permian Amb Formation, West Pakistan. Karachi University Studies. *Science and Technology*, 4(2), 88-95.
- International, C. F. C. A. O. P. (1998). The new vitrinite classification (ICCP System 1994). *Fuel*, 77(5), 349-358.99.
- Iqbal, S., Akhter, G., Bibi, S. (2015). Structural model of the Balkassar area, Potwar Plateau, Pakistan. *International Journal of Earth Sciences*, 104(8), 2253-2272.
- Iqbal, M.W.A., & Shah, S.M.I., 1980, A guide to the stratigraphy of Pakistan: Quetta, *Geological Survey of Pakistan Records*, 53(2), 34-39.
- Iqbal, N., yaseen, A., Lashari, R., Usmani, P., Ahsan, N. (2015). Some Palycepod Fossils from Chorgali Formation, Nurpur Area, Central Salt Range, Pakistan. *Sindh University Research Journal*, 43(2), 111-116.
- Iqbal, S., Jan, I. U., Hanif, M. (2014). The Mianwali and Tredian formations: An example of the Triassic Progradational deltaic system in the low-latitude western Salt Range, Pakistan. *Arabian Journal for Science and Engineering*, 39(7), 5489-5507.
- Iqbal, S., Jan, I. U., Akhter, G., Wagreich, M., Hanif, M. (2014). Triassic–Jurassic boundary: evidences from the Tethyan Salt Range, Pakistan and correlation with Europe. *Journal Himalayan Earth Science*, 36-37, 76-82.
- Jadoon, I.A.K., Frisch, W., Jaswal, T.M. Kemal, A., 1999. Triangle zone in the Himalayan Foreland, north Pakistan. *Geosciences* 2(6), 192-211.
- Jadoon, I. A., Frisch, W. (1997). Hinterland-vergent tectonic wedge below the Riwat thrust, Himalayan foreland, Pakistan: Implications for hydrocarbon exploration. *American Association of Petroleum Geologist Bulletin*, 81(3), 438-448.
- Jaswal, T. M. (1999). Triangle zone in the Himalayan foreland, north Pakistan. Himalaya and Tibet: mountain roots to mountain tops. *Journal Himalayan Earth Science* 1(2), 28-33.
- Jaswal, T.M., Lillie, R.J. Lawrence, R.D., 1997. Structure and evolution of the Northern Potwar deformed zone, Pakistan. *American Association of Petroleum Geologist Bulletin*, 81(2), 308-328.
- Jain, A. K. (2014). When did India–Asia collide and make the Himalaya. *Current Science*, 106(2), 254-266.
- Jaswal, T. M., Lillie, R. J., Lawrence, R. D. (1997). Structure and evolution of the northern Potwar deformed zone, Pakistan. *American Association of Petroleum Geologist Bulletin*, 81(2), 308-328.

- Johnson, B. D., Powell, C. M., Veevers, J. J. (1976). Spreading history of the eastern Indian Ocean and Greater India's northward flight from Antarctica and Australia. *Geological Society of America Bulletin*, 87(11), 1560-1566.
- Jungslager, E. H. (1999). Petroleum habitats of the Atlantic margin of South Africa. *Geological Society, London, Special Publications*, 153(1), 153-168.
- Kadri, I. B. (1995). *Petroleum geology of Pakistan* (1st ed., Vol. 1, pp. 1-275). Karachi Pakistan Petroleum Limited, Ferozsons (pvt) Limited Press.
- Kazmi, A. H., Abbasi, I. A. (2008). *Stratigraphy and historical geology of Pakistan* (1st ed., Vol. 1, pp. 1-524). Peshawar, Department & National Centre of Excellence in Geology press.
- Kazmi, A. H., Jan, M. Q. (1997). *Geology and tectonics of Pakistan* (1st ed., Vol. 1, pp. 1-497). Nazimabad, Karachi – Pakistan, Graphic Publishers 5C, 6/10, Nazimabad, Karachi - Pakistan.
- Kazmi, A.H. Rana, R.A., 1982. *Tectonic map of Pakistan* (1st ed., Vol. 5, pp. 20-60). Karachi, Pakistan, Graphic publishers.
- Kearey, P., Brooks, M., Hill, I. (2013). *An introduction to Geophysical Exploration* (3rd ed., Vol. 1, pp. 20-272). New York, John Wiley and Sons Publishers.
- Kemal, A., Balkwill, H. R., Stoakes, F. A. (1991, November). Indus Basin hydrocarbon plays. In New directions and strategies for accelerating petroleum exploration and production in Pakistan: *International Petroleum*, 1(1), 76-105.
- Kemal, A., (1992) Geology and new trends for hydrocarbon exploration in Pakistan, in Ahmed, G., Kemal, A., Zaman, A.S.H., and Humayon, M., eds., New directions and strategies for accelerating petroleum exploration and production in Pakistan. *Ministry of Petroleum and Natural Resources*, 2(4) 16–57.
- Keym, M., Dieckmann, V., Horsfield, B., Erdmann, M., Galimberti, R., Kua, L. C., Podlaha, O. (2006). Source rock heterogeneity of the Upper Jurassic Draupne Formation, North Viking Graben, and its relevance to petroleum generation studies. *Organic Geochemistry*, 37(2), 220-243.
- Khalid, P., Yasin, Q., Sohail, G. M. D., Kashif, J. M. (2015). Integrating core and wireline log data to evaluate porosity of Jurassic formations of Injra-1 and Nuryal-2 wells, Western Potwar, Pakistan. *Journal of the Geological Society of India*, 86(5), 553-562.
- Khan, I. A., Bridge, J. S., Kappelman, J., Wilson, R., 1997. Evolution of Miocene fluvial environments, eastern Potwar plateau, northern Pakistan. *Sedimentology*, 44(2), 221-251.
- Khan MA., Ahmed R., Raza HA., Kemal A., (1986) Geology of petroleum in Kohat-Potwar depression, Pakistan. *American Association of Petroleum Geologist Bulletin*, 70(2), 396–414.

- Koyi, H. (1998). The shaping of salt diapirs. *Journal of Structural Geology*, 20(4), 321-338.
- Krzywiec, P. (2010). Triassic evolution of the Klodawa salt structure: basement-controlled salt tectonics within the Mid-Polish Trough (Central Poland). *Geological Quarterly*, 48(2), 123-134.
- Kumar, P., Yuan, X., Kumar, M. R., Kind, R., Li, X., Chadha, R. K. (2007). The rapid drift of the Indian tectonic plate. *Nature*, 449(7164), 894-897.
- Langford, F. F., Blanc-Valleron, M. M. (1990). Interpreting Rock-Eval pyrolysis data using graphs of pyrolizable hydrocarbons vs. total organic carbon (1). *American Association of Petroleum Geologist Bulletin*, 74(6), 799-804.
- Larter, S. R. (1984). Application of analytical pyrolysis techniques to kerogen characterization and fossil fuel exploration/exploitation. *Analytical pyrolysis*, 1(1), 212-275.
- Larter, S. R., Douglas, A. G. (1980). A pyrolysis-gas chromatographic method for kerogen typing. *Physics and Chemistry of the Earth*, 12(1), 579-583.
- Larionov, V. V. (1969). *Radiometry of boreholes* (2nd ed., Vol. 8, pp. 8-26). Moscow, Nedra Publishers.
- Lashin, A., 2007. Velocity modelling of the Upper Cretaceous Baharya reservoir, using variogram and principal component analyses, North of Qattara Depression, Western Desert-Egypt. *Journal Applied Geophysics*. 6 (1), 279-303.
- Lashin, A., Mogren, S., 2012. Analysis of well log and pressure data of the gasbearing sand reservoirs of Kafr El-Sheikh formation: case study from the offshore Nile Delta-Egypt. *International Journal of Physical Science*. 7 (35), 53-66.
- Lashin, A., Ahmed, G., Abd El Aal, M., 2006. Improving and predicting the petrophysical parameters of the reservoirs using Monte Carlo Simulation and Stochastic analysis. *Journal Egypt Geophysics Society*, 4 (1), 1-16.
- Lashin, A., El Shahat, W., Sharaf, M., 2003. Formation evaluation of the Cenomanian and Lower Cretaceous rocks in the north eastern part of Sinai. *Journal Egypt Geophysics Society*, 47 (2), 1297-1324.
- Lashin, A., Marta, E. B., Khamis, M. (2016). Characterization of the Qishn sandstone reservoir, Masila Basin–Yemen, using an integrated petrophysical and seismic structural approach. *Journal of African Earth Sciences*, 115(3), 121-142.
- Latif, M. A. (1970). Micropaleontology of the Galis Group, Hazara, West Pakistan. *Jahrbuch der Geologischen Bundesanstalt, Sonderband*, 15(1), 63-66.
- Levin, H. L. (2009). *The earth through time* (9th ed., Vol. 8, pp. 80-624). John Wiley and Sons Publishers.
- Levorsen, A. I., Berry, F. A. (1967). *Geology of Petroleum* (1st ed., Vol. 1, pp. 20-724). San Francisco: WH Freeman Company Publishers.

- Lewis, G. E. (1937). A new Siwalik correlation. *American Journal of Science*, 11(195), 191-204.
- Lewan, M. D. (1984). Factors controlling the proportionality of vanadium to nickel in crude oils. *Geochimica et Cosmochimica Acta*, 48(11), 2231-2238.
- Lillie, R. J., Johnson, G. D., Yousuf, M., Zamin, A. S. H., Yeats, R. S. (1987). Structural development within the Himalayan foreland fold-and-thrust belt of Pakistan. *American Association of Petroleum Geologists*, 3(1), (379-392)
- Loveless, J. P., Allmendinger, R. W., Pritchard, M. E., González, G. (2010). Normal and reverse faulting driven by the subduction zone earthquake cycle in the northern Chilean fore arc. *Tectonics*, 29(2), 112-17.
- Magoon, L. B., Dow, W. G. (1994). *The Petroleum System* (2nd ed., Vol. 6, pp. 3-24). Menlo Park, California U.S. Geological Survey Press,
- Kemal, A., (1986) *Geology and new trends for Petroleum Exploration in Pakistan* (1st ed., Vol. 1, pp. 3-24). New directions and strategies for accelerating petroleum exploration and production in Pakistan, New York, USGS Publisher.
- Maqsood Malik, A., Ahmed, N. (2014). Paleocene Carbonate of Kohat-Potwar Sub-Basin of Upper Indus Basin, Pakistan. *Science International*, 26(5), 62-69.
- McDougall, J. W., Khan, S. H. (1990). Strike-slip faulting in a foreland fold-thrust belt: The Kalabagh Fault and Western Salt Range, Pakistan. *Tectonics*, 9(5), 1061-1075.
- Memon, A. D., Siddiqui, I. (2005). *Petroleum Geology and Hydrocarbon Prospects of Sindh, Pakistan* (1st ed., Vol. 6, pp. 3-20). Hyderabad, Allah Dino Memon Publishers.
- Mehmood, W., Aadil, N., Jadoon, Y. K. (2015). Evaluation of Petrophysical Properties for Reservoir Characterization of Eocene Age in Meyal Field, Potwar Basin–Pakistan. *Science International Lahore*, 27(5), 4187-4190.
- Moghal, M.A., Hameed, A., Saqi, M.I. Bugti, M.N., 2003. Subsurface geometry of Potwar sub-basin in relation to structuration and entrapment. *Pakistan Association of Petroleum Geologist Bulletin*, 7(5), 85-98.
- Moghal, M. A., Hameed, A., Saqi, M. I., Bugti, M. N. (2007). Subsurface geometry of Potwar sub-basin in relation to structuration and entrapment. *Pakistan Journal of Hydrocarbon Research*, 17(2), 61-72.
- Mohadjer, S., Bendick, R., Ischuk, A., Kuzikov, S., Kostuk, A., Saydullaev, U., Molnar, P. (2010). Partitioning of India-Eurasia convergence in the Pamir-Hindu Kush from GPS measurements. *Geophysical Research Letters*, 37(4), 24-31.
- Molnar, P., Tapponnier, P. (1981). A possible dependence of tectonic strength on the age of the crust in Asia. *Earth and Planetary Science Letters*, 52(1), 107-114.

- Molnar, P. (1990). A review of the seismicity and the rates of active underthrusting and deformation at the Himalaya. *Journal of Himalayan Geology*, 1(2), 131-154.
- McGuinness, D. B. Hossack, J. R. 1993. The development of allochthonous salt sheets as controlled by the rates of extension, sedimentation, and salt supply: Rates of geological processes. *Gulf Coast Section*, 1(2), 127-139.
- Najoui, Z., Riazanoff, S., Deffontaines, B., Xavier, J. P. (2018). Estimated location of the seafloor sources of marine natural oil seeps from sea surface outbreaks: A new "source path procedure" applied to the northern Gulf of Mexico. *Marine and Petroleum Geology*, 91(3), 190-201.
- Nabawy, B.S., Rochette, P., Geraud, Y., 2009. Petrophysical and magnetic pore network anisotropy of some Cretaceous sandstone from Tushka basin, Egypt. *Geophysics Journal International*. 177 (1), 43-61.
- Nederlof, M. H. (1979). The use of habitat of oil models in exploration prospect appraisal: Proceedings of the 10th World Petroleum Congress. *Bucharest Romania*, 81(2), 13-21.
- Nixon, R. P. (1973). Oil source beds in Cretaceous Mowry Shale of northwestern interior United States. *American Association of Petroleum Geologist Bulletin*, 57(1), 136-161.
- Noetling, F. (1901). *Beiträge zur Geologie der Salt Range: insbesondere der permischen und triassischen Ablagerung* (1st ed., Vol. 1, pp. 24-198). E Schweizerbart'sche Verhandlungen (E. Nägele). Stuttgart, Germany, Schweizerbart science publishers
- Oil and Gas Development Corporation [OGDC], 1996, *Pakistan Petroleum Prospects. An overview: Islamabad* (1st ed., Vol. 1, pp. 24-68). Oil and Gas Development Corporation Press.
- Orife, J. M., Avbovbo, A. A. (1982). Stratigraphic and unconformity traps in the Niger Delta. *American Association of Petroleum Geologist*, 1(2), 23-28.
- Ortoleva, P. J. (1994). Basin Compartments and Seals, *American Association of Petroleum Geologist*, 1(2), 61-66.
- Onajite, E. (2013). *Seismic data analysis techniques in hydrocarbon exploration* (1st ed., Vol. 31, pp. 1-256). New York, Elsevier Publishers.
- Orr, W. L. (1986). Kerogen asphaltene sulfur relationships in sulfur-rich Monterey oils. *Organic Geochemistry*, 10(1-3), 499-516.
- Peters, K. E. (1986). Guidelines for evaluating petroleum source rock using programmed pyrolysis. *American Association of Petroleum Geologist Bulletin*, 70(3), 318-329.
- Peters, K. E., Cassa, M. R. (1994). Applied source rock geochemistry: Essential elements. *American Association of Petroleum Geologist Bulletin*, 2(1), 18-25.

- Peters, K. E., Whelan, J. K., Hunt, J. M., Tarafa, M. E. (1983). Programmed pyrolysis of organic matter from thermally altered Cretaceous black shales. *American Association of Petroleum Geologist Bulletin*, 67(11), 2137-2146.
- Peters, K. E., Peters, K. E., Walters, C. C., Moldowan, J. M. (2005). *The biomarker guide* (1st ed., Vol. 7, pp. 750-900). UK, Cambridge University Press.
- Peters, K. E., Moldowan, J. M., Sundararaman, P. (1990). Effects of hydrous pyrolysis on biomarker thermal maturity parameters: Monterey phosphatic and siliceous members. *Organic Geochemistry*, 15(3), 249-265.
- Peters, K. E., Moldowan, J. M. (1993). The biomarker guide: interpreting molecular fossils in petroleum and ancient sediments. *American Association of Petroleum Geologist Bulletin*, 2(1), 18-25.
- Pennock, E. S. (1988). Structural interpretation of seismic reflection data from the eastern Salt Range and Potwar Plateau, Pakistan. *American Association of Petroleum Geologist*, 1(1), 841-857.
- Pennock, E. S., Lillie, R. J., Zaman, A. S. H., Yousaf, M. (1989). Structural interpretation of seismic reflection data from eastern Salt Range and Potwar Plateau, Pakistan. *American Association of Petroleum Geologist Bulletin*, 73(7), 841-857.
- Petroconsultants, (1996), *Petroleum exploration and production* (1st ed., Vol. 1, pp. 12-27). Petroconsultants: Islamabad, Oil and Gas Development Corporation Press.
- Pickett, G. R. (1970). Applications for borehole geophysics in geophysical exploration. *Geophysics*, 35(1), 81-92.
- Pilgrim, G. E. (1926). The Tertiary formations of India and the interrelation of marine and terrestrial deposits. *Pan-Pacific Science*, 2(3), 896-931.
- Pixler, B.O. (1969). Formation Evaluation by Analysis of Hydrocarbon Ratios. *Journal Petroleum Technology*, 21 (6), 665-670.
- Poupon, A., Gaymard, R. (1970, January). The evaluation of clay content from logs. In SPWLA 11th Annual Logging Symposium. *Society of Petrophysicists and Well-Log Analysts*, 1(2), 11-17.
- Quadri, V.N., Quadri, S.M.J.G., 1998, Failure-to-success targets may lie in Pakistan basins: *Oil and Gas Journal*, 72(2), 43-54.
- Quadri, Viqar-un-Nisa, Quadri, S.M.G.J. (1996), Exploration anatomy of success in oil and gas exploration in Pakistan. *Oil and Gas Journal*, 94(3), 20-28.
- Quirk, D. G., Schødt, N., Lassen, B., Ings, S. J., Hsu, D., Hirsch, K. K., Von Nicolai, C. (2012). Salt tectonics on passive margins: examples from Santos, Campos and Kwanza basins. *Geological Society, London, Special Publications*, 363(1), 207-244.

- Rana, R. A., Asrarullah. (1982). Tectonic map of Pakistan. Government of Pakistan, Min. of Petroleum and Natural Resources. *Journal Petroleum Technology*, 12 (7), 465-485.
- Raza, H.A., Ahmed, Riaz, Alam, Shaji, Ali, S.M. (1989). Petroleum zones of Pakistan: *Pakistan. Journal of Hydrocarbon Research*, 1(2), 21–56.
- Raza, S.M., 1967, Stratigraphy and palaeontology of Gandhian-Dartian area, Hazara District, West Pakistan. *Geology Bulletin University Punjab*, 5(1), 111 -114.
- Rider, M.H., 1986. *The geological interpretation of well logs* (1st ed., Vol. 1, pp. 1-280). New York, NY, (USA). John Wiley and Sons Publishers;
- Russell, W. L. (1955). *Structural geology for petroleum geologists* (1st ed., Vol. 3, pp. 23-75). McGraw-Hill, New York. Scientific Research an Academic Publisher.
- Schlumberger Charts (1977. *Log Interpretation charts. Schlumberger* (3rd ed., Vol. 3, pp. 1-58). New York, America Publishers.
- Schlumberger Charts, L. I. (1983). *Log Interpretation charts. Schlumberger* (5th ed., Vol. 6, pp. 1-45). New York, America Publishers.
- Schultz-Ela, D. D., Jackson, M. P., Vendeville, B. C. (1993). Mechanics of active salt diapirism. *Tectonophysics*, 228(3-4), 275-312.
- Schowalter, T. T. (1979). Mechanics of secondary hydrocarbon migration and entrapment. *American Association of Petroleum Geologist Bulletin*, 63(5), 723-760.
- Segesman, F. F. (1980). *Well-logging method. Geophysics* (1st ed., Vol. 3, pp. 1-79). New York, NY, (USA). John Wiley and Sons Publishers;
- Serra, O. E. (1983). *Fundamentals of well-log interpretation* (8th ed., Vol. 8, pp. 1-118). McGraw-Hill, New York. Scientific Research an Academic Publisher.
- Selley, R. C. (1996). *Ancient sedimentary environments and their sub-surface diagnosis* (4th ed., Vol. 17, pp. 121-142). New York, USA Psychology Press.
- Shah, S. I. (2009). *Stratigraphy of Pakistan* (1st ed., Vol. 1, pp. 1-340). Government of Pakistan Ministry of Petroleum and Natural Resources Geological Survey of Pakistan. Islamabad Geological Survey Press.
- Shah, S.M.I. (1977). Stratigraphy of Pakistan. *Pakistan Geological Survey Memoirs*, 12(1), 138-143.
- Shah, S. B. A., Abdullah, W. H. (2017). Structural interpretation and hydrocarbon potential of Balkassar oil field, eastern Potwar, Pakistan, using seismic 2D data and petrophysical analysis. *Journal of the Geological Society of India*, 90(3), 323-328.
- Shah, S. B. A., Abdullah, W. H. (2016). Petrophysical properties and hydrocarbon potentiality of Balkassar well 7 in Balkassar oilfield, Potwar Plateau, Pakistan. *Bullet in of the Geological Society of Malaysia*, 62(1), 73-77.

- Shami, B. A., Baig, M. S. (2002). Geomodeling for the enhancement of hydrocarbon potential of Joya Mair field, Potwar, Pakistan. *Pakistan Association of Petroleum Geoscientists-Society*, 2(1), 124-145.
- Sheriff, R. E. (1980). Nomogram for Fresnel-zone calculation. *Geophysics*, 45(5), 968-972.
- Sheriff, R. E., Geldart, L. P., (1995), *Exploration Seismology* (2nd ed., Vol. 4, pp. 1-70). UK, Cambridge University Press.
- Snyder, D. D., Fleming, D. B. (1985). Well logging a 25-year perspective. *Geophysics*, 50(12), 2504-2529.
- Sorkhabi, R. B., Tsuji, Y. (Eds.). (2005). *Faults, fluid flow, and petroleum traps* (1st ed., Vol. 1, pp. 24-300). McGraw-Hill, New York. Scientific Research an Academic Publisher.
- Stach, E. (1982). *Stach's textbook of coal petrology* (3rd ed., Vol. 2, pp. 24-542). Germany, Gebruder Borntraeger Publishers.
- Stewart, S. A. (2006). Implications of passive salt diapir kinematics for reservoir segmentation by radial and concentric faults. *Marine and Petroleum Geology*, 23(8), 843-853.
- Sweeney, J. J., Burnham, A. K. (1990). Evaluation of a simple model of vitrinite reflectance based on chemical kinetics. *American Association of Petroleum Geologist Bulletin*, 74(10), 1559-1570.
- Suggate, R. P. (1998). Relations between depth of burial, vitrinite reflectance and geothermal gradient. *Journal of Petroleum Geology*, 21(1), 5-32.
- Tahirkheli, R. K. (1979). Geology of Kohistan and adjoining Eurasian and Indo-Pakistan continents, Pakistan. *Geology Bulletin University Peshawar*, 11(1), 1-30.
- Tarback, E. J., Lutgens, F. K., Tasa, D., Tasa, D. (2005). *Earth: an introduction to physical geology* (11th ed., Vol. 2, pp. 270-850). UK, Pearson Publishers.
- Telford, W. M., Geldart, L. P., Sheriff, R. E. (1990). *Applied Geophysics* (2nd ed., Vol. 1, pp. 1-770). UK, Cambridge University press.
- Teichert, C. (1967). Nature of the Permian glacial record, Salt Range and Khisor Range, West Pakistan. *Neues Jahrbuch für Geologie und Paläontologie, Abhandlungen*, 129(2), 167-184.
- Thomas, D. (1988). Geochemical precursors to seismic activity. *Pure and Applied Geophysics*, 126(2-4), 241-266.
- Timur, A. (1968, January). An investigation of permeability, porosity, and residual water saturation relationships. *Pakistan Association of Petroleum Geoscientists-Society*, 2(1), 124-145.

- Tissot, B. P., Welte, D. H. (1984). *Geochemical Fossils and their Significance in Petroleum Formation* (1st ed., Vol. 1, pp. 20-666). In *Petroleum Formation and Occurrence*. Berlin, Heidelberg. Springer Publishers.
- Trusheim, F. (1960). Mechanism of salt migration in northern Germany. *American Association of Petroleum Geologist Bulletin*, 44(9), 1519-1540.
- Van Golf-Racht, T.D., 1982. Fundamentals of fractured reservoir engineering (1st ed., Vol. 22, pp. 20-42). Norway Elsevier Publishers.
- Van Overmeeren, R. A. (2001). Hagedoorn's plus-minus method: the beauty of simplicity. *Geophysical Prospecting*, 49(6), 687-696.
- Van der Pluijm, B. A., Marshak, S. (2004). *Earth structure: An introduction to Structural Geology and Tectonics* (2nd ed., Vol. 1, pp. 36-672). WW Norton and Company. New York, USA WW Norton and Company Publishers.
- Van Krevelen, D. W. (1961). Coal: Typology. Chemistry, Physics, Constitution. *Elsevier Science & Technology*, 3(1), 238-262.
- Vendeville, B. C. (2002). A new interpretation of Trusheim's classic model of salt-diapir growth. *American Association of Petroleum Geologist* 52(1), 943-952.
- Wandrey, C. J., Law, B. E., Shah, H. A. (2004). *Patala-Nammal composite total petroleum system, Kohat-Potwar geologic province, Pakistan* (1st ed., Vol. 1, pp. 6-17). US Department of the Interior, US Geological Survey Publishers.
- Waples, D. W. (1985). Maturity modeling: thermal indicators, hydrocarbon generation, and oil cracking. *Memoirs-American Association of Petroleum Geologists*, 3(2), 285-285.
- Watts, N. L. (1987). Theoretical aspects of cap-rock and fault seals for single-and two-phase hydrocarbon columns. *Marine and Petroleum Geology*, 4(4), 274-307.
- Wyllie, M. R. J., Gregory, A. R., Gardner, G. H. F. (1958). An experimental investigation of factors affecting elastic wave velocities in porous media. *Geophysics*, 23(2), 459-93.
- Wynne, A. B. (1878). *Geology of the Salt Range in the Punjab* (1st ed., Vol. 1, pp. 2-77). Government of India Press.
- Zahid, M., Khan, A., ur Rashid, M., Saboor, A., Ahmad, S. (2014). Structural interpretation of Joya Mair oil field, south Potwar, Upper Indus Basin, Pakistan, using 2D seismic data and petrophysical analysis. *Journal of Himalayan Earth Sciences Volume*, 47(1), 73-86.

LIST OF PUBLICATIONS AND PAPERS PRESENTED

PUBLICATIONS

1. **Shah, S. B. A.**, Abdullah, W. H, & Shuib, M. K (2019). Petrophysical properties evaluation of Balkassar oilfield, Potwar Plateau, Pakistan: implication for reservoir characterization. *Himalayan Geology*, 40(1), 50-57.
2. **Shah, S. B. A.**, & Abdullah, W. H. (2017). Structural interpretation and hydrocarbon potential of Balkassar oil field, eastern Potwar, Pakistan, using seismic 2D data and petrophysical analysis. *Journal of the Geological Society of India*, 90(3), 323-328.
3. **Shah, S. B. A.**, & Abdullah, W. H. (2016) Petrophysical properties and hydrocarbon potentiality of Balkassar well 7 in Balkassar oilfield, Potwar Plateau, Pakistan. *Bulletin of the Geological Society of Malaysia*, 62(1), 73 – 77.
4. **Shah, S. B. A.**, & Abdullah, W. H. (2017). Reservoir rock evaluation of Balkassar oilfield Potwar plateau, Pakistan using geophysical wireline Logs. *International Journal of Advances in Science Engineering and Technology*, 5(1-2), 108-110.

PAPER PRESENTED

1. **Shah, S. B. A.**, & Abdullah, W. H. (2017). *Reservoir rock evaluation of Balkassar oilfield Potwar plateau, Pakistan using geophysical wireline Logs*. Paper presented at International Conference on Environmental Science and Development (ICESD) Malacca, Malaysia 2nd - 3rd December 2016.